



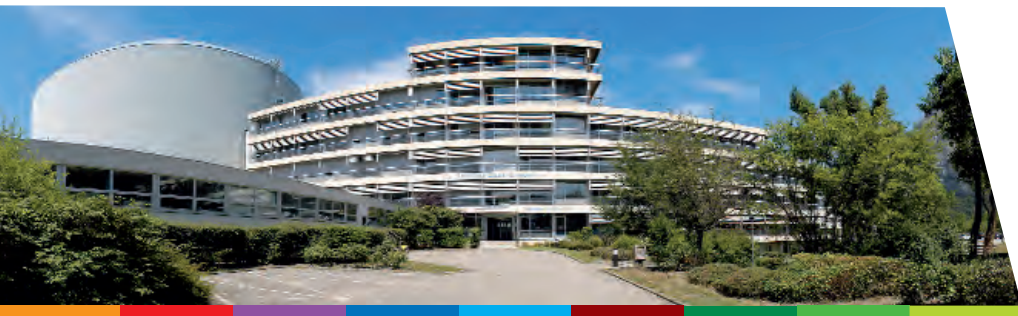
# 2006

## Annual Report

Institut Laue-Langevin



NEUTRONS  
FOR SCIENCE

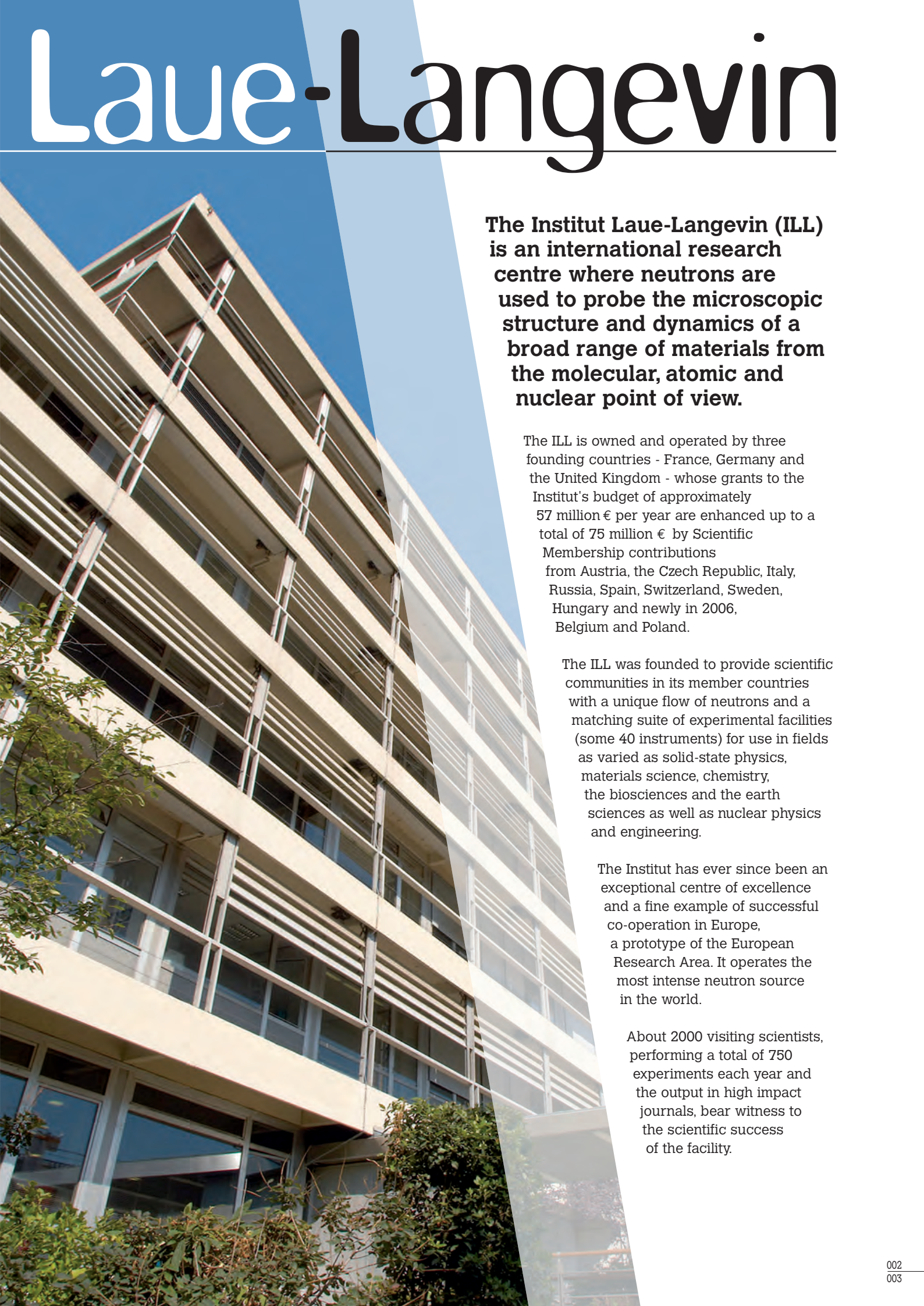


*“ The world's leading facility  
in neutron science and technology ”*

# The Institut



# Laue-Langevin



**The Institut Laue-Langevin (ILL) is an international research centre where neutrons are used to probe the microscopic structure and dynamics of a broad range of materials from the molecular, atomic and nuclear point of view.**

The ILL is owned and operated by three founding countries - France, Germany and the United Kingdom - whose grants to the Institut's budget of approximately 57 million € per year are enhanced up to a total of 75 million € by Scientific Membership contributions from Austria, the Czech Republic, Italy, Russia, Spain, Switzerland, Sweden, Hungary and newly in 2006, Belgium and Poland.

The ILL was founded to provide scientific communities in its member countries with a unique flow of neutrons and a matching suite of experimental facilities (some 40 instruments) for use in fields as varied as solid-state physics, materials science, chemistry, the biosciences and the earth sciences as well as nuclear physics and engineering.

The Institut has ever since been an exceptional centre of excellence and a fine example of successful co-operation in Europe, a prototype of the European Research Area. It operates the most intense neutron source in the world.

About 2000 visiting scientists, performing a total of 750 experiments each year and the output in high impact journals, bear witness to the scientific success of the facility.

**We warmly thank  
everyone who  
contributed to the  
production of this report**



**Editors:**

Giovanna Cicognani and Christian Vettier

**Production team:**

Katja Jenkins, Martin Boehm, Emmanuel Farhi,  
Peter Fouquet, Isabelle Grillo, Marie-Hélène Lemée-Cailleau,  
Roland May, Claudia Mondelli, Christian Plonka, Anne Stunault

**Design and Typesetting:**

Synthese ECA  
Tel: +33(0)4 76 90 02 73 - Fax: +33 (0)4 76 04 95 92

**Photography:**

ILL and Artechnique - artechnique@wanadoo.fr

**Printing:**

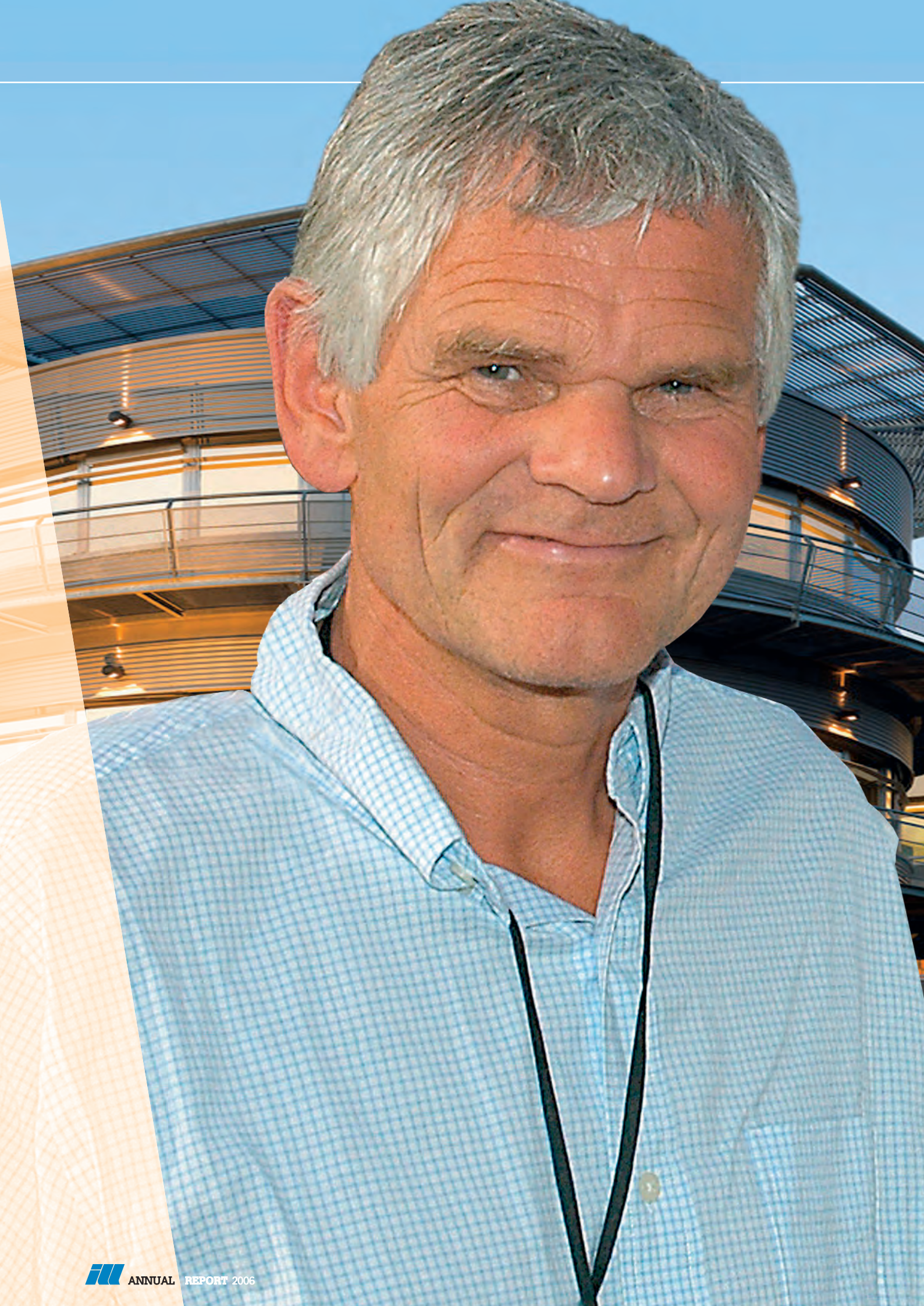
Imprimerie Pont de Claix

**Further copies can be obtained from:**

Institut Laue-Langevin  
Scientific Coordination Office (SCO)  
BP 156 - F-38042 Grenoble Cedex 9 (France)  
Tel: +33 (0)4 76 20 72 40 - Fax: +33 (0)4 76 48 39 06  
email: sco@ill.fr - web: www.ill.fr

# C CONTENTS

<b>Director's foreword</b>	006
<b>What is the ILL ?</b>	008
<b>Scientific highlights</b>	010
• Magnetism	016
• Materials	028
• Chemistry	030
• Soft matter	036
• Biology	042
• Liquids and glasses	048
• Nuclear and particle physics	052
• Spectroscopy, modelling and theory	056
<b>Looking to the future</b>	064
<b>Millennium programme and technical developments</b>	066
• Millennium programme	068
• Technical and computing developments	078
• New experimental techniques	090
<b>Experimental and user programme</b>	094
• User programme	096
• Instrument list	098
• Beamtime allocation	100
• Instrument performance	102
<b>Reactor operation</b>	104
<b>Workshops and events</b>	108
<b>Administrative matters</b>	116
<b>Facts and figures</b>	118



I take it as a great privilege, at the end of my first year at the ILL, to prepare my first Director's Foreword to the Annual Report.

The year has seen major changes in the ILL's Management team. Colin Carlile left his post as Director of the ILL to join the Swedish European Spallation Source Initiative in Lund. Andrew Harrison has joined us as the new British Director, taking over as Head of the Projects and Techniques Division from Werner Press. Werner, after four years at the ILL, has returned to the University of Kiel. Finally, Norbert König, who had served the ILL for five years as Head of Administration has returned to the German Ministry for Education and Research. He was replaced in good time by Amin Saidoun. There remain, of course, Christian Vettier – French Director of the Science Division – and Hervé Guyon – as the head of the Reactor Division – who will both continue to contribute their most valuable experience to the new Management Board.

The year 2006 was, indeed, an eventful year for the Institut. The reactor restart in June marked the end of an extremely productive 11-month shutdown. Our user programme was immediately resumed, on schedule, thanks to substantial efforts by all our staff.

The long shutdown had been used to replace the front-ends of our H1 and H2 neutron guides – which channel cold and thermal neutrons to some 20 instruments – and to refurbish the vertical cold neutron source. There was also intense activity on instrument and infrastructure projects under the ongoing Millennium Programme. Since its launch in 2000 the Millennium Programme has allowed the ILL to build or upgrade eleven different instruments and their associated infrastructure. The Institute can now boast more than a nine-fold increase in average instrument efficiency.

At the ILL's 2<sup>nd</sup> Millennium Symposium in April our user community gave us overwhelmingly positive feedback on these achievements and on our ambitions for extending the Millennium Programme. Constructive criticism was received on the limits to our sample environment facilities, and we have responded immediately with the launching of an appropriate investment programme.

In 2006 also the number of research proposals submitted for ILL appraisal reached its highest level ever. This is clear evidence that demand for ILL beamtime remains as healthy as ever. It also shows that the Millennium Programme is already paying dividends in terms of new scientific opportunities for ILL's users. High levels of activity, of course, generate high workloads, and we are particularly grateful to both the Peer Review Subcommittees of the Scientific Council and the ILL's User Support Team, who continue to deliver with efficiency and skill.

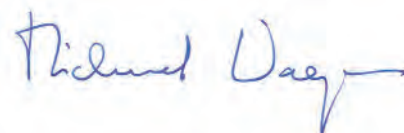
In October the European Strategy Forum on Research Infrastructures (ESFRI) published its first European Roadmap on research infrastructures. The Roadmap singled out the ILL as "...the world's most productive and reliable source of slow neutrons for the study of condensed matter". This may pave the way towards European funding, and this can only be good news for the ILL's commitment to continuous modernisation. Our plans in this respect can be consulted in the 2006 strategy document "Future Perspectives and Opportunities for the ILL".

*"...the world's most productive and reliable source of slow neutrons for the study of condensed matter".*

Our strategy proposals have been well received by the ILL's Associates, who have made long-term commitments to its funding. The plans have also been welcomed with enthusiasm by our 10 Scientific Members. Belgium and Poland joined our community in 2006 and we extend a very warm welcome to them.

Our Grenoble site is one of the most admired in Europe. It can boast not only the ILL but also the ESRF and the EMBL's Grenoble outstation. The time is now ripe to transform what is already a lively campus into a recognised centre of scientific excellence for European researchers. Plans have been drawn up by the three institutes on the site and we are optimistic that funding will soon be available for this purpose under the new financial framework to be agreed between the French State and the Region for the period 2007-2013.

We are therefore fully confident of a very bright future – surely the best of preparations for celebrating the ILL's 40<sup>th</sup> anniversary in 2007!



**Richard Wagner**  
Director of the ILL

# The ILL is a world-renowned international research centre for the study of matter

Formally, the ILL is a non profit-making French company under civil law, which is governed by an International Convention signed at Foreign Ministry level by three countries - France, Germany and the United Kingdom. Our Associates - the CNRS and the CEA representing France, the FZ Jülich representing Germany and the CCLRC representing the United Kingdom - own and administer the Institut. They are also responsible for all liabilities and eventual decommissioning costs. With the signing of the Fourth Amendment of the ILL Intergovernmental Convention on 4 December 2002, the ILL's life has been formally extended until at least 31 December 2013.

Although the ILL is an international organisation, its staff are not paid tax-free salaries, but instead they are enveloped within the French tax, employment and social security systems, which has marked advantages but also marked disadvantages from whichever point of view you look at it. The Institut is answerable to French legal bodies and to French security authorities. We exist and operate within the French Labour law (Code du Travail). Our staff representative bodies, as laid down by French law, are a significant presence in the ILL's daily life. We have strong links to the Mairie of Grenoble and surrounding communities, to the Préfecture of the Isère and to the Council of the Rhône-Alpes Region.

*The ILL's neutron source is the finest in the world*

Whilst our Associates own the facility and contribute the largest amount to the almost 75 M€ annual operating costs, the ILL also benefits from the scientific partnerships of ten other nations - Austria, the Czech Republic, Italy,

Spain, Switzerland, Russia, Sweden, Hungary and newly in 2006 Belgium and Poland - who together contribute ~17% of the operational and investment costs of the Institut. All ten partner countries in addition can and do contribute to capital projects at the Institut, within the Institut's priorities but according to their own priorities also.

Our governing body is the Steering Committee, which meets twice-yearly and is made up of representatives of the Associates and the Scientific Partners together with Directors and Staff Representatives. Within the framework of the International Convention, the Steering Committee has the ultimate responsibility for determining operational and investment strategies for the Institut.

The Institut has a Director and two Associate Directors, one from each of the Associate countries, appointed on short-term contracts normally of five years. The Director's role is generally taken alternately by the German and British appointee. The two Associate Directors are responsible for the Science Division and the Projects and Techniques Division respectively. The Head of the Administration Division is also appointed on a short-term contract, whereas the Head of the Reactor Division is a permanent ILL employee. These five people together constitute the Management Board of the Institut and are responsible for its day-to-day operation.

The scientific life of the Institut is guided by the Directors, with input from the ILL's ten scientific colleges. A Scientific Council, comprising seventeen external scientists from the member countries, advises the Directors on scientific directions for the Institut, on the evolution of the instrument suite and technical infrastructure to best meet the needs of the user research programme, and to assess the scientific output of the Institut. It is helped in this process by the Instrument Sub-Committee and by the Chairmen of the nine Scientific Sub-Committees who twice-yearly peer review the experiment proposals.

The ILL is composed of four Divisions, each with its distinct role and, it is true to say, its own culture. Efforts have been made to bring those cultures closer together whilst recognising the need for differences. The Science Division staffs the instruments and delivers the science; the Projects and Techniques Division designs and builds new instruments, develops new concepts and maintains beamlines and instruments operational; the Reactor Division delivers the neutrons, operates and mans the reactor 24 hours per day every day of the year and has responsibility for all aspects of security; the Administration Division deals with Personnel matters with particular responsibility for interactions with staff representative bodies, with Purchasing, with Finance and with Site and Building maintenance; and the Director's Services deal with Radiological safety, with conventional safety and with Health and Working Practices.

*Our community of users is world-wide with scientists from non-partner nations also having a chance to apply for beamtime with outstanding research proposals*

The ILL's neutron source is the finest in the world, being based on a single element 58.3 MW nuclear reactor designed for high brightness. The main moderator is the ambient D<sub>2</sub>O coolant surrounding the core which delivers intense beams of thermal neutrons to 11 beamlines and to four neutron guides. A graphite hot source operating at 2400 K delivers hot neutrons - energies up to 1eV and wavelengths down to 0.3 Å - to 3 beamlines. A renewal project has resulted in the installation of a new hot source and beam tubes during 2003. Two liquid deuterium cold sources at 25 K deliver cold neutrons - energies down to 200 μeV and wavelengths up to 20 Å - to some 17 instruments. An ultra-cold neutron source fed from the top of one

# What is the ILL ?

## Why neutrons

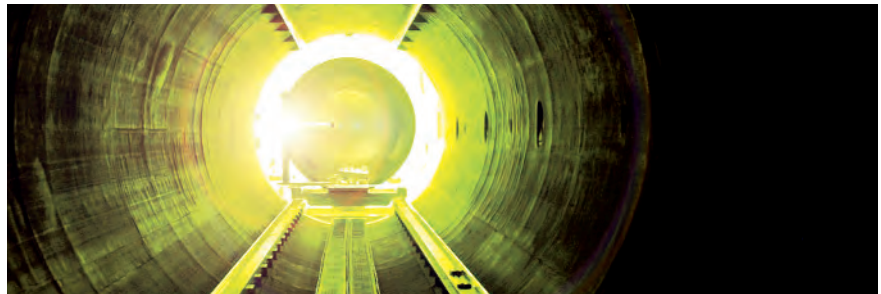
of the cold sources delivers neutrons vertically through the reactor pool to 5 instruments on the operational floor of the reactor. In all there are more than 50 measuring stations, 27 of which have full public access.

Our community of users is world-wide with scientists from non-partner nations also having a chance to apply for beamtime with outstanding research proposals. This broader community of users enriches the scientific life of the Institut.

Our interactions with our user community have been enhanced over the recent years: five years ago the ILL convened the first Millennium Symposium to launch an ambitious modernisation programme of instruments and infrastructure called the ILL Millennium Programme. Five years of hard work by the ILL staff in all divisions, with enthusiastic support from our users, have further expanded the ILL's suite of unique world-class instruments and yielded many-fold gains in efficiency and quality on several existing instruments. The Second Symposium with our users was held at the end of April 2006 to demonstrate the achievements of the Millennium Programme to date, and to boost the ILL's ambitious plans for the coming decade. Last but not least, the "Future perspectives and opportunities" document, produced in September 2006, presents the ILL strategy for the next 10 years.

The ILL monitors the papers published as a result of the use of our facilities. This gives a figure of around 500 papers per year. With a total annual budget of ~ 75 M€, the cost per published paper is around 150 k€. We pay particular attention to papers published in high impact journals. About 80 such papers per year are published from data taken on ILL instruments which is a factor of two higher than the second most productive neutron source in the world.

Beam days delivered for science during three reactor cycles amount to 4174 in 2006. The cost per beam day of science therefore stands at a very cost effective 17.9 k€ per day.



Neutron beams have the power, when used as a probe of small samples of materials, to reveal what is invisible using other radiations. Neutrons can appear to behave either as particles or as waves or as microscopic magnetic dipoles and it is these specific properties which enable them to uncover information which is often impossible to access using other techniques.

### Electrically Neutral

Neutrons are non-destructive and can penetrate deep into matter making them an ideal probe for biological materials and samples under extreme conditions of pressure, temperature, magnetic field or within chemical reaction vessels.

### Microscopically Magnetic

They possess a magnetic dipole moment which makes them sensitive to magnetic fields generated by unpaired electrons in materials. Precise details of the magnetic behaviour of materials at the atomic level can be investigated. In addition, the scattering power of a neutron by an atomic nucleus depends on the orientation of the neutron and the spin of the atomic nuclei in a sample thereby providing a powerful tool to detect the nuclear spin order.

### Wavelengths of Ångstroms

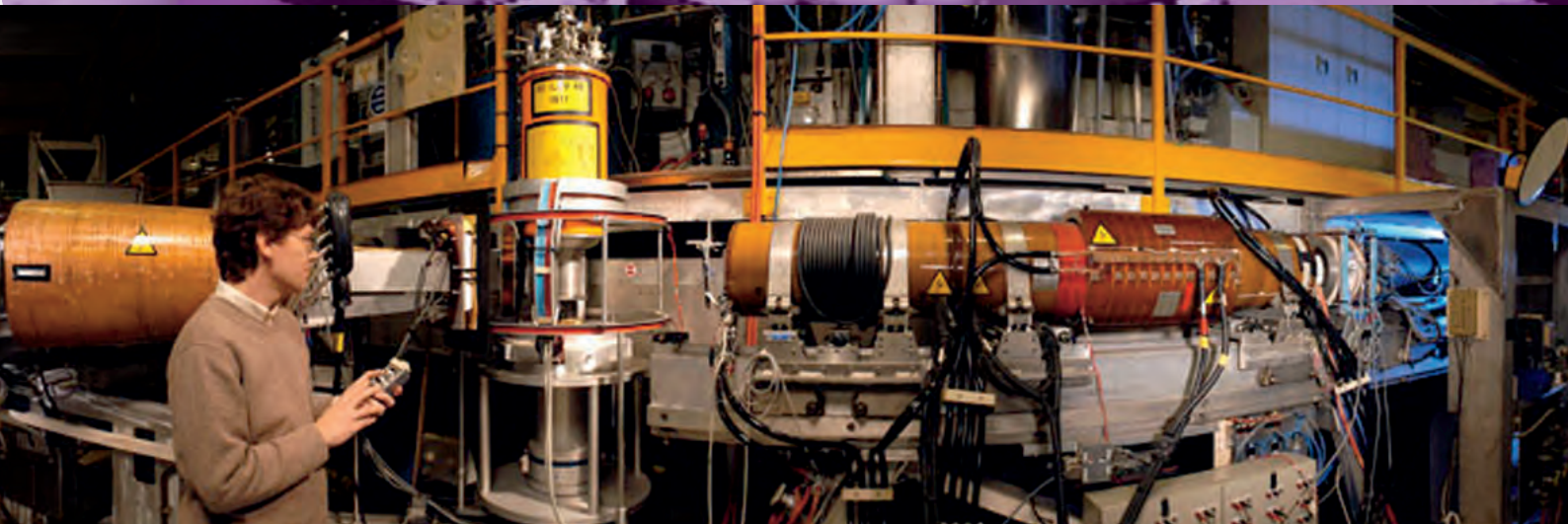
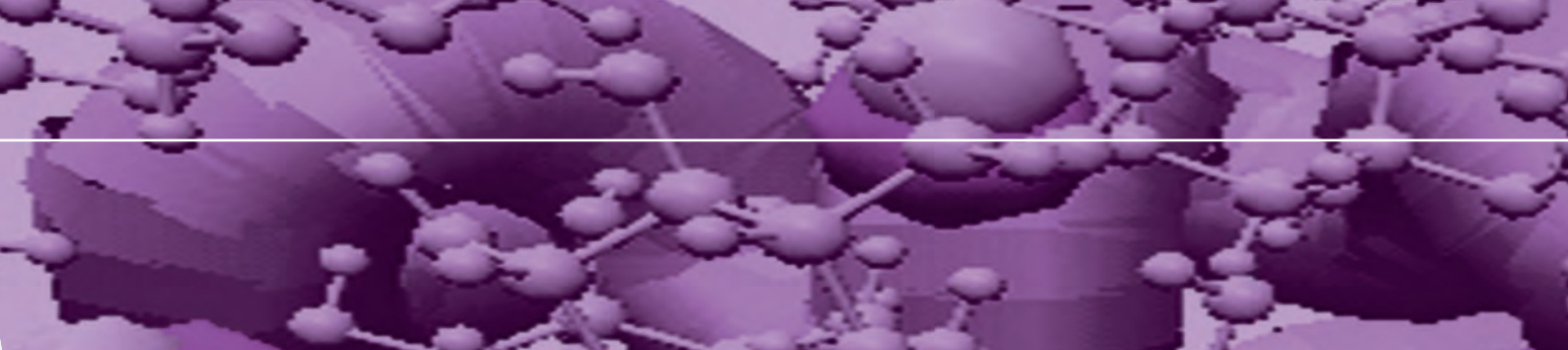
Their wavelengths range from 0.1 Å to 1000 Å making them an ideal probe of atomic and molecular structures ranging from those consisting of single atomic species to complex biopolymers.

### Energies of millielectronvolts

Their energies are of the same magnitude as the diffusive motions in solids and liquids, the coherent waves in single crystals (phonons and magnons) and the vibrational modes in molecules. An energy exchange between the incoming neutron and the sample of between 1 μeV (even 1 neV with spin-echo) and 1eV can readily be detected.

### Randomly sensitive

The variation of scattering power from nucleus to nucleus in a sample varies in a quasi-random manner. This means that light atoms are visible in the presence of heavy atoms and neighbouring atoms may be distinguished from each other. In addition, isotopic substitution (for example D for H, or one nickel isotope for another) can allow contrast to be varied in certain samples thereby highlighting specific structural features. The neutron is particularly sensitive to hydrogen atoms and therefore is a powerful probe of hydrogen storage materials, organic molecular materials, and biomolecular samples or polymers.



- Magnetism
- Materials
- Chemistry
- Soft matter
- Biology
- Liquids and glasses
- Nuclear and particle physics
- Spectroscopy, modelling and theory

# Scientific highlights



The scientific impact of ILL results from scientific programmes achieved by our users and the research accomplished by ILL staff. The instrument suite that has been developed at ILL enables a large scope of highly successful experiments. However, ILL has decided to further extend the scope of interface laboratories in order to attract and help top class science experiments. In 2001 strong pro-active moves were made to facilitate access to neutron experiments in life sciences; the Deuteration Laboratory was established and was eventually incorporated into the Partnership for Structural Biology. In 2002 the ILL decided to develop a vigorous and ambitious programme to support the users' scientific programmes by offering interface facilities through which ILL users could optimise their beamtime on ILL instruments; the slogan '*more than simply neutrons*' was thus coined. The Partnership for Structural Biology, the Computer Modelling Laboratory and the FaME38 facility are the first examples of dedicated facilities to be built next to ILL neutron beams.

*2006 has been a highly productive period for ILL's scientific agenda ...*

*2007 will certainly be another obvious big success.*

In 2006 the Soft Matter Laboratory was created, which would enable Soft Condensed Matter scientists to characterise their samples before or during scheduled experiments. It is the ILL's clear intention to move from an embryonic laboratory for soft matter to a joint ILL-ESRF interface facility, which scientists may benefit from in order to optimise their research programmes on Soft Matter, which require neutrons or X-rays. Strategies to promote a fresh spirit of research on the joint ILL-ESRF-EMBL site are now bearing fruit! The ILL intends to remain the world's premier source of neutron beams for research.

Researchers are using neutrons to develop and optimise properties of new materials ranging from membranes and fibres to composite systems.



Scientists and engineers exploit the unique properties of neutrons, described as the gentle scattering probe: they are non-destructive, highly penetrating and sensitive to magnetic moments; they probe thermal and sub-thermal excitation spectra in materials. The selection of highlights presented below allows a small glimpse into the tremendous range of high quality science achieved on instruments at ILL.

2006 has been a highly productive period for ILL's scientific agenda despite the continuing heavy programme to retrofit the building infrastructures. With a Millennium Programme in full swing, and with the reactor operating for four cycles, 2007 will certainly be another obvious big success. The ILL relies on its many collaborators who submit their contributions, to illustrate the range of research performed on ILL's instruments; I personally wish to warmly thank all of you who have eagerly contributed to this year's version.

Finally, I invite all of ILL's users to contemplate the future. ILL is now celebrating its 40<sup>th</sup> anniversary. Considering all its past achievements and the momentum gained in the modernisation of the site, we are confident that ILL will remain a model for European science. Just imagine a fully optimised ILL surrounded by an attractive science park!

**Christian Vettier**  
Associate Director

## Magnetism

Neutron scattering is an unchallenged tool in the study of many aspects of magnetism, in more and more complex systems, from exotic magnetic structures to unconventional superconductivity and low-dimensional systems.

While X-ray experiments on  $\text{GdB}_4$  could show some interference between anisotropic magnetic and charge scattering amplitudes, only neutron polarimetry could demonstrate the non-collinear character of the magnetic structure (Blanco *et al.*), questioning the involved interactions.

Neutron spectroscopy remains unique to characterise excitations and better understand exchange mechanisms in unconventional superconductors. Kuwahara *et al.* evidence the existence of non-magnetic quadrupolar interactions in the skutterudite  $\text{PrOs}_4\text{Sb}_{12}$  and their close connection to the superconducting transition. In  $\text{UPd}_2\text{Al}_3$ , the superconductivity is intimately connected to the magnetic dynamics in the system. Blackburn *et al.* show its itinerant character with all the  $5f$  electrons participating in the development of the superconductivity. In geometrically frustrated antiferromagnets short range correlations lead to clusters with local order and fluctuations, with a wide variety of ground states. In the Kagome bilayer  $\text{SrCr}_{9x}\text{Ga}_{12-9x}\text{O}_{19}$ , Mutka *et al.* show the existence of slow dynamics involving the interplay of spin-lattice coupling and quantum phenomena.

Complex mechanisms are also involved in Griffiths phases, responsible for colossal magnetoresistance in manganites. Magen *et al.* show the development of such a phase in  $\text{Tb}_5\text{Si}_2\text{Ge}_2$ , attributed to the competition between  $4f$ - $4f$  indirect exchange within the rare-earth atomic planes and superexchange involving the Si/Ge atoms.

Closer to applications, the study of ferromagnetic  $\text{Co}_{70}\text{Fe}_{30}$  stripes on an antiferromagnetic  $\text{Mn}_{83}\text{Ir}_{17}$  substrate by polarised neutron reflectometry lead to a better understanding of the relationships between the geometry and the exchange bias field contribution.

The diversity of the studies involve most types of instruments available at the ILL: powder and single-crystal diffractometers ( $\text{GdB}_4$  on D3), time-of-flight, three-axis ( $\text{PrOs}_4\text{Sb}_{12}$  on IN14) and spin-echo ( $\text{UPd}_2\text{Al}_3$  and  $\text{SrCr}_{9x}\text{Ga}_{12-9x}\text{O}_{19}$  on IN11) spectrometers, small-angle scattering instruments ( $\text{Tb}_5\text{Si}_2\text{Ge}_2$  on D16) and reflectometers ( $\text{Co}_{70}\text{Fe}_{30}$  on ADAM). For the near future, newly commissioned multi-analyser stages on several instruments will still enhance their capabilities: the flat cone option on IN20 and IN14, the RITA type multi-analyser IMPS on IN8, and the new analyser bench on D7, will allow new experiments, formerly barely feasible considering the huge counting times needed.

**Anne Stunault, College 5B Secretary**  
<http://www.ill.fr/Colleges/C5B>

**Martin Böhm, College 4 Secretary**  
<http://www.ill.fr/Colleges/C4>

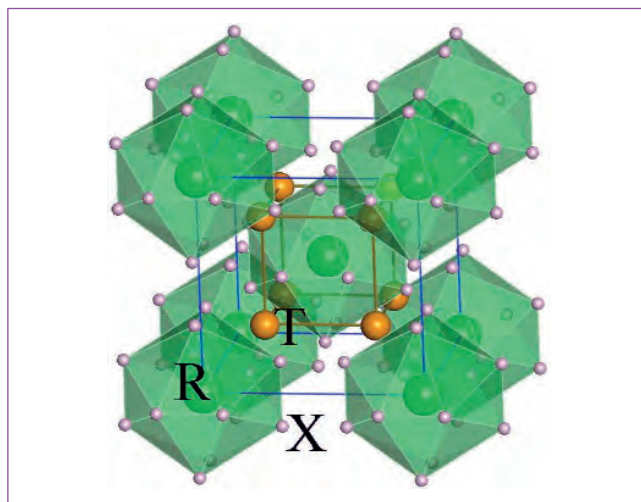
## Materials

College 1 has recently been created in order to discuss research proposals associated with applications of neutron methods (scattering and imaging). The upgrades of D1A, D11 and D22 and the construction of the strain scanner SALSA have boosted ILL's capabilities to deal with technological applications. The Neutrograph and the Tomography station are now used in a routine mode. Today, the ILL suite of instruments offers a wide range of tools for applied science. Additionally, the FaME38 facility <http://www.ill.fr/fame38/> has been set up in order to help users in the preparation and characterisation of samples for engineering science.

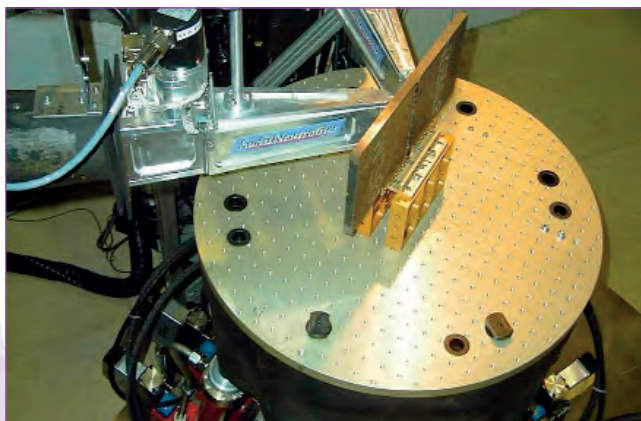
Research proposals which have been submitted to College 1 deal with residual stresses in railway rails, development and validation of construction codes and standards, archaeology and cultural heritage studies.

Obviously, topics regarding innovative instrumentation, simulation of guides, instruments, neutron optics and virtual experiments, medical applications are also in the remit of College 1.

**Emmanuel Farhi, College 1 Secretary**  
<http://www.ill.fr/Colleges/C1>



**Magnetism:** The crystal structure of the filled skutterudite superconductor  $\text{PrOs}_4\text{Sb}_{12}$  (IN12 and IN14, p. 22).



**Materials:** SALSA hexapod platform (p. 28).

## Chemistry and structure

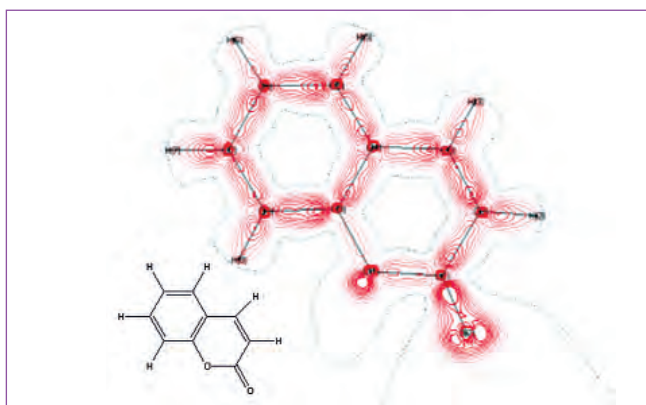
2006 was a short year in terms of neutron days but with a high-quality scientific production, in particular concerning the activities in chemistry and structures, traditionally associated with College 5A 'Crystallography'. We have this year selected three highlights from among the numerous and excellent experiments carried out at the ILL. These illustrate the diversity of current scientific trends investigated by our users in collaboration with ILL scientists.

In the field of zeolites, a subject of constant scientific and technological interest, J. Hunger *et al.* have explored the structural modification of adsorption complexes in a NaX zeolite at different water loadings, thanks to an experimental approach combining advanced infrared spectroscopy measurements with high resolution neutron powder diffraction on D2B. This shows that new water hexamers, analogous to ice Ih, can form between the faujasites supercages and are stabilised by a dense network of hydrogen bonding.

In the present context of energy saving, solid-oxide fuel cells attract a lot of interest because of an improved conversion of petrol into electrical current. W. Paulus *et al.* present an *in situ* study of the controlled intercalation of oxygen and show that solid oxides can relax towards new ordered structures already at ambient temperature, making questionable the well established general assumption that good ionic conduction is always accompanied by structural disorder and vice versa.

Finally, the new capabilities offered by thermal-neutron Laue diffraction and VIVALDI to frontier problems in chemistry, are illustrated by several recent and quite different examples (J.M. Cole *et al.*). This highlight shows how this high performance technique is especially well suited for small crystals, rapid chemical crystallography, reciprocal space surveys or studies of phase transitions, and demonstrates yet again that the Laue experiment is becoming as easy as a powder diffraction experiment, and often just as fast, but with the additional qualities of single-crystal diffraction.

**Marie-Hélène Lemée-Cailleau, College 5A Secretary**  
<http://www.ill.fr/Colleges/C5A>



**Chemistry:** Electron deformation density map of the coumarin laser-dye precursor (VIVALDI, p. 33).

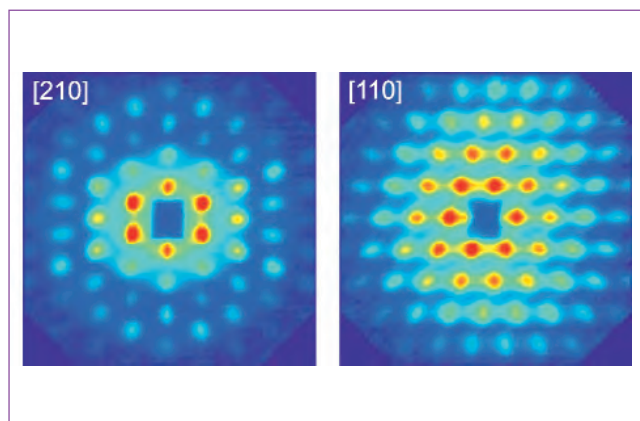
## Soft matter

This year, a major event for College 9 at the ILL was the Soft Matter User Meeting (SMUM), held on 22-24 November in the ESRF Auditorium. More than 110 scientists, mainly from Europe, attended the meeting. The aim of the meeting, presided by the College 9 Chairman, Stefan Egelhaaf (University of Düsseldorf), was to discuss the recent neutron research in soft matter and to identify the needs of the community from the perspective of a Partnership for Soft Condensed Matter (PSCM). From the discussions, it appears that complementary techniques that allow the characterisation and control of samples before or after the neutron experiments, would help make better use of beamtime and raise the quality of scattering experiments. The PSCM would also enable the pooling of resources in data analysis and modelling. In conclusion, this new facility would create an attractive and stimulating atmosphere from which both external users as well as scientists on site would profit. The ILL Steering Committee meeting held one week after the SMUM, accepted the idea of a PSCM on the ESRF/ILL site.

As there was no autumn proposal round in 2005, due to the reactor shutdown during the Refit Programme, the number of proposals submitted in April 2006 for College 9 reached a record 99 proposals - a number demonstrating the importance and the need of neutron scattering techniques for the soft matter community.

Three highlights have been selected this year. Two of them illustrate the importance of *in situ* measurements and how 'soft' materials may re-arrange and form new structures upon external mechanical constraint (Förster *et al.*) or with time (Imperor-Clerc *et al.*). The third report (Eastoe *et al.*) shows how the surfactant molecules are sensitive to the solvent environment that can trigger the aggregation properties.

**Isabelle Grillo, College 9 Secretary**  
<http://www.ill.fr/Colleges/C9>



**Soft matter:** *In situ* shear-induced ordering of soft crystals (D11, p. 37).

## Biology

The major event in the scientific life of College 8 was the introduction, in spring 2006, of Block Allocation Group (BAG) proposals. The first BAGs were proposed in the fields of membrane proteins (MP BAG), of Complexes and Solvent Environment (CSE BAG) and of deuterated proteins (P BAG).

The aim of the BAGs is to promote scientific interactions and exchange between biologists interested in, but not necessarily familiar with the use of neutrons, and to enhance flexibility in the allocation of beamtime, thus optimising its use.

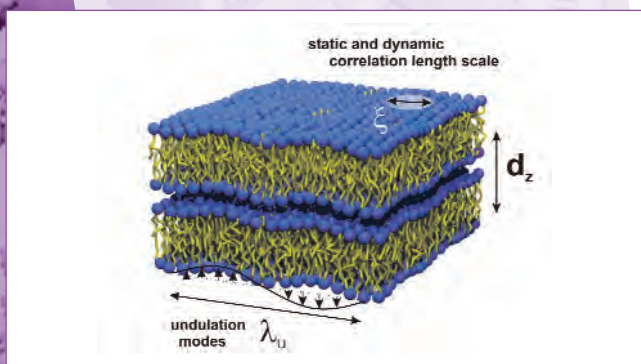
Initially, these proposals were put forward by internal members of the College. At the occasion of a BAG user meeting in May 2006, three external co-ordinators were named, and the beamtime was allocated giving priority to high-grade proposals, but also allowing for some short tests on less advanced, interesting systems. Beamtime was scheduled in blocks of 4 to 7 days at the beginning of every month, and the detailed time distribution was done at relatively short notice. This system was a full success with respect to flexibility, but requires improvements with respect to its administration and to the availability of the users to stay for longer periods of time.

Three scientific highlights were selected for this Annual Report. The first deals with an important structure, that of apolipoprotein B-100, the only protein found in low-density lipoprotein (LDL; 'bad cholesterol'). The structure of the detergent-solubilised protein could be obtained by SANS using contrast variation to render the detergent 'invisible' for neutrons. Thus, a structure of the whole lipoprotein particle could be proposed, whilst it is not amenable to a direct determination.

The second highlight describes how improvements in neutron instrumentation, sample preparation and environments allow one to study collective excitations and the role of water in the dynamics of membrane model systems, and to interpret their role in the physiological and biological function in these models with the aim to extrapolate this knowledge to real systems.

The third highlight of biological relevance, contributed by the Theory Group, explains pore stabilisation by packing.

**Roland May, College 8 Secretary**  
<http://www.ill.fr/Colleges/C8>



**Biology:** Structure of lipid bilayers (IN11, IN15 and IN10, p. 43).

## Liquids and glasses

Disordered systems, in particular liquids and glasses, exhibit complex behaviours. Proper understanding of these systems require a multidisciplinary approach - combining neutron experiments and computer simulations have provided deeper insight into properties of disordered systems.

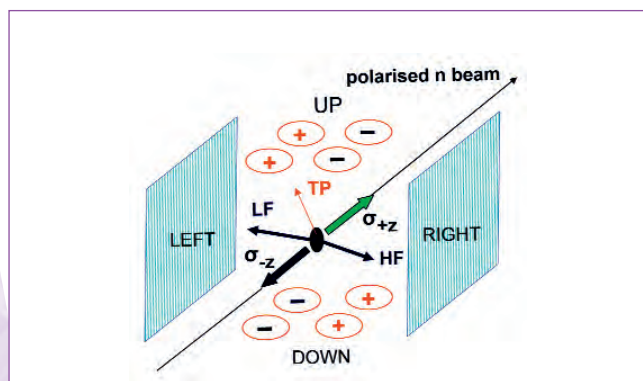
A good example of this development is the work by P. E. Mason *et al.* where neutron diffraction with isotopic substitution is combined with molecular dynamics simulation of aqueous solutions of D-glucose and D-xylose in order to extract a maximum of information about the structure of these systems. MDS were performed in order to understand the origin of the different peaks in the experimental radial correlation function making it possible to interpret the data in terms of specific correlations between pairs of individual atoms.

Another hot topic at present is the investigation of the effects of confinement on model systems. In this context, D. Morineau *et al.* show how both the structure and the dynamics of an archetype liquid crystal may exhibit enormous changes when the latter is confined in parallel channels in silicon wafers. Neutron diffraction data show a strong alteration of the phase diagram. Thus, they observe a depression of crystallisation on cooling and the formation of unstable crystalline phases, while the expected nematic-smectic transition is absent in the confined system. Measurements of molecular dynamics of the confined fluid by quasi-elastic neutron scattering also evidence an anomalous molecular mobility in the confined fluid as compared to the bulk.

**Claudia Mondelli, College 6 Secretary**  
<http://www.ill.fr/Colleges/C6>



**Liquids and glasses:** D-glucose sample (D4, p. 49).



**Nuclear and particle physics:** Fission of rotating nuclei (PF1B, p. 52).

## Nuclear and particle physics

The nuclear and particle physics group at the ILL maintains four instruments: PN1 'Lohengrin' - Fission product spectroscopy of exotic neutron rich nuclei; PN3 'GAMS' - Ultra-high precision measurements of gamma-rays emitted by nuclei after neutron capture; PF1B - High-intense (polarised) cold neutron facility; PF2 - Ultra-cold neutron (UCN) facility. The four instruments cover a broad range of physical phenomena in atomic, nuclear and particle physics and make use of the neutron as a tool for investigating the four known forces of Nature.

In the field of nuclear physics, two highlights were selected for this Annual Report: the discovery of a non-uniform rotation of the fission compound (in the reaction  $^{235}\text{U}(n,f)$ ) where rotating angles around  $0.1^\circ$  were observed in shifts of the angular distributions of the ternary alpha particles when flipping the spin of the neutrons (which induced the fission).

In another experiment, the precise energies and the lifetimes of the low-lying levels of  $^{150}\text{Sm}$  - a nucleus that is very close to the phase transition between spherical and quadrupole axial symmetry shapes - was studied.

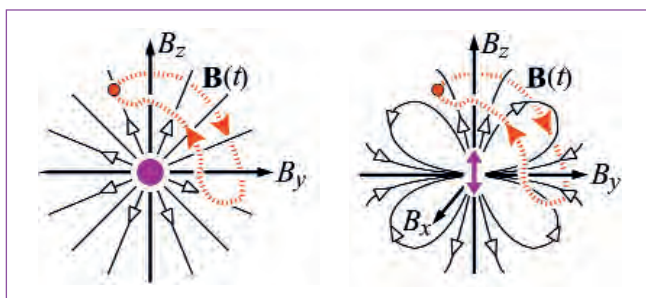
In particle physics, the neutron is used to test the Standard Model at low energies. The neutron decay is determined by three parameters at most and the precise measurement of these parameters sets limits on the existence of right-handed currents, on a deviation of the Cabibbo-Kobayashi-Maskawa matrix from unitarity, and on a violation of time reversal invariance. Closely connected to the latter is the search for an electric dipole moment, which is subject of ongoing research at the ILL.

Two important topics are highlighted: the recently installed spectrometer Perkeo III at PF1B aims to determine the parameters of the neutron decay with improved statistical and systematic error. The spectrometer benefits from the Perkeo principle of a  $2\times 2\pi$  solid-angle acceptance for the decay particles and a 10 times larger decay volume as in the past.

The precise value of the neutron lifetime is of fundamental importance to particle physics and cosmology. The present situation has become unsatisfactory as the lifetime result of a very recent UCN wall storage experiment differs by more than six standard deviations from the world average of 885.7(0.8) s. Magnetic storage of UCN is seen as a viable alternative to the former methods. The ongoing experiment of a Russian-French-German collaboration at PF2 - based on this technique - could help to solve the discrepancy in the near future.

**Christian Plonka, College 3 Secretary**

<http://www.ill.fr/nfp/npp/Home.htm>



*Spectroscopy, modelling techniques: the Berry phase (p. 63).*

## Spectroscopy, modelling and theory

In this year's annual report the papers on Spectroscopy, Modelling and Theory have been grouped together to underline the particularly strong advancement of combined experimental and theoretical studies in spectroscopy both in user groups and in ILL in-house science. Of the four papers in this section, two showcase the large mutual benefits of combining theory and experiments in spectroscopy. The following two papers from the ILL theory department show exciting progress in the theoretical analysis of spintronics and quantum computing.

Whereas many applications of nanotechnology, such as nanorobots, are still in the realms of science fiction, the creation of porous materials with nanometre sized pores is well advanced and they are used even in the ink of this document. For catalysis applications in particular, it would be a huge asset to know how liquid molecules actually move in these confinements. P. Fouquet and colleagues show how the potential energy surface between liquid molecules and the pore surface can be determined to an accuracy of a few meV - sufficient to map the weak interaction potential between benzene molecules and a graphite surface - by using neutron and helium spin-echo spectroscopy in combination with molecular dynamics simulations.

Skutterudites are very promising materials for ecological thermoelectric power generation, as they produce an electrical current when a temperature gradient is applied. A notorious problem in these materials is that one needs to maintain a high electrical conductivity while reducing as much as possible the thermal conductivity. M. Koza and colleagues eliminate, by combining neutron spectroscopy and numerical modelling, proposed models of localised rattling modes in filled skutterudites as the mechanism for the reduced thermal conductivity.

The first paper from the ILL theory group belongs to the realm of spintronics. Spin is the only internal degree of freedom of an electron and utilising it in new generations of semiconductor devices is nowadays the main technological challenge. Needless to say that exploiting spintronics is impossible without far-reaching fundamental research in this area. Whereas many important questions have been discussed rather extensively in the literature, there are only a handful of quantitative investigations. The work by G. Bouzerar and T. Ziman is in fact the first paper where recent, exciting, but puzzling observations of ferromagnetism in nominally non-magnetic semiconductors have been put on a firm theoretical basis.

R. Whitney's contribution is also motivated by promising applications of nano-systems to store information and quantum computing. However, the inevitable interactions of the nano-object with local environment, i.e. noise and decoherence, leaves their use still at a conceptual stage. The work presented in this section reaches the remarkable conclusion that noise itself has certain topologically stable characteristics, which can be disentangled from the properties of a quantum memory cell. Neutron experimentation conducted at the ILL this year by the user group from Vienna is an ideal tool to check this theoretical prediction.

**Peter Fouquet, College 7 Secretary**

<http://www.ill.fr/Colleges/C7/>

**Mark Johnson, Leader of Computing for Science**

<http://www.ill.fr/computing/club.html>

**Efim Kats, Head of Theory**

<http://www.ill.fr/Colleges/C2/TheoryCollegeHome.html>

# Observation of a Griffiths-like phase in the magnetocaloric compound $\text{Tb}_5\text{Si}_2\text{Ge}_2$

## Authors:

**C. Magen, P.A. Algarabel, L. Morellon and M.R. Ibarra** (ICMA, University of Zaragoza)  
**J.P. Araújo, A.M. Pereira and J.B. Sousa** (University of Porto)  
**C. Ritter** (ILL)

Within the so-called Griffiths model, a magnetic system in which a random distribution of the magnetic interactions is induced by disorder leads to a situation where different values of the exchange constant can be randomly assigned to the different sites of the lattice. In a certain temperature range above the ordering temperature  $T_C$ , the disordered system presents an intermediate regime, called the Griffiths phase, between the conventional paramagnetic phase and the ferromagnetic state characterised by a cluster-like state.

The rare-earth intermetallic system  $\text{Tb}_5(\text{Si}_x\text{Ge}_{1-x})_4$  was chosen as a serious candidate to host a Griffiths-like phase. The physical properties of these systems are strongly determined by their intrinsically layered crystallographic structure and the strong interplay between the magnetic and structural degrees of freedom. The crystal structure is conformed by the stacking of rigid two-dimensional layers (*slabs*) of Tb and T = Si/Ge atoms. The actual crystallographic phase and the nature of the magnetic interactions are controlled by the number of interlayer T-T covalent-like bonds connecting the slabs [1], as in these alloys two different magnetic interactions are playing part: the intralayer interaction ruled by the conventional 4f-4f RKKY indirect exchange, and the interlayer interactions, strongly influenced by an additional Tb-T-T-Tb superexchange-like interaction via the existing T-T bonds. Microscopic experimental evidence has been reported supporting that the intralayer magnetic structure is essentially ferromagnetic (FM), whereas the interlayer

coupling can be either FM or antiferromagnetic (AFM) [2]. In the case of  $\text{Tb}_5\text{Si}_2\text{Ge}_2$ , the high-temperature paramagnetic (PM) state crystallises in a monoclinic  $P112_1/a$

structure. On cooling, this compound experiences a second-order transition to an FM state at  $T_C = 110$  K, decoupled from the structural transformation to an

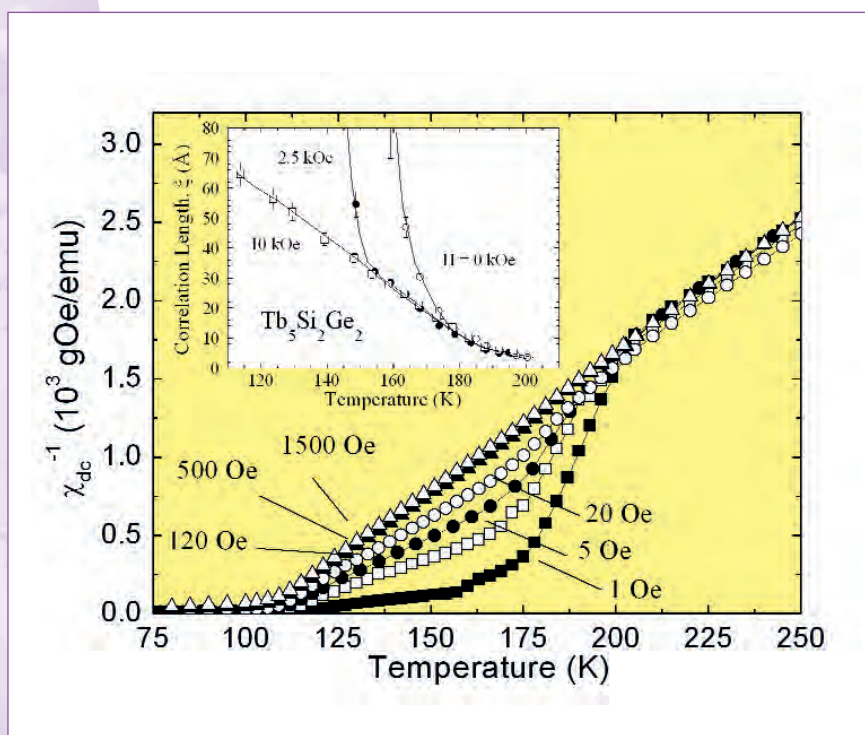


**Figure 1:** Temperature dependence of the inverse susceptibility ( $\chi^{-1}$ ) as a function of magnetic field, measured on heating. The inset shows the temperature and field dependence of  $\xi$  calculated from the Lorentzian fits of the SANS spectra.

orthorhombic Pnma phase taking place at  $T_t = 100$  K.

The existence of a Griffiths-like phase in  $Tb_5Si_2Ge_2$  in the form of an FM cluster system within a PM matrix, is firstly indicated by macroscopic magnetisation experiments. **Figure 1** presents the inverse dc magnetic susceptibility ( $\chi^{-1}$ ) as a function of temperature on heating in low magnetic fields. This picture clearly illustrates the anomalous behavior of  $\chi^{-1}$  that represents the fingerprint of a Griffiths phase [3]. In the conventional PM regime ( $T > 200$  K), the effective paramagnetic moment is  $9.8(1) \mu_B/Tb$ , which perfectly agrees with the theoretical value. However, below 200 K, a dramatic stair-like fall of  $\chi^{-1}$  is evident at very low fields ( $< 100$  Oe). On further increasing the magnetic field, only one plateau is observed, and the magnetic susceptibility at  $H \geq 500$  Oe becomes indistinguishable from the high-temperature values. It has been shown that the Griffiths phase is univocally characterised by a magnetic susceptibility exponent lower than unity, i.e.  $\chi^{-1} \propto (T-T_c)^{-\lambda}$ , where  $0 \leq \lambda \leq 1$  [4]. We have fitted the logarithmic representation of  $\chi^{-1}$  obtaining clearly different values for the exponent  $\lambda$  depending on whether we refine it in the anomalous region of  $\chi^{-1}$  ( $\lambda_G \cong 0.31$ ) or in the conventional PM phase ( $\lambda_{PM} \cong 0.064$ ).

The SANS instrument D16 is adequate to accurately probe the existence of FM clusters and characterise their size and temperature and magnetic-field evolution. The temperature dependence on cooling of the SANS intensity as a function of magnetic field, and at  $Q = 0.1 \text{ \AA}^{-1}$ , which is a typical intermediate value in the range of transferred momentum within the resolution of the instrument, is shown in **figure 2**. First, a remarkable increase of the SANS signal is observed from 200 to 175 K, this step being followed by a small plateau that extends down to  $\sim 150$  K. This anomalous contribution in the temperature range 150–200 K could be related with the nucleation of FM clusters within the PM region of  $Tb_5Si_2Ge_2$ . Below  $T \approx 150$  K, a huge increase of the signal is found associated with a strong rise of magnetic correlations in the vicinity of the Curie temperature of a second-order FM transition. A double peak is seen, at  $T_c = 115$  K and

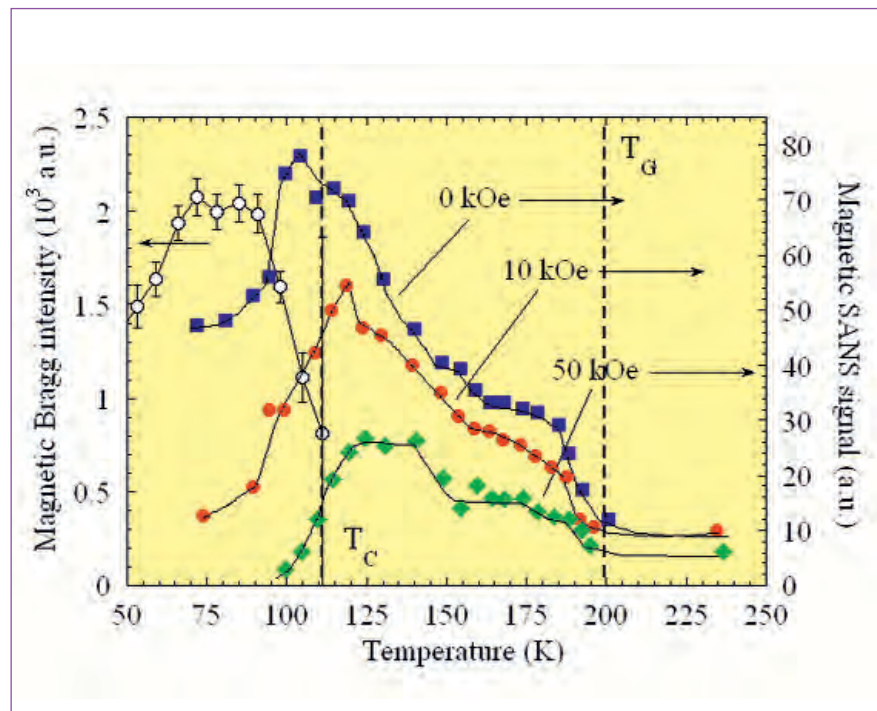


**Figure 2:** Temperature dependence of the magnetic SANS intensity collected in D16 at  $Q = 0.1 \text{ \AA}^{-1}$  in different magnetic fields (filled symbols), in comparison with the intensity of a magnetic Bragg peak (empty symbols). The region in which magnetic SANS signal exists, corresponds to the Griffiths-like phase.

$T_1 = 105$  K, which is associated with the decoupled magnetic-crystallographic transformation. Upon application of a magnetic field, the decrease of the SANS intensity in the whole temperature range is considerable. The correlation length ( $\xi$ ) extracted from the Lorentzian fits of the SANS spectra as a function of temperature and in different magnetic fields (see inset in figure 1) is the final proof of the existence of the FM cluster distribution that characterises the Griffiths-like phase. In zero-field, sizeable correlation lengths ( $\sim 5 \text{ \AA}$ ) are found around 200 K, its size progressively increasing up to a maximum at around  $T \approx 165$  K, where the cluster size rises beyond the experimental resolution of the instrument. SANS experiments demonstrate the existence of FM clusters within the monoclinic PM phase of  $Tb_5Si_2Ge_2$ , which characterise a Griffiths-like phase in the temperature range  $T_c < T < 200$  K. It is suggested [5] that the Griffiths-like phase originates from the intrinsic disorder within the crystallographic structure, and the competition of the

intra- and interlayer magnetic interactions ruling the microscopic behaviour of the naturally-layered structure, both factors promoting the segregation of nanometric regions with stronger FM interactions.

## References

- (1) W. Choe et al., *Phys. Rev. Lett.* **84** (2000) 4617
- (2) V.K. Pecharsky and K.A. Gschneidner, Jr., *Adv. Mater.* **13** (2001) 683
- (3) B. Salamon, P. Lin and S.H. Chun, *Phys. Rev. Lett.* **88** (2002) 197203
- (4) H. Castro Neto, G. Castilla and B.A. Jones, *Phys. Rev. Lett.* **81** (1998) 3531
- (5) C. Magen, P.A. Algarabel, L. Morellon, J.P. Araújo, C. Ritter, M.R. Ibarra, A.M. Pereira and J.B. Sousa, *Phys. Rev. Lett.* **96** (2006) 167201

# Determination of a non-collinear magnetic structure for $GdB_4$ using spherical neutron polarimetry

## Authors:

**J.A. Blanco and J. Fernandez-Rodríguez**

(University of Oviedo)

**P.J. Brown and A. Stunault** (ILL)

**K. Katsumata** (RIKEN Harima Institute, Hyogo)

**S.W. Lovesey** (RIKEN Harima Institute, Hyogo and ISIS Facility, Didcot)

**F. Iga and S. Michimura** (Hiroshima University)

Interest in the antiferromagnetic order of Gd ions in  $GdB_4$  was stimulated by results from resonant X-ray Bragg diffraction, enhanced at the  $GdL_3$  edge, in which anisotropic charge and magnetic scattering amplitudes interfere [1]. However, one could not distinguish between allowed collinear or non-collinear Gd configurations from X-ray diffraction results. The ambiguity has been fully resolved using spherical neutron polarimetry, which shows that the full tetragonal symmetry is preserved in the antiferromagnetic phase.

$GdB_4$  crystallises at room temperature in the tetragonal space group  $P4/mbm$  and orders antiferromagnetically below  $T_N=42$  K. The structure of the antiferromagnetic (AF) phase was originally inferred from susceptibility measurements on a single crystal since a neutron diffraction study is made extremely difficult by the high neutron absorption cross sections of natural Gd and B. Susceptibility measurements have shown that  $GdB_4$  orders antiferromagnetically below 42 K. The same measurements also give indirect information of the configuration of magnetic moments in  $GdB_4$ , indicating that the magnetic moments lie in the  $ab$  plane of the tetragonal unit cell [2]. More recently, magnetic X-ray scattering experiments have indicated a structure with zero propagation vector in which Gd atoms related by the centre of symmetry (1 & 2 and 3 & 4 in **figure 1**) have oppositely directed magnetic moments [1]. Some controversy has however arisen about the collinear (**figure 1**) or non-collinear (**figure 2**) character of this magnetic structure [1, 3].

With unpolarised neutrons it is very difficult to distinguish a non-collinear arrangement of moments from a collinear structure in which the crystal contains domains orientated at  $90^\circ$ , as the neutron reflection intensities predicted for the two models are almost identical. Spherical polarimetry [4] can readily confirm the correct model since the mixed domain model will give rise to characteristic depolarisation of the scattered neutrons.

For neutron diffraction experiments, two  $^{11}B$  enriched  $GdB_4$  single crystals were prepared, in the form of  $2 \times 2 \times 10$  mm<sup>3</sup> pillars, elongated parallel to [001] and the [010] directions, respectively. The neutron diffraction experiments were performed on the D3 diffractometer, at a short wavelength ( $\lambda = 0.545$  Å) to minimise the absorption, using CRYOPAD for spherical neutron polarimetry.

The polarisation matrices measured in the AF ordered phase at 2 K were all diagonal within experimental error. This shows that the crystal contains almost equal volumes of the two possible  $180^\circ$  domains. They also show clearly that for the (h0l) reflections, those with  $h = \text{odd}$  have magnetic interaction vectors lying in the (010) plane, whereas those of the  $h = \text{even}$  reflections are parallel to [010]. Since the magnetic structure factors of the  $h = \text{even}$  reflections depend on the vector sum of the moments

on the pairs of atoms 1 & 2 and 3 & 4, whilst those of the  $h = \text{odd}$  ones depend on their difference, this observation rules out all collinear models.

The polarisation matrices measured for the (hk0) reflections confirm that all the moments are in the (001) plane. Furthermore, they show that there is no

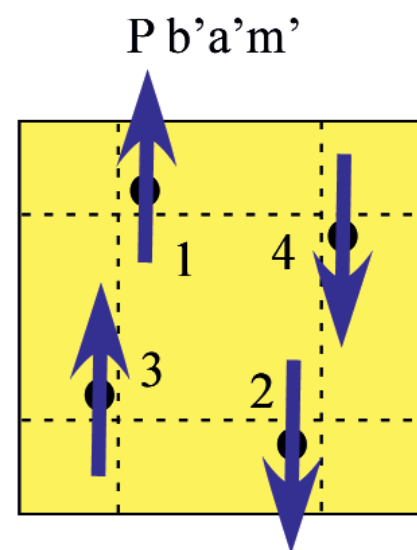


**Figure 1:** Collinear magnetic structure of the  $GdB_4$  on the  $ab$  plane with magnetic space group  $Pb' a' m'$ . It is worth noting that the atoms with antiparallel magnetic moments are related by inversion and time reversal symmetries.

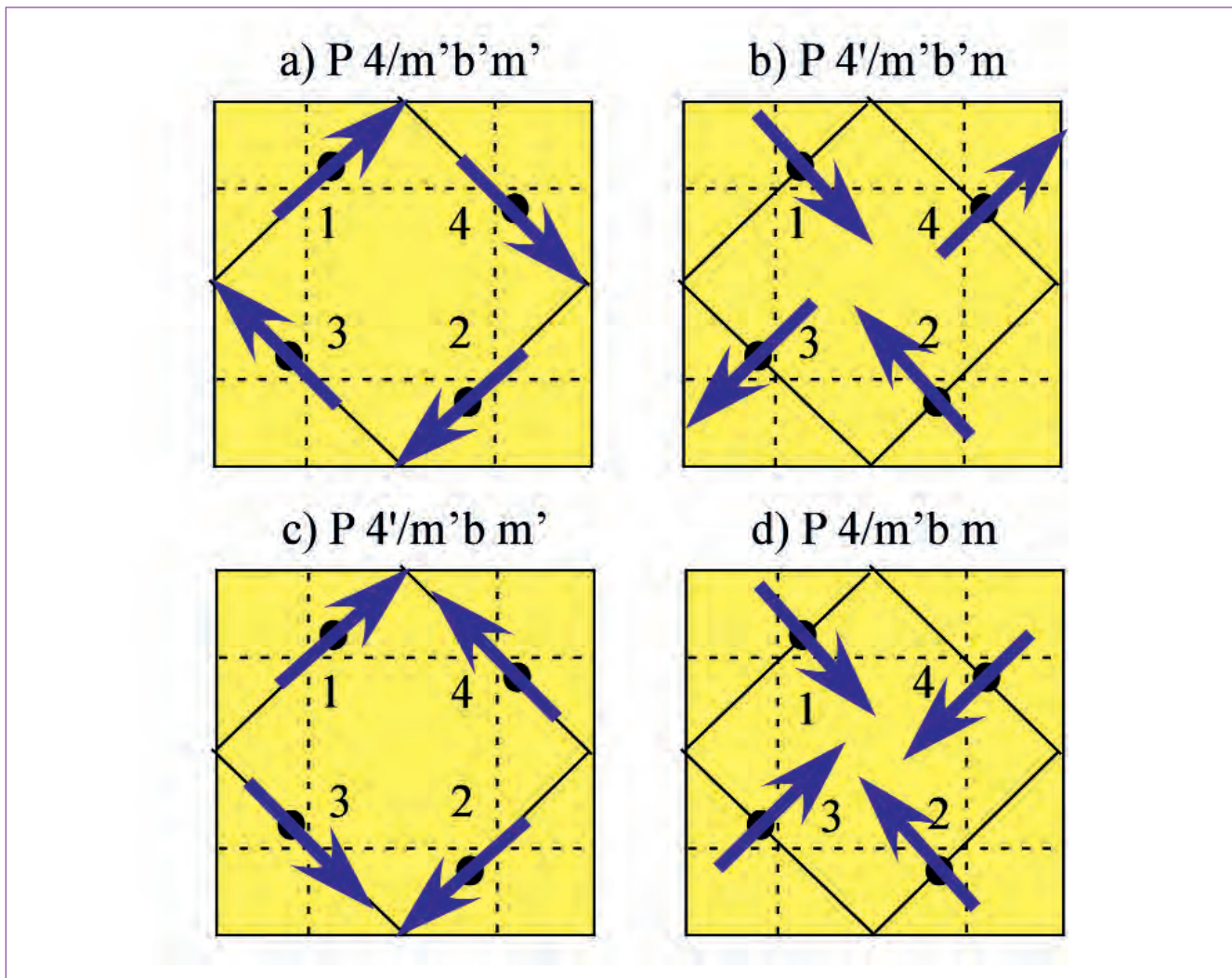


**Figure 2:** Non-collinear magnetic structures of the  $GdB_4$  with magnetic tetragonal space groups. It is worth noting that the atoms with antiparallel magnetic moments are related by inversion and time reversal symmetries.

magnetic scattering in the  $(hh0)$  reflections which implies that their magnetic structure factors are either zero or parallel (or antiparallel) to the scattering vector  $[110]$  giving a zero interaction vector.

A non-collinear structure would allow both reflections  $(hh0)$  and  $(h\bar{h}0)$  to have systematically zero magnetic interaction vectors. Taking into account the results for the  $(hh0)$  and  $(h0l)$  reflections, there is only one possible configuration for the magnetic structure of  $GdB_4$ : the magnetic space group is  $P4/m'b'm'$  with the Gd magnetic moments lying in the  $ab$ -plane of the tetragonal unit cell and parallel to the 4 different  $\langle 110 \rangle$  axes (**figure 2a**) [2].

A least square refinement of this structure was carried out using the diagonal elements of the polarisation matrices as data. The only free-parameter to be refined was  $|\vec{M}|$ , the modulus of the magnetic moment. The result obtained using scattering lengths  $Gd\ b = 12\ \text{fm}$  and  $^{11}B\ b = 6.65\ \text{fm}$  was  $|\vec{M}| = 7.14\ (0.17)\ \mu_B$ , with a goodness of fit  $\chi^2 = 3.8$ . Isotropic exchange interactions up to the first three nearest neighbours are unable to account for the observed magnetic arrangement.

Further research will be devoted to the exploration of the origin of the magnetic anisotropy needed to stabilise this non-collinear magnetic structure in  $GdB_4$ .

## References

- (1) S. Ji et al., *Phys. Rev. Lett.* 91 (2003) 257205
- (2) Z. Fisk et al., *Solid State Commun.* 39 (1981) 861; J. Fernandez-Rodriguez, *Phys. Rev. B* 72 (2005) 052407
- (3) J.A. Blanco et al., *Phys. Rev. B* 73 (2006) 212411
- (4) see e.g. P.J. Brown et al., *Proc. R. Soc. London, Ser. A* 442 (1993) 147; P. J. Brown et al., *Physica B* 267-268 (1999), 215

# Probing magnetisation dynamics in quantum systems

## Authors:

**E. Blackburn** (ILL and EC, JRC-ITU)

**A. Hiess and P. Fouquet** (ILL)

**N. Bernhoeft** (CEA-Grenoble)

**M.C. Rheinsadtler**

(University of Missouri, Columbia)

**W. Haussler** (TU Munich, Garching)

**G.H. Lander** (EC, JRC-ITU)

Fluctuations involving magnetic spins have been predicted to be responsible for the pairing mechanism for many unconventional superconductors, but a direct proof has remained elusive. Since neutrons can sense such fluctuations and their momentum dependence, they provide a unique probe. We have used the neutron spin-echo technique to extend the energy resolution available and look for fluctuations at very low temperatures.

One of the most favoured candidates for a magnetically mediated superconductor is  $\text{UPd}_2\text{Al}_3$ . The uranium atoms carry the magnetisation, presumably through the three 5f electrons, and the compound has an enhanced Sommerfeld coefficient  $\gamma = 150 \text{ mJ/mol K}^2$ , indicating a high electronic density of states near the Fermi level. It orders antiferromagnetically at  $T_N = 14 \text{ K}$  with almost  $1 \mu_B$  per uranium atom and a propagation vector  $Q_0 = (0 \ 0 \ 1/2)$ , and then becomes superconducting at  $T_{sc} \sim 2 \text{ K}$  whilst remaining antiferromagnetic. The magnetic excitation spectrum as investigated by three-axis spectroscopy (TAS) is structured in energy and momentum space. The experimental results were recently reviewed [1] and the magnetic response in the antiferromagnetic state at the zone centre  $Q_0$  as a function of temperature is shown in **figure 1**. Quasi-elastic scattering is experimentally observed at all temperatures above  $T_{sc}$  e.g. in the normal antiferromagnetically ordered state. Most interestingly, when the sample is superconducting at low temperatures, neutron scattering reveals the

appearance of an excitation with a gap of about  $0.4 \text{ meV}$  ( $\sim 3 k_B T_{sc}$ ) at the antiferromagnetic wavevector  $Q_0$  only. This excitation is thought to reflect the superconducting gap translational symmetry.

Neutron studies show that the dynamic magnetic response is intimately connected to the superconducting state. Two different mechanisms have been developed for the electronic behaviour; they differ in their treatment of the low-temperature magnetic fluctuations. In the fully itinerant model [2], all of the 5f electrons participate in the itinerant electron system responsible for the antiferromagnetic fluctuations and in the development of the superconductivity. In the superconducting state (most of) the 5f Fermi surface should be gapped and hence no (significant) quasielastic scattering should persist well below  $T_{sc}$ . In the dual model [3], only one of the three 5f electrons per uranium atom is itinerant and participates in the superconductivity, coupling to excitations generated by the remaining two localised 5f electrons. Fluctuations from the localised (crystal-field) states should exist at the lowest temperatures.

Unfortunately, as shown in **figure 1**, due to the TAS instrumental resolution, incoherent scattering and the low-energy inelastic excitations mask the region of interest for any such quasielastic scattering.

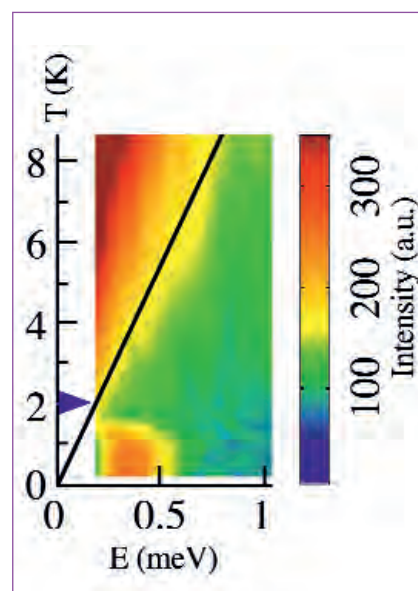
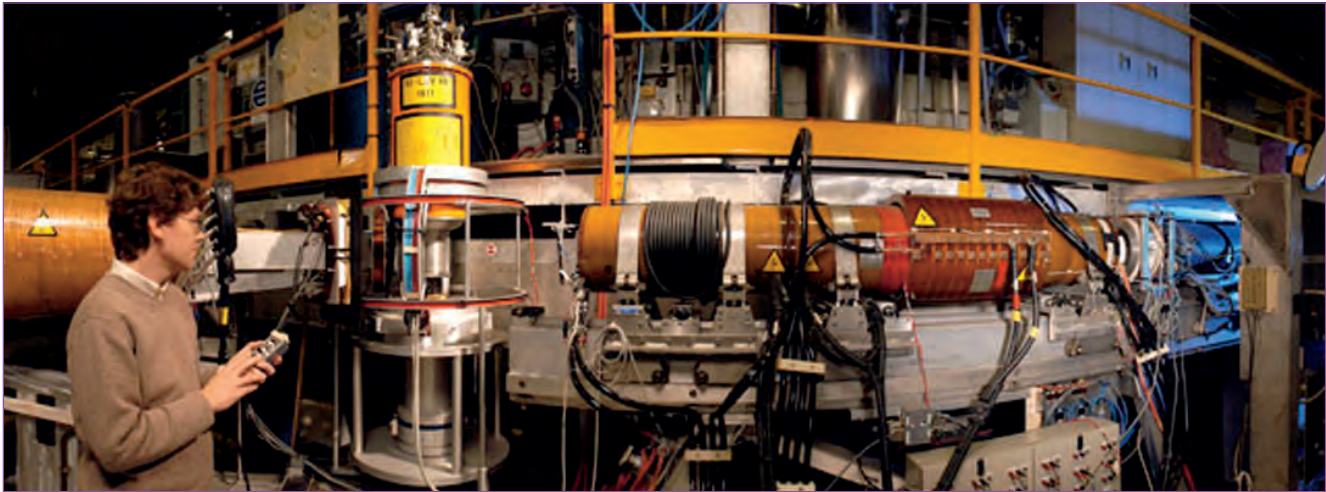


**Figure 1:** Contour plot of the magnetic dynamic response at the position  $Q_0 = (0 \ 0 \ 1/2)$  as a function of energy and temperature measured on the cold neutron three-axis spectrometer IN14. The superconducting transition temperature  $T_{sc}$  is marked by a blue arrow and the solid line gives the relationship  $E = k_B T$ . Notice first how the energy scale of quasielastic scattering intensity decreases and is obscured by the spectrometer resolution (white area) at low temperature. Secondly, below  $T_{sc}$  an inelastic scattering peak at  $0.4 \text{ meV}$  unique to the superconducting phase appears at this position of  $Q$ , which is related to the symmetry of the superconducting order parameter (1).



Peter Fouquet setting-up the spin-echo spectrometer IN11.

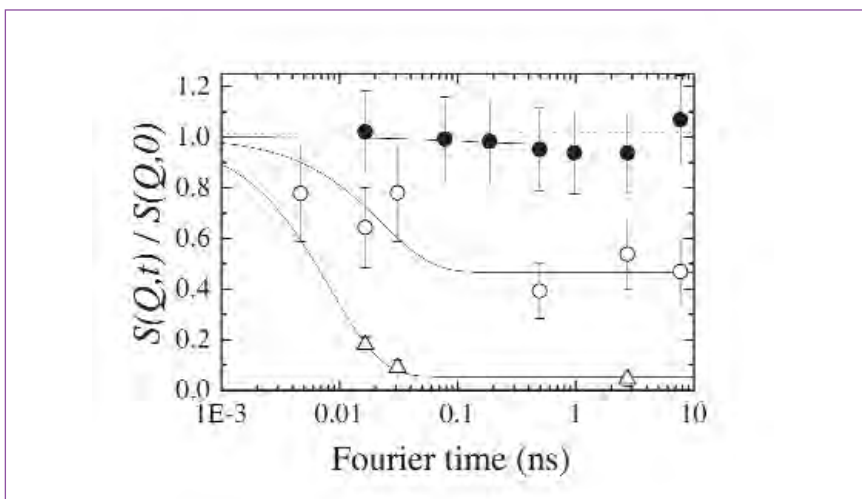


**Figure 2:** Momentum and time-dependent intermediate scattering function  $S(Q,t)$  normalised to  $S(Q,0)$  at 50 mK (solid circles), 2 K (open circles), and 15 K (solid triangles) measured on the spin-echo spectrometer IN11. The black lines are simple exponential fits. The gray lines are possible extremal decay curves at 2 K, illustrating the uncertainty at this temperature. The dash-dotted gray line is a numerical calculation of the predicted quasielastic response with (full width at half maximum) = 30  $\mu\text{eV}$  (4).

In order to enhance the resolution, we turned to neutron spin-echo (NSE) spectroscopy, using a single crystal to provide the necessary Q resolution. In the NSE technique the neutron time-of-flight is encoded in the precession of the neutron spins; changes due to small energy transfers to/from the sample can be matched and measured very precisely, to the order of 15 neV in certain cases, although for our experiment on IN11, the resolution was  $\sim 30 \mu\text{eV}$ . The magnetic dynamic response is strongest close to  $Q_0$ . However, to exploit the NSE resolution, the measurements

must be displaced slightly in Q to avoid elastic scattering from the Bragg peak, but close enough to  $Q_0$  to pick up any quasielastic response. The scattering wavevector  $Q' = (0.015 \ 0 \ 1/2)$  was found to offer the best compromise. As shown in **figure 2**, the scattering function clearly relaxes with time  $t$  at 2 K and 15 K, as inferred from the TAS energy width. At 15 K, there is  $\sim 8$  times more dynamic scattering than at 2 K. In the superconducting state at 50 mK, the data suggest a constant ratio  $S(Q', t)/S(Q', 0) = 1$ , indicating that the scattering is

purely static over the measured time window. This may be quantified to give a maximum fluctuation spectrum extending less than  $\sim 30 \mu\text{eV}$  around zero energy. From the absence of observed quasielastic response [4], the itinerant model is strongly favoured over the dual model.

The experimental and theoretical challenges encountered in using a single crystal and interpreting the data, are of major interest for further NSE investigations of the low-energy dynamical response at lowest temperatures. An example of current interest would be the low energy response in quantum phase transitions. Many other techniques, e.g. NMR and specific heat, already play a role in the study of such phase transitions; now neutrons, with their polarisation, energy and wave-vector selectivity, can be added to the arsenal of investigative techniques.

## References

- (1) A. Hiess et al., *J. Phys. Condens. Matter* 18 (2006) R437
- (2) K. Knöpfle et al., *J. Phys. Condens. Matter* 8 (1996) 901
- (3) N.K. Sato et al., *Nature* 410 (2001) 340
- (4) E. Blackburn et al. *Phys. Rev. Lett.* 97 (2006) 057002

# Direct observation of quadrupolar excitons in the filled skutterudite superconductor $\text{PrOs}_4\text{Sb}_{12}$

## Authors:

**K. Kuwahara, M. Kohgi, Y. Aoki and H. Sato** (Tokyo Metropolitan University)  
**K. Iwasa** (Tohoku University)  
**K. Kaneko and N. Metoki** (Japan Atomic Energy Agency, Tokai)  
**S. Raymond, M.-A. Méasson and J. Flouquet** (CEA-Grenoble)  
**H. Sugawara** (Tokushima University)

Low-energy magnetic excitations in single crystals of the filled skutterudite superconductor  $\text{PrOs}_4\text{Sb}_{12}$  have been studied by inelastic neutron scattering. The clear softening of the excitations at the wave vector  $Q = (1,0,0)$ , which is the same as the modulation vector of the field-induced antiferro-quadrupolar ordering, and the intensity analysis of the excitations directly evidence that the non-magnetic quadrupolar fluctuations are dominant in this system. Furthermore, the narrowing of the linewidths of the excitations in the superconducting phase indicates the close connection between the superconductivity and the excitations.

The relation between magnetism and superconductivity in strongly correlated electron systems is one of the most interesting research areas in condensed matter physics. Magnetic fluctuations, due to strong Coulomb repulsion and hybridisation between  $f$  electrons and conduction electrons, are believed to be at the origin of both the heavy-fermion behaviour and superconductivity. In general, however,  $f$  electrons in systems with high lattice symmetry also have non-magnetic quadrupolar degrees of freedom that can interact with conduction electrons through the orbital channels. Therefore, the non-magnetic quadrupolar fluctuations might also lead to new types of superconductivity.

The filled skutterudite compounds  $\text{RT}_4\text{X}_{12}$  (R: rare earth or actinide, T: transition metal, X: pnictogen) crystallise in the body-centered cubic space group  $Im\bar{3}$ , in which the R ion is surrounded by a cage of 12 X, as shown in **figure 1**.

These compounds show a wide variety of thermal, magnetic and transport properties due to a strong hybridisation and a rattling motion of the R ions resulting from their position at the center of a pnictogen cage [1]. Among them,  $\text{PrOs}_4\text{Sb}_{12}$  is the only Pr-based skutterudite material being both

heavy-fermion and superconductor with a superconducting transition temperature  $T_c = 1.85$  K [2]. The large specific heat jump at  $T_c$  suggests that heavy quasiparticles participate in the superconductivity. The occurrence of a field-induced antiferro-quadrupolar ordering near the supercon-

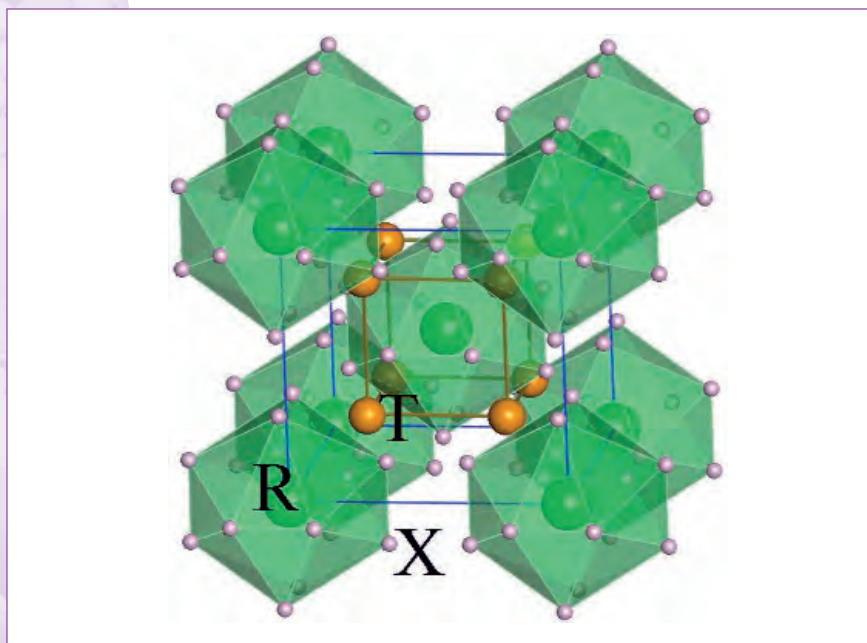


**Figure 1:** The crystal structure of the filled skutterudite  $\text{RT}_4\text{X}_{12}$ .

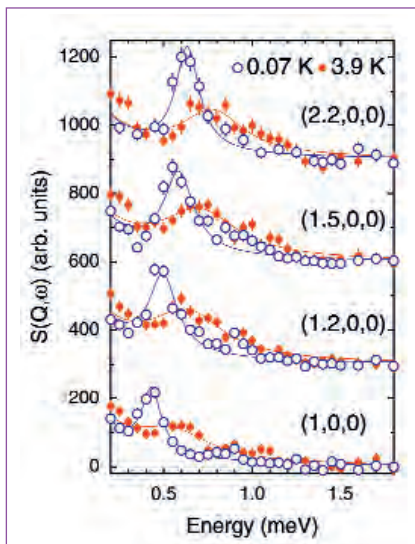


**Figure 2:** Energy spectra of the excitations in  $\text{PrOs}_4\text{Sb}_{12}$  with different  $Q$  vectors along the  $(1, 0, 0)$  direction at 0.07 K and 3.9 K.

ducting phase may naturally suggest that the heavy-fermion superconductivity is mediated by quadrupolar fluctuations [3]. Under the cubic crystal field, the  $4f$  electrons are well-localised. This is directly evidenced by inelastic neutron scattering experiments which show clear crystal field excitations [2, 4–7]. The energy gap between the singlet ground state and the triplet first excited state is 0.7 meV and other excited states are located at much larger energy above 10 meV. Focusing on the low-lying singlet-triplet excitations, we have performed high-resolution inelastic neutron scattering experiments on single crystals of  $\text{PrOs}_4\text{Sb}_{12}$  using the cold neutron three-axis spectrometers IN12 and IN14 located at the ILL.

**Figure 2** shows the dynamic structure factor  $S(Q, \omega)$  of  $\text{PrOs}_4\text{Sb}_{12}$  with different  $Q$  vectors along the  $(1, 0, 0)$  direction at the lowest temperature 0.07 K and at 3.9 K. The peaks around 0.4–0.8 meV correspond to the singlet-triplet transition. In both the normal and superconducting states, the energy of the excitations monotonically softens from the zone center to the zone boundary  $Q = (1, 0, 0)$ , corresponding to the field-induced antiferro-quadrupolar ordering wave-vector. This clear softening of the excitations at the zone boundary suggests that the crystal field states are modulated by



The three-axis spectrometer IN14.

intersite interactions and that some fluctuations are stronger at the zone boundary. If these interactions were magnetic in origin (magnetic excitons), the intensity of the excitation should be the strongest around the  $Q$  regions where the exciton energy is the weakest. However, the observed  $Q$  dependence of the excitation intensity is precisely reversed as shown in **figure 2** and thus does not correspond to this classical picture for magnetic excitons. This result provides direct evidence that the observed excitonic behaviour arises mainly from nonmagnetic quadrupolar interactions [8]. Within our knowledge, the excitation spectrum of  $\text{PrOs}_4\text{Sb}_{12}$  provides the first example of excitons due to quadrupolar interactions.

We also observed strong temperature dependence of the excitation spectra with a uniform softening of the singlet-triplet transition for all  $Q$  vectors with decreasing temperature. It is not clear whether the energy of the excitations decreases gradually or decreases with a distinct anomaly at  $T_c$ . On the other hand, the linewidths of the excitations exhibit a discontinuous decrease just below  $T_c$  as measured for  $Q = (1, 0, 0)$  [7], suggesting the close connection between the quadrupolar excitons and the superconductivity. This result is consistent with the exciton-based superconductivity theory which predicts that the life-time of excitons gets longer below  $T_c$  [9].

In summary, the observed low-energy excitations of  $\text{PrOs}_4\text{Sb}_{12}$  directly evidence that the non-magnetic quadrupolar fluctuations are dominant in this system. Furthermore, the temperature dependence of the excitations suggests that they are strongly connected to the heavy-fermion superconductivity.

## References

- (1) H. Sato et al., *International Conference on Magnetism, Kyoto, Japan, 2006 (PHYSICA B, in press)*
- (2) M.B. Maple et al., *J. Phys. Soc. Jpn.* 71 Suppl. (2002) 23
- (3) M. Kohgi et al., *J. Phys. Soc. Jpn.* 72 (2003) 1002
- (4) K. Kuwahara et al., *J. Phys. Soc. Jpn.* 73 (2004) 1438
- (5) E.A. Goremychkin et al., *Phys. Rev. Lett.* 93 (2004) 157003
- (6) S. Raymond et al., *Physica B* 359-361 (2005) 898-900
- (7) K. Kuwahara et al., *Phys. Rev. Lett.* 95 (2005) 107003
- (8) R. Shiina et al., *J. Phys. Soc. Jpn.* 73 (2004) 3453
- (9) M. Matsumoto and M. Koga, *J. Phys. Soc. Jpn.* 73 (2004) 1135

# Lattice vibrations drive relaxation in a highly frustrated magnet

## Authors:

**C. Payen** (Institut des Matériaux Jean Rouxel, Nantes)

**P. Mendels and D. Bono** (CNRS/LPS, Orsay)

**G. Ehlers** (SNS, Oak Ridge)

**H. Muika, P. Fouquet and J.R. Stewart** (ILL)

Very peculiar low-temperature properties of Kagomé bilayer compounds, such as  $\text{SrCr}_{9x}\text{Ga}_{12-9x}\text{O}_{19}$  (SCGO), highlight the fascinating physics of frustrated magnets. In spite of extensive studies using low-energy probes such as NMR,  $\mu\text{SR}$  and neutron backscattering spectroscopy, the dynamic response has been a persisting puzzle for theory and experiment. Neutron Spin-Echo (NSE) experiments have allowed the characterisation of the very short-ranged correlations and extremely slow, 'frozen' (elastic-like) response of part of the magnetic moment. The observation of a new feature - a phonon-assisted relaxation regime - in the SCGO compound, indicates that spin-lattice coupling is of importance in this frustrated magnet.

Geometric frustration in magnetic compounds [1,2] leads to many exotic phenomena. The incompatibility between local interactions and lattice symmetry induces a macroscopic degeneracy that often prevents long-range order while slow dynamics and freezing can occur at low temperatures. The energy scales associated with these features can fall orders of magnitude below the one of the dominating magnetic interactions and one can expect that other than purely magnetic degrees of freedom can influence the low-temperature properties as well as the selection of the ground-state, associated with the lifting of the degeneracy characteristic of frustrated magnets. In this context the role of spin-lattice coupling has recently received increased attention.

The pyrochlore slab compounds, also known as Kagomé bilayers, have triggered a vast amount of research since the discovery of the particular properties of  $\text{SrCr}_{9x}\text{Ga}_{12-9x}\text{O}_{19}$

(SCGO) in the late 80's and early 90's and later of  $\text{Ba}_2\text{Sn}_2\text{ZnCr}_{7x}\text{Ga}_{10-7x}\text{O}_{22}$  (BSZCGO) with similar trends. The static bulk susceptibility and high-temperature dynamics of both SCGO and BSZCGO are consistent with an antiferromagnetic exchange of  $J \approx 5$  meV between nearest neighbour  $\text{Cr}^{3+}$  ( $S=3/2$ ) ions that form a network of corner-

sharing tetrahedra. The absence of long-range order down to mK temperatures points out the strong geometrical frustration that governs the physics of these compounds. Associated with a spin-glass like freezing (at about  $T_g \approx 4$  K in SCGO and  $T_g \approx 1$  K for BSZCGO), an elastic-like neutron response appears as a broad hump

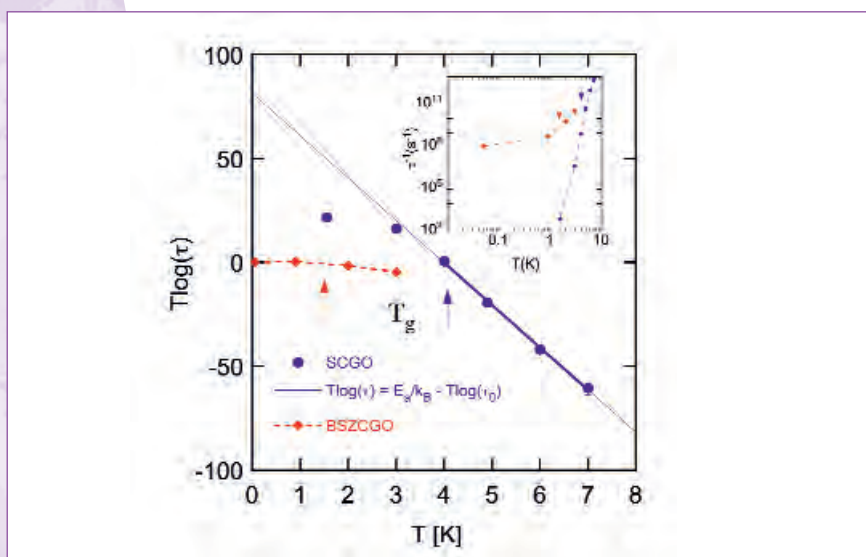


**Figure 1:** The temperature dependence of the NSE-determined relaxation rate shown as  $T\log(\tau)$  versus  $T$  for SCGO and BSZCGO. The arrows indicate the macroscopic freezing temperatures. The solid line is a fit to the SCGO data (for  $T > 4$  K) with a thermally activated law. The insert shows  $1/\tau$  vs.  $T$  on a log-log scale, highlighting the distinctly faster relaxation in the BSZCGO system. In both compounds the low  $T$  plateau indicates the establishment of a quantum regime [3].

with a  $Q$ -dependence characteristic of anti-ferromagnetic correlations limited to nearest neighbours, suggesting the existence of local clusters with essentially vanishing total moment. The neutron spin-echo (NSE) method, selective to magnetic excitations due to the use of polarised neutrons, and inherently sensitive to slow dynamics, is an ideal tool for the investigation of the low-temperature spin dynamics of these systems. We have used the IN11 NSE instrument to examine the temperature dependence of the magnetic response [3]. **Figure 1** shows the relaxation time  $\tau(T)$  plotted as  $T \log(\tau(T))$  versus  $T$ . For SCGO this plot shows a linear part indicating a thermally activated regime in which  $\tau(T) = \tau_0 \exp(E_a/(k_B T))$ , with  $E_a/k_B = 80 \pm 5$  K. In the temperature range just above the macroscopic freezing the relaxation occurs by overcoming a rather well defined energy barrier. This energy barrier cannot be associated with a particular excited state of magnetic origin since the magnetic response is totally featureless in the energy range corresponding to the observed activation energy. However, we found evidence of a phonon response at this energy both with neutron and Raman spectroscopy (see **figure 2**).

Our NSE results provide new insight into the puzzling low-temperature behaviour of the kagomé bilayer compounds and distinguish these materials with respect to usual spin-glasses. At the approach to the macroscopic spin-glass-like 'freezing', the spin fluctuations are accompanied by a slow response of part of the magnetic moments, with characteristic energy in the neV to  $\mu$ eV range. Unlike a standard spin-glass [4] the response does not show any critical divergence of the relaxation time at the apparent freezing temperature. A distinct new feature highlighted in SCGO is the slowing down regime above  $T_g$  in which the magnetic relaxation proceeds through a thermally activated process assisted by phonons with a well-defined energy. The  $Q$ -dependence of the magnetic response indicates that the relaxation must involve rearrangements of spins in local 'molecular' units that have essentially zero total moment and close to degenerate low lying energy levels. The specific vibrational mode observed by neutron and Raman spectroscopy influences the magnetic interactions and, in consequence, the energy levels in the clusters. Work in progress, in collaboration with the Scientific Computing group at the ILL

(M. Johnson and M. Zbiri) using *ab-initio* interatomic force field calculation of the phonon response, in association with more detailed neutron and Raman studies of the phonon density of states, will contribute to further microscopic understanding of these phenomena and the system-dependent features that distinguish SCGO and BSZCGO.



The wide-angle secondary coil/detector of IN11 is essential for the successful investigation of the low-energy magnetic response of frustrated magnets.

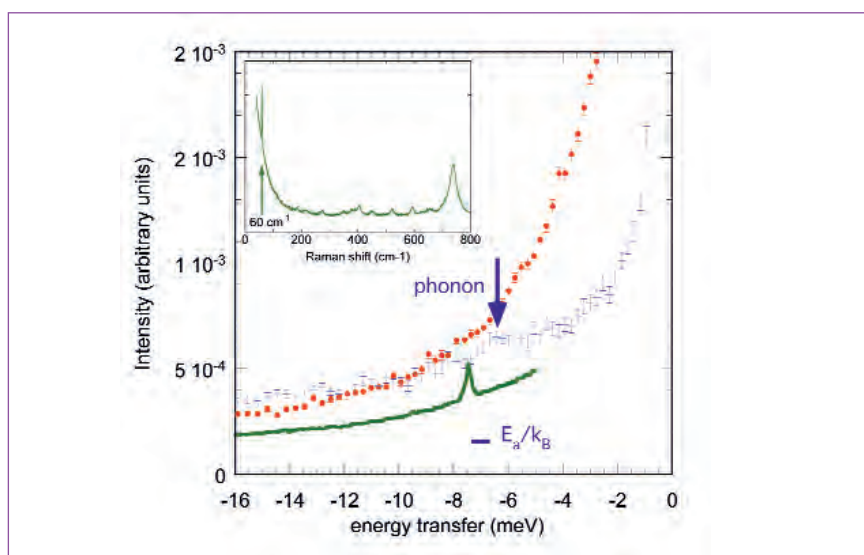


**Figure 2:** Neutron and Raman spectroscopy at room temperature show in SCGO a phonon mode at an energy of 7 meV ( $60 \text{ cm}^{-1}$ ). The inset shows the full Raman spectrum and the low-energy part has been converted and re-plotted for comparison with the neutron energy gain data obtained with the IN4 ToF spectrometer. Blue and red symbols correspond to the higher and the lower  $Q$ -range neutron data, dominated respectively by phonon and magnetic response [3].

## References

- (1) for reviews see e.g. A.P. Ramirez, *Handbook of magnetic materials*, vol 13 (2001) p. 318 and R. Moessner, *Can. J. of Phys.* 79 (2001) 1283
- (2) for additional insight see R. Moessner, A.P. Ramirez, *Physics Today* 59 (2006) 24
- (3) a full account is given in H. Mutka et al. *Phys. Rev. Lett.* 97 (2006) 047203 and *J. Phys: Condens. Matter*, in press
- (4) K. Pappas et al., *Phys. Rev B* 68 (2003) 054431

# Magnetic order in exchange bias patterns in a continuous film

## Authors:

**K. Theis-Bröhl, M. Wolff and H. Zabel**

(Ruhr-University Bochum)

**B.P. Toperverg** (Ruhr-University Bochum and PNPI Gatchina)

**J. McCord** (IFW Dresden)

**V. Höink, J. Schmalhorst and G. Reiss** (Bielefeld University)

**T. Weis, D. Engel and A. Ehresmann** (University of Kassel)

Continuous magnetic films, consisting of regions with different magnetic properties, are one alternative to patterned magnetic media, where the super-paramagnetic limit is approached at high package densities. For a detailed study of possible interactions between neighbouring magnetic elements in such a continuous film a model system was designed, allowing the efficient use of different experimental techniques as polarised neutron reflectometry and Kerr microscopy for complementary analysis.

Understanding and controlling competing exchange bias and exchange coupling effects is an important issue in the design of advanced antiferromagnetically-coupled hard disks with increasing storage density. The magnetic exchange bias effect - expressed by a field shift of the hysteresis loop - can be used for designing a magnetic pattern within a continuous film. Exchange bias occurs in ferromagnet (F) - antiferromagnet (AF) heterostructures when cooling the AF material through the blocking temperature in the field of the F layer. The exchange bias effect can be modified by bombarding the hetero-structure with light ions in an applied magnetic field. Magnetic patterning by ion bombardment combines both effects and changes the exchange bias in the ion exposed parts of the film, while keeping it unchanged in other regions. [1] We used He<sup>+</sup> ions for imprinting an opposite exchange bias in stripe-shaped parts of a 30 nm thick ferromagnetic Co<sub>70</sub>Fe<sub>30</sub> layer coupled by exchange bias to a

15 nm thick antiferromagnetic Mn<sub>83</sub>Ir<sub>17</sub> substrate [2]. In order to prevent bombardment of the complete sample, we partly covered it by photoresist. In the result we got a continuous film with an array of equally spaced 3 μm wide imprinted

magnetic stripes of oppositely oriented exchange bias.

The evolution of the domain structure along the hysteresis loop was studied by a combination of methods, including polarised neutron reflectometry and off-specular

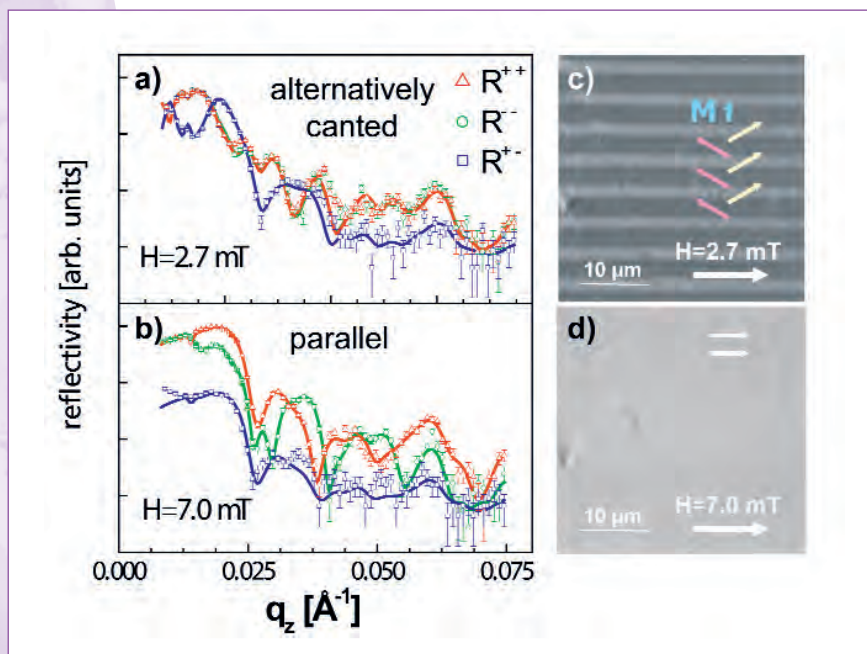


**Figure 1:** Data and fits of specular polarised neutron reflectivity measurements performed in the alternatively canted state (a) and in saturation (b). The neutron data are compared to Kerr microscopy measurements (c,d).

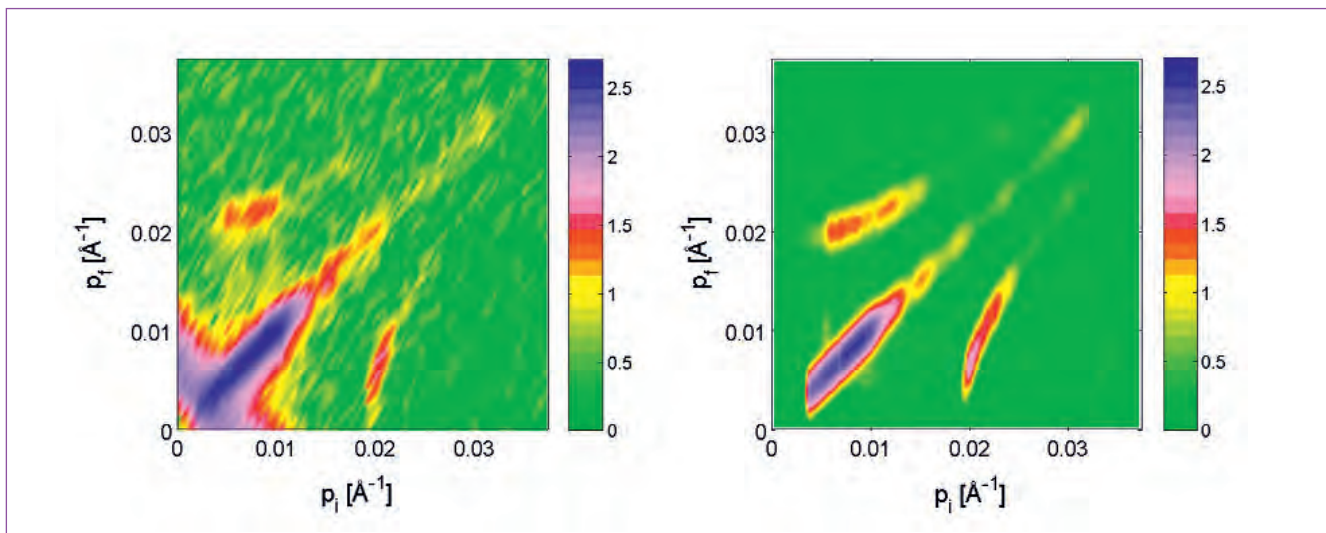


**Figure 2:** Experimental (left) and simulated (right) maps of the polarised neutron scattering intensity on a logarithmic scale. The experimental map was measured with neutrons in the “up” state at a field of 2.7 mT when the magnetisation is in the alternatively canted state. The intensity is plotted as a function of projections  $p_i$  and  $p_s$  of incident,  $k_i$  and scattered,  $k_s$  wave vectors.

scattering measured on the instrument ADAM, Kerr microscopy providing a vivid direct space image of the domain structure, as well as vector-MOKE measuring magnitude and direction of the net magnetisation. The quantitative analysis of the experimental data confirms that over a broad range of applied fields a lateral antiparallel order of neighbouring stripes exists as expected. However, the data also show that this lateral “antiferromagnetic order” coexists with a net magnetisation component normal to the stripes and to the magnetic field. This immediately follows from data on specular polarised reflectometry in **figure 1a**. Indeed, an appreciable spin-flip signal  $R^{+-}$  (and  $R^{-+}$ , not shown) in the specular channel, together with a vanishing splitting of non-spin-flip reflectivities  $R^{++}$  and  $R^{--}$ , signifies that the magnetisation averaged over the coherence length is substantially tilted with respect to the polarisation direction, and hence, to the stripe axis. On the other hand, the Kerr microscopy image in **figure 1c** reveals an alternating magnetic order and leads to a model illustrated by the arrows.

In saturation (see **figure 1b**) strong splitting of non-spin-flip reflectivities  $R^{++}$  and  $R^{--}$  and vanishing spin-flip reflectivities  $R^{+-}$  (and  $R^{-+}$ , not shown) account for a magnetisation arrangement along the stripe axis with no magnetic contrast seen in real space in the Kerr image in **figure 1d**.

From specular polarised neutron reflectometry alone one cannot draw any conclusions about the *lateral* arrangement of

magnetisation. The missing information can readily be inferred from fitting the off-specular scattering data to the model based on Kerr microscopy images. One representative example of data and the result of the fit are displayed in the left and right panel of **figure 2**. Here the diagonal ridge at  $p_i = p_s$  shows the intensity of specular reflection, while the curved bands correspond to Bragg diffraction. Some diffuse scattering seen at  $p_i \neq p_s$  is due to small ripple domains which can also be recognised in the Kerr images. Only the first-order Bragg reflections are seen, whereas the second-order ones are suppressed due to the equal width of adjacent magnetic stripes. The Bragg and diffuse scattering are purely of magnetic origin and vanish in saturation. From the fits performed over the whole scattering intensity maps for spin “up” and “down” neutrons we found, that the magnetisation vectors in neighbouring stripes make an angle of  $120^\circ$  resulting in a transverse film magnetisation.

For explaining these results one has to consider both, interfacial exchange bias across the F/AF interface and intralayer exchange coupling between adjacent stripes. The competition between these two interactions can be described in a simple phenomenological model [2].

The exchange bias field contribution is proportional to the number of interfacial pinning sites, i.e. to the area of the stripe, while the exchange energy between the stripes is proportional to the number of sites within the domain wall. Therefore, the ratio between bulk and interfacial contributions is roughly proportional to the square of the ratio (thickness/width). This means that one can suppress the tilt instability by either increasing the width of the stripes or by reducing the ferromagnetic film thickness, while keeping interfacial and bulk ferromagnetic exchange couplings unchanged. A set of newly designed samples is under fabrication in order to test these theoretical predictions.

## References

- (1) A. Ehresmann, *Recent Res. Dev. Phys.* 7 (2004) 401
- (2) K. Theis-Bröhl, M. Wolff, A. Westphalen, H. Zabel, J. McCord, V. Höink, J. Schmalhorst, G. Reiss, T. Weis, D. Engel, A. Ehresmann, U. Rucker and B.P. Toperverg, *Phys. Rev. B* 73 (2006) 174408

# Advances in fatigue life prediction of welds using neutron strain scanning

## Authors:

**M.N. James** (University of Plymouth)

**A. Steuwer** (University of Plymouth and FaME38 at the ILL-ESRF Grenoble)

**D. Hattingh and H. Lombard** (Nelson Mandela Metropolitan University, Port Elizabeth)

**D. Hughes and T. Pirling** (ILL)

The capabilities of the new SALSA strain scanning instrument and the materials characterisation facilities in the FaME38 laboratory have been utilised to generate a comprehensive set of residual strain line-scan data for a matrix of 12 butt welded specimens of RQT701 high-strength steel. The hexapod platform allows precise and reliable positioning of the neutron beam at the same relative depths for these heat-distorted specimens. Data were acquired along a selected line transverse to the weld. The quality and quantity of the SALSA measurements, obtained in only 4 days of beamtime, will provide meaningful insights into the complex and important engineering problem of highly variable fatigue strength often observed in high-strength welded steels. This is the first time such a wide range of weld process conditions have been considered on an advanced neutron strain scanning instrument.

Life prediction for welded structures is currently handled by design codes which are applicable to many conditions and grades of steel across a wide range of structures. Design lifing curves are available for a number of standard joint geometries. This makes fatigue design of structures relatively straightforward, but has limitations due to the inherent conservatism necessary in such a broad approach. These limitations become more apparent with higher strength steel grades where joints made under nominally similar conditions may exhibit differences in fatigue strength by a factor of 2, equivalent to a 10-fold difference in cyclic lives.

This problem has been considered in several major research projects [1-2] which identified the possibility that differences in fatigue performance might arise from residual stress influences. Measurements of resi-

dual stresses using hole drilling and surface X-ray techniques were, however, both inconclusive and contradictory. It was obvious to us that neutron strain scanning using an advanced instrument, such as SALSA at the ILL, had the potential to generate much more reliable data. High quality data would allow us to identify the influences of weld process factors (heat input, filler metal strength level and plate thickness) in joining high-strength steels and to explore the possibility of predicting fatigue life via strain and hardness gradients across the critical weld toe position.

SALSA is the new ILL strain imager dedicated to the determination of residual stresses in a broad range of applications in terms of components and materials. It is designed for diffraction measurements in 'real' engineering components and optimised for stress determination in metallic components. 4 days of beamtime on SALSA and a carefully designed experimental matrix allowed us to consider 2 heat inputs, 3 strength levels of filler metal and 2 plate thicknesses in RQT701 steel. This is a roller quenched and tempered structural steel with a yield strength > 690 MPa. We made measurements on 12 plates 300 mm long and

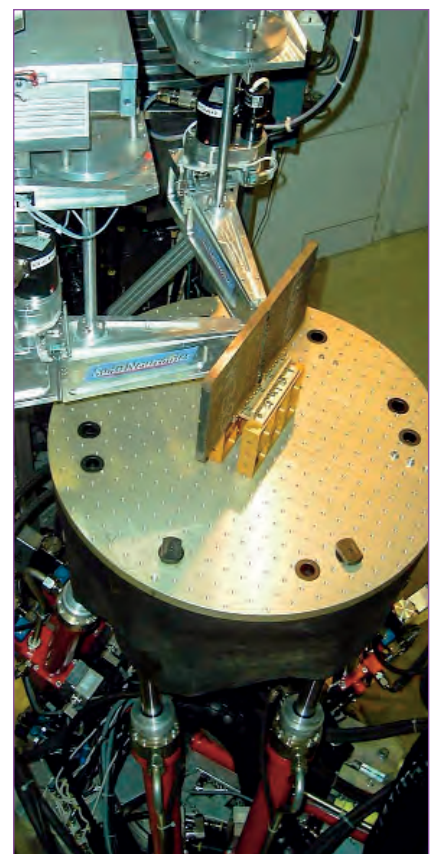


**Figure 1:** A welded specimen in position for strain scanning on the SALSA hexapod platform.

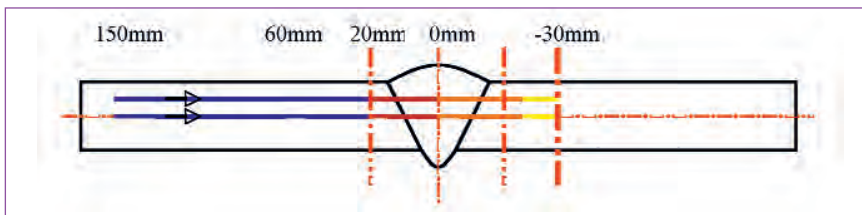


Figure 2: Schematic diagram of the weld cross-section showing the line scanning positions.

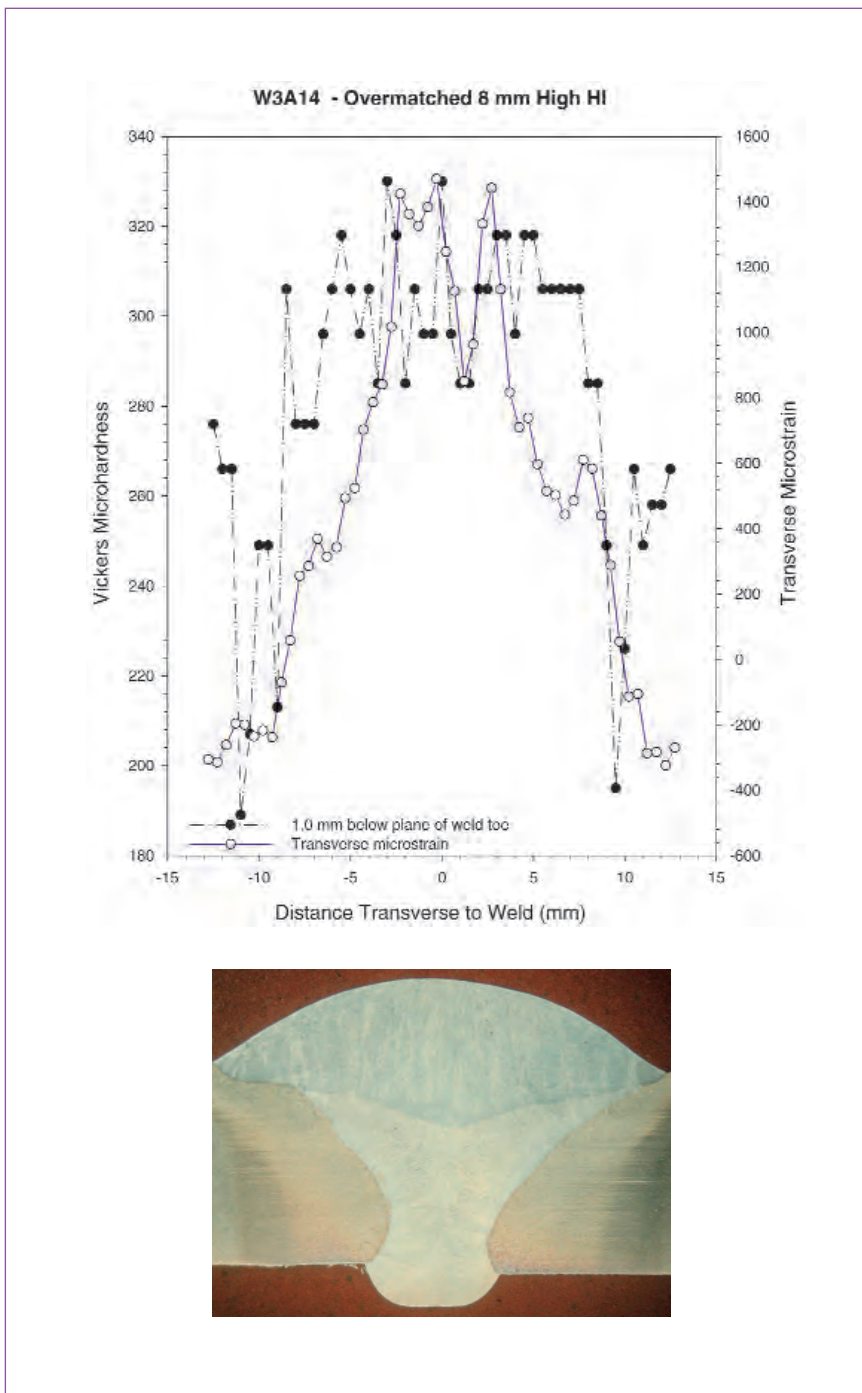


Figure 3: Illustration on the same size scale of transverse residual strain profile 1 mm below the plate surface, the Vickers micro-hardness profile, and their positions relative to the weld.

150 mm wide with a central butt weld parallel to the longer side. **Figure 1** shows a specimen mounted on the SALSA instrument.

**Figure 2** indicates the two line scans made in each specimen transverse to the weld run, along the centre of the plate thickness and along a line 1 mm below the plate surface on the cap side of the weld. These positions were chosen because fatigue cracks invariably start along the weld toe and are primarily influenced by the transverse residual strains. Steel welds are generally acknowledged to contain weld toe defects around 0.8-1.0 mm deep and the 1 mm line will reflect the residual strain values at this critical position. The mid-depth position is likely to reflect average residual strains arising from the heat input. Micro-hardness scans were done along the same lines using the automated testing machine in the FaME38 laboratory and metallographic specimens cut from plate positions adjacent to the strain scanning experiments.

Typical results are shown in **figure 3** as a composite image showing data for residual strain and micro-hardness on the same scale as a macrograph of the weld microstructure. These data will allow us to combine strain and hardness gradients across the weld toe in ways that are physically meaningful in terms of fatigue crack initiation and growth. We can then assess whether such a parameter can be used to predict the ranking order for fatigue performance in these welded specimens, assessed either by nominal surface stress, hot-spot stress or hot-spot strain.

## References

- (1) P.H. Bateson and C. Lindley, *Fatigue design of welded joints for increased design life*, ECSC Project 7210.KD/809 (1990)
- (2) P.H. Bateson and B. Holmes, *Residual stress and attachment thickness effects on the fatigue performance of welded joints*, ECSC Project 7210.MC/803 (1995)

# The formation of a cyclic water hexamer in zeolite NaX

## Authors:

**J. Hunger** (Max Planck Institute for Chemical Physics of Solids, Dresden)  
**H. Böhlig and B. Hunger** (University of Leipzig)  
**I.A. Beta** (Kansas State University, Manhattan)  
**C. Ling** (University of Sydney)  
**H. Jobic** (Institut de Recherches sur la Catalyse CNRS, Villeurbanne)

In order to understand the host-guest interactions in zeolite-water systems neutron powder diffraction measurements of faujasite NaX loaded with D<sub>2</sub>O have been combined with diffuse reflectance infrared Fourier transform spectroscopic (DRIFTS) measurements for determination of the adsorption complex structures. It has been shown that there is strong evidence to suggest formation of cyclic hexamers of water molecules localised in the 12-ring windows between faujasite supercages which are stabilised by hydrogen bonds to zeolite framework oxygen atoms.

The adsorption of water on zeolites is a subject of great scientific and technological interest due to the broad spectrum of zeolite applications as catalysts, adsorbents for separation processes, ion exchange, heat storage units, cooling devices and heat pump systems. However, besides some X-ray diffraction studies on fully hydrated faujasites, no convincing results have been reported so far in the literature about the arrangement of water molecules and extraframework cations in dependence on the water content in faujasite type zeolites. Recently, the structure of adsorption complexes of water in a NaX zeolite at lower loadings was published [1]. The results were interpreted together with DRIFTS measurements.

Samples of hydrated NaX were activated at 673 K under vacuum and loaded with D<sub>2</sub>O at room temperature. Neutron powder diffraction patterns of the samples were recorded at 5 K (D2B,  $\lambda = 2.4 \text{ \AA}$ ). The crystal structures have been solved using

a direct space global optimisation technique [2] and refined by the Rietveld method (figure 3). DRIFT spectroscopic experiments were carried out with a Perkin-Elmer 'System 2000R' spectrometer which allows temperature-programmed investigations between room temperature and 723 K in a carrier gas flow.

Neutron powder diffraction studies of zeolite samples loaded with 25, 48 and 72 D<sub>2</sub>O molecules per unit cell, respectively, reveal 4 to 6 possible positions of water molecules with respect to the zeolite framework and the extraframework sodium ions [1]. At all studied loadings, the water molecules on D<sub>2</sub>O positions W1 with the highest site occupation factors, are located in the 12-ring windows between the zeolite supercages. These molecules can interact with a sodium ion on SIII position (figure 1). While one of their D atoms points toward the O1 framework oxygen and forms a hydrogen bond with it, the other D atom remains localised in the 12-ring plane.

The presence of water molecules with hydrogen bonded and free OD bonds is in good agreement with the DRIFT spectra which show two broad associate bands at 3472 and 3236 cm<sup>-1</sup>, due to hydrogen bonding of water molecules, and two sharp bands at 3688 and 3636 cm<sup>-1</sup>, due to

the OH bonds free of hydrogen bonding. An attempted assignment for the two sharp bands would be as follows: the water molecules on W1 positions donate one hydrogen bond to an O1 framework oxygen atom. If one of these molecules would also donate a second hydrogen bond to a neighbouring water molecule, the latter would have a free H for hydrogen bonding.

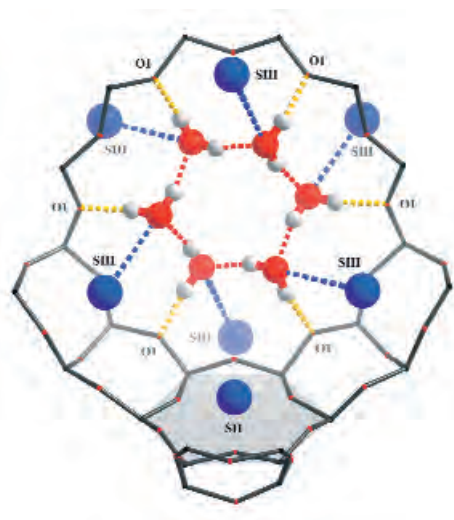


**Figure 1:** Cyclic hexamer of adsorbed water in NaX. Water molecules (in red) are located on W1 sites.

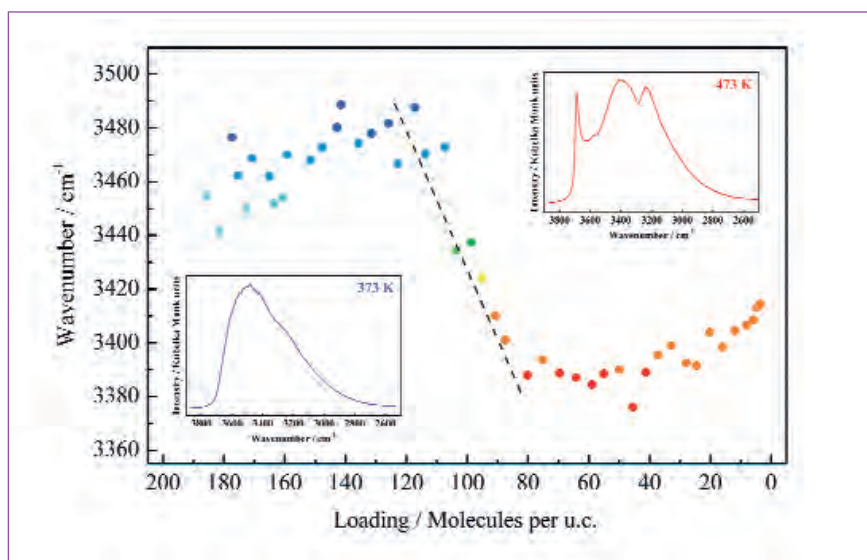


**Figure 2:** Relationship between the position of the high-frequency associate OH stretching band in dependence on the water loading obtained *in situ* by DRIFT spectroscopy during non-isothermal desorption of water in NaX.

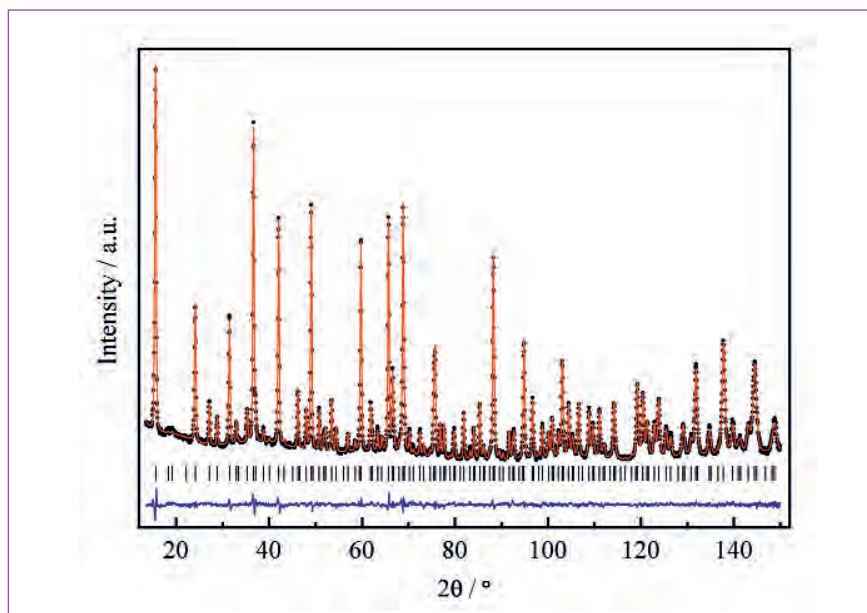


**Figure 3:** Rietveld refinement of the D2B neutron diffraction pattern for the crystal structure of zeolite NaX loaded with 72 D<sub>2</sub>O molecules per unit cell.

Therefore, it would be both a donor and an acceptor of hydrogen bonds. Based on quantum mechanical computations, the first species (only donor) will give rise to a higher frequency OH stretching mode than the donor-acceptor species. With increasing water loading and formation of larger water clusters, the number of free OH groups on donor-acceptor water molecules will steadily decrease. This prediction is in qualita-

tive agreement with the experimental observed decrease of intensity of the sharp low-frequency OH stretching mode with increasing water loading.

If all the six symmetry equivalent W1 positions in a 12-ring plane are occupied, cyclic D<sub>2</sub>O hexamers will be formed (**figure 1**). This structural motif which also occurs in ice Ih has been recently observed in water clusters trapped in liquid helium

droplets [3]. Cyclic water hexamers of different structures were also observed in metalorganic frameworks (see, e.g. [4]).

In case of water adsorbed on the NaX zeolite, besides the cooperative effect of hydrogen bonding inside the ring, an additional stabilisation of the hexamer occurs because of the hydrogen bonding to the zeolite framework. The geometrical parameters of the observed cyclic hexamer are quite similar to those in ice Ih.

The space group  $Fd\bar{3}$  was used for description of the structures of NaX samples loaded with 25, 48, and 72 water molecules per unit cell while the diffraction pattern of a NaX sample loaded with 120 D<sub>2</sub>O molecules per unit cell could not be indexed in this space group. This is evidence of the formation of at least one new phase. That fact can be interpreted in the sense of an intermediate state during an extensive reorientation of the D<sub>2</sub>O molecules after desorption of weakly adsorbed water molecules from the NaX zeolite. The restructuring results in the formation of the new adsorption complexes at lower loadings. This interpretation is supported by DRIFTS results which have shown a remarkable downshift of the high-frequency associate band between loadings of 120 and 70-80 water molecules per unit cell (see **figure 2**), indicating an increase of the average strength of the hydrogen bonds. However, a detailed clarification of this feature requires further experimental and theoretical studies which are in progress.

## References

- (1) J. Hunger, I.A. Beta, H. Böhlig, C. Ling, H. Jobic and B. Hunger, *J. Phys. Chem. B.*, 110 (2006) 342
- (2) V. Favre-Nicolin and R. Cerny, *J. Appl. Cryst.*, 35 (2002) 734
- (3) K. Nauta and R.E. Miller, *Science*, 287 (2000) 293
- (4) X.-M. Zhang, R.-Q. Fang and H.-S. Wu, *Crystal Growth & Design*, 5 (2005) 1335

# VIVALDI sets new frontiers in chemical crystallography

The new capabilities offered by thermal-neutron Laue diffraction and VIVALDI to frontier problems in chemistry are illustrated by four recent and quite different studies: the location of  $H^-$  in the Li cage of an organometallic complex; the C-H...F hydrogen bonding in a Zr-based organometallic catalytic complex; a multi-temperature study of the molecular disorder in pentachloronitrobenzene; and a charge-density study of the smelly organic molecule, coumarin, a chemical precursor to many laser dyes.

In the five years since receiving its first neutrons, the thermal-neutron Laue diffractometer VIVALDI has opened up several new fields of neutron research thanks to its ten- to one-hundred-fold gain in detection efficiency over conventional monochromatic single-crystal diffractometers. This gain is a product of the high incident flux in the un-monochromated neutron beam and the large solid-angle image-plate detector.

By far the most popular type of investigation on VIVALDI to date has been location and precise characterisation of hydrogen atoms in molecular structures with unit cells up to  $10000 \text{ \AA}^3$  in volume, often on crystals previously considered to be too small for neutron diffraction. The following four examples illustrate the diversity of topical chemical questions that can now be investigated by this novel instrument.

## Authors:

**J.M. Cole** (Cavendish Laboratory, Cambridge, UK)

**G.J. McIntyre** (ILL)

### Revealing a potential hydrogen-storage material

Metal-organic frameworks that can store hydrogen are of enormous contemporary interest given the industrial drive to develop hydrogen-based fuel cells.

In the study, illustrated in **figure 1**, an isolated hydride ion,  $H^-$ , encapsulated within a cage of lithium atoms in an organometallic complex, was discovered [1]. This is the first time a molecular main-group interstitial hydride has been reported using single-crystal neutron diffraction. The presence of this hydride was suspected from NMR results, X-ray diffraction data, and electron counting considerations, but it could only be confirmed using neutron diffraction.

### Realising the important role of C-F...H interactions in alkene polymerisation catalysis

For the first time, the presence of the contentious C-H...F-C interaction has been characterised by a single-crystal neutron diffraction study [2]. The results (**figure 2**), obtained using VIVALDI are important from a catalytic perspective because C-H...F-C contacts have been proposed in related 'post-metallocene' catalysts, but this is the first report demonstrating that such ligand-polymer interactions are experimentally feasible. Such weak attractive non-covalent intramolecular interactions, as opposed to the well-established agostic and co-catalyst...metal contacts, represent a new concept in polyalkene catalysis.

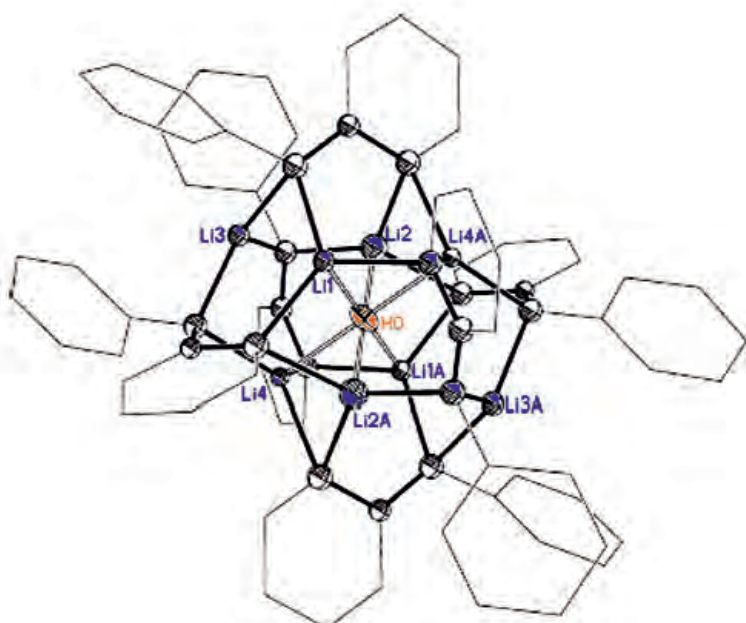


**Figure 1:** Crystal structure of the  $((tBu_2AlMe_2)_2Li)^- \{ (Ph(2-C_5H_4N)N)_6HLi_6 \}^+$  cation, highlighting the interstitial hydride,  $H^-$ , in orange, the surrounding metal cage, lithiums given in blue, connecting carbon atoms in black/white and an outline of the surrounding organic periphery in grey).

### Rapid multi-temperature crystal structure determinations of disordered molecules

The molecular disorder in pentachloronitrobenzene,  $C_6(Cl_5)(NO_2)$  was characterised over a wide temperature range by Laue diffraction [3], since the disorder (**figure 3**) causes the compound to possess anomalous dielectric properties. Molecular disorder is best analysed via multi-temperature crystal structure determinations since these can help differentiate between static and dynamic disorder. This investigation illustrates well the capabilities of VIVALDI for rapid multi-temperature studies since the atomic positional and anisotropic displacement parameters determined from this study compare very well to complementary X-ray diffraction measurements. Indeed, our results compare with the X-ray measurements better than those often observed when using slower monochromatic neutron diffraction. The use of VIVALDI has, therefore, a very relevant benefit for this type of work, given that neutrons are such a rare resource and are always in high demand.

### Speedy location of hydrogen positions for use in charge-density studies

The neutron diffraction study of this laser dye precursor, coumarin, provided hydrogen positions of sufficient accuracy to be

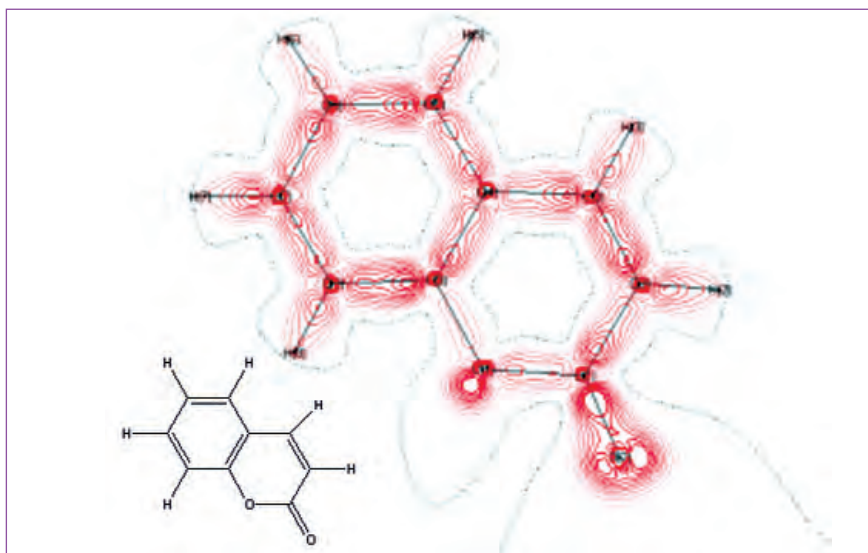


**Figure 4:** Electron deformation density map ( $\rho_{\text{multipolar}} - \rho_{\text{IAM}}$ ) of the coumarin laser-dye precursor, using the hydrogen positions derived from neutron diffraction on VIVALDI.

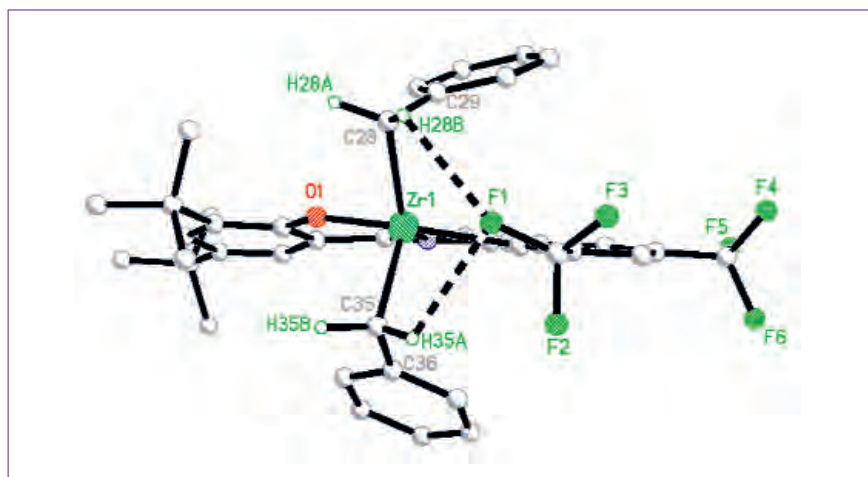


**Figure 2:** The C-H...F-C intramolecular interactions that play a key catalytic role in the Zr-based organometallic complex  $C_{41}H_{39}F_6NO_2$ .

used in combination with accurate X-ray diffraction data to perform a charge-density study [4]. The electron deformation density map derived from this work is shown in **figure 4**.

All four studies presented here were performed in the early days of operation of VIVALDI. Since then, improvements to the neutron guide feeding VIVALDI and improved image-plates have resulted in a ten-fold increase in efficiency. We can expect to see even more challenging frontier problems in chemical crystallography being successfully tackled in the near future.

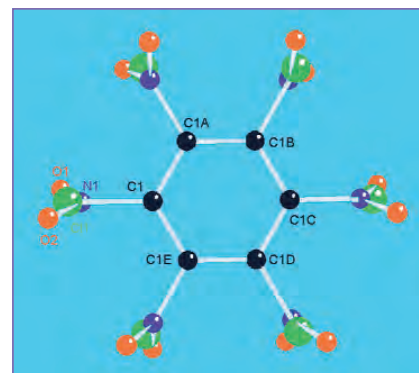


**Figure 3:** The molecular structure of pentachloronitrobenzene; the single nitro group and the five chlorine atoms are disordered over the six substituted positions of the benzene ring.

### References

- (1) S.R. Boss, J.M. Cole, R. Haigh, G.J. McIntyre, P.R. Raithby, R. Snaith, A.E.H. Wheatley, *Organometallics*, 23 (2004) 4527-4530
- (2) M.C.W. Chan, S.C.F. Kui, J.M. Cole, G.J. McIntyre, S. Matsui, N. Zhu and K.-H. Tam, *Chem. Eur. J.* 12 (2006) 2607-261
- (3) J.M. Cole and G.J. McIntyre, *Acta Crystallogr. B* (submitted, 2007)
- (4) J.M. Cole, S.L.G. Husheer, J.A.K. Howard, G.J. McIntyre and D. Yufit, unpublished results

# Engineering oxygen transport

## Authors:

W. Paulus, R. Le Toquin, T. Berthier, O. Hernandez and M. Ceretti  
(University of Rennes 1)

A. Cousson (LLB, CEA-Saclay, Gif-sur-Yvette)

C. Prestipino, C. Lamberti (University of Torino)

S. Eibl, H. Schober, M. Johnson and T. Hansen (ILL)

The requirements for new and clean energy sources, such as solid oxide fuel cells (SOFC), have stimulated considerable research activities in the last decade on solid oxygen ion conductors operating at moderate temperatures. SOFCs would offer enormous ecological benefit, provided that suitable materials with high oxygen permeability can be developed to operate at moderate temperatures. In order to better understand low-temperature oxygen diffusion mechanisms, the oxygen intercalation into  $\text{SrCoO}_{2.5}$  was investigated by *in situ* neutron diffraction and X-ray absorption spectroscopy at ambient temperature. In particular, three-dimensional oxygen ordering and evidence of the formation of  $\text{O}^-$  species during the intercalation were observed for the first time.

Ion conduction in solids is normally described in terms of a thermally activated hopping process with ions jumping from occupied into vacant sites. Oxygen ions are doubly charged and have a rather large radius of about 1.4 Å. The energy barriers to overcome during jumping are therefore high, requiring elevated temperatures for diffusion to set in, even in structures possessing rather large vacancy sites. In this context, it is rather surprising that there exist compounds into which oxygen ions can be intercalated reversibly at ambient temperature using 'gentle' electrochemical methods or other soft chemistry synthesis. At present two structure types are known to show such behaviour: the first one is the  $\text{La}_2\text{MO}_4+x$  ( $\text{M}=\text{Cu}, \text{Ni}, \text{Co}$ ) system with  $\text{K}_2\text{NiF}_4$  structure type and the second one concerns the deficient perovskites  $\text{SrMO}_{2.5}$  ( $\text{M}=\text{Fe}, \text{Co}$ ), with Brownmillerite structure type [1-3]. In particular,  $\text{SrMO}_{2.5}$  must be consi-

dered as a key system for the understanding of low-temperature reaction mechanisms involving oxygen diffusion, as it exhibits a particular high charge transfer of one electron per formula unit.

Perovskite oxides are networks of corner-sharing oxygen octahedra. Extracting rows of oxygen ions (see figure 1, left) in such a way as to create channels of parallel vacancies would lead to the Brownmillerite

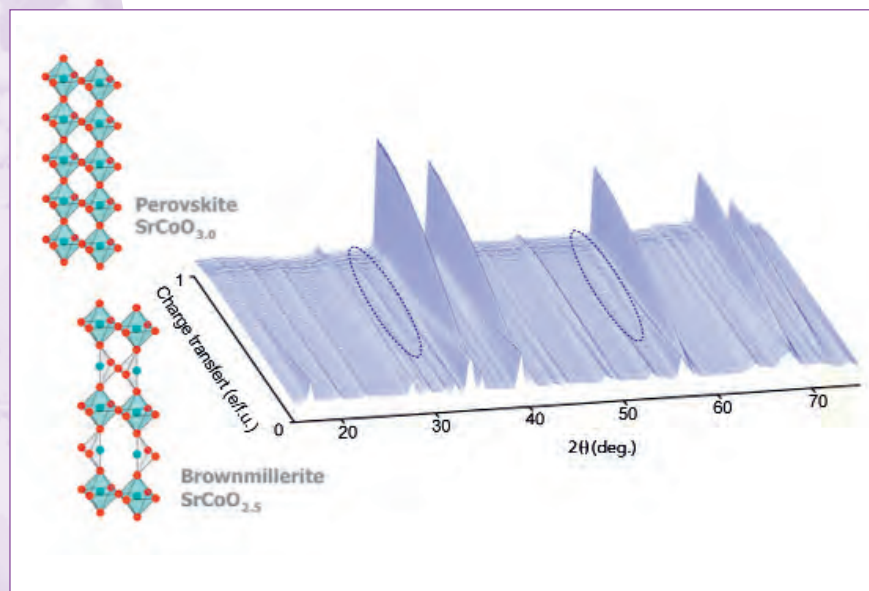


**Figure 1:** Right: Neutron powder diffraction patterns obtained *in situ* on D20 during the electrochemical oxidation of  $\text{SrCoO}_{2.5}$  vs. charge transfer. The diffractogram of the brownmillerite  $\text{SrCoO}_{2.5}$  is represented at the bottom, whereas the one of the perovskite  $\text{SrCoO}_{3.0}$  is at the top. The outlined ellipsoids indicate the positions of the superstructure reflection corresponding to  $\text{SrCoO}_{2.82\pm 0.07}$ . Left: Schematic transformation of the brownmillerite to the perovskite structure.

structure type. In the case of  $\text{SrCoO}_{2.5}$  these channels can be electrochemically re-oxidised at room temperature, thus coming back to the ordered  $\text{SrCoO}_3$  mother compound.

In a first step to understand what makes  $\text{SrCoO}_{2.5}$  so special, the structural and magnetic changes were monitored during electrochemical oxidation. Electrochemistry is in this context a very useful tool, as it allows controlling directly the charge transfer, i.e. the oxygen stoichiometry and also the reaction kinetics. *In situ* neutron diffraction, using a specially adapted electrochemical cell on the instrument D20, turned out to be the method of choice for this experiment. Neutrons are simply more suitable than X-rays when it comes to determine the oxygen ordering and stoichiometry.

In the first stage of the oxidation the original  $\text{SrCoO}_{2.5}$  phase coexists with  $\text{SrCoO}_{2.75}$ , a cubic deficient perovskite structure (see **figure 1**, left). Further oxygen uptake does, however, not proceed continuously to the cubic  $\text{SrCoO}_3$  but yields in an additional intermediate phase,  $\text{SrCoO}_{2.82 \pm 0.07}$ , establishing 3D oxygen ordering [4]. The latter phase is isostructural to the homologous  $\text{SrFeO}_{2.875}$  phase with tetragonal symmetry, which is related to the perovskite unit cell by  $a = b \approx 2a\sqrt{2}$  and  $c \approx 2a$ .

This is the first time that oxygen ordering has been detected during controlled intercalation at ambient temperature, i.e. far away from thermodynamic equilibrium. This implies the important message that solid oxides can indeed relax towards new ordered structures already at ambient temperature. The general assumption that good ionic conduction is always accompanied by structural disorder and that, reciprocally, structural disorder always favours ionic conduction, is thus a questionable concept. Complementary studies by X-ray absorption spectroscopy carried out *in situ* on the beamline BM29 at the ESRF have evidenced the formation of  $\text{O}^-$  species during the intercalation reaction [4]. This indicates that the oxygen sub-band is energetically higher than the cobalt band and further underlines the importance of possible valence fluctuations to support oxygen ion conduction following  $\text{Co}^{4+} + \text{O}^{2-} \leftrightarrow \text{Co}^{3+} + \text{O}^-$  which has in this sense more than only academic impact.

The fact that  $\text{CaFeO}_{2.5}$  is unable to intercalate oxygen by electrochemical oxidation while  $\text{SrFeO}_{2.5}$  does, demonstrates that the simple existence of vacancy channels solely is unable to explain the conduction mechanism. It becomes evident that also the lattice motion must play a decisive role. Inelastic neutron scattering (IN6) shows significant differences in the density-of-states for the homologous compounds  $\text{SrFeO}_{2.5}$  and  $\text{CaFeO}_{2.5}$  (**figure 2**).

Using these neutron data to validate numerical simulations, we obtain first evidence for a delicate interplay of structure *and* lattice dynamics. In particular, very small changes in the cell parameters may trigger instabilities, i.e. soft-going modes leading to dynamic disorder. According to our numerical simulations, the conduction channels in  $\text{SrFeO}_{2.5}$ , even at room temperature, are anything but rigid tubes. The tetrahedra, constituting the walls of these channels, display a very complex motion in a way to promote dynamically transport of oxygen ions along the channels. The equivalent motions do not exist in  $\text{CaFeO}_{2.5}$  thus offering an explanation why oxygen cannot be intercalated at ambient conditions.

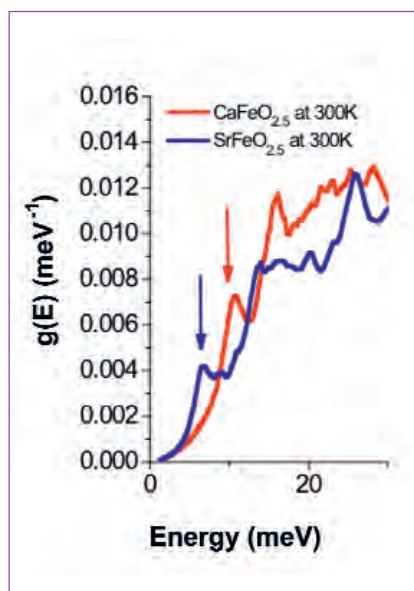
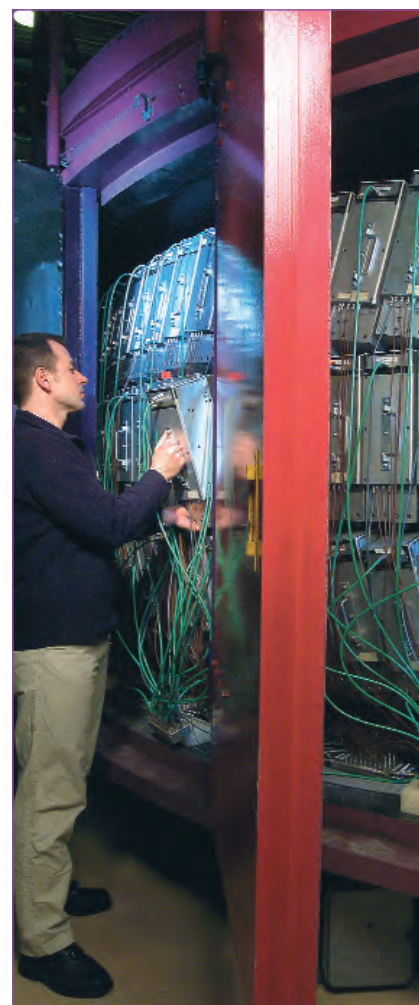


**Figure 2:** Density-of-states of  $\text{SrFeO}_{2.5}$  (blue) and  $\text{CaFeO}_{2.5}$  (red) obtained on IN6 at 300 K. The low energy modes were found for  $\text{SrFeO}_{2.5}$  at 7 meV and for  $\text{CaFeO}_{2.5}$  at 12 meV and are indicated by arrows.



Michael Koza on the time-of-flight spectrometer IN6.

## References

- (1) J.C. Grenier, A. Wattiaux, J.-P. Doumerc, L. Fournes, J.-P. Cheminade and M. Pouchard, *J. Solid State Chem.* 96 (1992) 20
- (2) A. Nemudry, P. Rudolf and R. Schöllhorn, *Chem. Mater.* 8 (1996) 2232
- (3) W. Paulus, A. Cousson, G. Dhalenne, J. Berthon, A. Revcolevschi, S. Hosoya, W. Treutmann and G. Heger, R. Le Toquin, *Solid State Sci.* 4 (2002) 565
- (4) R. Le Toquin, W. Paulus, A. Cousson, C. Prestipino and C. Lamberti, *J. Am. Chem. Soc.*, 128 (2006) 13161

## Formation of soft single crystals

### Authors:

C. Schellbach, A. Frömsdorf and  
S. Förster (University of Hamburg)  
P. Lindner (ILL)

The shear-induced ordering of soft crystals has been studied *in situ* using a specially adapted shear cell aligned in the neutron beam. Small-angle neutron diffraction experiments revealed for the first time how highly ordered soft single crystals are formed and how their degree of order is quantified. These experiments are of critical importance for the preparation of many ordered solid-state materials, such as photonic crystals, mesoporous materials and nanostructured surfaces.

Intuitively, we relate the term *soft* to the mechanical properties of a material, such as its elasticity or compliance. Typical soft materials are plastics, gels or creams. On a molecular scale, these properties are related to relatively weak interaction potentials with a weak or *soft* spatial dependence. Soft materials can spontaneously order and therefore tolerate to some extent imperfections such as a deviation in the size and shape of their constituent structures. Another very useful property is their large susceptibility to external fields. This means that even modest external fields are able to strongly induce a

macroscopic alignment in a particular direction. These properties are commonly exploited in modern materials science to produce highly ordered solid-state materials by templating highly ordered soft structures.

In this respect, the mechanisms and possible limitations of the shear-induced ordering of soft materials are of critical importance. The only direct way to investigate these processes on a molecular scale is by carrying out *in situ* measurements, where the materials are probed by diffraction experiments during shear. Such experiments can be performed at the small-angle neutron diffraction instrument D11 at the ILL Grenoble.

There, a specially adapted state-of-the-art rheometer can be aligned to the neutron beam to perform *in situ* rheological experiments. The particular material used in these studies was concentrated solutions of block copolymer micelles (PI-PEO) with a diameter of 40 nm that were known to order spontaneously into an *fcc*-lattice. The question was under what conditions (e.g. shear-rate, temperature, pretreatment) such solutions can be shear-aligned to achieve maximum order. Another very basic question was whether there is an experimental measurement to quantify the degree of order that has been achieved.

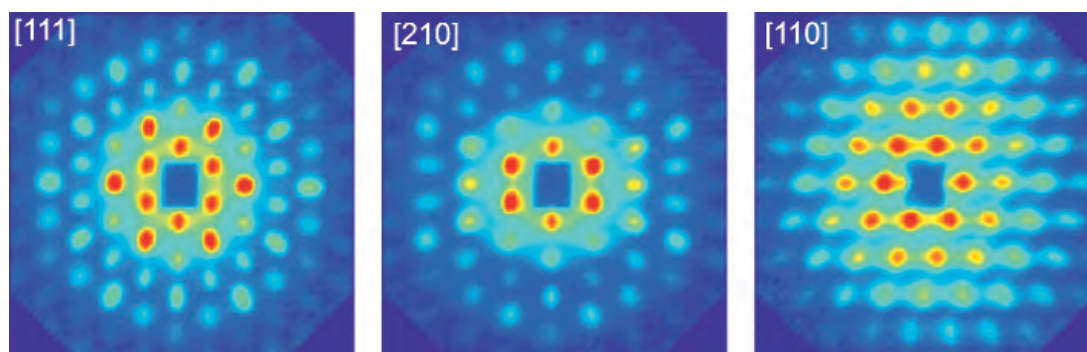
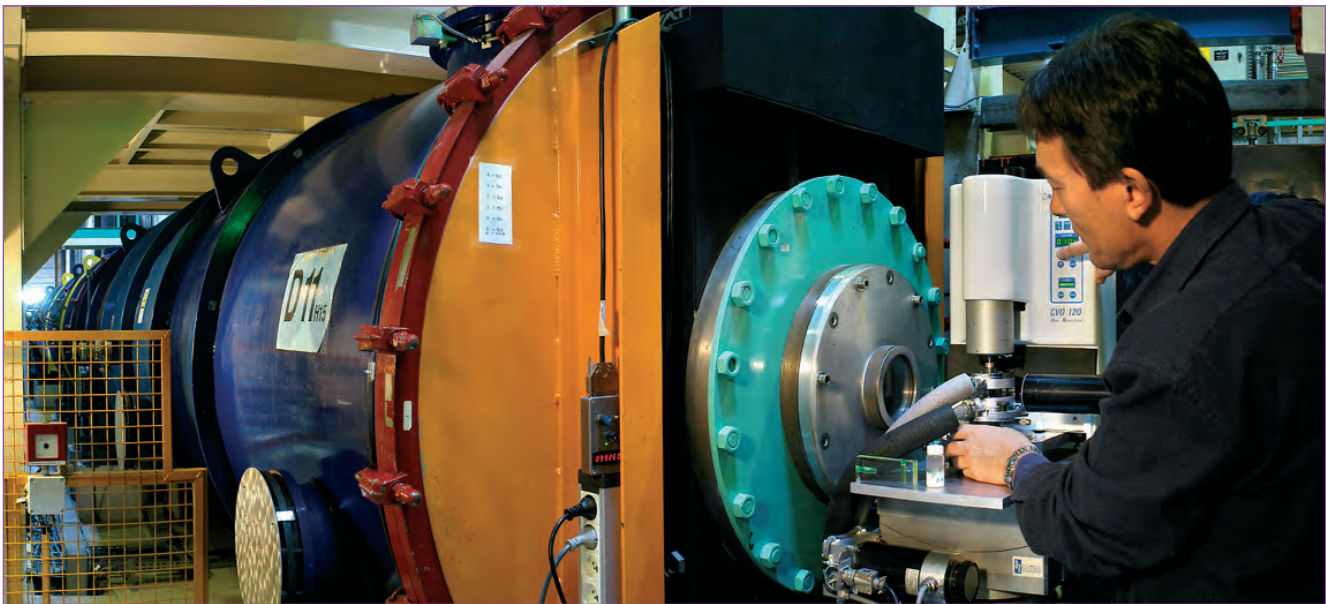


Figure 1: Scattering patterns obtained by passing the neutron beam at different angles through the shear cell. The crystalline orientations are indicated by their Miller indices  $hkl$ .



Peter Lindner on the small-angle neutron diffraction instrument D11.

Performed experiments showed first of all that the materials can only be made to develop long-range order and to align in the shear direction at the highest experimentally accessible shear rates of  $1000 \text{ s}^{-1}$ .

Secondly, the only way to trap the ordered state which developed at high shear rates is to suddenly stop shearing the material. This is in fact an empirically found method for processing such materials that is commonly used in many laboratories for

preparing ordered structures. The materials that are obtained in this way show an exceptionally large number of Bragg-peaks, as seen in **figure 1**.

By passing the neutron beam at different angles through the shear-cell, different crystalline projections of the fcc-lattice could be probed, which proved that a macroscopic fcc crystal had been formed (**figure 1**). With model calculations it was possible to reproduce the scattering patterns quantitatively.

From the relative peak intensities, the calculations yielded for the first time the coherence length of the lattice, which is a sensitive measure of its degree of long-range order.

Using a narrow neutron beam of only  $300 \mu\text{m}$  diameter, it was possible to scan through the gap of the shear cell to monitor the structural changes of the lattice within the gap during shear (**figure 2**). Indeed, it was found that within the gap, the two twins of the fcc crystal were phase separated, with one twin located at the outer wall and the other twin located at the inner wall of the shear cell.

These studies showed that performing *in situ* shear experiments in the neutron beam makes it possible to reveal details of the shear-induced ordering and orientation process of soft materials with high resolution and precision.

## References

- (1) S. Förster, M. Konrad, P. Lindner, *Phys. Rev. Lett.* 94 (2005) 017803
- (2) S. Förster, C. Schellbach, A. Frömsdorf, S.V. Roth, P. Lindner, submitted

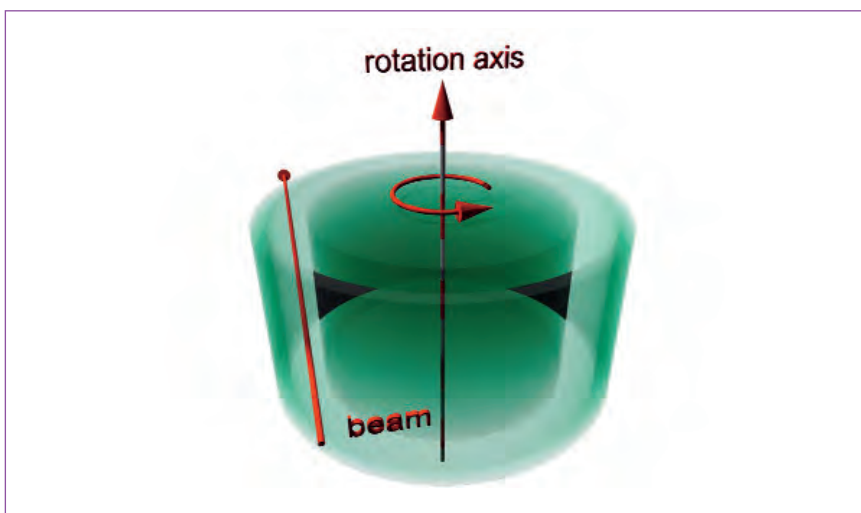


Figure 2: Schematic drawing of the shear cell with rotation axis and neutron beam direction as indicated.

## *In situ* SANS studies of the synthesis of mesoporous materials

The time-resolved *in situ* SANS has provided crucial information about the mechanism and kinetics of the synthesis of SBA-15 mesoporous silica. A three-stage cooperative self-assembly mechanism has been clearly identified. The first stage of SBA-15 synthesis involves formation of spherical copolymer micelles. The spherical micelles transform after 5 minutes of the reaction in the presence of silica precursor into cylindrical ones. Agglomeration of cylindrical micelles into two-dimensional hexagonal phase represents the third stage of SBA-15 synthesis.

Meso-structured materials (SBA-15 and related mesoporous materials [1]) with adjustable porous networks have shown a great deal of promise for the design of new heterogeneous catalysts, semiconductors, low dielectric devices and new separation processes. The pore diameter and the silica wall thickness are the major parameters, which influence their possible applications. One of the most promising mesoporous materials is the silica based SBA-15, prepared using non-ionic tri-block copolymers, such as Pluronic P123, as the structure-directing agent [1]. During the synthesis, silica precursors, tetralkylorthosilicates, are added to acidic solutions of the non-ionic copolymers at 30–100 °C. Under these conditions, the silica precursors are quickly hydrolysed and condense into silica oligomers growing upon time. The inter-

action of the oligomers with the copolymer micelles leads to the precipitation of a solid 2D hexagonal phase. The copolymers can be removed from the silica by calcination or solvent extraction. The structure of the resulting material is characterised by a 2D hexagonal array of mesopores with the pore diameter typically between 2 and 30 nm and the wall thickness up to 6 nm, which can be controlled to some extent by varying the reaction conditions.

Because of the difficulty to perform *in situ* studies, direct experimental information about the key initial stages of the synthesis is lacking. However, it is needed to understand how silica oligomers and copolymer micelles interact together upon time and to improve the properties of these materials for practical applications. Small-angle neutron scattering (SANS) experiments are particularly well suited for *in situ* studies under realistic conditions, because in contrast to TEM, NMR or EPR studies they do not

### Authors:

**M. Impéror-Clerc**

(LPS, Université Paris-Sud, Orsay)

**I. Grillo** (ILL)

**D. Durand** (BBMC, Université Paris-Sud, Orsay)

**A.Y. Khodakov** (UCCS, Université de Lille)

**V.L. Zholobenko** (Keele University)

require quenching procedures of the reaction mixture. Furthermore, the use of D<sub>2</sub>O instead of H<sub>2</sub>O considerably increases the contrast between the solvent and the polymer and allows one to investigate the evolution of the organic aggregates during the growth process which is not possible with other techniques, as SAXS [3, 4] or TEM [5] are mainly sensitive to the inorganic species.

The first *in situ* time-resolved small-angle neutron scattering (SANS) study of the initial stages of the SBA-15 synthesis was performed at the D22 instrument at the ILL [2]. The reaction mixture was circulating continuously through a 1-mm quartz flow-cell using a peristaltic pump. With the very high flux at the sample position, short acquisition times of the order of 30 seconds were used. The reaction was followed during 40 minutes.

Prior to the addition of the silica precursor (TEOS), the acidic copolymer solution



**Figure 1:** Images of the reaction medium at different reaction times taken during the *in situ* SANS experiments. The turbidity of the solution is increasing upon time until a white precipitate forms after 23 minutes.

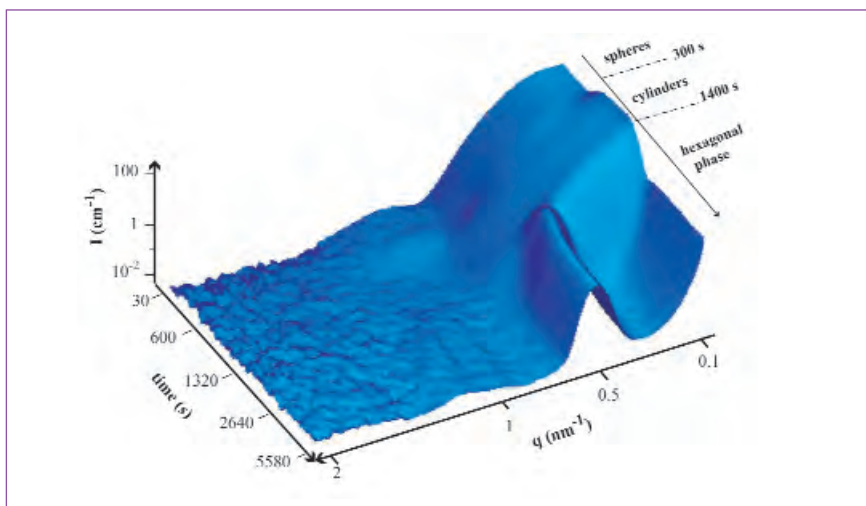


**Figure 2:** Evolution of the neutron scattering intensities with time. Only spherical micelles of P123 block copolymer are present in the synthesis mixture within the first few minutes of the reaction. Following the short induction period, hybrid organic-inorganic cylindrical micelles are detected. The Bragg peak is the signature of aggregation of the cylindrical micelles and formation of a 2D hexagonal SBA-15 phase.

appears transparent. The SANS data indicate the presence of copolymer spherical micelles of 7.1 nm radius. After the addition of TEOS, the solution becomes immediately turbid until a thick white precipitate forms after about 23 minutes of the reaction (**figure 1**).

The spherical copolymer micelles do not evolve during the induction period of 5 minutes after the TEOS addition (**figure 2**). Then, between 5 and 23 minutes, a continuous evolution of the scattered intensity is observed, characterised by the increase of the intensity at low  $Q$  and a  $Q^{-1}$  slope in a log-log plot that is the signature of 1D objects (**figure 3**). This corresponds to the

transformation of the shape of the micelles from spherical to cylindrical and their continuous growth in length up to few tens of nanometers. The turbidity of the solution is directly related to the growth of the micelles, and coincides with the beginning of the condensation of silica. The precipitation of the hybrid material is observed after 23 minutes (**figure 1**). Simultaneously, the (100) Bragg peak of the 2D hexagonal packing is viewed in the SANS patterns. The position of the peak corresponds to a distance between the cylinders of 14.2 nm.

The proposed three-stage mechanism of the cooperative self-assembly of the SBA-15

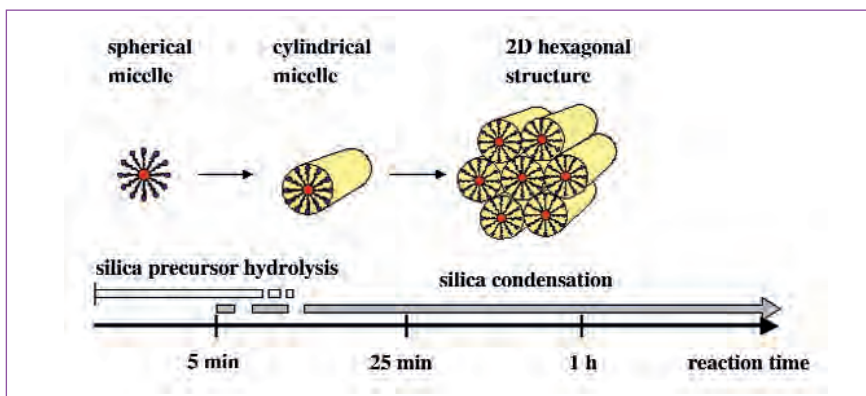


**Figure 4:** Sketch of the three-stage mechanisms of the synthesis. Silica oligomers are located in the yellow region.

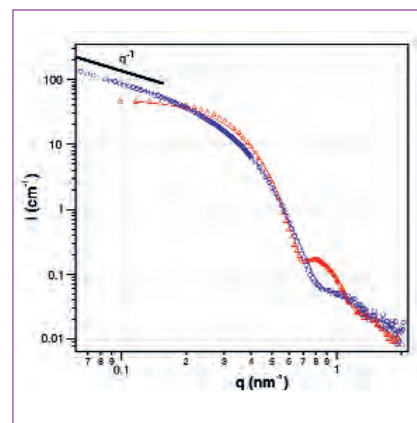


**Figure 3:** Example of scattering curves at two times of the reaction. The lines are a calculation of the form factor. ( $\Delta$ ): prior to TEOS addition, the micelles are well described by core-shell spheres, with an external radius of 7.1 nm. ( $\circ$ ): 15 minutes after the beginning of the reaction, the micelles can be viewed as cylinders of length 50 nm and radius 6.9 nm.

synthesis is illustrated in **figure 4**. The present SANS results suggest, in agreement with a recent TEM study [5], that the transformation from spherical to cylindrical micelles takes place before the precipitation of the ordered SBA-15 material, and that the precipitation is associated with the self-assembly of hybrid cylindrical micelles into the two-dimensional hexagonal structure of SBA-15.

## References

- (1) D. Zhao, J. Feng, Q. Huo, N. Melosh, G.H. Fredrickson, B.F. Chmelka and G.D. Stucky, *Science* (1998), 279, 548
- (2) M. Impéror-Clerc, I. Grillo, A.Y. Khodakov, D. Durand and V.L. Zholobenko, *Chem. Commun.*, 2007, issue 8, 834-836
- (3) K. Flodstrom, C.V. Teixeira, H. Amenitsch, V. Alfredsson, M. Linden, *Langmuir* (2004), 20 (12), 4885-4891
- (4) A.Y. Khodakov, V.L. Zholobenko, M. Imperor-Clerc, D. Durand, *Journal of Physical Chemistry B* 2005, 109 (48), 22780-22790.
- (5) S. Ruthstein, J. Schmidt, E. Kesselman, Y. Talmon, D. Goldfarb, *Journal of the American Chemical Society* (2006), 128 (10), 3366-3374.

# Triggered aggregation of nonionic surfactants in glycol mixtures

## Authors:

C. Seguin and J. Eastoe

(University of Bristol)

R.K. Heenan (ISIS Facility, Didcot)

I. Grillo (ILL)

Using mixtures of two mutually miscible hydrogen-bonding solvents has led to a surprising finding: it is possible to switch 'on' and 'off' aggregation of a nonionic surfactant. This unexpected behaviour may find uses in triggered release, targeted delivery and critical non-aqueous cleaning applications (1).

The solvents are ethylene glycol (EG, normal 'anti-freeze') and propylene glycol (PG), and the surfactant is  $C_{12}E_8$  (octaethylene monododecyl ether). Small-angle neutron scattering (SANS) was used to follow the solvent-induced changes, by employing contrast variation to highlight the surfactant molecules in the background sea of deuterated solvents. The 'on' state is achieved in pure EG, whereas if the solvent is pure PG then aggregation is strongly inhibited. For blends of EG and PG the extent of aggregation can be readily controlled by the EG:PG mixture ratio. These findings are made all the more surprising when it is realised that the solvents have very similar chemical structures, differing merely by an additional  $-CH_2-$  group for PG.

Small-angle neutron scattering (SANS) was used to characterise micellar aggregates of  $C_{12}E_8$ . SANS experiments were carried out at the D22 diffractometer at the ILL. Fully deuterated solvents provided contrast against the  $h$ -surfactant aggregates.

**Figure 1** shows SANS curves of  $C_{12}E_8$  surfactant in different solvents which are either pure deuterated d-EG, or d-PG, or their mixtures.  $C_{12}E_8$  was from Fluka BioChemika,

$\geq 98.0\%$  GC) and used without further purification. Fully deuterated ethylene and propylene glycol were obtained from  $Q_{max}$  laboratory (CDN isotopes).

Obviously, the nature of the solvent, and its composition in terms of the EG:PG ratio, has a strong effect on the measured intensity. Even without quantitative analysis (described below), it is clear that the strong aggregation seen in pure EG ( $\bullet$ ) is suppressed as the mixed solvent composi-

tion is made richer in PG ( $\times$ ). Detailed analyses of the SANS curves were performed using two related models describing anisotropic cylindrical, or ellipsoidal particles. For the EG-rich systems, the micelles appeared to be cylindrical in shape (described by a cross-sectional radius and a length). However, as the PG content is increased there is evidence for a subtle shape change to ellipsoidal micelles (described by principal radii  $r_1$  and  $r_2$ , and

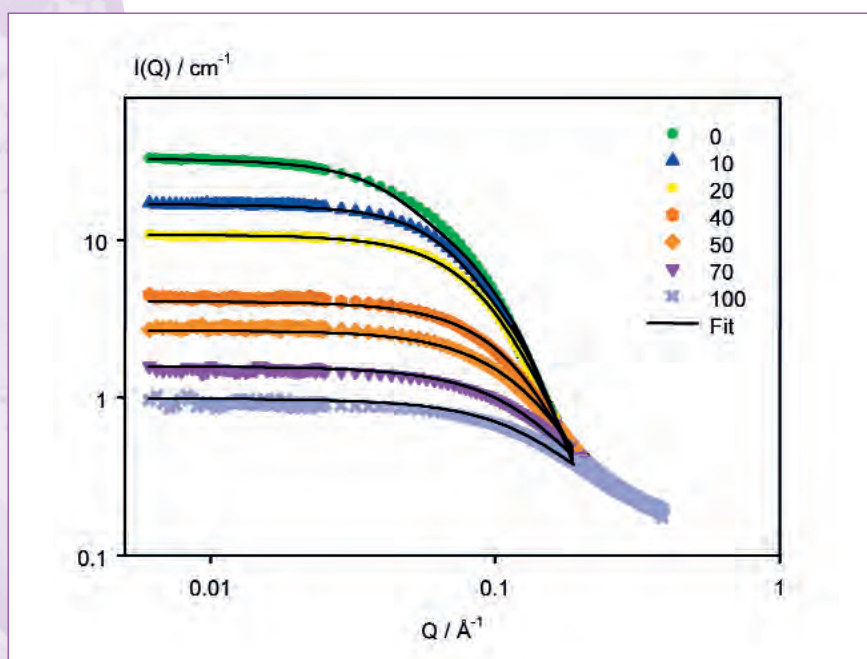


**Figure 1** shows SANS curves of  $C_{12}E_8$  surfactant in different solvents which are either pure deuterated d-EG, or d-PG, or their mixtures.

Solvent	R / Å	L / Å	V / (10 <sup>4</sup> Å <sup>3</sup> )
100% d-EG	19	143	17
90% d-EG	19	84	9
80% d-EG	18	58	6

Solvent	r <sub>1</sub> / Å	r <sub>2</sub> / Å	t / (Å) (thickness)	V / (10 <sup>4</sup> Å <sup>3</sup> )
60% d-EG	16	8	8	4
50% d-EG	16	5	5	2
30% d-EG	16	3	5	1
100% d-PG	16	1	3	1

**Table 1:** Parameters obtained by analysis SANS data from 10 wt% surfactant solutions of C<sub>12</sub>E<sub>8</sub>, in different deuterated glycol solvents at 25°C. Uncertainties: R, r<sub>1</sub>, r<sub>2</sub>, t all ± 2Å. Length L ± 10Å.

a shell thickness  $t$  to account for some weak solvent penetration into the outer surface of the micelles). These fitted functions are shown in **figure 1**. The values of internal micellar dimensions are consistent with those found in literature for this surfactant, by Lu *et al.* [2]. Using these parameters it has been possible to estimate the effective volume of each individual micelle  $V$ , which decreases dramatically as EG is systematically replaced by PG. It appears that changing the solvent from pure EG to PG causes a dramatic shift in surfactant properties, effectively switching 'off' aggregation. The tendency to cylinder formation in pure EG may be a result of a lower effective solvation of the EO headgroups compared to PG. This finding is also consistent with work of others [3], which suggested that EG can penetrate in the micelle and alter the micellar surface.

Aggregation of common nonionic C<sub>12</sub>E<sub>8</sub> surfactant was determined using SANS. When mixed EG/PG solvents are employed, aggregation and nature of the micelles were affected by the solvent composition. Therefore, ethylene glycol may be considered as a 'structure-making' solvent, whereas propylene glycol behaves as a 'structure-breaker'. The micelles tend to change from elongated rod-like aggregates in EG into ellipsoidal aggregates at higher PG content. This unusual behaviour

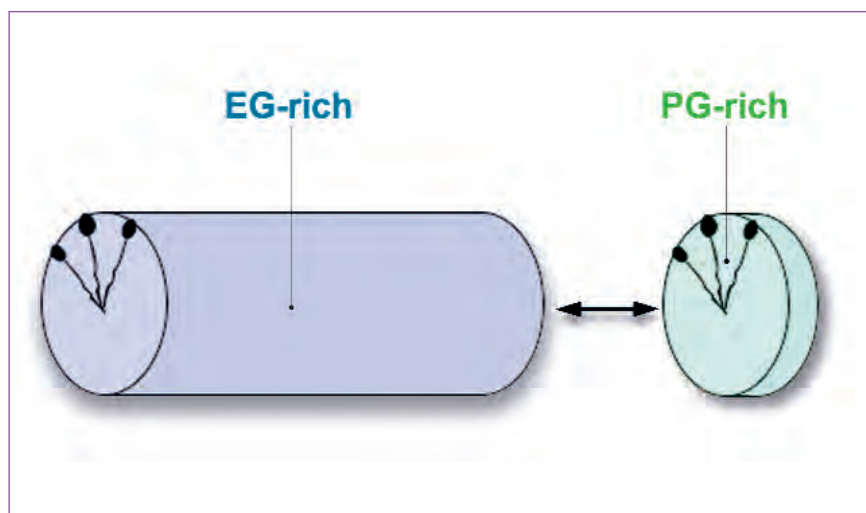


**Figure 2:** Switching from ethylene glycol (EG) to propylene glycol (PG) induces a massive change in the clustering and aggregation.

demonstrates potential for expanding the uses and applications of these two industrial solvents. Amongst others, this may have benefits for protein studies or conservation fluids. Furthermore, owing to special "anti-freeze" properties, EG also finds many commercial applications: now it is possible to consider high-performance cooling fluids containing surfactant micelles for added lubrication and cleaning functions.

## References

- (1) C. Seguin, J. Eastoe, R. Clapperton, R.K. Heenan, I. Grillo, *Colloids and Surfaces A* 282-283 (2006) 134-142; C. Seguin, J. Eastoe, R. Heenan, I. Grillo "Controlling aggregation of non-ionic surfactants using mixed glycol media" *Langmuir* (2007) 23, in press.
- (2) J.R. Lu, Z.X. Li, and R.K. Thomas, *J. Phys. Chem.* 98 (1994) 6559
- (3) C. Carnero Ruiz, *J. Colloid Interface Sci.* 221 (2000) 262

# Using neutron spectroscopy to study dynamics in model membrane systems

## Authors:

**M.C. Rheinstädter**

(University of Missouri-Columbia)

**T. Seydel** (ILL)

**W. Häussler** (TU Munich, Garching)

**T. Salditt**

(Institute for X-Ray Physics, Göttingen)

New developments and improvements in neutron scattering instruments, sample preparation and environments and, eventually, the more and more powerful neutron sources open up the possibility to study collective excitations, i.e. phonons, in artificial and biological membranes. The overall perspective is to establish relationships between collective dynamics and physiological and biological function in model systems, but also in their much more complex biological counterparts

The combination of different inelastic neutron scattering techniques enlarges the accessible window of momentum and energy transfer - or better: accessible length and time scales - and allows to study structure and dynamics on length scales from nearest neighbour distances of lipid molecules or lipid acyl chains to more than 100 nm and time scales from about 0.1 ps to almost 1  $\mu$ s. The fluctuations can be quantified by measuring the corresponding dispersion relations, i.e. the wave vector-dependence of the excitation frequencies or relaxation rates. As an important difference to 'hard' condensed matter, scattering experiments in soft-matter materials suffer from the often missing or unincisive periodic arrangement of the molecules. It is therefore not sufficient to determine the dispersion relation over one periodic unit in reciprocal space (Brillouin zone), i.e. a relatively small range of Q-values, only. Rather, to characterise the fluctuations and to compare experimental results with present membrane theories, the measurement must cover as large a range as possible in length and time scales. The overall objective is to establish dynamics-function relationships in artificial and

biological membranes to couple particularly the collective dynamics to, e.g. transport processes within and across the bilayers. The bilayers are prepared as highly-oriented multi-lamellar membrane stacks on Si-wafers. The 'sandwich samples' for the inelastic experiments consist of up to 20 substrates and about 100.000 stacked membranes (500 mg of deuterated lipids). The mesoscopic collective dynamics in

the model membrane system DMPC (1,2-dimyristoyl-sn-glycero-3-phosphatidylcholine) has been investigated using the spin-echo spectrometers IN11 and IN15 [1]. Highly energy-resolved experiments on the backscattering machines IN10 and IN16 shed light on the dynamics of the membrane hydration water, i.e. the water molecules in the water layer in between the stacked membranes [2].

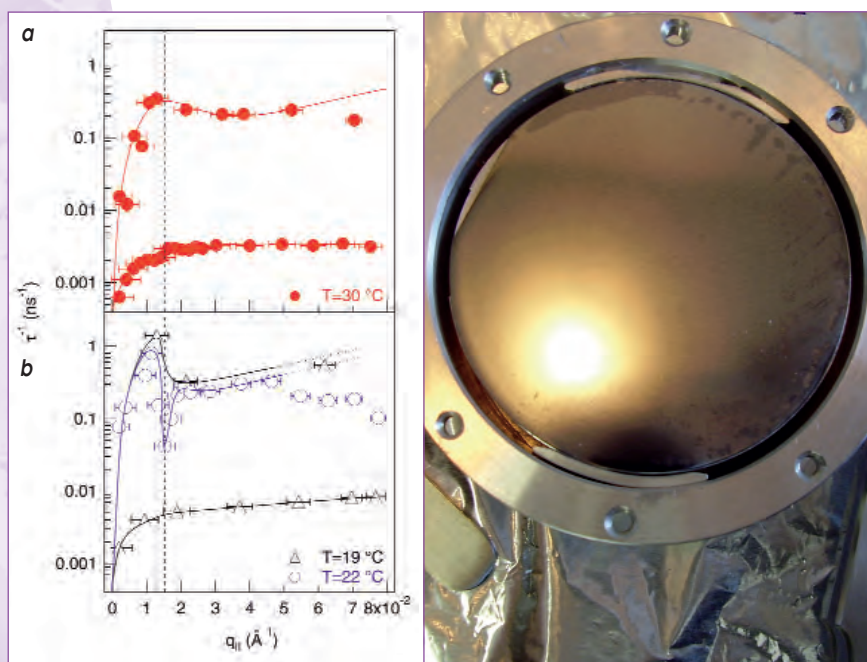


**Figure 1 left:** (a) Dispersion relations at  $T = 30$  °C. The solid line is a fit to a smectic hydrodynamic theory. (b) Dispersion relations in the gel (19 °C) and in the fluid phase (22 °C). A pronounced soft mode is observed at  $Q_{\parallel} = 0.015 \text{ \AA}^{-1}$  at 22 °C (dotted vertical line). Solid lines in (b) are guides to the eye. **Right:** Photograph of the sample.

## Mesoscopic Fluctuations

Fluctuations on the mesoscopic scale are determined by the elasticity parameters of the bilayers, i.e., the compressibility of the stacked membranes,  $B$ , and the bending modulus  $\kappa$ . The relaxations in this regime are in the nano-second time-range with accompanying small  $q$ -values. Spin-echo spectrometers, as IN11 and IN15, turned out to be highly suited for these experiments. **Figure 1** shows the dispersion relation in DMPC for different temperatures in the gel ( $T = 19^\circ\text{C}$ ), the fluid ( $30^\circ\text{C}$ ) phase and at an intermediate temperature, just above the main transition in phospholipid bilayers. For small  $Q$ -values, i.e. length scales of several hundred nanometers, the bilayers behave as liquid films and the corresponding dynamics is basically determined by the viscosity of the membrane water,  $\eta$ , with  $\tau^{-1} \sim Q^2$ . At higher  $Q$ -values and corresponding smaller length-scales the elasticity parameters of the membrane are probed. The critical length-scale for the transition from film to bulk elasticity regime is found to be about 45 nm. The experimental data in the fluid phase can be fitted to a smectic hydrodynamic theory and the elasticity parameters  $B$  and  $\kappa$  and the viscosity  $\eta$  determined to  $B = 1.08 \times 10^7 \text{ J/m}^3$ ,  $\kappa = 14.8 k_B T$  and  $\eta = 0.016 \text{ Pa s}$ . The viscosity of the membrane water appears to be much higher as compared to bulk water ( $0.001 \text{ Pa s}$ ) pointing to distinctly different dynamical properties of the two-dimensional layer of hydration water. As a remarkable feature we find a soft-mode, i.e. an extreme softening of the bilayers, in the critical swelling regime at  $T = 22^\circ\text{C}$ , which occurs on a well-defined length-scale of about 45 nm, probably related to the formation of gel and fluid domains in the co-existence region.

## Membrane Water Dynamics

By careful analysis of the 'elastic' scattering on IN10, that is scattering which is elastic within the excellent energy resolution of  $1 \mu\text{eV}$ , we could identify scattering contributions of the lipids, in particular the lipid acyl chains, and the membrane water, i.e. molecules in the water layer in between the stacked membranes, by their respective  $Q$ -values. The hydration water turns out to

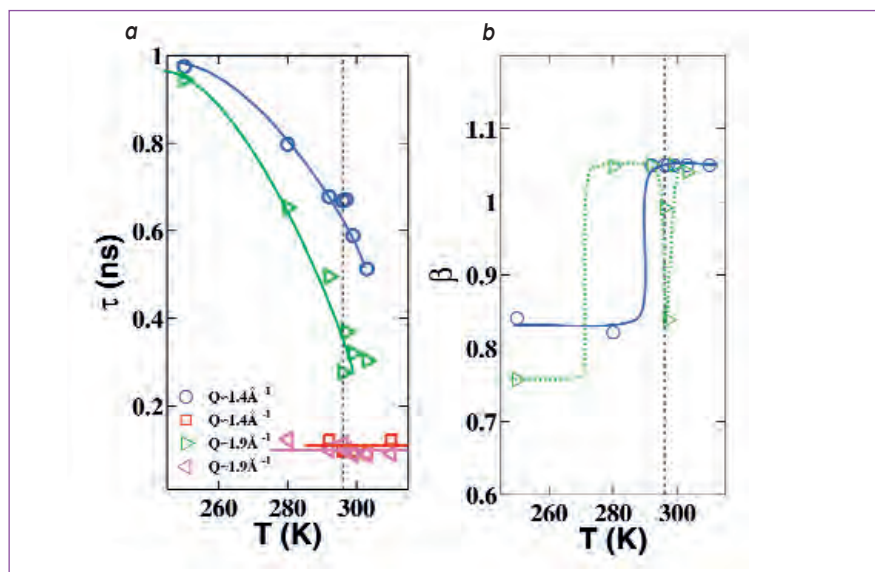
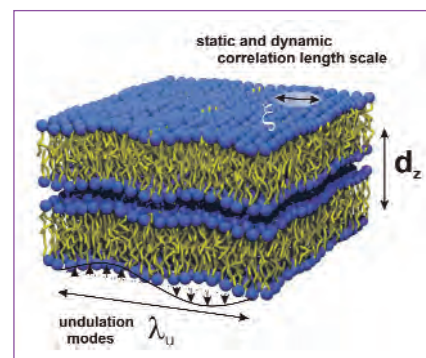


**Figure 2:** (a) Relaxation times at the lipid chain and the water position for all measured temperatures as determined from fits to quasi elastic data. (b) Exponents of the exponential decay as determined from fits of the intermediate scattering function. Solid lines are guides to the eye.

be super-cooled with a freezing temperature of 271 K, 7 K below the freezing of bulk heavy water ( $\text{D}_2\text{O}$ ). A recent experiment on IN16 now allowed determining the relaxation rates of acyl chains and water molecules separately but simultaneously. From a combined analysis in the energy and time domain, we could also determine the stretching exponent,  $\beta$ , for the two processes, i.e. the deviation from single exponential decays of the corresponding correlation functions. We find that the relaxation dynamics highly depends on the local environment in the regimes where lipid tails and water molecules are 'frozen' ( $T < 294 \text{ K}$  for the lipids and  $T < 271 \text{ K}$  for the water) with values for  $\beta$  of  $\beta < 1$ . In the respective fluid phases, the relaxations turn into single exponential. **Figure 2** shows the temperature-dependence of the corresponding relaxation times (a) together with the stretching parameter  $\beta$  (b). Note that in the regime of critical swelling, the water dynamics again develops a distinct 'stretched' character.

Elaborate future experiments should allow to simultaneously determine complete dispersion relations of lipids and water to quantify the corresponding dynamics. It is now widely accepted that the dynamics of biological systems cannot be fully understood without understanding the

dynamics of the aqueous surrounding as well, so that these experiments provide a unique and important insight.



Schematic of lipid bilayers.

## References

- (1) 'Dispersion relation of lipid membrane shape fluctuations by neutron spin-echo spectrometry', M.C. Rheinstädter, W. Häussler and T. Salditt, *Phys. Rev. Lett.* 97, 048103 (2006)
- (2) 'Nanosecond molecular relaxations in lipid bilayers studied by high-energy resolution neutron scattering and in situ diffraction', M.C. Rheinstädter, T. Seydel and T. Salditt, *Phys. Rev.* E75, 011907 (2007)

# Apolipoprotein B-100: a closer look at the protein moiety of a human blood cholesterol carrier

## Authors:

**A. Johs, I. Waldner, P. Laggner and  
R. Prassl** (Institute of Biophysics and  
Nanosystems Research, Graz)

**M. Hammel** (University of Missouri - Kansas City)

**R.P. May** (ILL)

Apolipoprotein B-100 (apoB-100) is the only protein found in human low-density lipoprotein (LDL), which is a key player in cholesterol metabolism. We have determined the low-resolution structure of lipid-free apoB-100 by small-angle neutron scattering (SANS) with contrast variation using advanced shape reconstruction algorithms.

The three-dimensional model of apoB-100 assumes a modular curved shape with a central cavity. In combination with a secondary structure prediction we have constructed a hypothetical domain organisation of apoB-100 on the low-density lipoprotein particle.

Low-density lipoprotein (LDL) is the principal cholesterol carrier in the blood and serves as a transport system for cholesterol from the liver to most tissues of the body. It is also known as 'bad cholesterol', contrary to high-density lipoprotein, HDL. LDL adopts the shape of a globular microemulsion particle consisting of a non-polar ('fatty') core of cholesteryl esters, triacylglycerols and an amphiphilic coating of phospholipid, cholesterol and a single protein component: apoB-100. This protein mediates the recognition, internalisation and lysosomal degradation of LDL by endothelial cells. Thus, apoB-100 plays a leading role in the metabolic pathway of cholesterol and hence in the premature development of atherosclerosis and cardio-vascular diseases.

ApoB-100 is one of the largest known monomeric proteins with 4,536 amino acid residues and a molecular mass of the glycosylated protein of

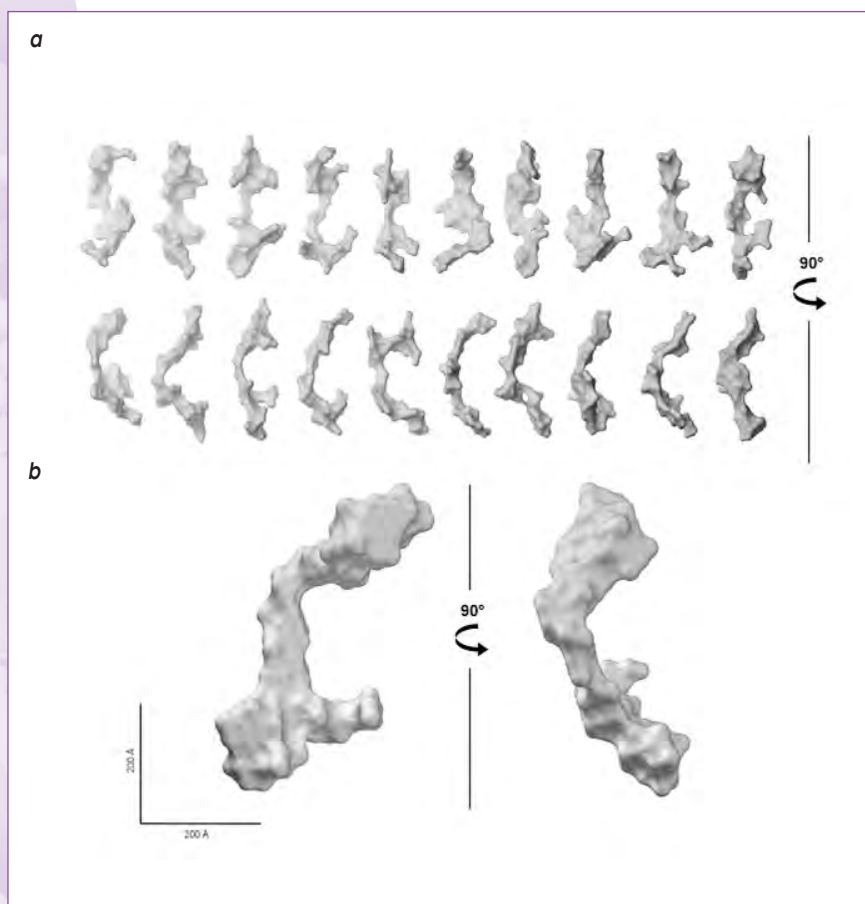
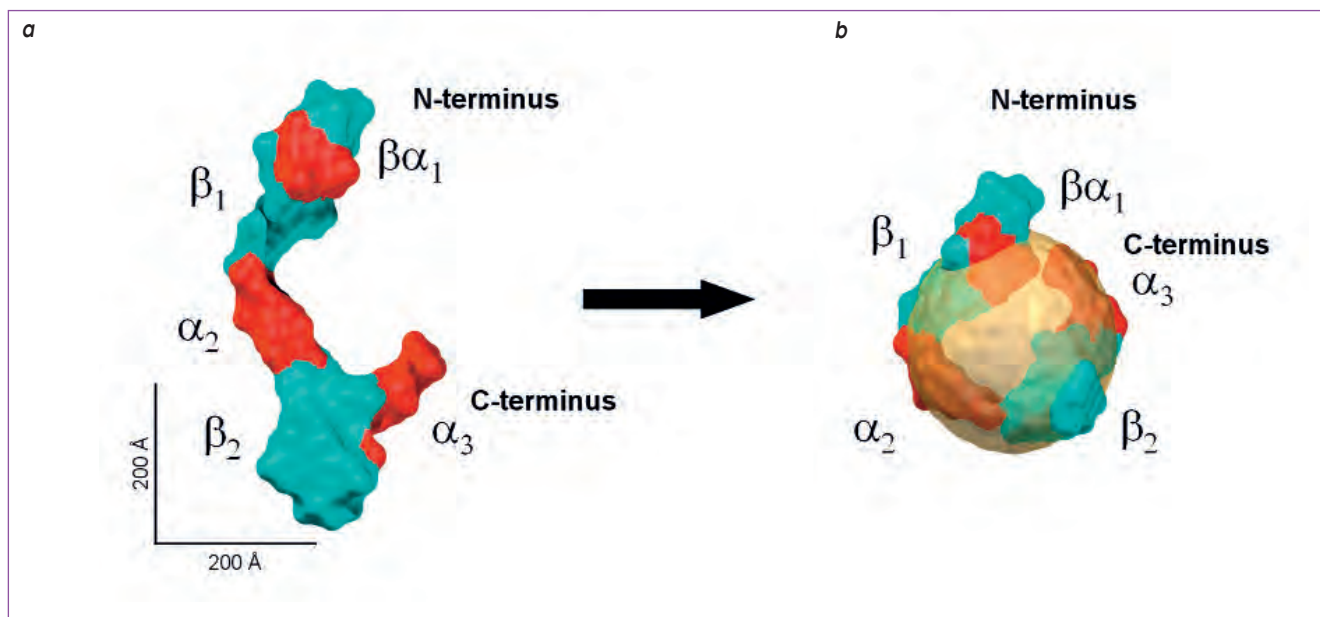


**Figure 1:** (a) Single reconstructed three-dimensional *ab initio* models of lipid-free apoB-100. (b) Average envelope shape of apoB-100.



about 550 kDa. A pentapartite domain structure of amphipathic  $\alpha$ -helices and  $\beta$ -sheets was postulated for lipid-associated apoB-100 [1] forming a long strand surrounding the LDL particle. Further, apoB-100 is characterised by a high hydrophobicity resembling membrane spanning proteins.

Despite extensive attempts to gain knowledge on the molecular structure of this protein by various methodologies during the last three decades, sound information on protein structure is still missing because of its huge size and hydrophobic nature. A reason for this difficulty may be seen in the size polydispersity and complex composition of the lipid moiety in LDL.

Nonidet P40 (nonylphenylpolyethylene glycol) was our surfactant of choice to separate the protein from LDL by removing all associated lipid components. The purified protein-detergent complex was used for SANS experiments at the instruments D11 and D22 of the ILL.

Scattering profiles were recorded while the scattering density of the solubilising detergent was matched at 18%  $D_2O/H_2O$ . Due to the size of the particles, data acquired at two sample-to-detector distances (14.0 and 2.8 m) were merged yielding a scattering profile over a total Q-range of

**Figure 2:** (a) Structure model of apoB-100 with colour-coded secondary structure information. Red:  $\alpha$ -helical structures, blue:  $\beta$ -sheet structures.

(b) Hypothetical model of the LDL particle after superposition of the apoB-100 structure model and a 250 Å diameter sphere representing the lipid components of LDL (yellow).

0.004–0.26  $\text{\AA}^{-1}$ . Indirect Fourier transformation of the scattered intensities yields a pair-distance distribution function that shows a tailing with a  $D_{\max}$  of 600 Å and incorporates separated maxima over a broad q-range. These features already suggest that apoB 100 is an elongated particle consisting of independent modules.

A series of single models was restored by *ab initio* shape reconstruction algorithms [2]. Superposition and alignment of ten separate models (figure 1a), which had similar qualities of fit, led to an averaged structure (figure 1b). The model reveals that apoB 100 has an elongated arch-like structure consisting of single domains connected by structurally flexible regions with a cavity located in the centre of the particle.

Finally, secondary structure elements derived from a secondary structure prediction were mapped onto the surface of the model proportionally to the fraction of their occurrence (figure 2a). Accordingly, we have proposed a hypothetical spatial arrangement of the apoB 100 molecule on LDL (figure 2b).

Taken together, the results of this work highlight the modular arrangement and structural flexibility of apoB-100 and constitute an important milestone in the elucidation of molecular fundamentals of lipid metabolism. The work reported here was selected 'Paper of the week' by the Journal of Biological Chemistry [3] stating it as a major contribution to the field.

## References

- (1) J.P. Segrest, M.K. Jones, V.K. Mishra, G.M. Anantharamaiah and D.W. Garber, *Arterioscler. Thromb.* 14 (1994) 1674-1685
- (2) D.I. Svergun, *Biophys. J.* 76 (1999) 2879-2886
- (3) A. Johs, M. Hammel, I. Waldner, R.P. May, P. Laggner and R. Prassl, *J. Biol. Chem.* 281 (2006) 19732-9

# Pore stabilisation by packing

The thermodynamics and kinetics of fluctuational membrane pore opening and growth in tensionless membranes is modelled in the case of short-range interactions between pores. It is shown that an isolated pore is always unstable irrespective of its size. However, excluded volume interactions in a system of many pores can stabilise pores of a given size in a certain range of external parameters.

## Authors:

**D.J. Bicout** (ILL and ENVL Lyon)

**F. Schmid** (ILL and University of Bielefeld)

**E. Kats** (ILL)

The opening of stable pores in biological membranes is a crucial step for the delivery of biological active molecules, drugs and genes into cells.

Additionally, the formation of pores is supposed to be one key step of the fusion of membranes.

The importance of the fusion of biological membranes is so clear that only a few words such as endocytosis, intracellular trafficking, and viral entry should suffice as a reminder to the reader.

Pores can form and grow in membrane in response to thermal fluctuations and external influences. Pore growth enhances the transport of biomolecules across the membranes and, besides its biological relevance, can produce new prospective biotechnological applications. Holes appear in the membrane via an activated process, and their subsequent growth is controlled by a line tension.

The model free energy  $F(n)$  for the formation of a single pore in a tensionless membrane contains two contributions: a purely energetic part as suggested by Litster [1], and an entropic part as modelled by Shillcock and Seifert [2],

$$F(n) = \begin{cases} 0 & ; 0 \leq n < n_0 \\ F_0 + (\lambda - k_B T \ln z)[n - n_0] & ; n \geq n_0 \\ + (2 - \alpha)k_B T \ln(n/n_0) & ; n \geq n_0 \end{cases}$$

where  $F_0$  is the free energy required to create or initiate a pore of smallest size  $n_0$ ,  $\lambda$  the line tension of the pore edge,  $k_B T = 1/\beta$  the thermal energy,  $z$  the connectivity constant of the matrix medium, and  $\alpha$  an exponent related to the entropy of the possible pore contour conformations.

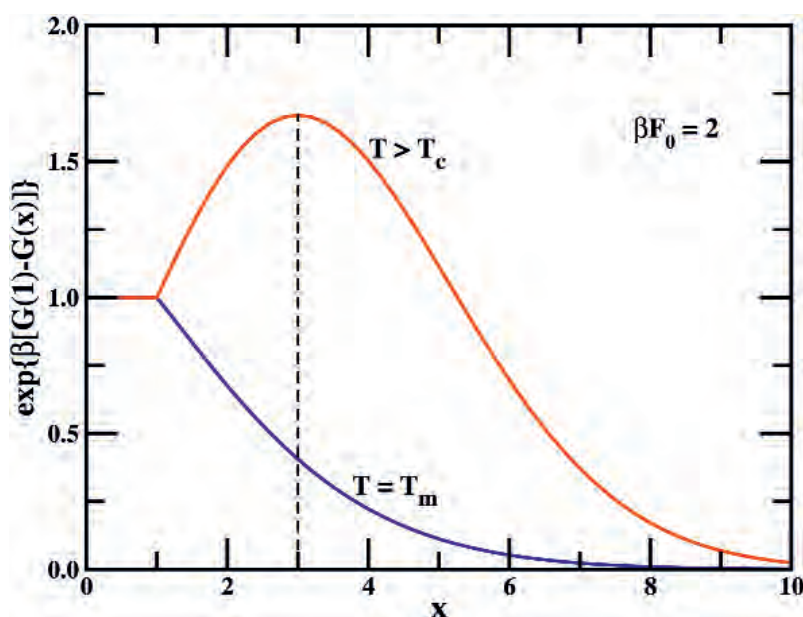


**Figure 1:** Reduced free energy as a function of the reduced pore size for different temperature regimes. The dashed vertical line indicates the maximum in the pore size distribution.

With the assumption that the pores do not interact unless close to each other (confirmed recently in [3]), only excluded volume interactions are considered, and using the mean field approach, the total free energy reads as

$$F = \sum_n N(n)F(n) - k_B T \sum_n N(n) \ln \left[ \frac{e^{(A - A_0)}}{a_0 N(n)} \right]$$

where  $N(n)$  counts the number of pores of size  $n$ , and  $A - A_0$  is the area accessible for pores,

$$A_0 = \sum_n N(n)a(n).$$

Here  $a(n)$  is the difference between the excluded and the actual pore area, which is nonzero due to the fractal shape of the pores and scales like  $a(n) = a_0(n/n_0)^{2\nu}$  with the Flory exponent  $\nu$ . In what follows, we will deal on the reduced pore size  $x = n/n_0$ , and introduce the characteristic quantities

$$Q_0 = n_0 \ln(z) \quad ; \quad T_m = \frac{l}{k_B \ln(z)}.$$

Single, independent pores grow indefinitely at the temperature  $T_m$ , thus destabilising the membrane, because the line tension becomes negative. In a multiple pore system, however, membranes remain stable even

beyond  $T_m$ . The excluded volume interaction between pores can stabilize membranes even in parameter regions where the line tension is negative. The pore size distribution in this case may have a maximum at nonzero contour length  $n$ . Three regimes can be distinguished (see details in our publication [4]): (i) At low temperatures,  $T < T_m$ , the line tension is positive, and the pore size distribution  $N(n)$  drops monotonically. (ii) At intermediate temperatures,  $T_m < T < T_c$ , the line tension is negative, and the pores are stabilised by the presence of other pores; the pore size distribution still drops monotonically. (iii) At high temperatures  $T > T_c$ , a maximum emerges in the pore size distribution, i.e. pores have a preferable size. **Figure 1** shows the effective pore energy  $G(x)$  for two temperatures above and below  $T_c$ . Above  $T_c$ , it has a minimum at finite  $x$ . In the packing stabilized regime, beyond  $T_c$ , one should thus expect that the membrane contains many long-lived pores with a size distribution exhibiting one preferred contour length. Indeed, such structures can be observed in membranes, and also found in simulations of simple model membranes (see **figure 2**).

In conclusion, a new excluded volume mechanism is proposed that stabilises structures with many pores. Such a process, which seems to have been overlooked in the literature up to now, promotes sieve-like membrane structures. There should be great benefits in applications in biotechnology and medicine in allowing the control of membrane permeability.

## References

- (1) J. Litster, *Phys. Lett., A*, 53 (1975) 193
- (2) J.C. Shillcock, U. Seifert, *Biophys. J.*, 74 (1998) 1754
- (3) C. Loison, M. Mareschal, F. Schmid, *J. Chem. Phys.*, 121 (2004) 1890
- (4) D.J. Bicout, F. Schmid, E.I. Kats, *Phys. Rev. E*, 73, 060101(R) (2006)

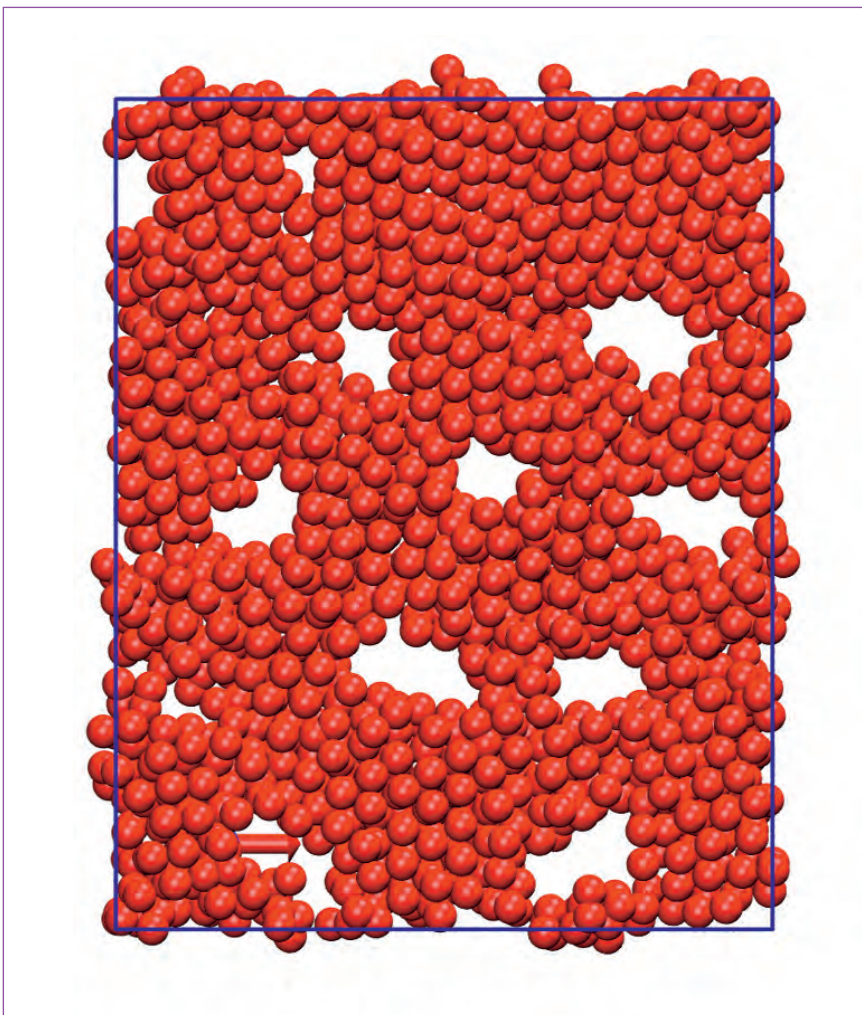


**Figure 2:** Simulation snapshot of a porous membrane.

## The solvation of complex species

### Authors:

**P.E. Mason and J.W. Brady**

(Cornell University, Ithaca)

**G.W. Neilson and J.E. Enderby**

(University of Bristol)

**M.-L. Saboungi** (CNRS Orléans)

**G.J. Cuello** (ILL)

Water is vital, both as a solvent in which many of the body's solutes dissolve and as part of many metabolic processes. Neutron diffraction experiments have been one of the most effective methods for providing atomic-resolution structural data about water and solutes in such solutions. However, these experiments on aqueous solutions of molecular species, such as sugars and amino acids, are notoriously difficult to interpret due to the complexity of the data obtained. A new approach, combining neutron diffraction with isotopic substitution experiments on specifically-labelled samples with molecular dynamics simulations, makes it possible to fully understand the structure of these biomolecules in the water environment.

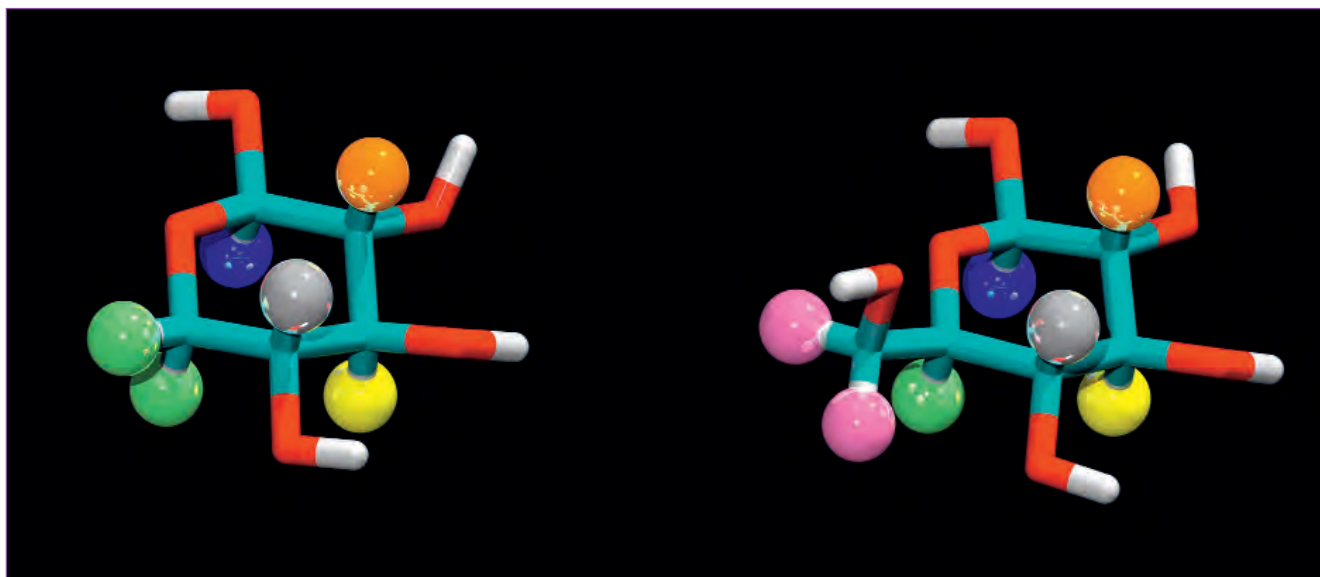
Although they have long been neglected compared to other classes of biological molecules such as proteins and nucleic acids, sugars are important for many reasons. As the end point of photosynthesis, carbohydrates are vital in biological energy storage in both plants and animals, and play important structural roles as well. Furthermore,

they are involved in a wide range of molecular recognition processes in phenomena as diverse as fertilisation of egg cells by sperm, infection by bacteria and viruses, cell adhesion, and vaccine design and function. Perhaps as importantly, sugars can serve as a general model for small biological molecules interacting with water. Sugars offer several advantages for neutron

diffraction experiments over other biological molecules such as amino acids: they are much more soluble at normal temperatures, are chemically stable, contain a number of functional groups and are relatively rigid, simplifying the interpretation of their interactions with the solvent. Sugars are known to interact strongly with water in aqueous solutions and to significantly affect the



**Figure 1:** Computer simulations of how water structures around D-glucose (right) and D-xylose (left). Regions of high density relative to bulk water are shown as contours at twice the bulk water density in light green for the glucose and yellow for the xylose.



properties of the systems that contain them, inhibiting freezing and increasing the viscosity, for example. Computer simulations have been used to explore how sugar solutes impose structure on the surrounding water, such as is shown in **figure 1**, and how the water affects the sugar conformation, but it has proven more difficult to explore such structuring experimentally using neutron diffraction.

Neutron diffraction measurements on an aqueous solution provide weighted averages of the partial structure factors for each pair of atom types in the system. The interpretation of these data for even relatively simple systems, such as solutions of monatomic ions in water, is complicated by the large number of peaks in the real-space radial correlation functions. The interpretation of experimental data for solutions of large asymmetric molecules like glucose, with 24 atoms, would seem to be hopeless. The technique of neutron scattering with isotopic substitution (NDIS) can be used to reduce the data into the structural correlations between one atom type and all other atom types in the system. Unfortunately, in a large chiral molecule like glucose, replacement of the non-exchangeable hydrogen atoms with deuterium still leaves a complicated average structure factor since each of these atoms is in a different structural environment. However, exploiting the beam intensity and instrument stability

**Figure 2:** Experiments were conducted on a series of D-glucose (right) and D-xylose (left) samples selectively labeled with a single H/D substitution at each position shown by the colored spheres. Double substitutions were made in the case of the C6 aliphatic hydrogen atoms of glucose, shown in light purple on the right, and in that of the C5 hydrogen atoms of xylose, shown in light green on the left.

available at ILL, it is possible to design an NDIS experiment that overcomes these difficulties. By synthesising a glucose sample with deuterium substituted at only one non-exchangeable position, it is possible to obtain diffraction data for the environment around that specific site with acceptable counting statistics. Even these highly specific structural data cannot be interpreted without further information. With the help of parallel molecular dynamics simulations on an identical system, however, the different peaks in the experimental radial correlation function can be assigned, making it possible to interpret the diffraction data in terms of specific correlations between pairs of individual atoms.

Such an approach was used to study aqueous solutions of D-glucose and D-xylose [1,2]. **Figure 2** illustrates the non-exchangeable hydrogen positions that have been individually labelled with deuterium in different samples. The individual peaks in the radial distribution functions for these molecules to specific intramolecular correlations could be clearly assigned. Since some of the interatomic distances in these molecules change as the hydroxyl and hydroxymethyl groups adopt different

rotameric conformations, constrained molecular dynamics simulations for each of the possible conformations have helped distinguish which conformation gives structure factors most consistent with the experimental data. These methods could identify the predominant conformation for the C4 hydroxyl group of D-xylose and the equilibrium conformational population for the exocyclic hydroxymethyl group of D-glucose. In a future extension of this work, the local structure of the solvent water will be studied around each of the substituted hydrogen atoms on the sugar molecule.

## References

- (1) *Neutron diffraction and computer simulation studies of D-xylose*, P.E. Mason, G.W. Neilson, J.E. Enderby, M.-L. Saboungi and J.W. Brady, *J. Am. Chem. Soc.* 127 (2005) 10991-10998
- (2) *Determination of a hydroxyl conformation in aqueous xylose using neutron scattering and molecular dynamics*, P.E. Mason, G.W. Neilson, J.E. Enderby, M.-L. Saboungi and J.W. Brady, *J. Phys. Chem. B* 110 (2006) 2981-2983

# “What does the bottle matter?” A liquid crystal confined into a nanocapillary

## Authors:

**D. Morineau, R. Lefort and R. Guégan**

(GMCM Rennes)

**M. Guendouz** (FOTON Lannion)

**B. Frick** (ILL)

Fluids confined in containers of nanometric size exhibit very exceptional properties, which would be different if they were filled in a container of macroscopic size. They show anomalous molecular mobility, peculiar phase transitions and unusual intermolecular ordering. These phenomena depend on the size of the nanocontainer and on the nature and strength of its interaction with the fluid. New surprising effects show up when confining liquid crystals, which are related to the morphology of the nanocapillary-liquid crystal interface.

“What does the bottle matter?”, provided the liquid inside retains its everlasting benefic properties... Alfred de Musset [1] would be surprised to learn that his passionate citation might only be true provided the bottle is not too narrow, and that the understanding of the physical properties of molecular phases

confined at a nanometer scale has become, two centuries later, of worldwide interest [2]. Indeed, when the size of a nanometric container compares with the typical lengths that rule the bulk properties of a system at the molecular level, strong geometric restrictions may become prevailing. For instance, they can disrupt crystalline order,

or inhibit putative cooperative relaxation processes in supercooled liquids. The energy of the high nanocontainer-fluid interfacial area is also crucial. This surface interaction may shift phase transitions temperatures and affect the molecular mobility. The situation is even more complex for anisotropic phases, which are expected to be

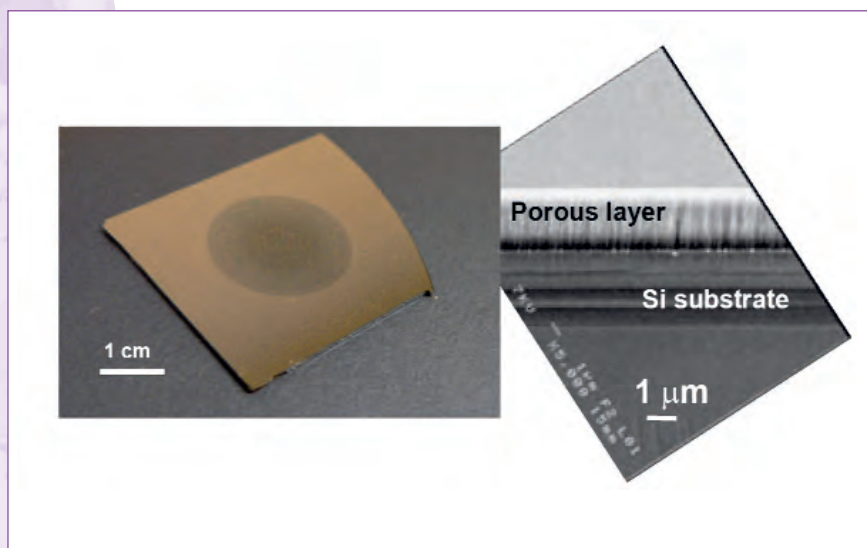


**Figure 1:** Complex fluids confined in capillaries of macroscopic dimension  
© <http://www.arc-international.com/presse/fichiers/arcoroc/ow/hurricane.jpg>

**Figure 2:** Nanocapillaries obtained from the columnar phase of porous silicon.  
Top view of the porous silicon wafer (left). The surface of the porous layer appears as a shaded disk.  
Side view of the porous layer by scanning electron microscopy (right).  
The nanochannels are aligned perpendicular to the surface of the porous layer.

sensitive to the dimensionality of the container as well.

A further effect, due to the morphology (irregularity) of the inner surface of the nano-container, has shown up in the case of confined liquid crystals and is related to the concept of frozen quenched disorder in confinement.

Liquid crystals are elastically soft materials and present anisotropic phases with weak orientational and translational orders, which are directly coupled to surfaces and external fields. The interaction between a confined liquid crystal and its nanoporous container acts as a quenched field, whose nature depends on the morphology of the porous solid. Strongly disordered porous materials can be used experimentally to introduce an almost spatially homogeneous random pinning of the liquid crystal [3]. Such a situation is mostly encountered for random porous materials (aerogels and aerosils dispersions), which are isotropic and homogeneous materials.

Random field effects for a simpler and anisotropic morphology were introduced by confining an archetype liquid crystal in porous silicon nanochannels [4]. Porous silicon layers were prepared with a parallel arrangement of unconnected uniaxial channels (diameter:  $\sim 30$  nm, length:  $30 \mu\text{m}$ ) running perpendicular to the surface wafer (figure 2). The preferential alignment of all the channels prevents powder average limitations when measuring anisotropic observables. Despite the apparent regular morphology of the porous container, strong anisotropic quenched disorder is expected from the highly corrugated inner surface of the channels at microscopic length scales, i.e.  $\sim 1$  nm.

Fully hydrogenated 4-n-octyl-4-cyanobiphenyl (8CB) has been chosen as a reference liquid crystal. It undergoes, with increasing temperature, the following sequence of phases: crystal (K), smectic A (A), nematic (N) and isotropic (I) with the following transition temperatures:  $T_{KA}=294.4$  K,  $T_{NA}=305.8$  K and  $T_{NI}=313.5$  K.

Extreme alteration of the phase diagram of 8CB in porous silicon has been observed by neutron diffraction (G6.1, LLB, Saclay) (figure 3). Crystallisation is strongly

depressed on cooling and leads to two crystalline phases below 250 K, which do not correspond to stable phases of bulk 8CB. More remarkable is the absence of a nematic-smectic transition, which is replaced by a reversible and gradual increase of a short-range translational order over an extremely wide temperature range. This study also proves that the increase of the smectic correlations on cooling first arises from thermal fluctuations, while an additional contribution due to static disorder dominates at lower temperatures. The balance between the strength of quenched disorder and the smectic elastic energy leads to the progressive growth of a saturating smectic correlation length from 3 nm at the bulk nematic-smectic transition temperature up to 12 nm at 250K, which supports recent theoretical predictions [3]. Because of the one-dimensional topology of the porous silicon channels, the short-range smectic order grows preferentially in the direction of the nanochannels long axis.

The temperature variation of the molecular dynamics of the confined fluid was monitored by incoherent quasielastic neutron scattering on IN16 (ILL) [5]. A large reduction of the translational diffusion is observed in the liquid phase at temperatures as high as 315 K, which is well above the isotropic-nematic transition. Even more striking is the molecular dynamics of the short-range-ordered smectic phase, which displays a 'glass-like' slowdown on decreasing temperature. Such strongly hindered molecular dynamics can find its origin at different levels. First of all, interfacial interactions can induce a dominant heterogeneous slowing-down, distributing molecular relaxation times from the surface to the centre of the pores. But this continuous slowing-down also follows the growth of the anisotropic static correlation length that reflects the unusual smectic phase behaviour of 8CB in porous silicon. This length is restricted to nanometric scale as a consequence of quenched disorder, and can therefore compete with the putative characteristic sizes that would measure the extent of cooperativity of the molecular dynamics.

As a matter of fact, the bottle matters!

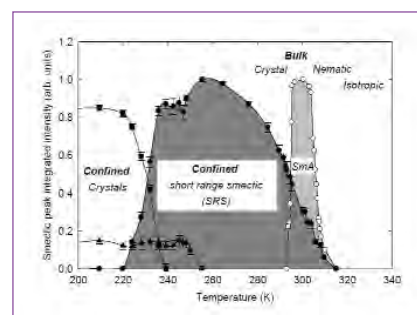


**Figure 3:** Phase behaviour of bulk and confined 8CB, deduced from the temperature-dependent intensity of selected Bragg peaks characteristic for different phases. The smectic Bragg peak of bulk (open circle) and confined 8CB (filled circles) is located at  $0.2\text{\AA}^{-1}$ . The crystalline Bragg peaks corresponding to two different phases appear successively for  $q$ -values of  $0.25 \text{\AA}^{-1}$  and  $0.15\text{\AA}^{-1}$  (squares and triangles respectively).

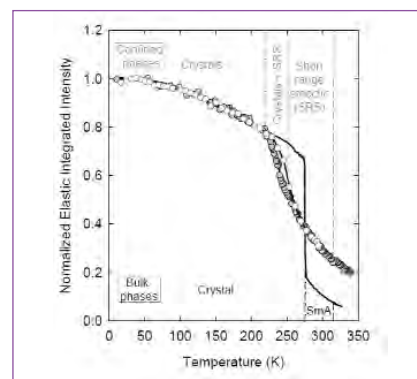


**Figure 4:** Energy resolved elastic scattering for 8CB confined in porous silicon (symbols) and for bulk (solid line), measured on the neutron backscattering spectrometer IN16 (filled symbols: cooling, open symbols heating curve; data are integrated from  $0.4$  to  $1.9 \text{\AA}^{-1}$ , corrected for empty sample contribution and are normalised at the lowest temperature).

## References

- (1) «What does the bottle matter?»  
A. de Musset, 'La coupe et les lèvres' (1836)
- (2) International Workshop on Dynamics in Confinement, ILL, (2006)
- (3) T. Bellini, L. Radzihovsky, J. Toner and N.A. Clark, *Science* 294 (2001) 1074
- (4) R. Guégan, D. Morineau, C. Loverdo, W. Béziel and M. Guendouz, *Phys. Rev. E* 73 (2006) 011707
- (5) R. Guégan, D. Morineau, R. Lefort, A. Moréac, W. Béziel, M. Guendouz, J.-M. Zanotti and B. Frick, *J. Chem. Phys.*, 126 (2007) 064902

# Fission of rotating nuclei

## Authors:

**A. Gagarski, I. Guseva and G. Petrov**  
(PNPI, Gatchina)

**F. Gönnenwein**  
(University of Tübingen)

**M. Mutterer** (Technical University  
Darmstadt)

**V. Nesvizhevsky and T. Soldner** (ILL)

In fission induced by cold polarised neutrons, it was discovered that the fissioning compound rotates at scission in the reaction  $^{235}\text{U}(n,f)$ . The rotation is non-uniform and the angles of rotation are extremely small. Rotation angles below  $0.1^\circ$  were revealed by observing the shifts in the angular distributions of ternary  $\alpha$ -particles upon flipping the spin of the neutrons inducing fission.

Fission reactions induced by polarised cold neutrons have so far mainly been used to study symmetry laws in fission, like e.g. parity conservation. In the context of these studies a startling phenomenon was observed. It was found that the fission axis, i.e. the axis along which the fission fragments are flying apart in opposite directions, is rotating in a plane perpendicular to the spin of the polarised neutron. Since following capture of a polarised neutron the compound nucleus is also polarised, a collective rotation of the fissioning system appears to be quite feasible. However, following scission the fragments are accelerated within times of some  $10^{-21}$  s up to their eventual velocity of about 1 cm/ns. The moment of the rotational inertia will increase with a similar time constant. For fragments at infinity the moment of inertia will be infinite also. Hence, for a given angular momentum the angular velocity will very quickly come to a virtual stop. For a typical angular momentum of 1h simple estimates yield integrated total angles of rotation of much less than  $1^\circ$ . In the past, such small angles appeared to be not measurable in fission experiments.

In the present experiment, ternary fission in the reaction  $^{235}\text{U}(n,f)$  with cold polarised neutrons was under investigation. Ternary fission is a rather rare process where besides the two main fission fragments a third light charged particle – in most cases an  $\alpha$ -particle – is ejected. A characteristic feature of this process is the angular distribution of the ternary particles which is centred roughly perpendicular to the fission axis. This is readily understood as being due to the Coulomb forces being exerted by the

two fission fragments on the  $\alpha$ -particle. The experimental set-up sketched in **figure 1** takes these angular correlations into account. In the experiment a thin  $^{235}\text{U}$  target is irradiated by a neutron beam with spin polarisation pointing either parallel or anti-parallel to the beam direction. Fission fragments and ternary particles are intercepted near a plane perpendicular to neutron beam and polarisation. If now the nucleus undergoing fission is rotating, the  $\alpha$ -particles will experience a rotating

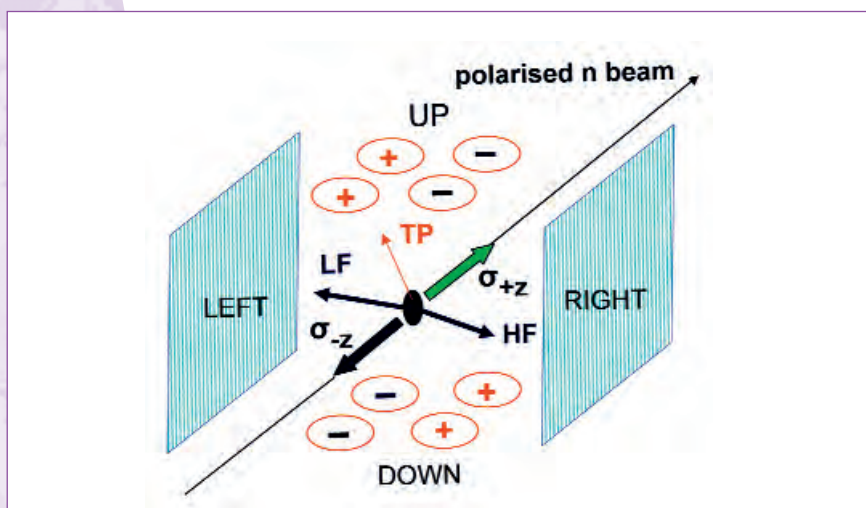
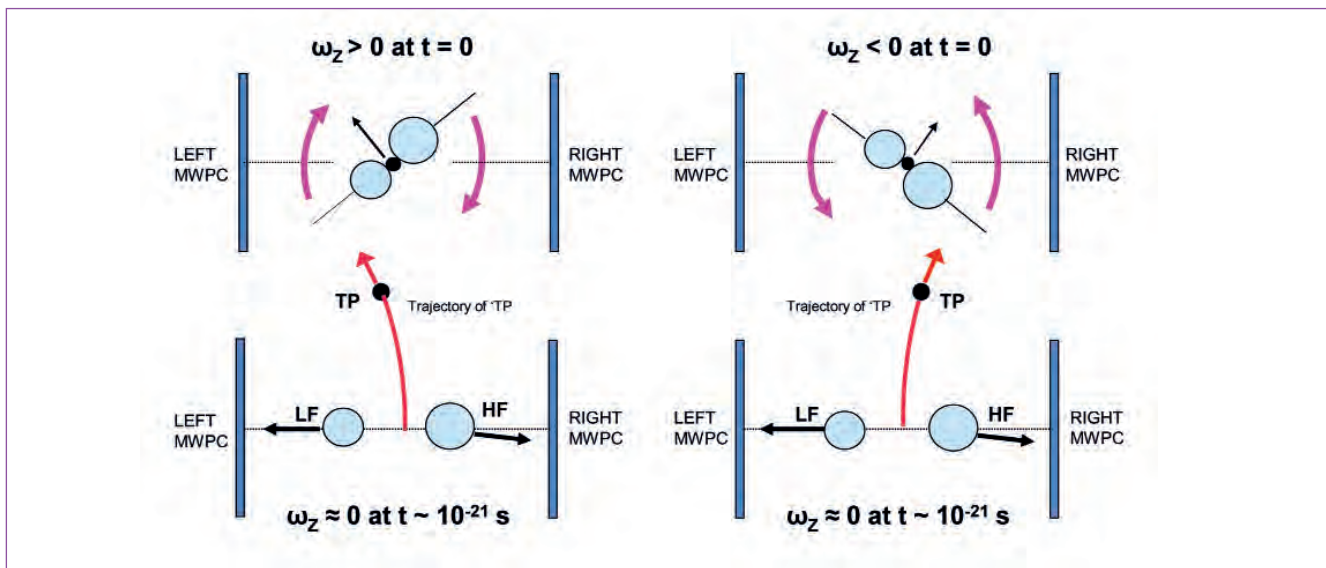


**Figure 1:** Sketch of the experimental set-up. The  $^{235}\text{U}$  target at the centre of a reaction chamber is irradiated by a neutron beam with spin polarisation either parallel ( $\sigma_{+z}$ ) or anti-parallel ( $\sigma_{-z}$ ) to the beam. The two complementary fission fragments are measured by Multi-Wire-Proportional-Counters (in the figure to the Left and Right) while the ternary particles are picked up by two arrays of 4 large surface barrier detectors each (in the figure labelled Up and Down). For the signs labelling the  $\alpha$ -detectors see text.



Coulomb field and at least partly will follow the rotation. Their trajectories will hence be slightly bent which means that their angular distributions will be shifted as compared to a non-rotating nucleus. In the experiment, flipping the neutron spin leads to an inversion of the sense of rotation of the fissioning compound. Flipping periodically the neutron spin the angular distributions of the  $\alpha$ -particles will wobble back and forth. This is illustrated in **figure 2** for a neutron beam perpendicular to the drawing plane. Depending on the sense of rotation  $\omega_z > 0$  or  $\omega_z < 0$  at the time of scission  $t = 0$  or  $\omega_z < 0$  at the time of scission  $t = 0$  the trajectories are bent in opposite directions.

Intercepting the  $\alpha$ -particles to the right and left of the most probable angle, i.e. on the slopes of the angular distributions as in the set-up of **figure 1**, the count rates measured will be sensitive to very small shifts in the distribution. When evaluating the asymmetry  $A = (N^+ - N^-) / (N^+ + N^-)$  with  $N^+$  and  $N^-$  the count rates for opposite senses of rotation, a characteristic pattern of signs for  $A$  is observed, as indicated in **figure 1**. On average the modulus of  $A$  equals  $|A| = 3.30(13) \cdot 10^{-3}$ . Albeit small the effect having been dubbed the "ROT effect" is seen to be manifest for the reaction investigated. Assuming that the fissioning compound is rotating with a given angular momentum around the neutron beam and spin axis, trajectory calculations for  $\alpha$ -particles have been performed in a rotating lab system. With a reasonable value of  $1\hbar$  for the angu-

**Figure 2:** Model to explain how the rotation of the fission axis is measured. Left (right) panels are for rotations clockwise (anti-clockwise) in figure 1. Top panels sketch the configuration at scission ( $t = 0$ ). Bottom panels represent the final situation some  $10^{-21}$  s later with light (LF) and heavy (HF) fragments prone to be detected. Ternary particles (TP) escape with their angular distributions being shifted in opposite directions for the two senses of rotation. The figure is not to scale.

lar momentum of rotation, asymmetries compatible with experiment are found. The interesting figure to be deduced is the final angle of rotation of the fission axis. The angle is smaller than  $0.2^\circ$ . In summary, the surprising fact is less that nuclei undergoing fission induced by pola-

rised neutrons are rotating than the power of the spin flip technique allowing to measure angles well below  $1^\circ$  in a violent nuclear reaction like fission. For theoreticians, the challenge will be to understand which properties of the fissile nuclei govern the outcome of the ROT effect.

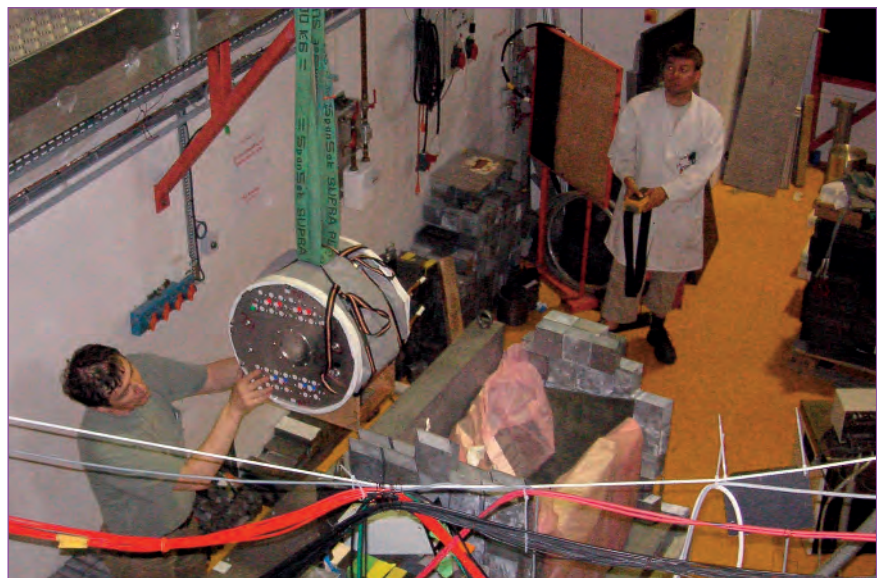


**Figure 3, from left:** Alex Gagarski and Torsten Soldner setting up the experiment at the beam position PF1B. The fission chamber is arriving and about to be buried in a lead house to shield neighbouring installations against fission neutrons and gammas.

# Low energy phonon structure of $^{150}\text{Sm}$

## Authors:

**H.G. Börner, P. Mufti and M. Jentschel** (ILL)  
**N.V. Zamfir** (Yale University, New Haven and NIPNE, Bucharest)  
**R.F. Casten and E.A. McCutchan** (Yale University, New Haven)  
**R. Krücken** (Yale University, New Haven and TU Munich, Garching)

The low-lying decay scheme of  $^{150}\text{Sm}$  was studied with the GAMS spectrometers. Precise energies, as well as lifetimes measured with the GRID technique, provided important structural information. A comparison with the predictions of Interacting Boson Model calculations confirmed that this nucleus is very close to the phase transition between spherical and quadrupole axial symmetric shapes, lying just prior to the critical point on the spherical side of the transition.

The nature and evolution of collectivity and coherence in atomic nuclei is one of the most fundamental issues in nuclear structure. One of the long-persisting issues which has been under intense study in recent years is whether finite nuclei can exhibit phase coexistence and phase transitional behaviour of the type observed in other physical systems. It has long been thought that true phase transitional behaviour was impossible, at least at low-excitation energies where the level densities are low and states are discrete. Recent evidence [1-3], however, in  $^{152}\text{Sm}$  suggests that phase transitions and phase co-existence may indeed exist in atomic nuclei. Level sequences representing deformed and spherical-type states have been identified. These coexisting deformed and spherical structures have been reproduced in both Interacting Boson Approximation (IBA) Model and Geometric Collective Model (GCM) calculations [4, 5]. These results prompted the development of the X(5) critical point model [6] by F. Iachello, to describe nuclei at the

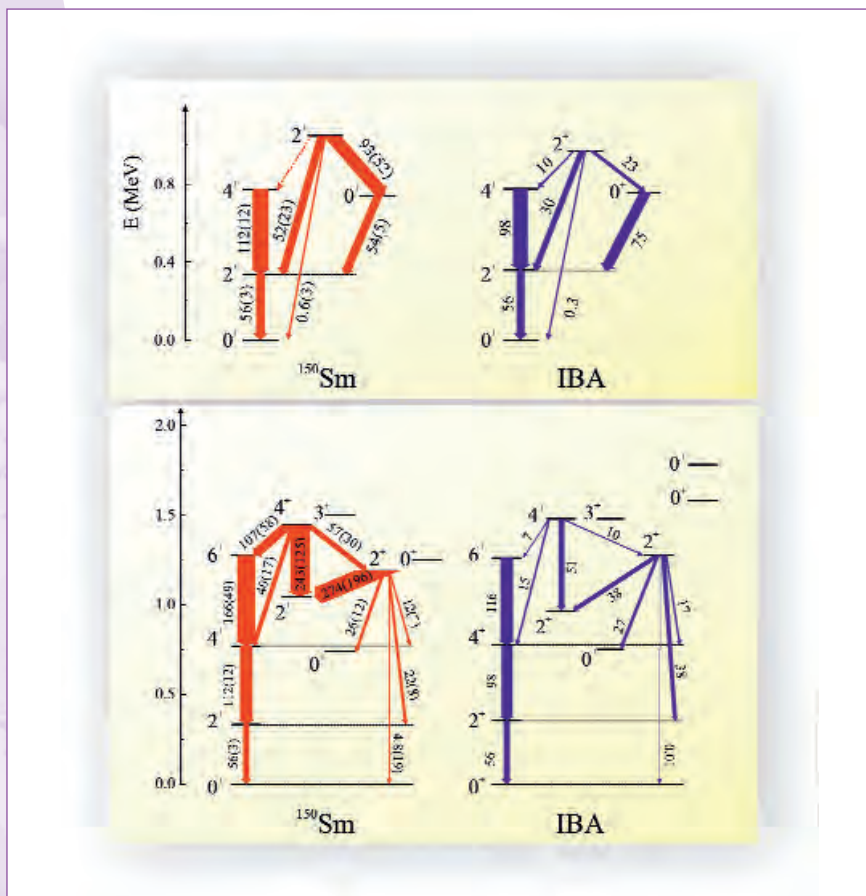


**Figure 1:** (Top) Experimental absolute electromagnetic transition rates compared with the IBA predictions for transitions from the  $4_1^+$ ,  $2_2^+$ , and  $0_2^+$  levels belonging to the 2 quasi phonon multiplet. The thickness of the transition's arrows is proportional to the transition rate. (Bottom) Same as top, but for the transitions from  $6_1^+$ ,  $4_2^+$ , and  $2_3^+$  levels belonging to the 3 quasi phonon multiplet.



The Gams 5 spectrometer which was used to determine lifetimes and gamma-ray transition energies in the experiment.

critical point of the phase transition from spherical to axially deformed shapes. The predictions involve a more deformed ground-state structure and a less deformed band built on the  $O_2^+$  level.  $^{152}\text{Sm}$  was the first nucleus identified (see for instance ILL Annual Report 2000) to exhibit a structure close to the X(5) predictions.

The purpose of the study presented here was to provide a very precise decay scheme of neighboring  $^{150}\text{Sm}$  populated in the  $(n,\gamma)$  reaction. Precise gamma-ray energies were measured using the ultra-high resolution GAMS4 crystal spectrometer and level lifetimes were determined using the GRID technique. With the help of the lifetimes one can deduce the electromagnetic transition probabilities. **Figure 1** presents the comparison of the empirical low-lying spectrum and transition strengths of  $^{150}\text{Sm}$  with the IBA calculations. A phonon-like structure is evident in both the experimental spectrum and the IBA calculations. The

energies and decay strengths suggest that the  $4_1^+$ ,  $2_2^+$  and  $O_2^+$  states (**figure 1** top) are members of the 2 quasi-phonon multiplet while the  $6_1^+$ ,  $4_2^+$ , and  $2_3^+$  states (**figure 1** bottom) are members of the 3 quasi-phonon multiplet. This establishes the ground state of  $^{150}\text{Sm}$  as close to a spherical vibrator. Experimentally, a single excited  $O^+$  state is observed around the 3-phonon multiplet energy, whereas the IBA predicts two closely spaced  $O^+$  states at a similar energy. The identification of the  $O_2^+$  state as possibly corresponding to a deformed structure would indicate that the character of the level sequences in  $^{150}\text{Sm}$  is opposite to that of  $^{152}\text{Sm}$ , with a spherical ground state and a deformed excited state structure.

This suggests that  $^{150}\text{Sm}$  is located before the phase transitional point in the evolution from spherical to deformed structures. In conclusion, the comparison of the new data with detailed IBA calculations, allowed

identifying the quasispherical phonon structure of this nucleus and a possible coexisting deformed state.

## References

- (1) R.F. Casten et al., *Phys. Rev. C* 57 (1998) R1553
- (2) N.V. Zamfir et al., *Phys. Rev. C* 60 (1999) 054312
- (3) T. Klug, A. Dewald, V. Werner, P. von Brentano and R.F. Casten, *Phys. Lett. B* 495 (2000) 55
- (4) F. Iachello, N.V. Zamfir, R. F. Casten, *Phys. Rev. Lett.* 81 (1998) 1191
- (5) J.Y. Zhang, M.A. Caprio, N.V. Zamfir and R.F. Casten, *Phys. Rev. C* 60 (1999) 061304
- (6) F. Iachello, *Phys. Rev. Lett.* 87 (2001) 052502

# The interaction potential between benzene and graphite surfaces resolved using spin-echo spectroscopies and MD calculations

## Authors:

P. Fouquet and M. Johnson (ILL)  
 A.P. Jardine, H. Hedgeland,  
 G. Alexandrowicz, W. Allison and J. Ellis  
 (University of Cambridge)

Dynamics of liquids in mesoporous confinements have been a field of intense study recently as many interesting effects are observed, such as a change in the glass transition temperature with the pore diameter (1). The establishment of a general model for these systems is hindered at present by the fact that the dynamic interaction between molecules and the matrix surface is scarcely known since the dynamics of the molecules situated close to the surface cannot be extracted generally from bulk experiments. A new approach has been developed, combining bulk and surface high-resolution dynamics studies with molecular dynamics (MD) modelling, applied to the benchmark system of benzene diffusion on graphite.

Extracting the dynamics of near surface atoms from bulk studies is generally not straightforward as timescales of diffusion vary gradually when the distance from the surface increases. Computer simulations would be a very useful tool here, but no method has been validated so far to model the surface-molecule interaction in these systems well enough. We present an approach that will solve many of the open questions. The key point of the method is to reduce the system to a (sub-)monolayer of surface-adsorbed molecules. We have studied a system of benzene in carbonous confinements, reduced in this way, with a combination of high-resolution spectroscopies and computer simulations. For diffusion with relaxation times in the ps to ns range, spin-echo spectroscopies [2] and MD simulations are the only available tools. Neutron spin-echo

(NSE) spectroscopy has, in fact, been used successfully in many recent studies of dynamics in confinements.

For the study of surface diffusion we have recently built a spin-echo spectrometer which replaces the neutron as probe parti-

cle by  $^3\text{He}$  atoms [3, 4]. As He atoms do not penetrate into the sample,  $^3\text{He}$  spin-echo (HeSE) spectroscopy is exclusively surface sensitive. SE spectroscopy uses the Larmor precession of the nuclear magnetic moment to measure atom displacements as a function of time, i.e. it measures the

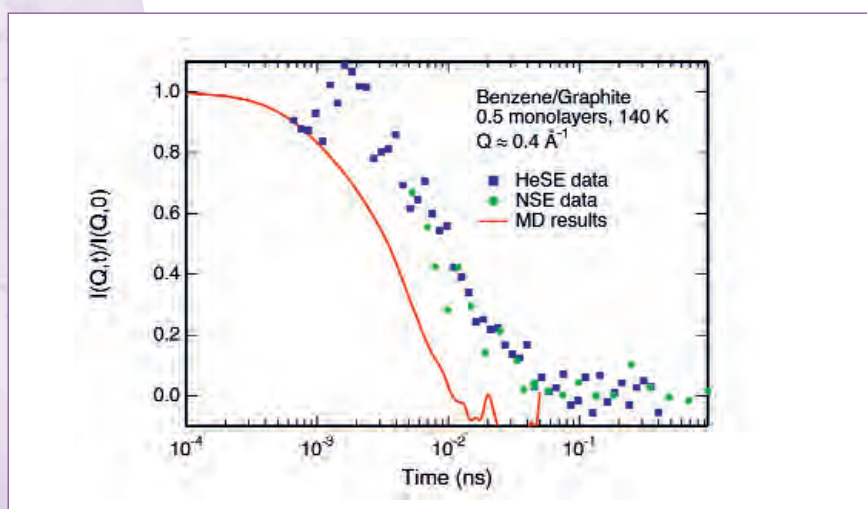


Figure 1: Intermediate scattering functions  $I(Q,t)$  measured using HeSE (blue squares) and NSE (green circles) spectroscopy and calculated using MD simulations based on the force-field COMPASS (solid line).

# Spectroscopy, modelling and theory

intermediate scattering function  $I(Q,t)$  on the 0.1 ps to 100 ns time scale. **Figure 1** shows the results of HeSE measurements of only half a monolayer of benzene molecules on a  $1 \times 1 \text{ cm}^2$  HOPG sample. As our aim is to give a solid base for the analysis of bulk confinement studies, the dynamics found in this surface science study were compared to the benchmark method NSE to exclude possible variation in the results due to the difference in the probe-sample interaction. In the case of diffusion on graphite surfaces, direct comparison is possible as the signal on the ILL spectrometer IN11 has recently been dramatically increased, allowing the use of Papyex exfoliated graphite as substrate, which is essentially a stack of thousands of thin graphite samples with a surface area of about  $20 \text{ m}^2$  per gramme. For comparison, we show IN11 results in **figure 1** alongside our HeSE measurements. The agreement between the data sets means that a future extrapolation of HeSE results for the analysis of NSE bulk studies is viable.

From the spin-echo measurements we can gain a good general understanding of the diffusive dynamics of the benzene films by extracting the relaxation times for different momentum transfers, which indicates the diffusion mechanism, and different temperatures, giving activation energies. From our analysis we conclude that the diffusion is essentially Brownian without any trace of jump diffusion. The activation barrier of the diffusion is very small (about 15 meV). Thus, a pure van der Waals interaction should model the interaction very well.

The information gained using NSE and HeSE spectroscopies remains averaged over very large numbers of molecules. A detailed understanding of what is happening to each molecule needs the help of computer simulations. As density functional theory calculations are far too slow and do not supply accuracies in the meV range, as needed here, MD calculations were performed. The aim for the simulations was twofold: firstly, we wanted to validate forcefields and programs which are widely available in the scientific community (using Cerius2 and Materials Studio by Accelrys for MD

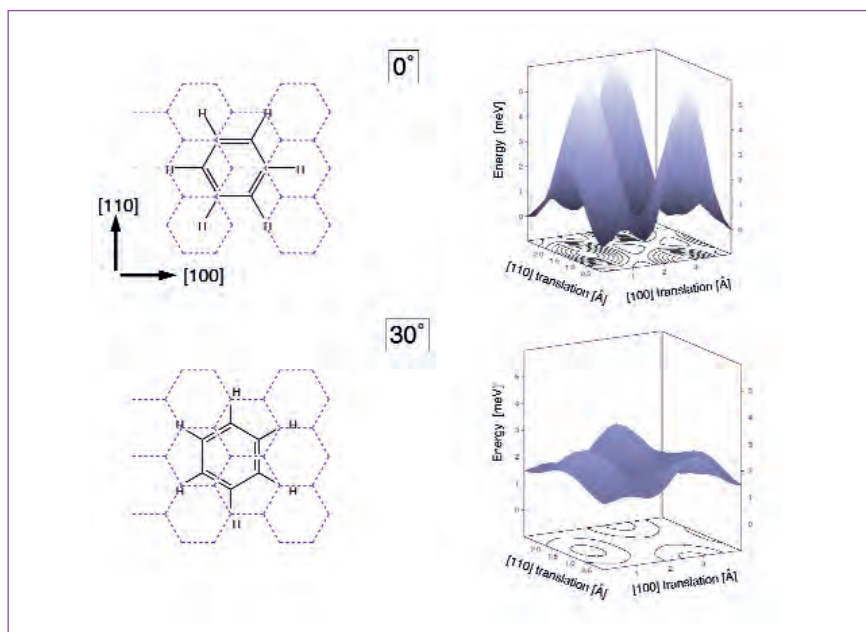


**Figure 2:** The excellent agreement between our MD calculations and measurements allows us to calculate the potential energy surface (PES) for the translational and rotational motion of benzene molecules on a graphite surface. Here, the translational PES is shown for a single molecule whose rotation angle is in phase with the graphite substrate ( $0^\circ$ ) and perfectly out of phase ( $30^\circ$ ). If the molecule is out of phase the translational barrier is strongly decreased.

calculations and the freeware package nMoldyn for analysis) to allow for the transfer of the knowledge gained here to further systems. Secondly, we aimed at analysing the benzene/graphite system in more detail to link the ensemble averaged experimental results to the microscopic motion of single molecules.

The MD calculations turned out to give a surprisingly good agreement with the experimental results (**figure 1**) [5]. In particular, the DFT based forcefield COMPASS can reproduce all qualitative features of the experiments and gives a very good quantitative result. Thus, COMPASS-based calculations of benzene diffusion in mesoporous confinements should give a very accurate description of the surface contribution. In addition, it was found that the COMPASS-derived interaction potential surface has a dependence on the molecule's angular orientation (**figure 2**). In the calculations this lead to a preferential selection of an orientation angle that is out of phase with the substrate structure and we found a coupling between rotational motion and lateral diffusion which merits further detailed studies.

In conclusion, the interaction between benzene and carbon surfaces can be understood in detail by combining NSE and HeSE with MD calculations. Second generation force-fields, such as COMPASS, were validated, giving excellent results for the benzene-graphite interaction, such that they form a solid foundation for the description of the surface interaction in future studies of benzene and similar molecules in carbonous confinements.

## References

- (1) see for example: C. Alba-Simionesco et al., *Eur. Phys. J. E* 12 (2003) 19
- (2) F. Mezei (Ed.), *Neutron Spin Echo, Lecture Notes in Physics, Vol. 128*, Springer, Berlin, 1980
- (3) A.P. Jardine et al., *Science* 304 (2004) 1790
- (4) P. Fouquet et al., *Rev. Sci. Instrum.* 76 (2005) 053109
- (5) P. Fouquet et al., to be submitted to *J. Chem. Phys.*

# Filled Skutterudite structures: future materials for an ecological power generation?

## Authors:

**M.M. Koza, M.R. Johnson and H. Mutka**  
(ILL)

**R. Viennois** (University of Geneva)

**L. Girard and D. Ravot**  
(University of Montpellier II)

In the search for efficient thermoelectric materials the reduction of lattice thermal conductivity is crucial. We have examined filled Skutterudite materials in which localised vibrational rattling modes were proposed to be the main factor in reducing the thermal conductivity. In disagreement with the earlier hypothesis the phonon properties of filled Skutterudites are those of harmonic crystals with the supposed localised modes being due to low lying optical modes coupling to zone boundary acoustic branches.

At the beginning of the 19<sup>th</sup> century, Thomas Johann Seebeck established the effect of generation of a voltage and, hence, an electrical current along a temperature gradient applied to a metallic material. The efficiency of the Seebeck effect, the transformation of thermal to electrical power, is determined by electrical and heat transport properties. Efficient thermoelectric (TE) materials require a low thermal conductivity but a high electrical conductivity.

The concurrent fulfillment of both conditions poses a serious obstacle for the production of efficient TE devices. Only recently the search for efficient TE materials has been accelerated due to appreciable advances in materials synthesis techniques. Modern TE materials have complex crystalline structures allowing the exploitation of different physical effects for a suppression of thermal conductivity.

In general, modern TE materials have a high number of atoms  $N$  per unit cell, reducing the fraction of heat carrying acoustic phonons to  $1/N$ . Disorder added to their crystalline matrix by a random atomic substitution enhances the scattering of acoustic phonons.

Alloying with heavy elements, like rare-earth atoms, lowers the atomic vibration frequencies and hence the thermal conductivity. However, all these material processing techniques reduce as well the electrical conductivity.

In this respect, nano-cage structures incorporating guest atoms are considered the most promising basis for TE materials. Here, electron and heat conductivity are decoupled, whereby the nano-cage framework serves as host for the electronic transport. On the other hand, the encaged guests form a hindrance for the heat transport by acoustic phonons.

For example, the Skutterudite  $\text{Co}_4\text{Sb}_{12}$  can be tuned - by adding La or Ce - from an empty cage structure to the filled Skutterudite  $\text{RFe}_x\text{Sb}_{12}$  ( $\text{R} = \text{La}, \text{Ce}$ ) passing through a range of intermediate compositions  $\text{R}_x\text{-Fe}_y\text{Co}_{4-y}\text{Sb}_{12}$  ( $0 < x < 1, 0 < y < 4$ ).

The Skutterudite structure is sketched in **figure 1**. The lattice thermal conductivity of the filled structure remains more than one order of magnitude below the one of the unfilled modification at room temperature and above [1]. Hence, Skutterudite structures offer the opportunity to study changes in the microscopic dynamics upon successive filling of the cages in a simple and smart way. Indeed, despite the experimentally established dependence of the thermal conductivity on the filling of the voids, the fundamental microscopic process leading to a reduced heat transport is not understood. As a rather phenomenological approach towards a classification of TE materials they have been termed as 'phonon glasses and electron crystals' [2]. In this scenario the encaged atoms are supposed to behave like independent 'rattlers' in cages, dissipating heat randomly - a picture that is often referred to when low-energy phonon properties in glasses are discussed.

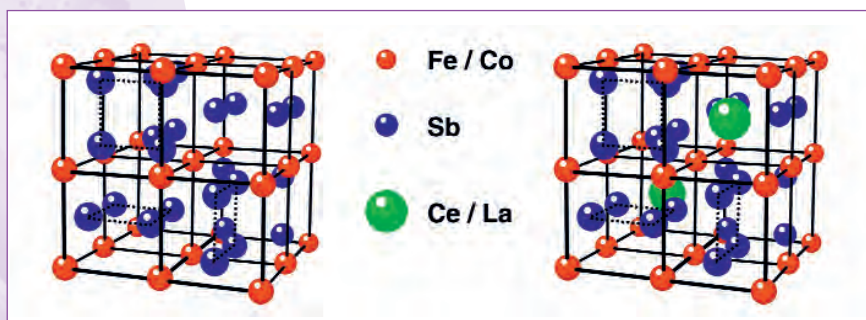


**Figure 1:** Sketch of the structure of the empty (left) and filled (right) Skutterudite system.

# Spectroscopy, modelling and theory

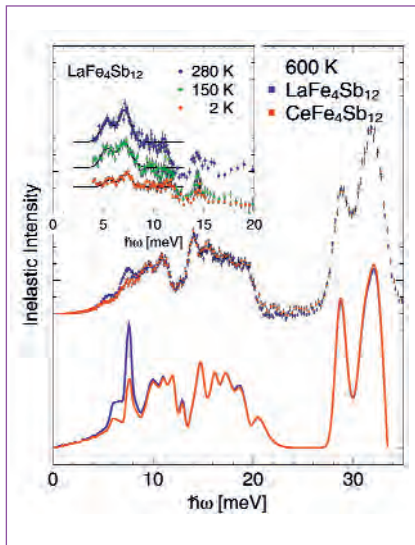


**Figure 2:** Inelastic response of the Ce and La filled Skutterudite structure measured at IN6 and IN4 (inset) at different temperatures. *Ab initio* lattice dynamics calculations are indicated as well.

Note the peaked features at about 7 meV correspond to the van Hove singularities of the guests' acoustic and optic phonon sheets (4).

The hypothesis of such rattling mode was checked using the combination of high-resolution time-of-flight neutron spectroscopy with extensive lattice dynamics calculations. Indeed, the application of La and Ce as guest atoms is a favorable case. Despite the almost identical masses of these elements, their predominantly coherent cross sections differ by a factor of three. Hence, from the contrast in the inelastic response of La and Ce filled Skutterudites one is able to extract directly all information on the phase correlations of the guest atoms in a wide range of energy and momentum. Moreover, combining cold- (IN6) with thermal- neutron (IN4) spectroscopy it is possible to examine the harmonicity of the guest modes in a temperature range of 2 – 600 K (figure 2) [3].

High-quality computed data are indispensable for discriminating between different dynamic scenarios and to prove or disprove the supposed 'phonon glass and electron crystal' idea. To achieve this goal a new approach was developed, based on *ab initio* structure determination and lattice dynam-

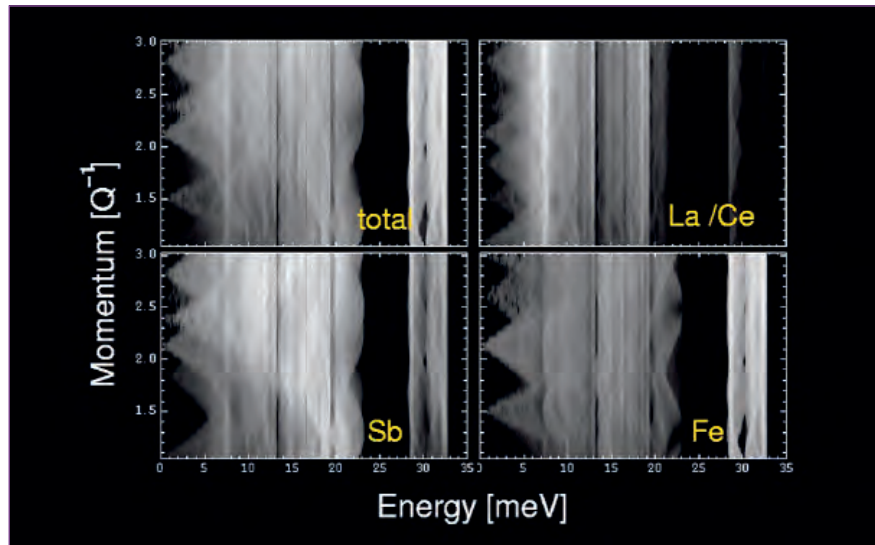


**Figure 3:** Contrast plot of the computed inelastic intensities matching the wide energy-momentum phase space of our time-of-flight experiments on IN6.

ics for computing time-of-flight data. The lattice dynamics calculation is based on the generation of a random set of Q points from which the coherent dynamic structure factor is computed, matching the phase space map of the instruments. The calculated data comprise the partial contributions of the elements. Hence, the inelastic response of the intercalated guests can be directly compared with the contrast data of the experiments. **Figure 3** demonstrates the extensive information comprised in the computed dynamic structure factor. The experimental data supported by *ab initio* lattice dynamics calculations demonstrate that the filled Skutterudite materials behave as harmonic crystalline structures [4]. The simple picture of the guest atoms behaving like 'rattlers in cages' is not satisfying and, accordingly, the term of a 'phonon glass' for Skutterudite structures does not apply. In the case of the heavy elements La and Ce, the lattice dynamics is characterised by low-energy van Hove singularities of acoustic and optic phonon sheets, leading to enhanced Umklapp-scattering as the major source of the low thermal conductivity in filled Skutterudite structures.

Computing the coherent time-of-flight inelastic response from *ab initio* calculations is a generic technique which has been successfully introduced here. It can be

applied to any polycrystalline substance and, moreover, compared to complementary techniques like Molecular Dynamics. The analysis of data beyond the usual incoherent approximation provides not only the opportunity of discriminating trivial mass effects from complex properties of chemical bonding and the possibility of identifying anharmonic effects in the vibrational dynamics. It is, in particular, a powerful tool for identifying cooperative dynamic coupling between distinct atomic species in a compound sample.

## References

- (1) G.P. Meisner et al., *Phys. Rev. Lett.* 80 (1998) 3551
- (2) G.A Slack, in "CRC Handbook of Thermoelectrics" edited by D.M. Rowe (CRC Press London, 1995) 407
- (3) R. Viennois, L. Girard, M.M. Koza, H. Mutka, D. Ravot, F. Terki, S. Charar, and J.-C. Tedenac, *Phys. Chem. Chem. Phys.* 7 (2005) 1617
- (4) M.M. Koza, M.R. Johnson, R. Viennois, H. Mutka, L. Girard, D. Ravot, IEEE publication 06TH8931 (2006). <http://www.its.org/taxonomy/term/286>

# d<sup>0</sup> ferromagnetism in oxides

## Authors:

G. Bouzerar (CNRS, Grenoble)

T. Ziman (ILL)

We have recently developed a theory of vacancy-induced magnetism in oxide materials. As well as providing a possible conceptual basis of a range of puzzling phenomena in films, this has suggested possible new ferromagnets based on substitution of wide-band semiconductors.

In the last twenty years, oxides have provided a number of unexpected new phenomena which may not only provide materials with useful new properties, but also provide challenges to understanding co-operative phenomena in solids. Some of the latest discoveries concern a number of exciting effects when ferromagnetism is seen in unexpected places. These are apparently unrelated to traditional transition metal magnetism and are seen in oxides such as HfO<sub>2</sub>, ZrO<sub>2</sub> [1], CaO, ZnO, and related materials such as hexaborides (CaB<sub>6</sub>). What is puzzling is that thin films of materials, which in bulk have neither magnetic moments nor magnetic order, may be ferromagnetic well above room temperature. HfO<sub>2</sub> or ZrO<sub>2</sub> are both wide-band insulating material with high dielectric constant; the possibility of making them ferromagnetic could widen their possible application in the field of spintronics. There are too few magnetic impurities in the ZrO<sub>2</sub> films to explain the magnetism and the cation (nominally Zr<sup>4+</sup>) should be in a non-magnetic d<sup>0</sup> configuration. The term 'd<sup>0</sup> ferromagnetism' was coined to describe this general phenomenon.

There had long been suggestions that intrinsic cation or anion vacancies may provide a source of magnetic ions. Vacancies do two important things: first, because of the dif-

ference of the charges of the missing ion and the vacancy, they introduce holes in the oxygen band; and second, because of the missing charge on the vacancy, the holes are attracted back close to it. It is the balance between the two effects that can lead to moments which are not simply localised on a single site of the original lattice. This gives a possible source of magnetic moments but what has been lacking so far was an understanding of how the moments could interact to order up to relatively high temperatures. The situation is complicated further by the fact that experimental results are still 'unstable'. Simple models for vacancy-induced ferromagnetism can help

identify critical parameters, (as an example: the nature and concentration of vacancies,) and propose new materials where controlled substitutions could replace the vacancies. Indeed, while oxygen vacancies were originally suggested as the source of magnetism in HfO<sub>2</sub>, density functional calculations indicated that moments were more likely in partially depleted oxygen orbitals around Hf vacancies. These considerations lead us [2] to formulate a simple model Hamiltonian for d<sup>0</sup> magnetism. The original model was formulated for cation vacancies in oxides such as HfO<sub>2</sub>, ZrO<sub>2</sub> and CaO, but the obtained results suggested the occurrence of more general

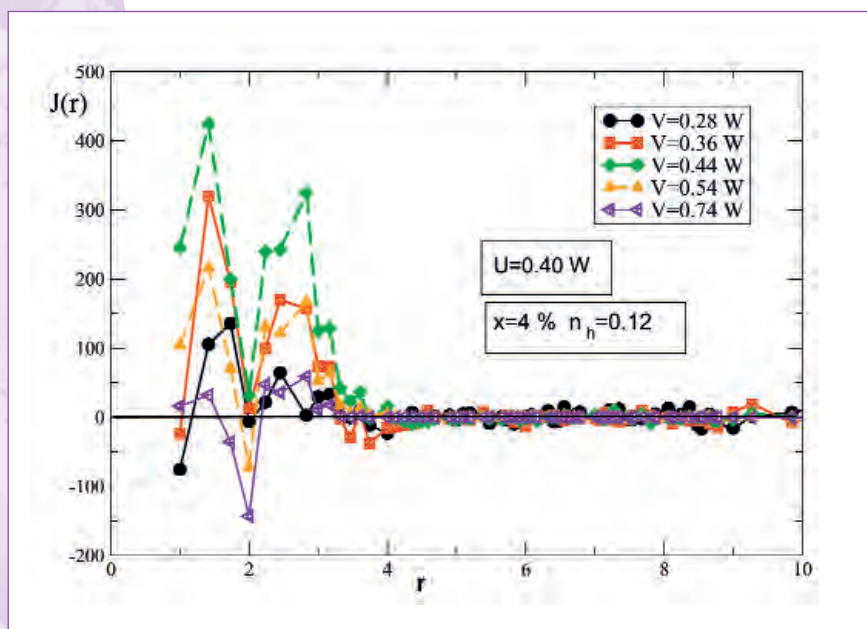


Figure 1: Magnetic couplings calculated for different distances between vacancies. Different colours correspond to varying potentials  $V$ . As  $V$  is tuned through an optimal value (green curve) the couplings increase and are all ferromagnetic.

# Spectroscopy, modelling and theory

phenomena, in which a vacancy or substitutional defect creates an *extended* magnetic moment on neighbouring atoms. The magnetic moment is distributed over several originally non-magnetic oxygen atoms of the host and there is no clear separation between the holes forming the moment and those mediating the interactions.

In theoretical terms, a single-band Hubbard model of oxygen orbitals with bandwidth  $W$  and correlation  $U$  is used, with a novel correlated form of disorder. A 'defect' does not alter the regular geometry of the oxygen lattice, but introduces attractive potentials  $V$  on the neighbouring oxygen orbitals. First, the magnetic couplings are to be estimated at all distances between the different impurity-induced moments; then, the Curie temperature is to be assessed for the effective dilute Heisenberg model where each 'spin' represents the total moment, which is quite large, spread over several oxygen atoms.

**Figure 1** shows the calculated couplings averaged over different impurity configurations. The potential  $V$  is varied, but the vacancy concentration is fixed at  $x = 4\%$  and the number of holes per vacancy at  $n_h/x = 3$ . For small  $V$ , the couplings oscillate with distance, but with antiferromagnetic nearest neighbour coupling. As  $V$  increases the couplings become more ferromagnetic, but with further increase some become antiferromagnetic again. Thus, from **figure 1** there is a range of values  $V$  where the couplings, while fluctuating, are all ferromagnetic. This is associated with the incipient development of a visible impurity band just at the band edge. This ferromagnetic bias in the 'RKKY-like' oscillations corresponds to the resonant form of the impurity band. Once we understand the couplings we can calculate the Curie temperature within SC-LRPA, a simple but powerful method developed at the ILL [3].

**Figure 2** shows the Curie temperature, optimised for other variables of the model, as a function of the crucial variable which is the number of holes per vacancy. The concentration of vacancies is too large for equilibrium but quite feasible for films. There is a window of concentrations where TC becomes very large; outside this window there may exist local moments but no long-range ferromagnetic order. Interestingly,

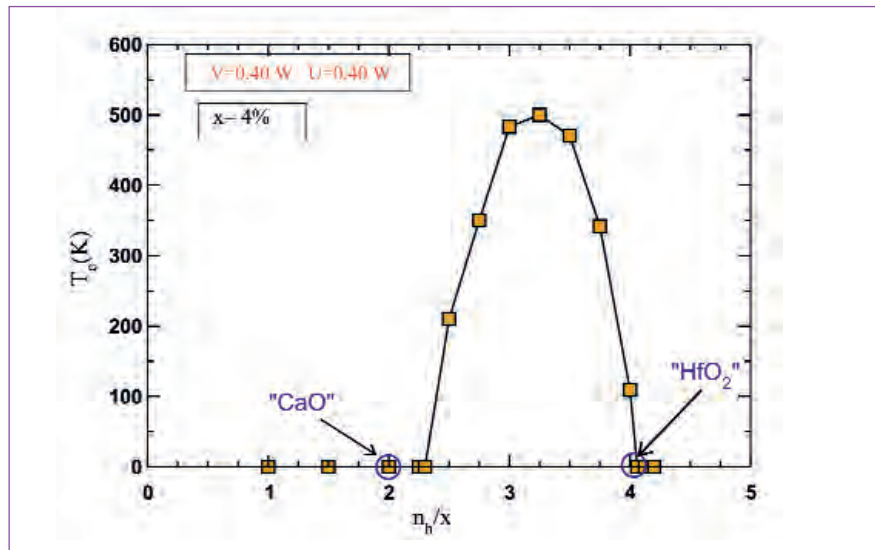


**Figure 2:** Optimal Curie temperatures as a function of the number of holes for 4% vacancies. Ferromagnetism occurs over a range between 2 (a simplified model of anion vacancies in CaO) and 4 (same for HfO<sub>2</sub>) holes per vacancy and is strongest around 3.

the formal charges of vacancies in HfO<sub>2</sub> or CaO are near the edges of stability of ferromagnetism for the parameters chosen, assuming *only* cation vacancies. This may suggest an explanation for the extreme sensitivity of current results to sample history: presence of defects other than those associated with magnetic moments may well vary the carrier density and destabilize long-range magnetic order.

One of the purposes of this theoretical work is to provide a simple conceptual framework for understanding intriguing results. Measurements of local moments should take into account that the moment may be primarily spread over oxygen orbitals. It is hoped that future reflectivity experiments with neutrons and X-rays with films will make clearer the crucial questions of densities of different vacancies and their correlation with ferromagnetism, as has been useful in diluted magnetic semiconductors [4]. It would also be interesting to measure the profile of the density of states (e.g. by photoemission) to see whether it does indeed correspond to the proposed picture. The calculations suggest that a promising avenue for stabilizing or increasing the Curie temperature experimentally may be to use non-magnetic substitution of Hf(Zr) by Li, Na, K, Rb or Cs rather than Hf(Zr) vacancies which are difficult to

control. This has suggested a new class of materials which, hopefully, will be synthesized soon. Band structure calculations, made in collaboration with the Prague group [5] taking into account all bands and the actual structure, support the idea: for example, of substituting K for Zr in ZrO<sub>2</sub>. This may be attractive since it might be realized in bulk as well as films. Calculations show that Curie temperatures above room temperature may be achievable for a few per cent of vacancies or substitutions. This is a high concentration for vacancies, but may be possible for substitution even in equilibrium.

## References

- (1) M. Venkatesan, C.B. Fitzgerald, and J.M.D. Coey, *Nature (London)* 430 (2004) 630
- (2) G. Bouzerar and T. Ziman, *Phys. Rev. Lett.* 96 20762 (2006)
- (3) G. Bouzerar, T. Ziman and J. Kudrnovský, *Europhys. Lett.*, 69 (2005) 812-818
- (4) B.J. Kirby et al., *Phys. Rev. B* 69, 081307(R) (2004)
- (5) F. Maca and J. Kudrnovský, (unpublished)

# From qubits to neutrons and back again: Berry phase in dissipative quantum mechanics

**Author:**

**R.S. Whitney (ILL)**

The push towards quantum computing has re-invigorated the field of dissipative quantum mechanics. Neutrons are ideal for investigating many of the issues that are relevant there. In this context we discuss our recent work, which has overturned the notion that the Berry phase is insensitive to the effects of dissipation. We look forward to the experiments by the Atominstitut, Vienna, which will use the ILL ultra-cold neutron source to probe these issues.

Soon computer chips will become so small that quantum mechanics and the discreteness of electrons cannot be ignored. This will require new architectures for the chips, and possibly even new concepts of computing. One extremely exciting avenue being explored is that of *quantum computing*, which is as different from present-day computing as quantum mechanics is from Newtonian mechanics. A quantum computer would start with all input data in *qubits* (quantum logic-states) which are in a quantum superposition of zero *and* one ( $|0\rangle$  and  $|1\rangle$ ). It would thereby run calculations for all possible inputs at the same time, and then systematically collapse all these states to give a single desired outcome. Imagine for a moment that you were simulating a complicated system of many particles and wanted to find the lowest energy configuration. It is hoped that a quantum algorithm could be constructed that would calculate the energy of all possible states in parallel and then output the state with the lowest energy.

The fly in the ointment is errors due to noise. A quantum computer would be incredibly sensitive to noise. It is an analogue device, so an algorithm may fail if  $a, b$  are accidentally changed even slightly in the state  $a|0\rangle + b|1\rangle$ . However, even more crucial is the fact that quantum computing requires coherence. A coherent quantum system is one which has kept its phase information (the phase of the complex numbers  $a$  &  $b$  above). This phase is easily washed-out by noise, making quantum computation impossible. Clever error correction techniques exist, which will work if each *qubit* remains coherent (retains its phase) for at least 10,000 gate operations. To achieve such coherence times is *the* technical challenge for any of the proposed technologies (from superconducting-circuits to interacting spins in nuclei) to overcome.

## **Dissipative quantum mechanics**

In addition to technology-specific challenges of reducing noise, there are fundamental questions to be asked about noise in quantum systems; this is the field of *dissipative quantum mechanics*. Quantum systems interact with noise generated by their environments, which typically contain many degrees-of-freedom with different natural frequencies, this noise causes dissipation (relaxation and decoherence).

While the study of these effects is as old as quantum mechanics, the push towards quantum computing has led to new questions being asked and answered in both theory and experiments. A forthcoming experiment by the Atominstitut, Vienna, will use the ultra-cold neutron source at the ILL to address some of these questions. The intrinsic coherence of the neutron's spins is comparable to the best present-day qubits, while the experimental set-up is more flexible. They plan to trap the neutrons and expose them to a random magnetic field, allowing them to probe almost any aspect of dissipative quantum mechanics. It is their intention to study the effect of dissipation on Berry phase with this set-up.

## **Berry phase in dissipative quantum mechanics**

It has been suggested that geometric phases, such as the Berry phase, would be intrinsically insensitive to noise, making it ideal to utilise them for quantum computing [1]. The Berry phase is the phase acquired by a particle's wave function due to its Hamiltonian being slowly rotated around a closed loop [2]. Berry found a very pretty aspect of quantum mechanics, when he noted that this phase depended only on the geometry of the path, not the rate or manner in which it is followed. For a spin-half

# Spectroscopy, modelling and theory

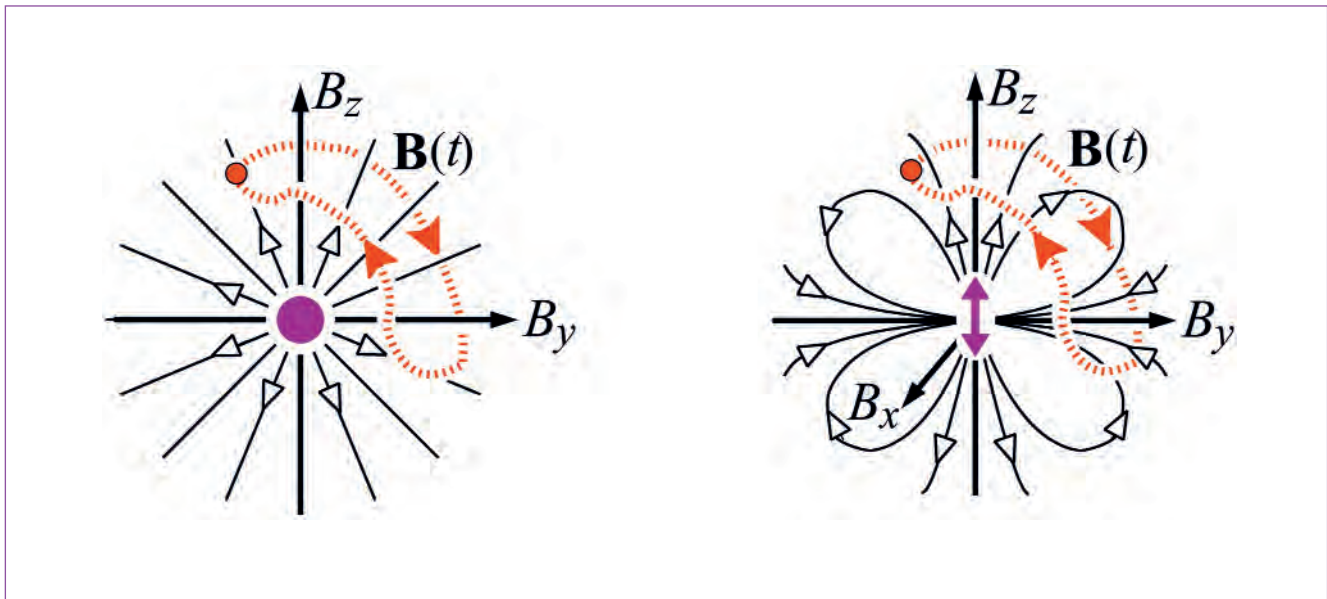


**Figure 1:** In dissipative quantum mechanics the Berry phase becomes the flux of two fields enclosed by the slowly varying  $B$ -field (discontinuous line). The monopole field (left) is that found by Berry, while the quadrupole-like field (right) is noise-induced. The latter field has a complex prefactor whose magnitude goes like the square of the noise amplitude.

(a *qubit* or a neutron), a Berry phase can be generated by the slow rotation of an applied magnetic field, then the Berry phase will be half the solid-angle enclosed by the magnetic field. Berry then gave a mathematical description of this phase as the flux due to a monopole sitting at the origin in the parameter space (given by the  $x,y,z$ -components of the magnetic field, **figure 1**). The Berry phase has now been shown to be important in areas as diverse as chemical reactions and vortices in superconductors.

Recent theoretical work has shown that the Berry phase is not insensitive to either quantum noise [3] or classical noise [3, 4]. Indeed, the phase of the spin is washed-out at approximately the same rate, independent of whether there is a Berry phase present or not. If this is confirmed experimentally, then it directly contradicts the notion in ref. [1], making it unlikely that Berry phases would be ideal for quantum computing. However, we also reach the

remarkable conclusion that the Berry phase itself is different in dissipative quantum mechanics. It remains geometric, but gains a *quadrupole-like* component [3], in addition to the monopole component found by Berry (**figure 1**). Further, this new noise-induced geometric term is complex, with its imaginary part being a small geometric contribution to decoherence.

### ...and back again

While neutron sources are extremely unlikely to be used for quantum computing, experiments with coherent neutrons can shed significant light on aspects of quantum mechanics which are absolutely fundamental to quantum computing. By introducing noise artificially, one can study dissipative quantum mechanics in a situation where (unlike in qubits) even the noise is completely controllable. Thus, the exchange of ideas between the two fields is guaranteed to be highly productive.

### References

- (1) S. Lloyd, *Science*, 292 (2001) 1669
- (2) M.V. Berry, *Proc. R. Soc. Lond.* 392 (1984) 45 and A. Shapere and F. Wilczek (Eds.), *Geometric Phases in Physics* (World Scientific, Singapore, 1989)
- (3) R.S. Whitney and Y. Gefen, *Phys. Rev. Lett.* 90, (2003) 190402 and R.S. Whitney, Y. Makhlin, A. Shnirman and Y. Gefen, *Phys. Rev. Lett.* 94 (2005) 070407
- (4) G. De Chiara, G. Massimo Palma, *Phys. Rev. Lett.* 91 (2003) 090404

# Looking to



# the future →

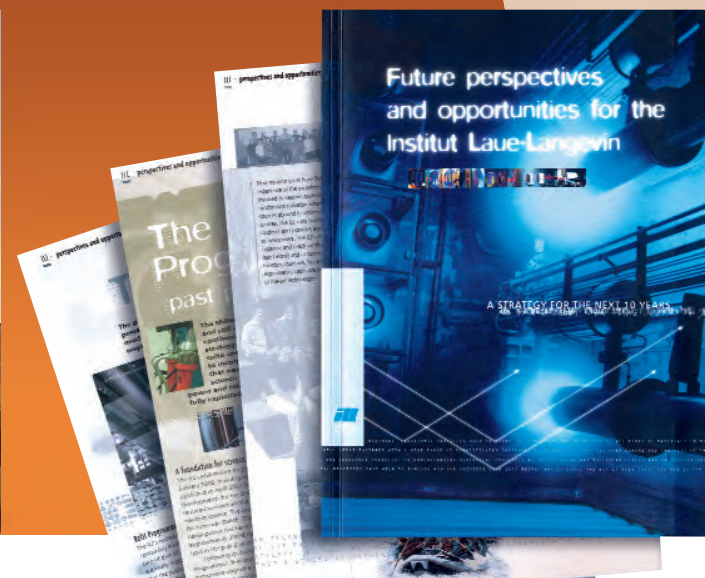
## Future Perspectives and Opportunities

**“The ILL has firmly established itself as a pioneer in neutron science. The new ‘Perspectives and Opportunities’ document lays out the strategy plan for the next 10 years and presents the future opportunities that will keep the ILL a world-leader for the next 15 years. We all at the ILL have demonstrated once again the worth of investing in our Institut for the future. This is now accepted without question.”**

**Colin Carlile**  
(ILL Director, 2000-2006)



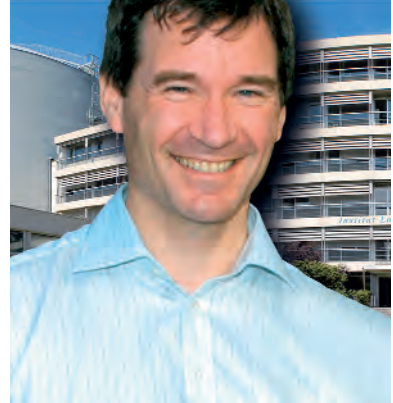
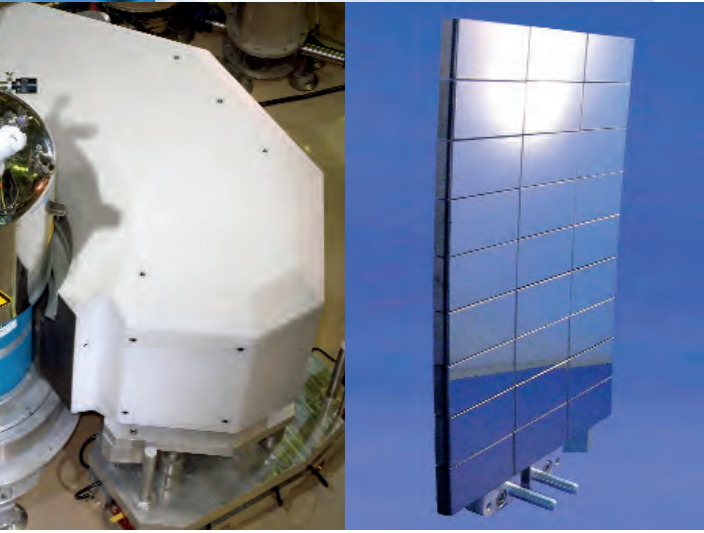
A lot has happened at the ILL since the Millennium Programme was first launched in 2001. The result is that our instruments can deliver eight times as much high-quality data as they did in 1999. It has been 5 years since the ILL produced its first Roadmap, and we therefore felt the need of producing a revised paper. The “Perspectives and Opportunities” document has appeared after 2 years of preparative study and considerable effort by the ILL management team, in close collaboration with a large number of people. It identifies the technical initiatives that are possible together with the investments that are needed with the aim of keeping the ILL at the forefront of neutron science for the next 15 years.





- Millennium programme
- Technical and computing developments
- New experimental techniques

# Millennium programme and technical developments



2006 has been a year of change and challenges for the Millennium Programme. It also provided an opportunity for reflection: the 2<sup>nd</sup> Millennium Symposium, held in April, showcased what has been achieved to date, and provided a forum to discuss future priorities.

June marked the end of an intense period of installation work during a long reactor shutdown.

This furnished us with greatly improved neutron guides to serve the main guide-hall of ILL7. In parallel, many new or improved instruments were either completed or brought much closer to fruition, including BRISP, FlatCone, SALSA, D2B, D7, D19, LADI-III and IN5.

The Perspectives and Opportunities (P & O) document was published in the autumn, presenting a vision for the ILL for many years to come, and redefining the various stages of the Millennium Programme. The M0 phase comprises those projects that are finished or approach completion, and we highlight some of its successes in the following pages.

The M1 phase embraces 7 new instruments and supporting infrastructure, poised to leap from the drawing board to the instrument halls. Finally, the M2 phase includes projects that will not start until some time in the next decade but which will soon require planning to ensure that we maintain our momentum.

## *A vision for the ILL many years to come...*

The year ended well with the promise by our Associates to increase the budget for the M1 phase to the extent that most of what has been proposed can actually be achieved in the next 5 or 6 years. Such a long-term commitment brings a new focus to our planning.

At the centre of this is the decision about the location of the third cold source, which, combined with priorities and constraints for the M1 instruments will define our Millennium strategy for at least the next 5 years.

Watch this space!

**Andrew Harrison**  
Associate Director

# The Millennium Programme

**Author:**

**A. Harrison (ILL)**

The 2<sup>nd</sup> Millennium Symposium was held in Grenoble in late April, highlighting the science that has already been enabled by new instruments and upgrades and taking soundings from our user communities who provided strong endorsements of the Programme to date, and pointers for future priorities.

A long reactor shut-down ended in June with a restart that was remarkably free of trouble despite the pressure to finish a tremendous amount of work. Most ambitious of these projects was the renewal of 100 m of in-pile sections of the 12 H1/H2 guides which supply the main guide-hall in ILL7, and

needed 20,000 hours of manpower. The upgrade to  $m = 2$  supermirror guides, and realignment of sections at the junction between the reactor and the guide-hall provides an average flux gain of more than 60% for the thermal and cold guides.

A number of instruments have also been completed or commissioned. The **Flat-Cone** detector, which provides a roving multide-tector for triple-axis instruments, enabling much faster mapping in  $Q$  and  $\omega$  at high resolution, is now available for scheduled experiments after successful tests on IN3, IN8, IN14 and IN20.

**SALSA** is establishing itself as the world-leading instrument for residual stress determination in engineering components using neutrons, and enjoys a gain factor of almost 3 in flux from the refurbished H22 guide.

The thermal neutron diffractometer **D19** took delivery of a new multiwire 'banana' detector last year, giving an angular coverage of  $120^\circ \times 30^\circ$ , twice as large as any other detector of this type. A new monochromator housing, incorporating 3 take-off angles has also been installed and commissioning tests should be finished in 2007.

The time-of-flight (TOF) Brillouin Spectrometer, **BRISP**, an Italian-German CRG, also became operational in 2006, after improvements to the shielding led to a reduction in the background level by two orders of magnitude.

**D7**, the cold-neutron TOF spectrometer with polarisation analysis, will receive its last new analyser bank early in 2007, delivering a 70-fold increase in flux on the old instrument – a reward for almost a year of sputtering to produce 250 m<sup>2</sup> of Co/Ti supermirrors; in addition, a new Fermi chopper enables spectral analysis to be performed at a resolution of 0.2 – 0.5 meV



*Figure 1: View of the work to install the new in-pile section of the H1/H2 guides.*

A number of ongoing projects have also seen major advances in 2006. The largest visible addition to ILL7 is the new shielding for the secondary spectrometer of the TOF cold neutron instrument **IN5B**, which has already led to a four-fold decrease in background. This will accommodate a TOF vacuum chamber due to arrive early in 2007, and 30m<sup>2</sup> of position-sensitive linear detector modules, designed and patented by ILL, and fabricated on site in a hall specially equipped for the purpose.

Work on the backscattering spectrometer **IN16B** progresses, with the Doppler drive testing successfully in IN16, and tests for the phase-space transformer – a high-speed graphite chopper that promises a flux gain factor of 4 – are scheduled for 2007.

**LADI-III**, the new Laue diffractometer arrived in June and we anticipate that the new detector will provide a 3-fold gain over the old LADI. The design of **FIGARO** – the horizontal-plane reflectometer approaches completion, and work has already started at Astrium on the new carbon fibre choppers.

Finally, projects to revitalise ILL's original small-angle instrument **D11** are converging, with design complete for a new collimating guide. This, combined with the former D22 detector with renewed electronics, offers large gains in flux.

The Millennium infrastructure programme has also seen remarkable progress. A new world record of 76 % has been set in the polarisation of <sup>3</sup>He **spin-filters on a neutron instrument**; this has arisen from improvements to the Tyrex polarised <sup>3</sup>He filling station, combined with a more efficient transfer of the gas to cells and delivery to the instrument.

The versatility of **NOMAD**, the new control environment for ILL instruments, is starting to become apparent: a recent experiment on IN5 required the chopper timing to be related to that of a pulsed laser directed at the sample, and this could be set up rapidly and tailored to the changing needs of the experiment. Our commitment to the development of cryogen-free cryostats is bearing fruit, with greatly improved cooling times for devices that should eventually replace our more conventional 'Orange' cryostats.

The promise of extra funding for the Millennium Programme by our Associates is a very exciting development, presenting

us with a stiff challenge to plan well and then deliver, but also promising a very bright future for the ILL.

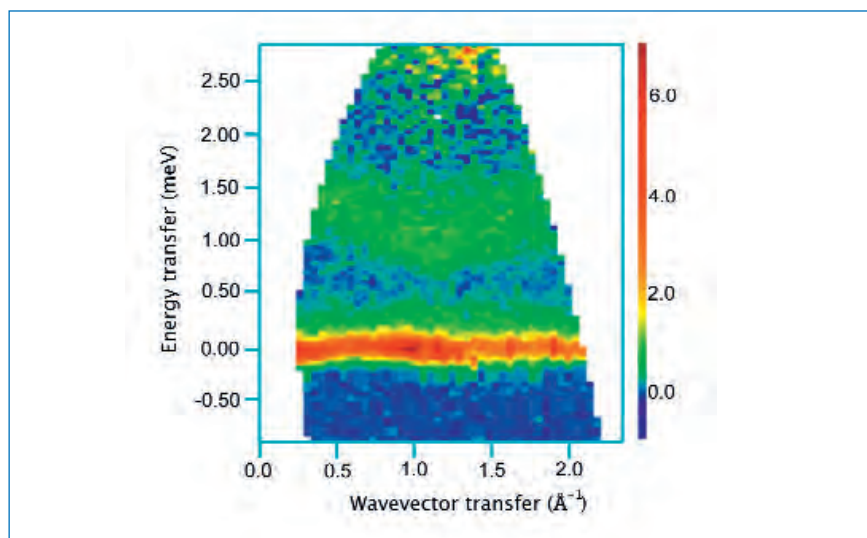


**Figure 2:** Inelastic magnetic scattering at 900 mK from a powder sample of the geometrically frustrated magnet  $Tb_2Sn_2O_7$ , measured on D7.



**Figure 3:** Completed detector modules for IN5, each 3 m in length.

## Engineering users warm to SALSA

### Authors:

T. Pirling and D.J. Hughes (ILL)

SALSA, the ILL instrument for engineering and materials science, came on line at the end of 2005 and the three reactor cycles for users of 2006 have shown its excellent performance. A surprisingly wide range of experiments have included stress determination in superconducting wires at a temperature of 4 K, investigation of welded steel joints used in the construction industry, understanding fatigue in nickel single-crystal tensile specimens and near-surface stress determination in a 120 kg bearing used in the shaft of a wind-powered electricity generator.

In 2006 SALSA has evolved into the world-leading instrument for residual stress determination in engineering components using neutrons. During the last year significant strides forward have been made. Behind the scenes, SALSA has also benefited from the refurbished neutron guide H22 which now provides a 'raw' flux gain of a factor of  $\approx 3$ .

When the instrument was commissioned the beam-defining optics were incident and detector slits. These provide a high-flux solution to many bulk measurement experiments. From the last cycle of 2006 radial-focussing oscillating collimators were available as an option. These allow better definition of small measuring volumes with high peak-to-background ratios whilst also suppressing spurious effects arising

when measurements are made through surfaces [1]. Users are therefore able to perform detailed peak-shape analysis even near surfaces.

One of the principal challenges when measuring strain in complex samples is the location of the measuring volume with respect to the sample. To assist sample alignment we have developed a 3D-camera assisted metrological system. A set of three cameras are focused on the measurement location, providing a spatial resolution of  $\approx 20 \mu\text{m}$ . Intelligent pattern-matching routines allow the simple determination of the centre-of-rotation for the instrument, a very important tool for instrument alignment. The same technique is applied to locate reference marks on the sample. Measurements of distances, angles and positions can be performed on screen. **Figure 1** shows a screen-shot during the alignment of a complex shaped aircraft engine turbine ring section. The specimen had first been digitised using the co-ordinate measuring machine (CMM) in the FaME38 laboratory.

Continued developments are planned for 2007 including: further improvements to the camera system; installation of a portable laser scanner at the instrument to digitise the sample surface and determine the absolute position of the sample relative to the translation stage; providing a more flexible range of beam definition optics (slits/collimators/supports).

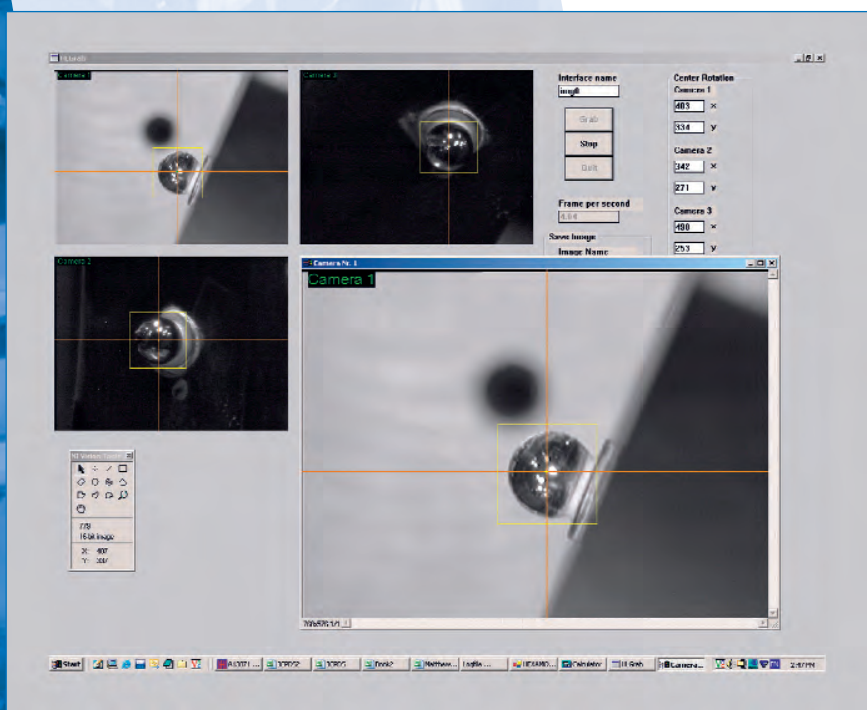


**Figure 1:** Alignment of a turbine section on SALSA. The screen shot shows steel balls of 4 mm diameter, used for alignment, automatically detected by the pattern matching routine. The crosses mark the gauge volume position.

## Experimental highlights

Ultrasonic Impact treatment (UIT) is a novel mechanical surface treatment, capable of introducing a deep layer of compressive residual stress into engineering materials. The technique is particularly suited to the protection of known failure locations at welded joints in the aerospace industry. UIT has been shown to be highly effective in increasing fatigue strength and damage tolerance. The UIT treatment involves the deformation of the surface of the treated material by impacts of a free needle indenter vibrating at  $\approx 27$  kHz. These impacts create severe plastic deformation of the near surface region (depth 1-3 mm typically for steel) and an ultrasonic stress wave that propagates deep into the material (10-12 mm). As part of a project to investigate the effectiveness of this treatment, the full thickness residual stress distribution was measured on SALSAs (Alex Evans). The results show a 1 mm deep region of beneficial compressive residual strain produced by the process (figure 2), accompanied by plastic deformation revealed by peak broadening.

Considering the current drive to lower emission energy sources, increasing focus is falling upon electricity generation by wind power. A recent study (Matthew Peel) using SALSAs attempted to measure the residual stress in the wall of a wind turbine central axis roller bearing. The sheer scale of wind turbines combined with the near-constant running the often remote location, sometimes offshore, poses some difficult engineering questions. The central bearing of the drive axis is a key component which experiences complex stress states both in the bulk and on the surfaces in contact with the shaft on one side and the rollers on the other. Conventional surface treatments to impose compressive surface stresses have led to unexpected failures, probably due to the occurrence of balancing tensile stresses in other locations. An ongoing project in collaboration with Swedish company SKF intends to fully characterise the residual stresses in a complete bearing of 60 cm diameter and 120 kg weight (figure 3). The measurements required flexible sample positioning, high spatial resolution and substantial penetration for which the hexapod and the beam optics on SALSAs are very effective.

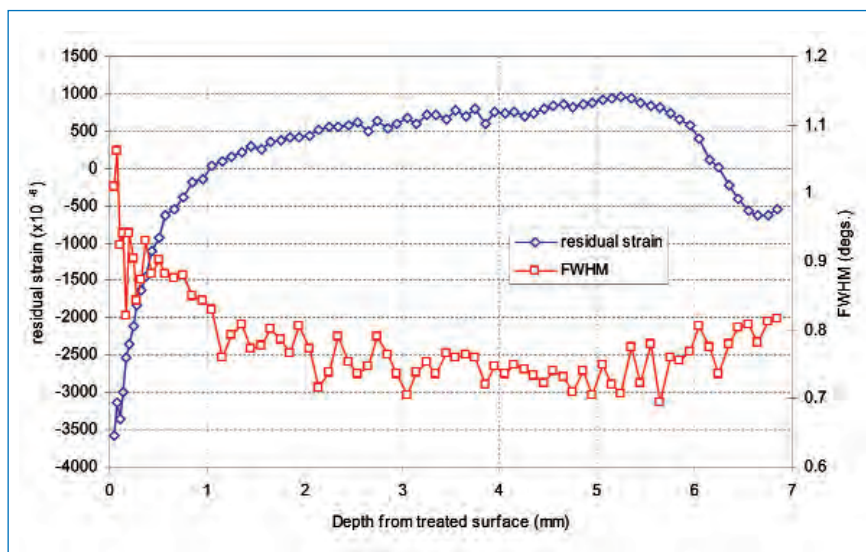


**Figure 2:** Longitudinal residual strain and peak width evolution in an UIT treated steel sample. Data analysis is in progress, but it can already be seen from the peak width that the plastically deformed region is well correlated with the region of compressive stresses. This analysis is only possible with the radial focusing collimator set-up.



**Figure 3:** Wind turbine and bearing mounted on the SALSAs hexapod.

The roller bed is positioned vertical by tilting the hexapod.

## References

(1) ILL annual report, 2000, p. 8

Further Information: 'First impressions of SALSAs: The new engineering instrument at ILL'. D.J. Hughes, G. Bruno, T. Pirling and P.J. Withers. *Neutron News* 17, 3 (2006), 28-32

# The *FlatCone* multianalyser for three-axis spectrometers

Our report covers the experimental tests of the recently developed secondary spectrometer module simultaneously covering a scattering angle range of  $75^\circ$  and offering a choice between two final neutron wave numbers of  $k_f = 1.5 \text{ \AA}^{-1}$  and  $3 \text{ \AA}^{-1}$ . This new device provides improved momentum resolution and enhances data collection rate in experiments mapping the inelastic response over extended areas in the  $(\mathbf{Q}, \omega)$  space.

Neutron inelastic scattering studies using three-axis spectrometers (TAS) are often synonymous with measuring dispersion relations of elementary excitations in crystalline solids. At present such experiments are giving way to studies of other objects such as continuum modes in low-dimensional

quantum spin systems and fluctuations related to ordering processes, both on short and long ranges. Such experiments no longer need to rely on the traditional  $\mathbf{Q} = \text{constant}$  scanning mode, which necessitated a complex combination of spectrometer movements for each scan step, and

therefore they can be easily accelerated by multiplexing the momentum and energy analysis of the scattered neutrons.

The *FlatCone* device displayed in **figure 1a** consists of an array of 31 discrete analyser/detector channels covering an angular range of  $75^\circ$ . In each channel the first of the analysers is tuned to the final neutron wave-number of  $3 \text{ \AA}^{-1}$  and the second one to  $1.4 \text{ \AA}^{-1}$ , the actual energy being chosen by selecting the corresponding beam path to the detector as indicated in **figure 1b**. The analyser crystals consist of packs of elastically bent Si (111) blades, focusing monochromatically onto the sample and scattering neutrons upwards into detectors, lying parallel to the horizontal plane without any direct sight of the sample position.

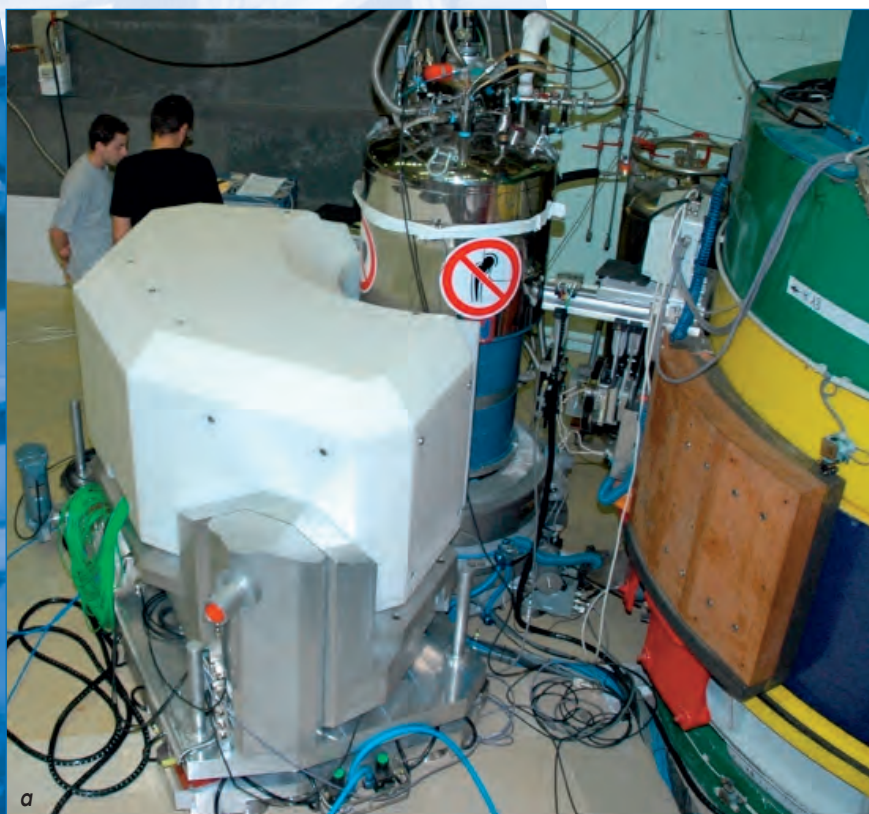


**Figure 1a:** View of the *FlatCone* multianalyser mounted together with the 4T horizontal cryomagnet on IN20 in September 2006.

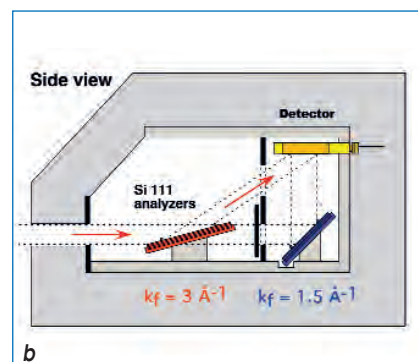


**Figure 1b:** Schematic sketch of a vertical cut through one of the *FlatCone* channels; the arrows represent the neutron flight path of the scattered neutrons with  $k_f = 3 \text{ \AA}^{-1}$  (thermal beam).

Absorbing partition walls (borated aluminium alloy) minimise the cross talk between neighbouring channels. The whole analyser array is protected by a 300 mm thick polyethylene shielding case, mounted on a dedicated Tanzboden unit with a lifting and tilting stage, providing the access to the flat

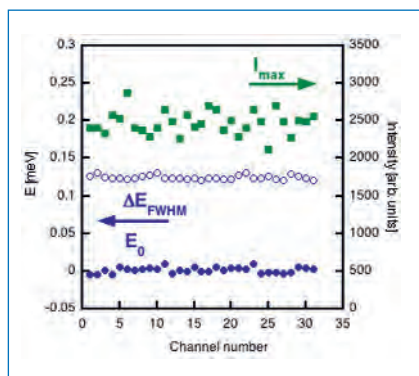


**Figure 2:** Results of FlatCone calibration runs with a standard vanadium sample on IN14 ( $k_f = 1.4 \text{ \AA}^{-1}$ ); the relative r.m.s. spread of the peak count rate ( $I_{max}$ ), energy offset ( $E_0$ ) and energy resolution ( $\Delta E_{FWHM}$ ) is less than 5% between individual channels.

cone geometry [1] and the adaptation to neutron beam levels at different instruments. After successful preliminary tests of the thermal neutron part in summer 2005 we carried out commissioning tests of both the thermal (IN20, July 2006) and cold neutron (IN14, November 2006) analyser parts. Calibration scans performed with a standard vanadium sample prove excellent uniformity of the count rate, energy resolution and energy offset of all the multianalyser channels, as illustrated by the IN14 results displayed in **figure 2**. Another advantage of the Si (111) analyser crystals is the absence of second order contamination, which permits to avoid the otherwise mandatory use of pyrolytic graphite or beryllium filters in the scattered beam. The sensitivity (signal/noise ratio) of any of the analyser channels is about equivalent to that of a traditional TAS with a single analyser/detector thanks to the massive PE shielding and to the internal layout minimising parasitic scattering and avoiding direct view between the detectors and the sample area.

After its commissioning tests in summer, the high energy analyser array was used for

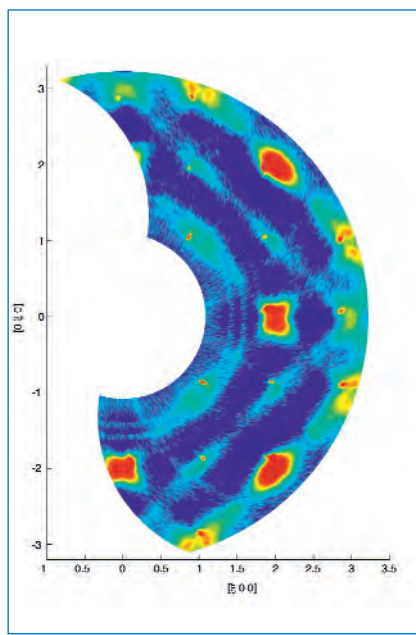


**Figure 3:** Map of inelastic response in PZN-8%PT at  $\Delta E = 3 \text{ meV}$  collected with FlatCone on IN20.

several in-house and regular user experiments investigating lattice vibrations in relaxor ferroelectrics PZN-8%PT ( $\text{PbZn}_{1/3}\text{Nb}_{2/3}\text{O}_3$ -8%  $\text{PbTiO}_3$ ) and PMN ( $\text{PbMg}_{1/3}\text{Nb}_{2/3}\text{O}_3$ ), magnetic ordering in a heavy fermion compound  $\text{PuCoGa}_5$  and spin-1/2 soliton dynamics in a 1D-antiferromagnet  $\text{CsCoBr}_3$ . Maps providing an overview of the inelastic response over several Brillouin zones for samples of habitual size are readily obtained within 1-2 hours of measurement time. In order to obtain a detailed coverage of the  $(\mathbf{Q}, E)$  range of interest, the dead angles between the channels have to be covered by combining data from two sweeps obtained with the multianalyser bank displaced by  $1.25^\circ$ . As an example, **figure 3** displays the inelastic response at a constant energy transfer of 3 meV in PZN-8%PT, one of the most studied relaxor ferroelectrics [2]. The new finding in these data are the diagonal  $[110]$  ridges of diffuse inelastic scattering, bearing potential information on the dynamics of the frequently discussed polar nanoregions, expected to be responsible for the exceptional dielectric properties of the relaxors. The strong intensity maxima, close to the Brillouin zone centres, carry information on the waterfall anomaly of the

phonon dispersion and have been subject to extensive studies in this material using the classical TAS configuration [3]. On the other hand the presence of the same anomaly in another member of the family of relaxor perovskites, the PMN, has been subject to extensive discussions so far [4].

**Figure 4** displays a cut through a three-dimensional block of scattering data from PMN collected by a series of  $E = \text{constant}$  sweeps, which brings evidence for the almost vertical phonon dispersion in PMN as well; the slight asymmetry between the left- and right-hand side of the response is due to focusing effects in the  $(\mathbf{Q}, E)$  space.

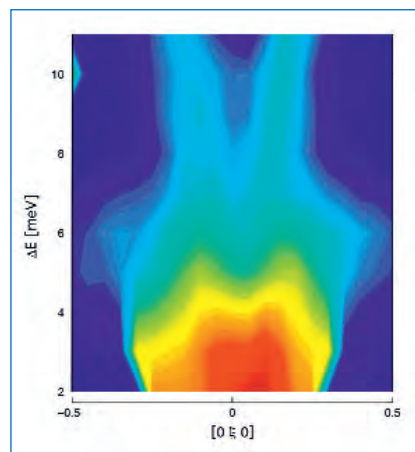


**Figure 4:** The waterfall phonon dispersion anomaly in PMN; a  $(\mathbf{Q}, E)$  cut through a series of  $E = \text{constant}$  maps collected with FlatCone on IN20.

## References

- (1) R. Born, D. Hohlwein, *Z. Phys. B* 74 (1989) 547
- (2) P.M. Gehring, S.E. Park, G. Shirane, *Phys. Rev. Lett.* 84 (2000) 5216
- (3) J. Hlinka, S. Kamba, J. Petzelt, J. Kulda, C.A. Randall, S.J. Zhang, *Phys. Rev. Lett.* 91(2003) 107602
- (4) S.N. Gvasaliya, B. Roessli et al, *J. Phys.: Condens. Matter* 17 (2005) 4343

# FIGARO: a new reflectometer to investigate fluid interfaces

**Authors:**

*G. Fragneto, R. Cubitt and I. Sutton (ILL)*

We report on the progress in the project for a new reflectometer for the study of thin films from horizontal samples that will complement studies on the D17 reflectometer at the ILL. The instrument will be devoted to soft matter and biology for the characterisation of layers at fluid interfaces with a fraction of nanometer resolution. Performances in terms of flux will be similar to those of D17.

**FIGARO** (Fluid Interfaces Grazing Angles Reflectometer) will be a high flux, flexible resolution, time-of-flight reflectometer with a vertical scattering plane, which will be commissioned at the ILL by spring 2008. It will be used for studies of thin films at air/liquid and liquid/liquid interfaces mainly in the realms of soft matter and biology. Applications involve the study of the interaction of

proteins with lipid monolayers, surface behaviour of surfactants, polymers and other amphiphiles at liquid/air and liquid/liquid interfaces. A polarised neutron option will not be available on day one, although this is an option not excluded for the future.

Unique features of the instrument include the simultaneous use of a Brewster Angle

Microscope during the reflectivity measurements and the possibility to strike the interface from above and below in a wide Q-range. With an incoming beam of wavelengths comprised between 2 Å and 30 Å, it will be possible to attain a Q-range from  $\sim 0.002 \text{ \AA}^{-1}$  to  $\sim 0.32 \text{ \AA}^{-1}$  by using two incoming angles of  $0.7^\circ$  and  $3^\circ$ .

The instrument will be fed by a 28 m long  $m=2$  supermirror guide, of 80 mm width and 15 mm height at the reactor beam port (H17).

The guide height will be increased up to 30 mm at the instrument to take up the divergence of the beam in the low resolution measurements. **Figure 1** shows a simulation at the end of the guide of the neutron flux integrated over the full divergence vs. wavelength (simulation by K. Andersen, ILL).

**Figure 2** shows a simplified drawing of the instrument. The first component of the instrument is a series of three guides containing frame-overlap mirrors to remove wavelengths bigger than 30 Å, 20 Å and 10 Å, respectively. Four choppers follow, with carbon fiber discs of 800 mm diameter and  $45^\circ$  aperture, independently rotating in pairs at a speed up to 4500 rpm, depending on the wavelength range used. The distance between the discs is such that 6 different wavelength resolutions can be obtained, ranging from 1.2 to 10%, by keeping the projected chopper openings equal

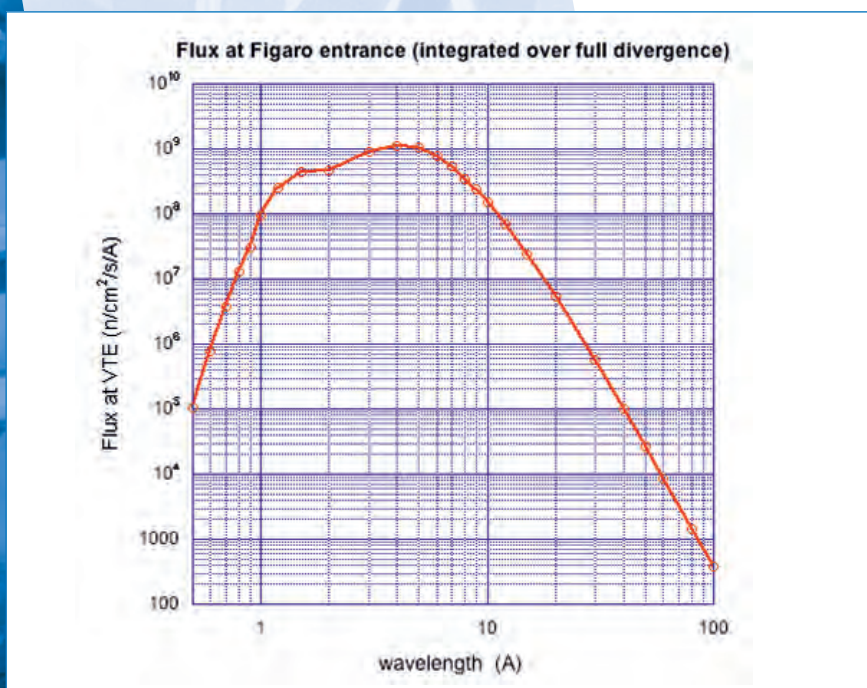


**Figure 1:** Simulation of the flux at the exit of the H17 guide.

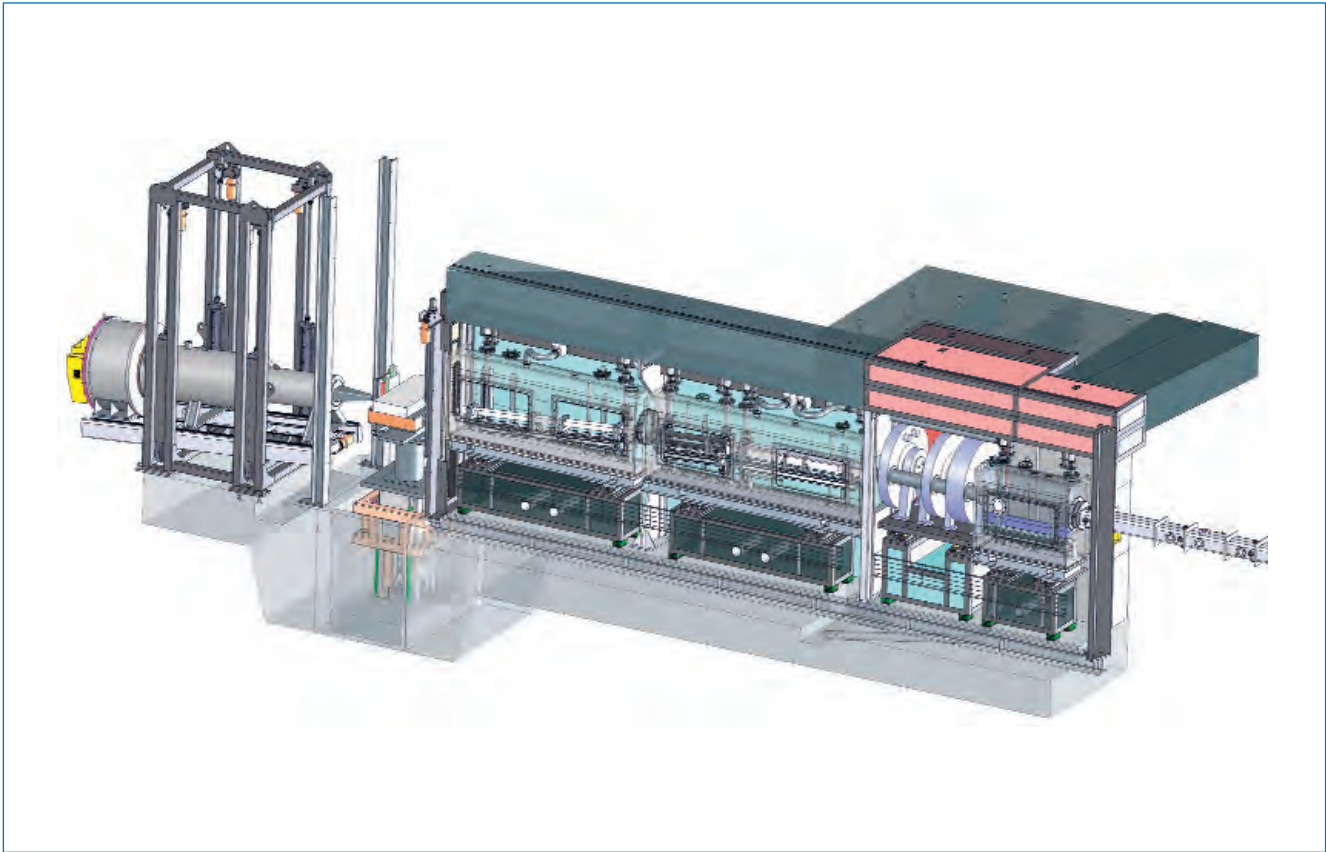


Figure 2: Schematic view of the instrument FIGARO.

to zero. The system is being assembled at Eads Astrium Ltd. (Freiburg, Germany).

Choppers are followed by two guide sections covered with supermirrors of  $m=4$  deflecting downwards and upwards to allow incoming angles of the neutron beam between  $\pm 0.3$  and  $\pm 4^\circ$ . Angles are not fixed and therefore a wide choice of selected  $Q$ -ranges is allowed. These elements are also used to focus the beam in the horizontal plane. For liquid/liquid interfaces it is important that the incoming beam can approach the interface from above or below the horizon as one liquid phase may be far more easily penetrable than the other.

The deflecting guides are followed by a 2 m collimation section, in order to eliminate off-specular scattering arising from the two supermirrors, comprising two slits and an absorbing guide on the top and bottom faces and  $m=4$  supermirror sides to carry

on the horizontal focusing down to 40 mm. A gas filled monitor will be used to measure the intensity of the incoming beam for data normalisation at high angles (i.e. wide slit opening).

The sample stage is equipped with active and passive anti-vibration systems, x-y-z translation axis, goniometer for solid samples. A Brewster Angle Microscope (Nanofilm, Germany) will be mounted on a Langmuir trough when studies of insoluble monolayers are carried out, for simultaneous detection of in-plane features. The imaging of thin films at the gas-liquid interface is often used for studying in-plane features. Images will be collected during the neutron measurements for different reasons, one being a quality check of samples that cannot be characterised fully before the neutron reflectivity measurements and also to quantitatively assess the in-plane features and their possible modifications during the acquisition as

for example in kinetics scan. The lateral resolution of the microscope is  $2 \mu\text{m}$ .

A two-dimensional multitube detector will be positioned at 3 m from the sample. It will be able to move horizontally up to 1 m distance from the sample, and up and down to detect the reflected and direct beams at all angles. It consists of an Aluminium plate with 64 squared holes of 7,5 mm internal side and 2 mm resolution along the 250 mm length. This detector will allow measurements of specular and off-specular reflectivity as well as GISANS. A high count rate will give the possibility of measuring the direct beam signal for data normalisation at the first angle with wider slits than what is now allowed on D17 and therefore faster measurements will be possible.

The detector technology is novel but very similar to that of multitubes. If the prototype tests fail, the multitubes option will be used.

# IN15: stronger and longer

**Authors:**

*B. Farago, P. Falus and C. Gomez (ILL)*

We report the improvements achieved on the IN15 high resolution neutron spin-echo spectrometer during the nine month reactor shutdown. The wavelength range has been extended toward shorter wavelengths while improving intensity across the board. As a result of the higher intensities and a careful realignment half microsecond Fourier time has been reached with a resolution function still above 0.3.

## 0.1 Stronger

The IN15 spin-echo spectrometer is situated on the H51 cold neutron guide. This is a 40 mm x 120 mm cold neutron guide which is shared between the instruments D22 and IN15. D22 uses the upper 55 mm and to accommodate both instruments IN15 uses the lower 55 mm with a splitter, which consists of Si plates deviating the beam at 3 degree. At the time of construction only m=2 super mirrors were available, which cut off all wavelengths below about 8.5 Å. This beam was then polarised further downstream with a V shaped cavity polariser (also m=2 but polarising super mirror).

The advantage of the V-shape transmission polariser is that it maintains the beam direction. However, when used for a very broad wavelength range the V-polariser only works well if the neutron guide is properly illuminated at all divergence angles. If the guide is not completely illuminated, it could happen that the polariser diverts the direct beam sideways depleting the middle of the beam, leading to serious intensity losses after collimation.

With the excellent collaboration of the ILL Neutron Optics Group and Technical Services the splitter has been changed to an m=3.2 polarising FeSi super mirror, and

the V polariser was removed. With the new splitter mirror we expected the wavelength band to extend down below 6 Å and eliminate the need of a polariser for  $\lambda < 15$  Å. Simultaneously our ILL made selector was changed to an Astrium selector in order to be able to reach 6 Å while expecting a better transmission too.

The absolute neutron flux at the sample position was calibrated by measuring the scattering intensity from 0.5 mm thick water. Absolute scale was achieved using a few reference gold foil activation measurements (**figure 1**). **Figure 2** shows the inten-

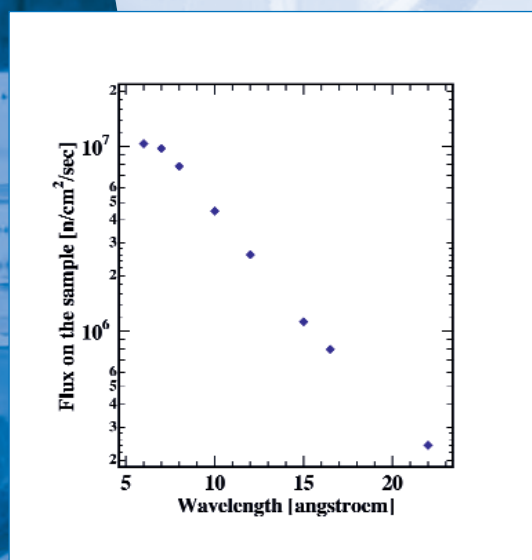


**Figure 1:** Neutron flux at the sample position of IN15 (July 2006).

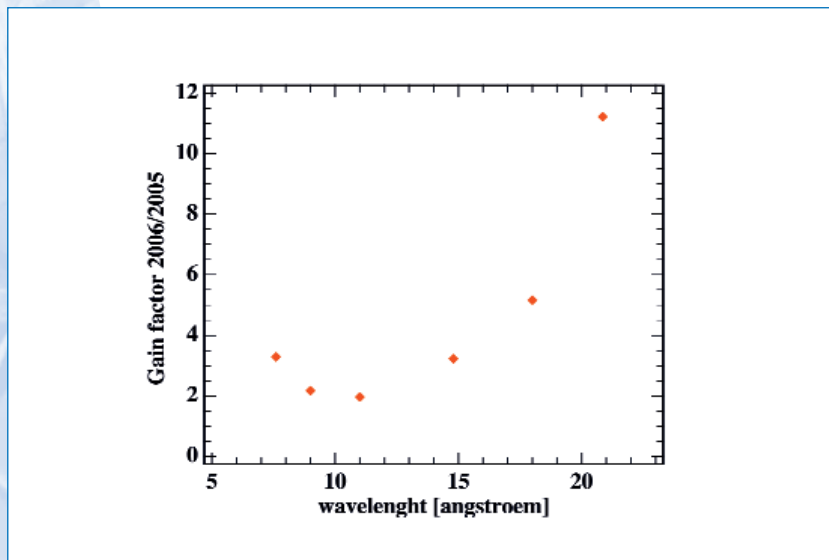
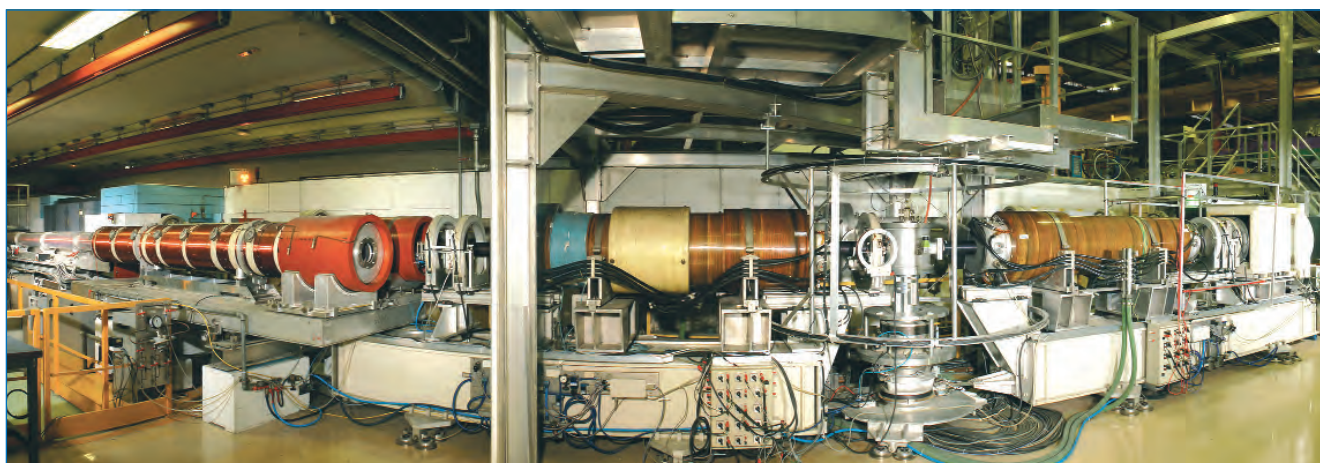


**Figure 2:** Intensity gain as a function of wavelength compared to the situation in 2005.



The high resolution spin-echo spectrometer, IN15.

sity gain compared to the situation in 2005. The improvements are much bigger than what we anticipated. The gain at short wavelength was expected because of the higher m super mirror. However at long wavelength the removal of the V polariser was much more beneficial than we anticipated. The real surprise is that there is a gain even in the 9 - 12 Å range. This improvement is partly due to the new selector, the rest is probably the result of the better reflectivity of the splitter. These intensities might improve even further in the near future if we slightly relax the collimation to take advantage of the full 55 mm height of the neutron guide.

We are in the process of reinstalling a much shorter V polariser to improve beam polarisation at the longest wavelengths, while not reducing the intensity of the shorter wavelengths. Presently the polarisation drops to about 50% at 22 Å.

## 0.2 Longer

In spin-echo measurements the longer is the neutron wavelength we use, the longer spin-echo times are reached and the better the energy resolution is. There are two limits on using longer and longer wavelengths. First the neutron flux from the cold source

sharply drops towards longer wavelengths, making experiments harder and harder. The second limitation is that for longer wavelengths it is more difficult to keep the magnetic field integrals the same for all trajectories, thus the instrumental resolution may not stay at sufficient levels. Since the intensity at 22 Å improved by more than an order of magnitude, the intensity should not be a limitation. How about resolution? Indeed with neutron spin echo, as it measures in Fourier time instead of energy space, the raw  $S(Q,t)$  measured on a sample is simply divided by the resolution function. While this is tremendously more simple than deconvolution, there is still a limit, namely if the echo curve of an elastic scatterer (the resolution) drops to zero, division by it is problematic. In practice, except in some special cases, it is not worthwhile to go beyond the point where the resolution drops below  $1/e$ . During the shut down we have undertaken an exercise to rigorously realign the instrument, and simultaneously re-optimised the positioning of the correction elements. As a result the resolution curves improved for all wavelengths, and we reached a new milestone of  $0.55 \mu\text{sec}$  at 22 Å as illustrated in **figure 3**. We should note here, that these resolutions were obtained with the maximum sample size (30 mm x 30 mm rectangular shape), thus they could be further improved if the sample size is decreased.

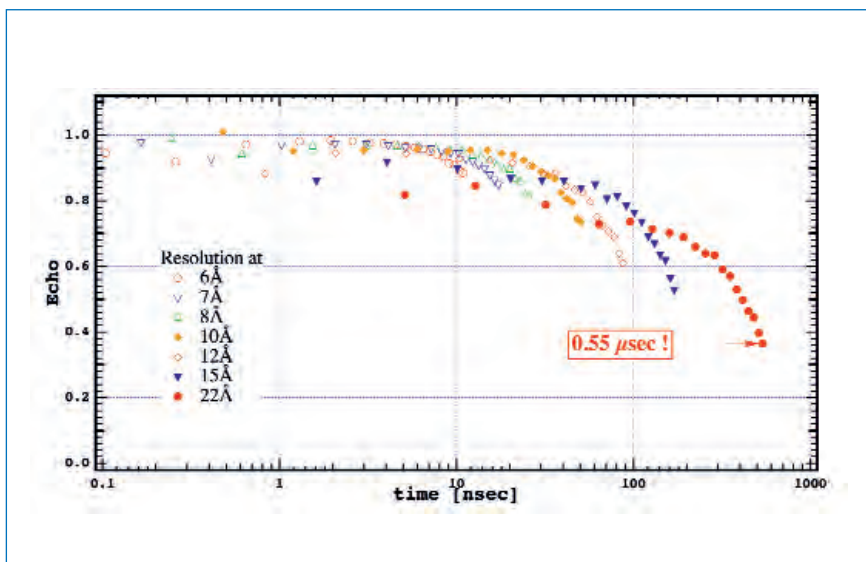


Figure 3: Instrumental resolutions for the available wavelength range of IN15 (July 2006).

# Towards perfect $^3\text{He}$ spin-filters

## Authors:

D. Jullien, P. Mouveau, A. Petoukhov,  
E. Babcock, K.H. Andersen,  
E. Lelièvre-Berna and F. Tasset (ILL)

2006 has been the year in which neutron spin-filters 'came of age' at the ILL. The levels of performance and usage on the instruments show that they have made the phase transition from developing technique to standard tool for polarised neutrons.

2006 has been an eventful year for the  $^3\text{He}$  spin-filter group. The departure of two staff members, one of whom has not yet been replaced, has presented a challenge in workload and continuity, while at the same time an opportunity for more efficient group work and for moving forwards in new directions. It is also the year in which Tyrex, the ILL  $^3\text{He}$  filling station, finally broke the 80% barrier in the optical-pumping cells (OPCs), delivering spin-filter cells to neutron instruments with polarisations in excess of 75%. The big jump in performance this year is due to the combination of improved laser optics and new electrodes for the RF dis-

charge in the optical pumping cells. **Figure 1** shows the polarisation in the OPCs during steady optical pumping (static mode) and while operating the compressor to fill a neutron spin-filter cell (dynamic mode). The polarisation values quoted below were measured with neutrons on D22 and PF1B.

**Figure 2** shows the development of  $^3\text{He}$  polarisation delivered to the instruments as a function of time. Also shown in the graph is the transmission of an unpolarised neutron beam through a  $^3\text{He}$  spin-filter adjusted to give a polarising power of 90% and 95% (corresponding to a flipping ratio

of 20 or 40). Compared to 2001, the  $^3\text{He}$  polarisation has increased by 20% (from 55% to 75%), which does not sound earth-shattering. However, this apparently modest increase in polarisation has given rise to an increase in neutron transmission (at constant flipping ratio) by a factor of two. **Figure 3** shows the neutron polarisation and transmission which are obtained with the current level of  $^3\text{He}$  polarisation. The "Opacity" is the product of the cell pressure, cell length and neutron wavelength. It can be adjusted for any wavelength to pretty much any value to give the desired compromise of transmission versus polarisation.

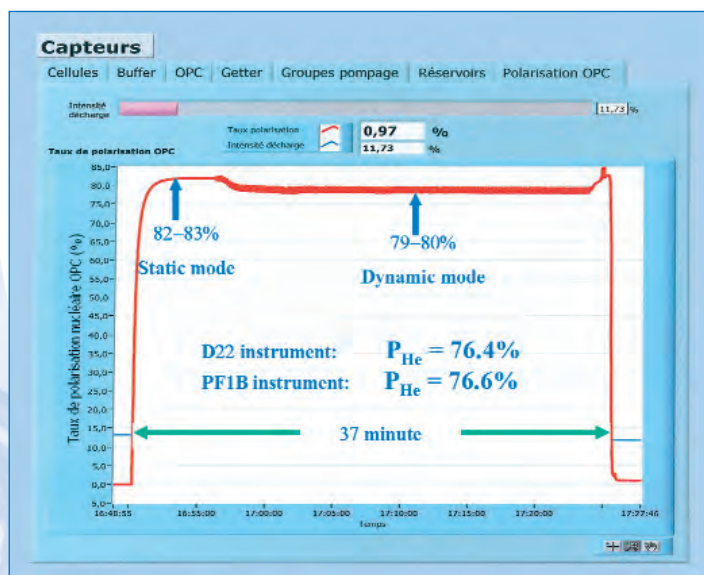


**Figure 1:** Polarisation in the OPCs during steady optical pumping (static mode) and while operating the compressor to fill a neutron spin-filter cell (dynamic mode).

◀ The  $^3\text{He}$  spin-filter group at the ILL standing in front of Tyrex. From the left: Pascal Mouveau, David Jullien, Sasha Petoukhov and Earl Babcock.

# Technical and computing developments

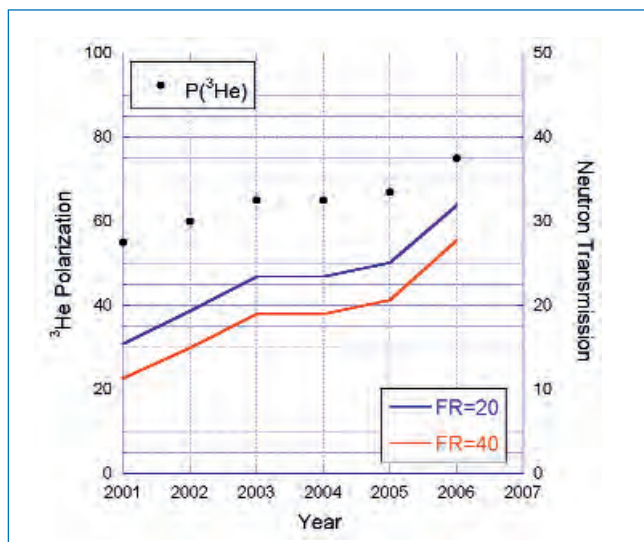


Figure 2: <sup>3</sup>He polarisation delivered to the instruments as a function of time.

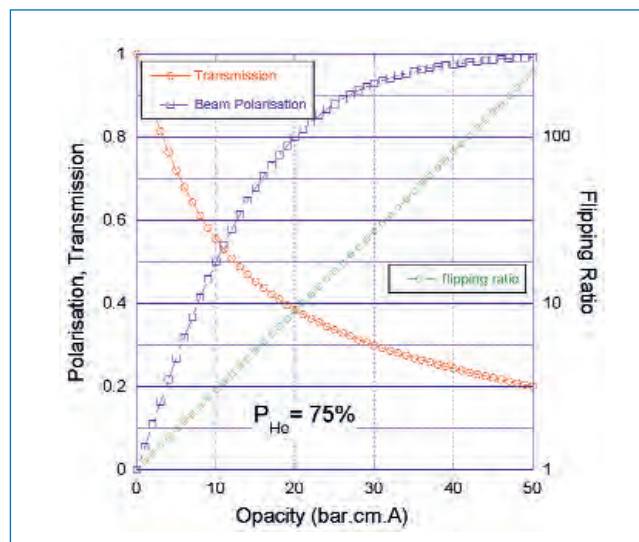


Figure 3: Neutron polarisation and transmission which are obtained with the current level of <sup>3</sup>He polarisation.

<sup>3</sup>He spin-filters have now reached a level at which their performance matches that of polarising crystals and supermirrors across the board. Other factors than bare performance, including convenience, cost-effectiveness, neutron background and resolution effects, should now be used to drive the

choice of polarisation technology for new instruments or instrument upgrades.

The year 2006 also saw an enormous increase in the number of spin-filter cells provided to neutron instruments. Figure 4 shows the time-evolution of the number of

spin-filter cells prepared by the <sup>3</sup>He group. The number of cells provided to the instruments more than doubled between 2005 and 2006. Part of the increase in production in 2006 is due to an increase in the number of instruments requesting <sup>3</sup>He spin-filters for characterising their instruments, allowing absolute determination of their beam polarisation with negligible systematic errors. However, the major increase in demand in 2006 comes from scheduled user experiments. Seeing as the cells are typically replaced every day, the number of cells corresponds quite closely to the number of beam days delivered.

Now that <sup>3</sup>He spin-filters have become a standard and indispensable option on a large range of instruments, we need to start preparing to safeguard future provision and performance. Spin-exchange Optical Pumping (SEOP), the alternative <sup>3</sup>He polarisation technique to that used on Tyrex, in which the <sup>3</sup>He gas is mixed with an alkali metal vapour, is now also being actively pursued at the ILL. A new laboratory is being installed in the office space adjacent to the laboratory vacated by the first ILL filling station "Cow", which is being transferred to the PNPI in Gatchina, Russia. An *in situ* repolarising SEOP system is currently being designed for the PF1B fundamental physics beam line. A similar system will also be installed on D3.

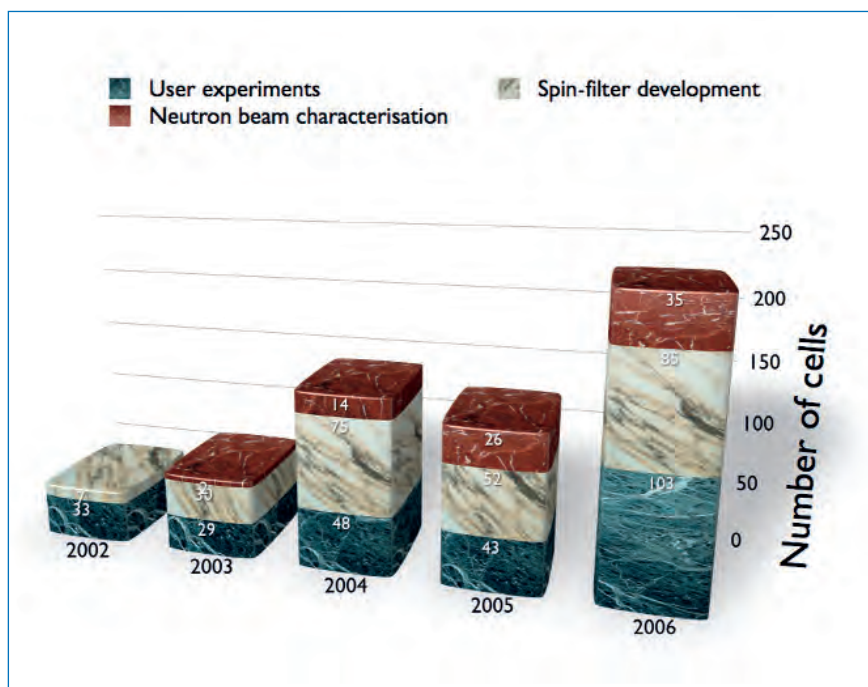


Figure 4: Time-evolution of the number of spin-filter cells produced at the ILL.

# New Bragg optics for ILL instruments

## Authors:

*P. Courtois, J. Baudin Cavallo, T. Guiblain, R. Hehn, E. Hetzler, C. Menthonnex, B. Mestrallet, T. Bigault, K. Ben Saïdane, A. Bouvier, D. Gorny, W. Graf and K.H. Andersen (ILL)*

Several new monochromators have been installed at the ILL over the last year. Large gains in instrument performance are expected as a result of the good crystal quality which can now be obtained. Progress has also been made in the performance of polarising Fe-Si supermirrors, which are approaching  $m=4$ .

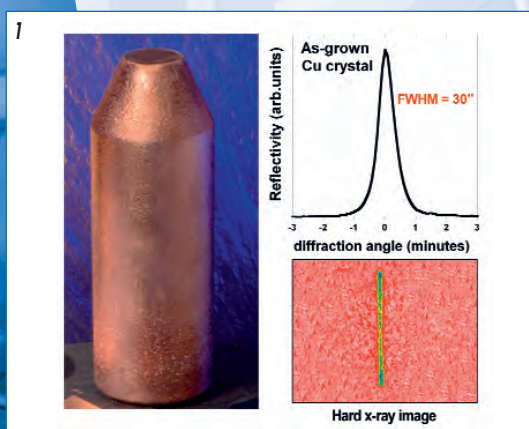
The 2006 has been a particularly productive year for the ILL monochromator group, with the completion of no less than six large,

focusing monochromator/analyser arrays: a new copper monochromator for D3, a germanium multi-analyser for IN8,

a Heusler analyser for IN22, and no less than three new monochromators for D19: PG(002), Cu(220) and Ge(115).

Instrument	Crystal	Mosaic	Experimental peak reflectivity	Theoretical peak reflectivity	Number of crystals	Dimensions (mm)	Positioning accuracy
D19	Cu(220)	0.25°	40 % (at 1.1 Å)	49 %	21	46 x 28 x 8	+/- 0.03°
D19	Ge(115)	0.20°	17 % (at 1.1 Å)	22 %	42	23 x 28 x 10	+/- 0.03°
D19	PG(002)	0.45°	75 % (at 2.4 Å)	85 %	28	46 x 22 x 2	+/- 0.05°
D3	Cu(200)	0.25°	50 % (at 1.1 Å)	56 %	44	50 x 10 x 8	+/- 0.02°
IN8C	Bent Ge(111)	0.30°	45 % (at 1.8 Å)	56 %	36	40 x 30 x 7	+/- 0.02°
IN22	Heusler	0.45°	24 % (at 1.8 Å)	27 %	33	40 x 17 x 5	+/- 0.02°

Table 1: Typical crystal specifications and neutron properties for the new monochromators completed in 2006.



**A number of key technical developments lie behind for this impressive production:**

- **Towards perfect Copper single crystals**

Using the Bridgman technique, we are now able to grow large copper single crystals with a very narrow and uniform mosaic spread of down to 30 seconds of arc (figure 1). Although such a small mosaic distribution is too narrow to be used directly for neutron monochromators, these almost-perfect crystals provide the ideal starting point for controlling the mosaic spread in a reliable and reproducible way. They are also of great interest for the construction of a gamma-ray Laue lens for astrophysical applications [1].

# Technical and computing developments

## • Towards mosaic Germanium single crystals

We have succeeded in growing good quality Ge single crystals with a neutron mosaic spread of up to  $0.1^\circ$  (**figure 2**). Such Ge crystals can be used directly for neutron monochromators where high resolution and no  $\lambda/2$  contamination are required. In addition, their mosaic properties can be combined with a controlled curvature in order to increase the total wavelength band selected by the bent crystal.

## • Manipulation of crystal mosaic

Starting from high-quality single crystals of copper and germanium, plastic deformation at high temperature is used to increase the mosaic spread up to the value which matches the instrument requirements on divergence, flux and resolution. Ge(115), Cu(220) and Cu(200) crystals with different mosaic spreads were produced for the D19 and D3 Millennium projects (**figure 3**). This technique was also successfully used to bend germanium crystals into a radius of curvature of 5 m for the IN8 multi-analyser (**figure 4**).

## • Neutron reflectivity

The peak reflectivity of Cu and Ge mosaic crystals was measured on the T13A test beam using a perfect germanium monochromator (**figure 2**). Because of extinction processes and structural defects, the measured peak reflectivity of mosaic crystals is generally somewhat less than the theoretical values calculated from the Darwin model of ideal imperfect mosaic crystals (**table 1**). It is remarkable to note that except for very small mosaic spreads (i.e. FWHM  $< 0.2^\circ$ ), where secondary extinction is important, the value of the copper reflectivity is very close to the theoretical data ( $R_{\text{exp}} = 85 - 95 \% R_{\text{th}}$ ). This result is mainly due to the very good homogeneity of the mosaic structure of the deformed crystal.

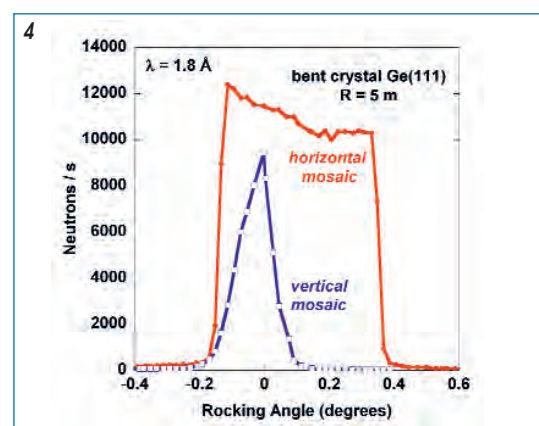
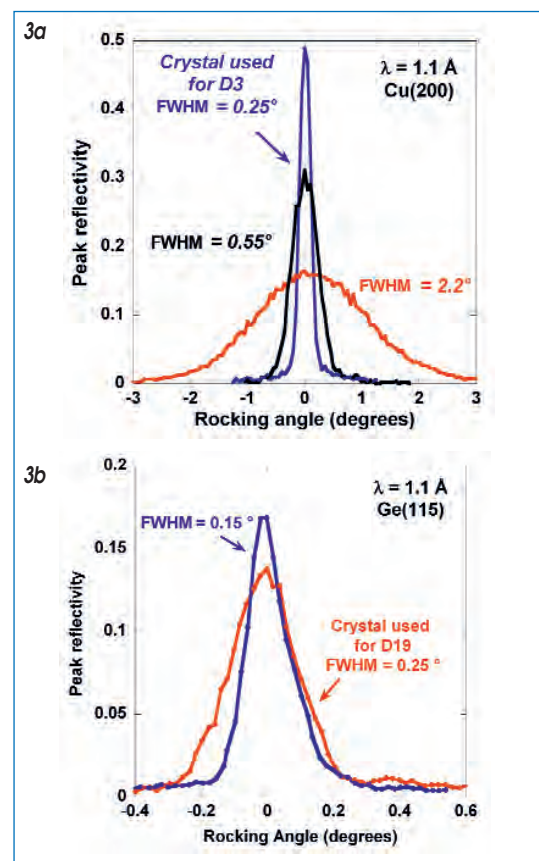
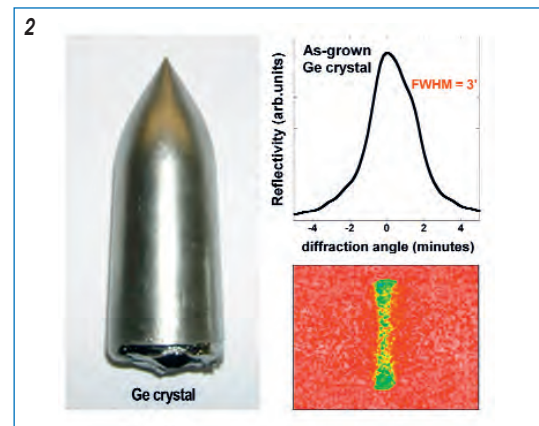
The as-grown Ge single crystals also present good reflectivities. Non-uniformity of the mosaic distribution is probably responsible for the slightly smaller reflectivity observed in the plastically deformed germanium crystals, which is still up to 80% of the calculated values.

**Figure 1:** Large copper single crystal of length 250 mm and diameter 80 mm grown at ILL and the corresponding hard X-ray diffraction image and peak profile.

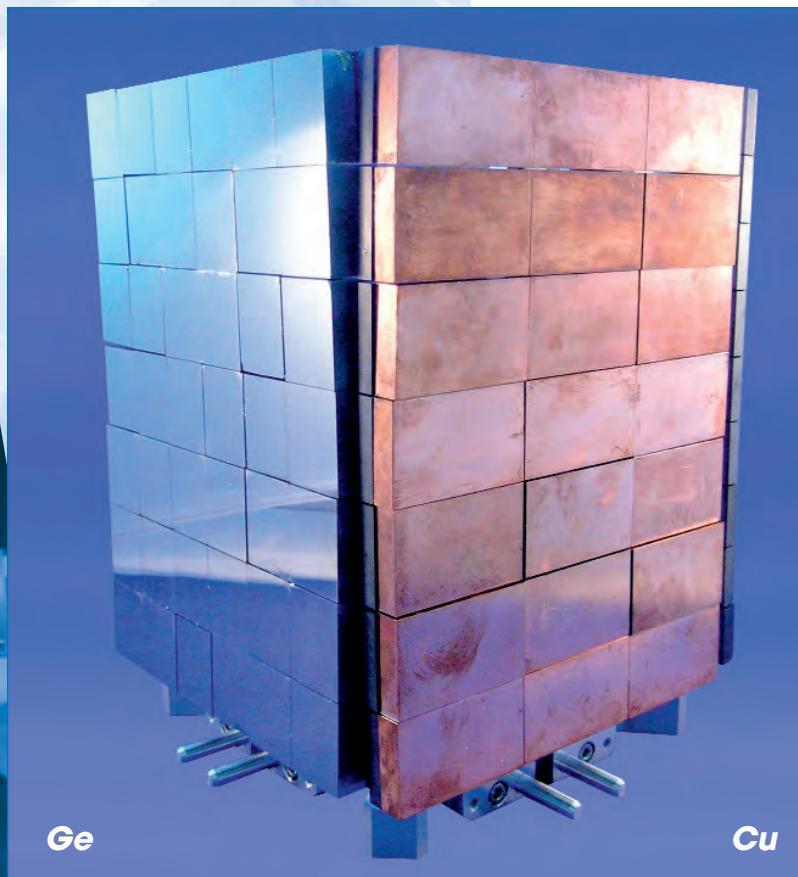
**Figure 2:** Mosaic Ge single crystal produced at ILL and the corresponding hard X-ray diffraction image and peak profile.

**Figure 3:** Rocking curves and neutron peak reflectivities from Cu(200) (**Figure 3a**) and Ge(115) (**Figure 3b**) crystals of different mosaic distribution obtained by plastic deformation at high temperature.

**Figure 4:** Rocking curves from a Ge(111) crystal after bending by plastic deformation (radius of curvature  $R = 5\text{m}$ ).



From left to right, the Ge(115), Cu(220) and PG(002), monochromators of the "4-face" monochromator unit for the **D19** Millennium project. Each face is a double fixed horizontal and vertical focus monochromator. The three crystals (6 for Ge) in each of the rows are glued on a precision-machined support of  $B_4C$  with their crystallographic planes inclined by angles corresponding to horizontal curvature. The rows are then positioned on an aluminum frame, which is machined to achieve the vertical focusing.

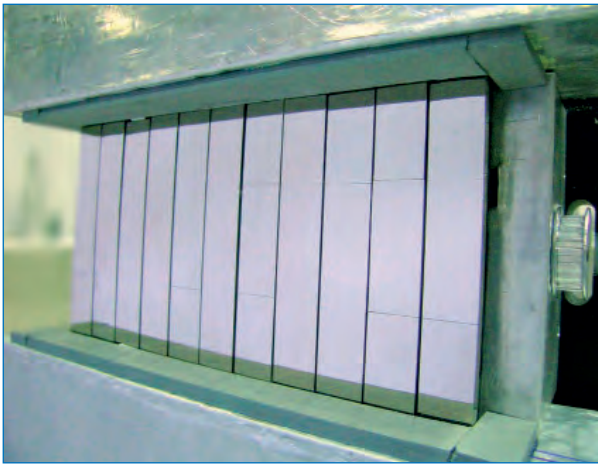


Combined with a  $^3\text{He}$  neutron spin-filter, the aim of the new vertically-focusing Cu(200) monochromator for the **D3** diffractometer will produce a monochromatic beam of polarised neutrons at short wavelengths (0.3 to 0.9 Å). In order to optimise the resolution of the instrument at high take-off angles, several Cu(hhl) planes reflections are accessible when rotating the crystals with respect to the Bragg angle.



# Technical and computing developments

The new Ge(111) multi analyser for **IN8** with its 9 columns of bent Ge crystals was installed in December 2006. Each column can be rotated independently. As a result, the **IN8** spectrometer can work either as a conventional TAS or in a dispersive mode. This will enable the mapping of selected regions in  $(Q, \omega)$  space. The use of Ge(111) crystals has the advantage of avoiding second-order contamination.



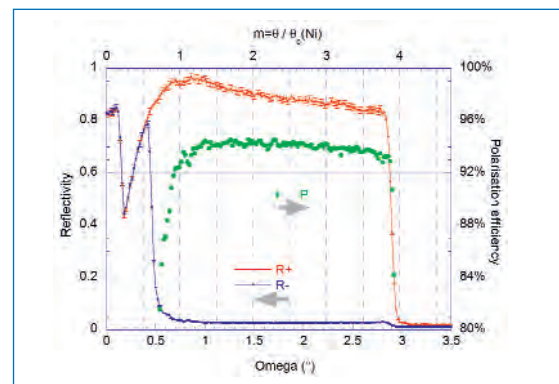
The new Heusler analyser for **IN22**.



## A little further with Fe/Si polarising supermirrors

Neutron supermirrors are a very efficient means of reflecting and polarising cold neutron beams. Magnetic and non-magnetic layers are alternated with a continuous variation in thickness, giving rise to Bragg diffraction within a continuous d-spacing range and extending the polarising behaviour to a much larger angular (or wavelength) range. For a monochromatic beam, the  $m$  value characterises the angular extension with reference to the critical angle of nickel for total reflection:  $\mu = \theta_{\max}/\theta_{\text{Ni}}$ . Optimising polarising supermirror coatings involves difficulties inherent in high- $m$  supermirrors [2], as well as a few additional difficulties. For instance, one has to match precisely the scattering length densities of both materials for one spin state. In 2006, the year in which the magnetron sputtering coating machines were relocated and recommissioned due to the Seismic Refit Programme, the performance of supermirror coatings went on progressing at the ILL. As an example, the figure shows the reflectivity of an  $m=3.8$  Fe/Si supermirror for both spin states, and the deduced polarisation efficiency. Note that the measured polarisation efficiency is limited here by the upstream polariser efficiency. The real polarising efficiency is certainly higher.

Fe/Si coatings are particularly well adapted for designing transmission polarisers [3], solid state polarisers [4] or reflection polarisers when activating materials cannot be used due to the high neutron flux. Work continues to push the performance of these coatings even higher.



## References

- (1) P. Courtois, K.H. Andersen and P. Bastie, *Copper Mosaic Crystals for Laue Lenses*, EXPA2006 (in press)
- (2) P. Boni, D. Clemens, M. Senthil Kumar and S. Tixier, *Physica B* 241-243 (1997) 1060
- (3) P. Courtois et al., *Physica B* (in press)
- (4) A. Stunault et al., *Physica B* (in press)

# Neutron diffraction on levitated liquids at the D4 diffractometer

## Authors:

**L. Hennef, I. Pozdnyakova, S. Brassamin, D. Zanghi and D.L. Price** (CRMHT, Orléans)  
**M.-L. Saboungi** (CRMD, Orléans)  
**V. Cristiglio, G.J. Cuello, P. Palteau and H.E. Fischer** (ILL)

Neutron scattering is an important source of structural information on disordered materials. For the past few years, the combination of aerodynamic levitation and laser heating at neutron sources has enabled structural investigations on liquid materials at very high temperature that was not previously possible with classical furnaces. The use of 3 mm spherical samples is a major challenge, however, since the irradiated volume is much smaller than that normally used with neutron scattering.

The molten state is a crucial stage in various industrial processes like glass manufacture, metallurgy and crystal growth. For all these applications, knowledge of the thermophysical properties of the liquid material is important.

Most of the physical properties of a high temperature liquid are related to its atomic structure, which also has an obvious fundamental interest. It is thus necessary to develop devices capable of probing the local environment of the atoms in the liquid sample. At very high temperature, it is difficult to use conventional furnaces because of several problems. In particular, the sample can be polluted by the container and its structural properties thereby modified. This has led to the development of various containerless techniques and their first use at neutron sources a few years ago [1].

We have developed a new high-temperature environment for wide-angle neutron diffraction measurements. The set-up is based on aerodynamic levitation and laser heating and has been specifically adapted to the D4 diffractometer. Aerodynamic levitation is

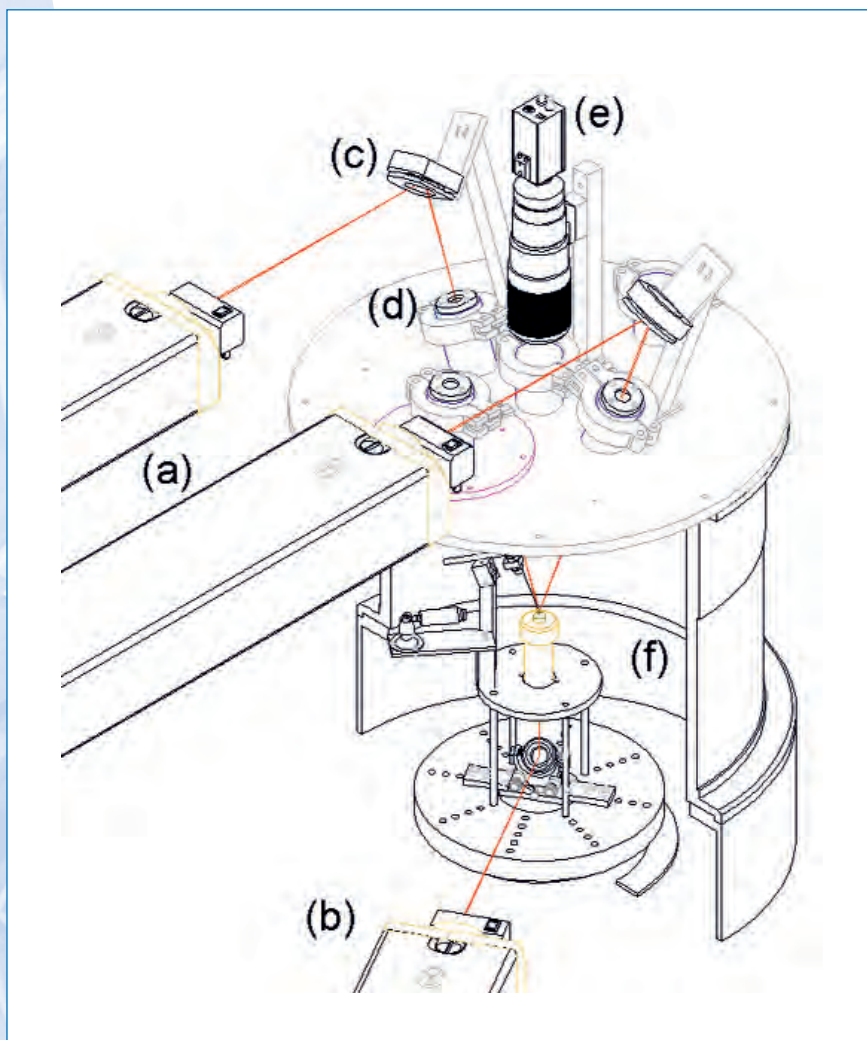


**Figure 1:** Schematic view of the experimental arrangement: laser heads (a,b), spherical mirrors (c), NaCl windows (d), video camera (e), levitation device (f).

a simple way to suspend samples which can then be heated with CO<sub>2</sub> lasers. The advantages of this technique are the simplicity and compactness of the device, making it possible to integrate it easily into different kinds of experiments. In addition, all types of samples can be used, including glasses, ceramics and metals [2].

The principle is relatively simple. A spherical sample with a diameter of about 3 mm is placed on a levitator. This device contains a convergent-divergent nozzle that channels a regulated gas flow onto the sample from below. For neutron diffraction, the nozzle is made of vanadium since this material has a very small coherent neutron scattering length, allowing easy subtraction of its diffraction intensity.

The sample is heated to the desired temperatures by two 125-W CO<sub>2</sub> lasers (figure 1). The infrared laser beams are focused onto the sample from above by means of spherical mirrors at two different angles in order to obtain a homogeneous temperature distribution. The laser beams enter the chamber through NaCl windows, transparent to the 10.6 μm wavelength.

A third laser directed at the sample through the nozzle from below is used to compensate the cooling of the sample from the gas flow. The temperature is measured with an optical pyrometer placed inside the chamber to avoid window corrections. Several video cameras (vertical and horizontal) are used to monitor the sample during the heating process.

The total structure factor  $S(Q)$  of liquid YAG (Y<sub>3</sub>Al<sub>5</sub>O<sub>12</sub>) at 2373 K (inset of figure 2) was measured at D4 using a wavelength of 0.5 Å over the 1.5°–135° angular range, giving a usable  $Q$  range of 0.3–23.2 Å<sup>-1</sup>. The total counting time was three hours including detector movements. The first of several peaks in  $S(Q)$  occurs at 2.1 Å<sup>-1</sup> and is very weak compared to its intensity measured with X-rays [3]. This implies that it corresponds mostly to cation-cation correlations that have relatively low weighting factors with neutrons compared to X-rays. *Ab initio* Molecular Dynamics (AIMD) simulations performed at the ILL reproduce this small peak exactly, which is seen to be due to Y–Y, Y–Al, and Al–Al correlations as postulated experimentally.

The total pair-distribution function  $G(r)$ , obtained via Fourier transformation of  $S(Q)$ , shows various peaks (figure 2). The first one at 1.76 Å corresponds to the nearest-neighbour distance for the Al–O bond and the second at 2.22 Å is due to Y–O correlations. Integration under the two first peaks gives coordination numbers of 4.1 and 5.5 for Al–O and Y–O bonds respectively, in agreement with the X-ray work. The AIMD simulations reproduce the experimental  $G(r)$  and  $S(Q)$  quite well (figure 2) and make it possible to determine the six partial pair-distribution functions.

The present study shows that this new apparatus [4] developed for the D4 diffractometer is a powerful tool for studying liquid materials at very high temperatures. Thanks to the high flux at the ILL, we find that the use of relatively short counting times with small samples is sufficient for obtaining high-quality structure factors over a large  $Q$  range. It is then possible to derive reliable results for the liquid-state structure with good resolution in real space. The experimental results are well modelled by AIMD simulations.

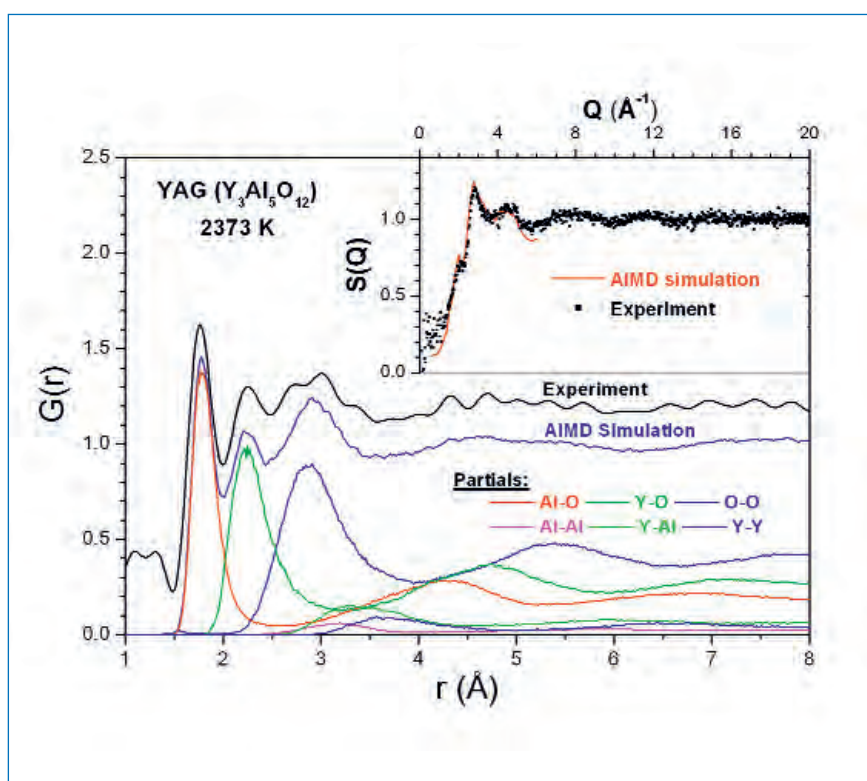


**Figure 2:** Total pair-distribution function  $G(r)$  for liquid YAG at 2373 K: comparison between experiment and AIMD simulations (the experimental curve is shifted up). The lower curves depict the 6 partial pair-distribution functions obtained from the simulations. The inset shows the experimental total structure factor  $S(Q)$  measured over 3 hours, as compared to the simulation results.

## References

- (1) C. Landron et al., *Phys. Rev. Lett.* 86 (2001) 4839
- (2) S. Krishnan and D.L. Price, *J. Phys.: Condens. Matter* 12 (2000) R145
- (3) J.K.R. Weber et al., *Phys. Rev. Lett.* 84 (2000) 3622
- (4) L. Henet et al., *Rev. Sci. Instrum.* 77 (2006) 053903

# Genetic algorithms produce an optimum design for the wide-angle spin-echo spectrometer WASP

## Authors:

**P. M. Bentley** (Hahn-Meitner Institut, Berlin)  
**P. Fouquet, R. Hölzel and M. Crawford** (ILL)

As neutron instrumentation is becoming increasingly complex, traditional methods of optimisation are often prohibitively time consuming, and are likely to stop far short of a global optimum. We have taken an evolutionary step forwards by borrowing from the artificial intelligence community, and developing instruments that – by breeding in a virtual environment – evolve themselves into a superior design. We present here the use of genetic algorithms (GAs) in the design of magnetic fields for the next-generation spin-echo instrument ‘WASP’ that will replace IN11 as part of the ILL Millennium Programme.

Neutron instrument design has changed enormously since the pioneering work at the first neutron reactors, and neutron data acquisition rates have increased by orders of magnitude. The success of the ILL Millennium Programme illustrates the gains that can be made by careful

design of neutron instruments. Human efforts can, however, only push instrument design to a certain point, before further optimisation can become a real headache. For a modern spectrometer, the process often reduces to a search through a high-dimensional parameter space with preva-

lent local optima and where the parameters are strongly correlated. In addition, because of the instrument complexity, it is convenient to use Monte Carlo methods to assess the instrument’s performance, which means that the parameter space is noisy and partial derivatives are unreliable.

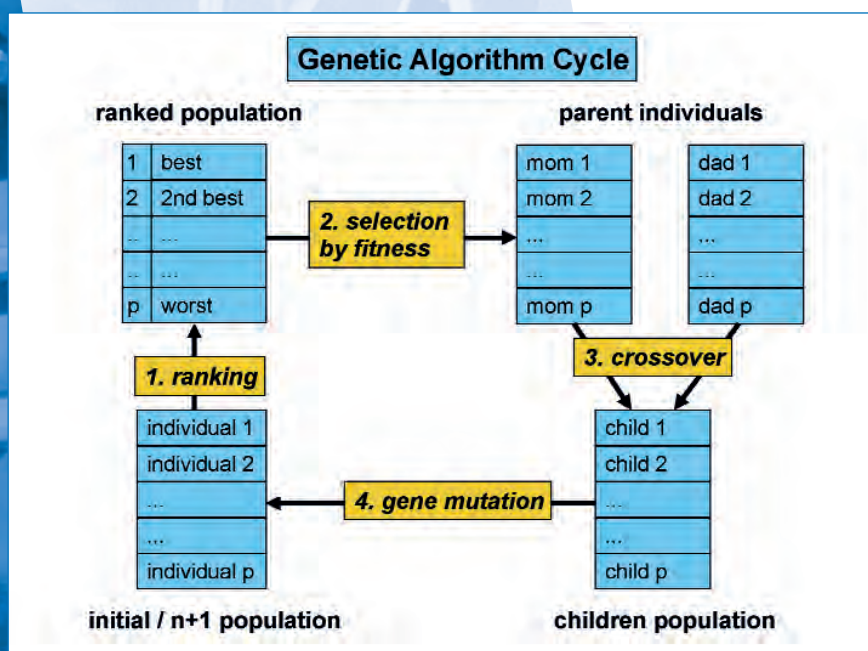


**Figure 1:** Overview of the steps performed in a genetic algorithm to establish a next generation. This cycle is typically performed a few hundred times to guarantee convergence of the calculations.

The optimisation of the neutron spin-echo spectrometer WASP (Wide Angle SPin-echo) involves all the difficulties pointed out above. In the neutron spin-echo technique the Larmor precession of the neutron spin in a magnetic field is used to encode the velocity of the neutrons. By comparing the precession angles of the neutron spins, in identical fields before and after scattering from the sample, tiny velocity changes (or energy changes) can be measured. An optimum spectrometer design possesses the quality that all neutrons are exposed to exactly the same field integral, irrespective of their differing trajectories. In addition, there are regions in the spectrometer where the magnetic field directions are rotated and a guide field is needed to prevent the loss of neutron polarization. All these features can be analysed and optimised by a combination of analytic magnetic field calculations on ensembles of trajectories created using a Monte Carlo approach. Although our analytical calculations are extremely quick and

# Technical and computing developments

accurate when compared to a finite element approach, we quickly reached a point where further manual optimisation was impossible. At this point we chose to apply optimisation algorithms.

GAs are a branch of artificial intelligence that exhibit machine-learning, and they excel in noisy and strongly-correlated parameter spaces with local optima. They are based on the ability of life forms to self-adapt to meet the demands imposed by their environment [1], and were first developed in computer science by Holland [2]. Whilst they have been successfully deployed in finance, engineering, and the military, within the neutron community they are a relatively untapped resource, seeing use primarily as a superior tool for *ab initio* determination of structure from diffraction data [3].

The first step in using GAs is to encode the instrument parameters into 'chromosomes'. In the first instance, this is rather trivial because numbers are stored in memory in binary-based encoding, providing us with 'gene' symbols, i.e. '1's and '0's. The next and most crucial step is to formulate a figure of merit, which encapsulates the knowledge of the designer, and is used to compare competing instrument designs in a quantitative way. For WASP, this figure of merit was calculated from the field integral (resolution) and the field homogeneity (linked directly with polarisation losses). It also enforced constraints on instrument size and guide fields [4].

The final stage is to create a *virtual population* of creatures, i.e. solutions, which are both autonomous and independent. The evolutionary process in each generation involves several different mechanisms (figure 1). Parents are chosen pseudo-randomly from the top of the gene-pool, and their genetic code is mixed to create child solutions (*uniform cross-over*). During this process mutations occur, so that ~ 0.7 % of genes is miscopied, i.e. a '1' is written instead of a '0' or vice-versa. Note that the mutation produces a random-distance jump in a parameter value, meaning solutions can easily hop out of local minima. 15 % of the creatures were cloned into the

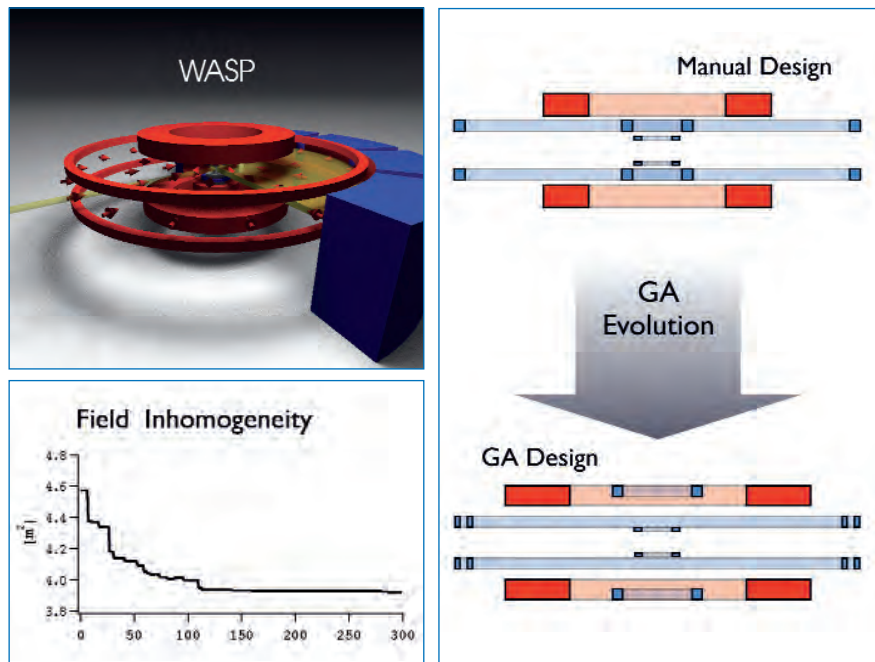


**Figure 2:** Evolution of the WASP magnetic coil design using a genetic algorithm. The upper left hand corner shows an artists view of the new spectrometer. On the right hand side vertical cuts through the instrument are compared for the instrument developed by a manual search (starting point for the GA) and the optimised design. The graph shows the 15 % decrease of the inhomogeneity of the field by the GA optimisation. The red rectangles represent the main magnetic field coils, whereas the blue rectangles stand for correction coils that reduce the field at critical points of the set-up.

next generation, which simulates the existence of older creatures who are sufficiently successful to have multiple children. The best creature in the whole generation is always cloned, a process known as *elitism*. This keeps the best solution and causes the population to converge faster. These processes are typically repeated over a few hundred generations, and a superior instrument design emerges just like a superior species design in the natural world.

Using genetic algorithms, we have successfully arrived at an optimised magnetic field design for the WASP spectrometer [4]. The optimisation still required a substantial effort, in particular for establishing an efficient and appropriate figure of merit. However, we found that the concentration of the instrument designer's work on creating a good figure of merit forces the developer to formulate clear and quantifiable conditions for a good instrument. Finally, one of the biggest advantages of our approach is that once a good figure of merit is set, any

changes in the boundary conditions due to technical developments can be implemented by a quick (~ 24 hour) re-optimisation of the whole instrument – an invaluable advantage in the construction phase.

## References

- (1) C.R. Darwin, 'On the Origin of Species by Means of Natural Selection' (Murray, London, UK, 1859)
- (2) J.T. Holland, 'Adaptation in Natural and Artificial Systems' (MIT, Cambridge, MA, USA, 1975)
- (3) P. Juhás, D.M. Cherba, P.M. Duxbury, W.F. Punch, S.J.L. Billinge, *Nature* 440 (2006) 655
- (4) G. Hölzel, P.M. Bentley and P. Fouquet, *Rev. Sci. Instrum.* 77 (2006) 105107

# Virtual experiments: combining realistic neutron scattering instruments and sample simulations

## Authors:

**E. Farhi and M.R. Johnson** (ILL)

**V. Hugouvieux**

(University of Montpellier II and ILL)

**W. Kob** (University of Montpellier II)

A new sample component is presented for the Monte Carlo, ray-tracing program, McStas, which is widely used to simulate neutron scattering instruments. The new component allows the sample to be described by the dynamic structure factor, which is separated into coherent and incoherent contributions. Absorption and multiple scattering are treated. The sample component can also be used to treat any scattering material which may be close to the sample and therefore contaminate the total, measured signal. We present an example of simulated scattering from I-Rb on an IN6-type instrument.

The signal measured with neutron instruments may be contaminated in certain experiment configurations. Data analysis raises questions concerning various contributions to the total signal such as background, coherent and incoherent scattering, self-shielding and multiple scattering.

Indeed the experimental signal is the convolution of the instrument response (including sample environment) and the signal due to the interaction between neutrons and the sample (structure and dynamics). The precise knowledge of both these contributions is required to allow the separation of instrument and sample signals.

This paper presents the new *Isotropic-Sqw* component in the McStas code [1] which allows the sample scattering function  $S(Q, \omega)$  to be included in a Monte-Carlo neutron scattering instrument simulations and therefore to model accurately liquids, glasses, powders, polymers and gases. In particular we

focus on the possibilities of such a numerical approach for handling multiple scattering and labelling most contributions arising in the total signal.

The method is based on the expression for the neutron partial differential cross section [3],

where the dynamic structure factor  $S(Q, \omega)$  is used as a probability function in order to improve the Monte-Carlo variance reduction. The implementation can be summarised in four steps:

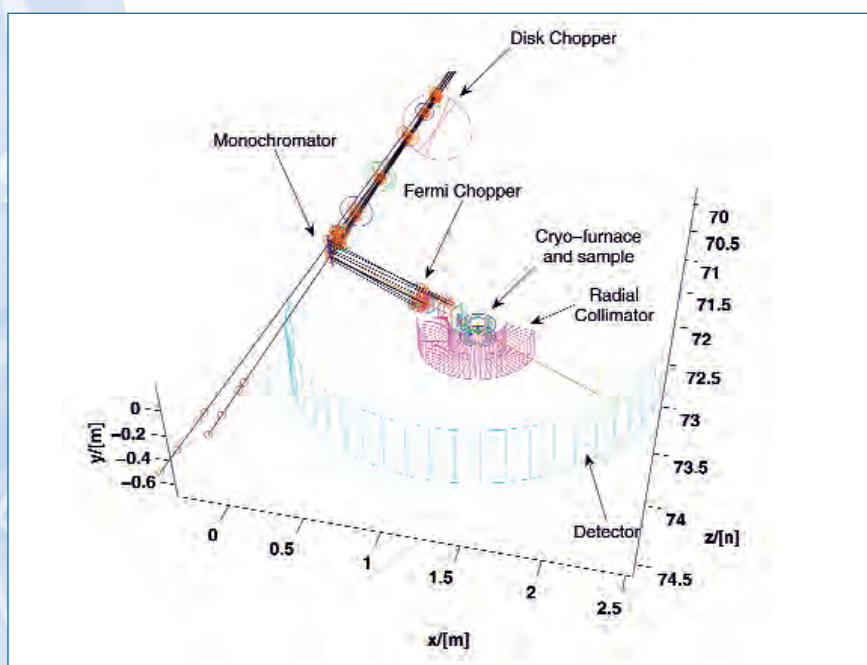


Figure 1: A view of the time-of-flight model instrument produced by McStas.

# Technical and computing developments

1. Determination of the probability of interaction for each neutron along the path as a function of the material density  $\rho$ , the path length  $d$  in the material and the integrated total cross section  $S$  over the accessible dynamic range. This sets the total scattered intensity from the sample [2].
2. Weighting of the neutron interaction with the absorption probability, and selection of the type of interaction (coherent or incoherent).
3. Selection of the wave vector and energy transfer from the dynamic structure factor  $S$  used as a probability distribution. This step requires the density of states and the density of wave vector transfers for each energy transfer to be computed. Then we account for the detailed balance.

4. Checking that selection rules can be solved and choose randomly an angle on the scattering cone.

This procedure is iterated until the neutron leaves the sample.

## Example

In order to demonstrate the use of the component, we built a model of a direct geometry time-of-flight machine based on the IN6 design (figure 1). In our model, a liquid rubidium sample at 350 K obtained from classical molecular dynamics in a niobium cylindrical container ( $\phi=1.6$  cm) was inserted in a cryo-furnace made of 4 aluminium/niobium shields. The spectrometer was operated at  $\lambda=3.4$  Å. The virtual experiment records scattered neutrons just as in a real experiment (upper data set of figure 2),

but we may trace each neutron history in order to separate contributions from the sample and the environment. Further study shows that results are in agreement with both real measurements and previous multiple scattering estimation codes [4]. Typical simulation times are considerably faster than real data acquisition. The simulation helps greatly to identify signals which are not directly related to the expected sample physics.

The new *Isotropic-Sqw* component is freely available to users within the McStas package [1], together with a limited data base of materials (powders and liquids). This latter is currently being extended by means of extensive molecular dynamics simulations, in order to cover the usual materials used for neutron experiments.

McStas is jointly developed by Risø and ILL. It is supported as a JRA of the NMI3 network by the European Commission under the 6<sup>th</sup> Framework Programme through the Key Action: Strengthening the European Research Area, Research Infrastructures.

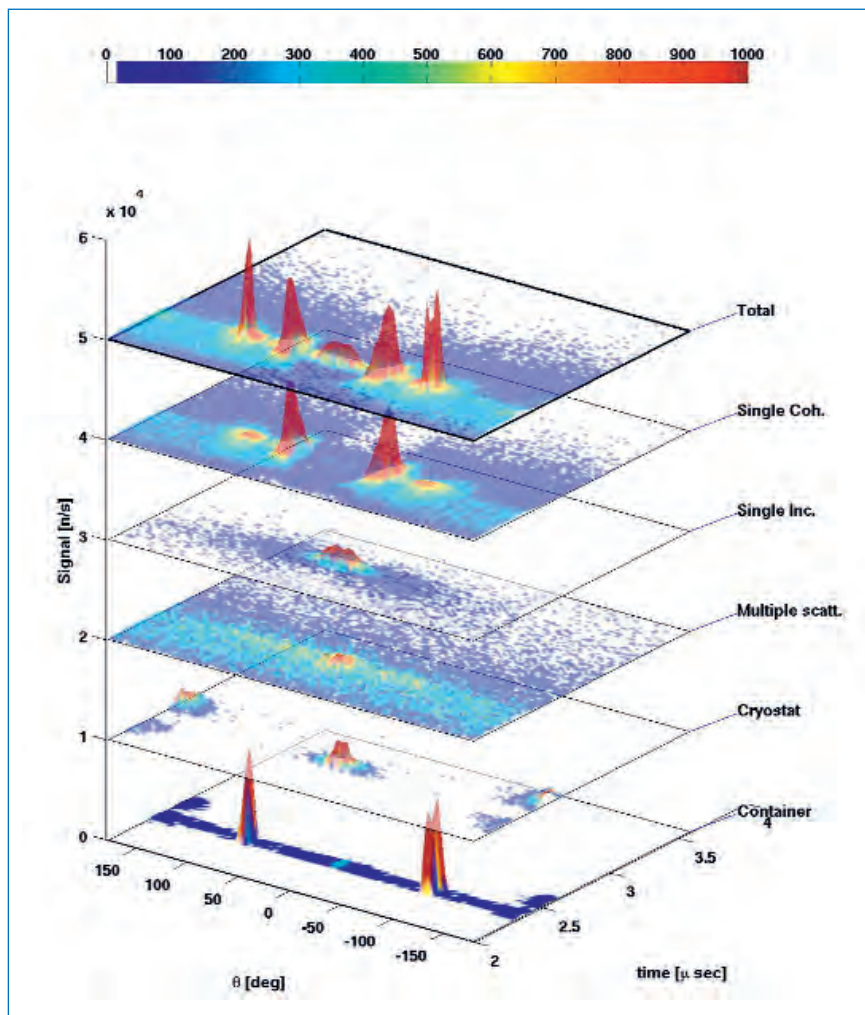


**Figure 2:** The simulated total signal from I-Rb at 350 K is separated into the coherent, incoherent, multiple scattering, cryostat, and container contributions. The cryostat and multiple scattering have been multiplied by a factor 10.

## References

- (1) K. Lefmann and K. Nielsen, *Neutron News* 10 (1999) 20 and P. Willendrup, E. Farhi and K. Lefmann, *Physica B* 350 (2004) 735. See website <http://www.mcstas.org/>
- (2) V.F. Sears, *Adv. Phys.* 24 (1975) 1
- (3) P.A. Egelstaff, *An introduction to the liquid state*, Academic Press, London (1967)
- (4) J.R.D. Copley and J.M. Rowe, *Phys. Rev. A* 9 (1974) 1656 and *Phys. Rev. Lett.* 32 (1974) 49

## How to gain a factor of 100 in flux on D17

**Author:**

**R. Cubitt (ILL)**

The ILL is presently the most powerful source of neutrons in the world but will soon be overtaken by new spallation sources in the USA (SNS) and Japan (JPARC). The proposed European source, the ESS, will be even more powerful still and yet will have approximately the same mean flux as the ILL. The reason these sources gain so much is that they are naturally pulsed whereas at the ILL, in order to establish the wavelength, we are obliged to either monochromate or to chop the beam. In both of these processes the vast majority of neutrons are thrown away without even hitting the sample. If we could find a detector which not only measures the scattered position of a neutron but tells us its wavelength as well, we could use all the available neutrons and would have a source that rivals the ESS.

This article explores the possibility of using the optical process of refraction to detect the neutrons wavelength without the use of choppers or monochromators.

As with light we can define a refractive index for neutrons at an interface. It is only a function of the wavelength and the scattering length density (Nb) difference at

the interface. When a well collimated beam strikes a flat surface (with a positive Nb against air) the transmitted beam bends towards the plane of the interface and is

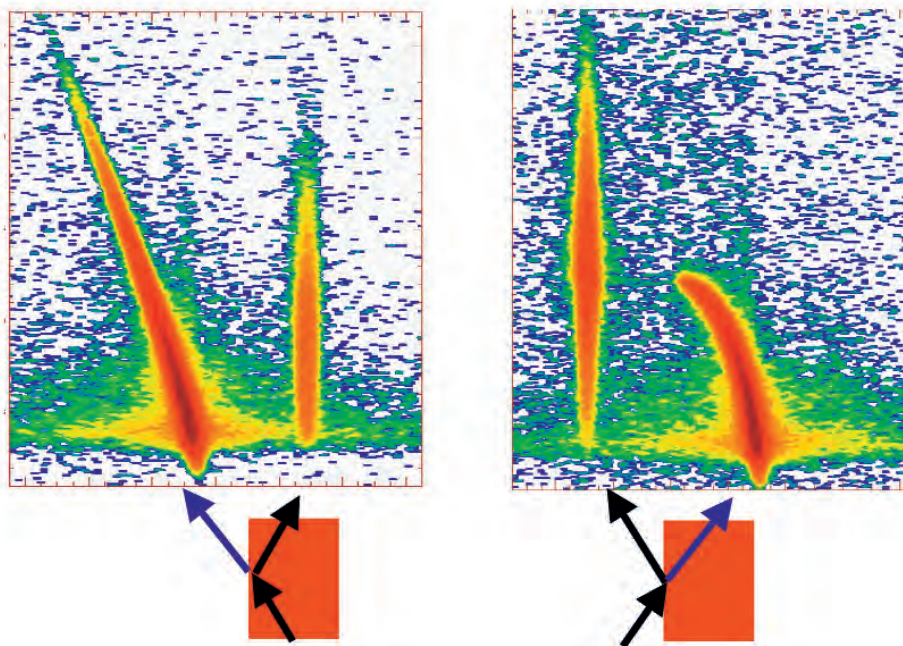


**Figure 1:** Two approaches for refraction with the incoming beam from inside (left) and outside (right) the refracting material. The vertical axis is wavelength 0-30 Å and the horizontal axis covers 4.5°.

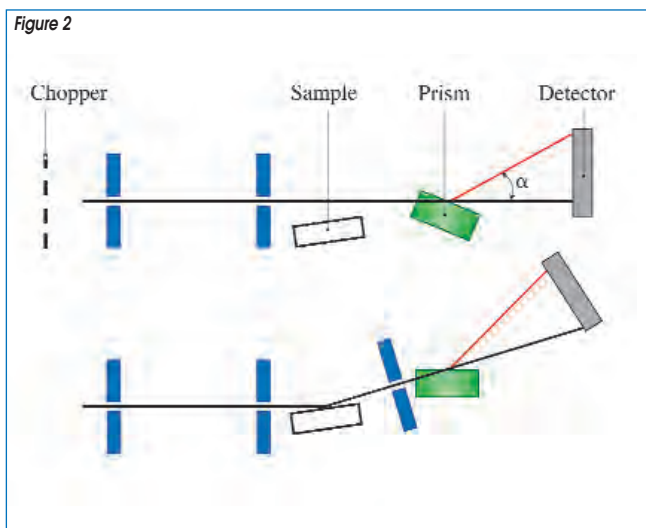


**Figure 2:** The instrumental set-up for a reflectometry experiment using a refractive interface to encode the neutrons wavelength by deflection.

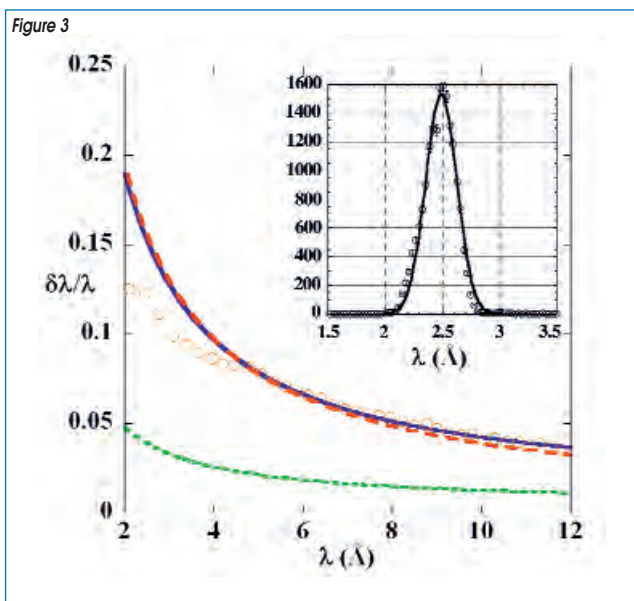


**Figure 3:** Measured resolution with a surface waviness of  $0.03^\circ$  (orange circles) compared with that of a chopper with opening  $7^\circ$  (red dashes) and theory (blue line). The lower green dotted line shows what could be achieved with a waviness of  $2 \times 10^{-3}$  degrees resulting in gains of up to a factor 100. The refracting interface was a  $140 \times 80$  mm slab of single crystal sapphire at an angle of  $0.18^\circ$  to the incoming beam.

parallel to it at a wavelength just below the wavelength corresponding to total reflection. In this case the deflection of the beam goes as the square of the wavelength but is linear if we strike the interface from the inside at very small angles. In this manner all wavelengths are deflected by a different angle allowing us to recover the intensity as a function of wavelength from the intensity distribution as a function of deflected angle.

**Figure 1** demonstrates the effect for the two possibilities of incoming beam. The approach from air leads to very good resolution near the total reflection region but the wavelength range is restricted by the presence of total reflection. With the beam coming from inside the material, there is no total reflection and the almost linear deflection with wavelength is appropriate for coding wavelengths over a wide range such as that required by a time-of-flight (TOF) reflectometer. D17 at the ILL has a TOF mode and the nature of reflectometry naturally requires a well collimated beam making it ideal for the use of refractive wavelength encoding. Experiments use a wavelength band of  $2\text{--}20 \text{ \AA}$  with a typical resolution no worse than  $\Delta\lambda/\lambda = 5\%$ . In order to achieve this resolution by refraction we require a detector with resolution

better than  $0.5 \text{ mm}$  at  $3.4 \text{ m}$  and the interface should not have waviness worse than  $10^{-3}$  degrees [1].

Good candidates for the refracting material with a high Nb and low absorption are single crystal  $\text{MgF}_2$  and  $\text{Al}_2\text{O}_3$  with Nb of  $5.13 \times 10^{-6} \text{ \AA}^{-2}$  and  $5.7 \times 10^{-6} \text{ \AA}^{-2}$  and absorption lengths of  $327 \text{ mm}$  and  $83 \text{ mm}$ , respectively for  $20 \text{ \AA}$  neutrons. In addition to the absorption we must also take into account the finite reflectivity of the beam at the interface. Taking  $\text{Al}_2\text{O}_3$  and a beam width and detector resolution of  $0.3 \text{ mm}$ , a detector distance of  $3.4 \text{ m}$  and no waviness then we can resolve  $2 \text{ \AA}$  with  $5\% \Delta\lambda/\lambda$ . The transmission of a single chopper designed to achieve this resolution is only  $0.5\%$ . Measured losses with refraction due to reflection and absorption amount to less than  $25\%$  at  $2 \text{ \AA}$  and  $40\%$  at  $12 \text{ \AA}$ . This corresponds to a gain of a factor 80 at this resolution.

In practice the measurement would proceed as follows as shown in **figure 2**. In order to calibrate the deflection as a function of wavelength choppers would be employed with the main beam striking only the refractive interface. After this, the choppers can be

stopped so the intensity as a function of deflection can be measured with the full beam. Then the sample is inserted into the beam with the refractive interface rotated with the detector to capture the reflection. To obtain reflectivity the last two measurements are simply divided. The results of a real measurement to test the resolution are shown in **figure 3**. In this case the resolution was limited only by the waviness of the refractive interface which was  $0.03$  degrees.

This method shows that gains of up to two orders of magnitude are possible in useful flux allowing very fast kinetic measurements to be made. The only disadvantage is that off-specular measurements can no longer be made in parallel with specular as the multidetector is effectively converted to a single detector. Real reflectivity experiments are planned with a prototype high-resolution multi-detector developed at the ILL and a refractive interface machined to the appropriate waviness.

## References

- (1) R. Cubitt, H.M. Shimizu, K. Ikeda and N. Torikai, *NIM A V558 (2006) 547-550*

# Quantitative texture analysis on D19 using the new 120° curved area PSD

## Authors:

F. Léon (CRISMAT, Caen and ILL)  
 D. Chateigner (CRISMAT, Caen)  
 B. Ouladiaz and D. Richard (ILL)

Quantitative texture analysis has recently been developed on the D19 diffractometer at the ILL. The newly developed detector ranks this instrument as nearly the quickest world-wide for this kind of experiment, with potentialities in dynamic texture measurements.

Quantitative Texture Analysis (QTA) relies on the measurements of many pole figures, each being acquired for a typical scan of around 1400 measurement points when using point detectors, giving rise to prohibitive acquisition times for most materials at low-flux neutron centres. Neutron QTA has been developed for several decades at many neutron centres [1]. Only in the 1980's time measurement could be reduced to typically one day on D1B, then to a few hours around a decade later when intense beam became available and curved PSD developed, like on D20 [2]. We show here that

this measuring time can still be reduced by increasing the solid-angle range spanned by the detector, as recently became possible on the D19 diffractometer. In order to characterise the upgraded instrument in terms of QTA, we measured a Belemnite rostrum from the cretaceous, which can be considered as a standard sample. The rostrum is the fossilised calcitic part of this ancient species from the Cephalopoda, which exhibits a planar texture (one crystallographic direction is aligned at random in a macroscopic plane) with c-axes randomly oriented around the rostrum axis. The crystal orientation typically culminates at around

8 times the powder value along this axis. A typical texture experiment requires the acquisition of 1368 diagrams measured in as many sample orientations using a 5°x5° grid in  $\varphi$  and  $\chi$ . In such samples, statistically reliable diagrams are obtained in 10 seconds of integration, giving a total of around 4h of acquisition time per pole figure (using a 1D detector) or per sample (using a PSD), not including dead times due to motor increments and data storage. By using the D19 position-sensitive curved area detector, we measured Debye-Scherrer diagrams of the textured Belemnite rostrum (figure 1a), in approximately one hour.

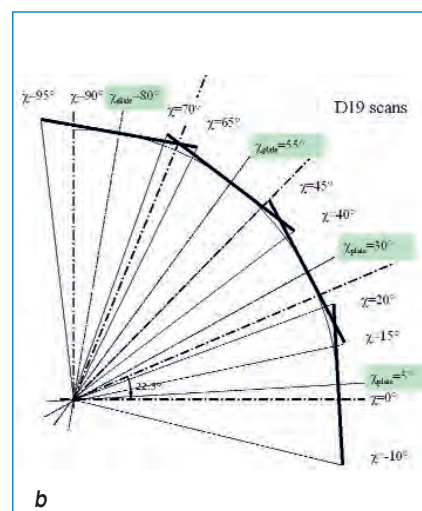
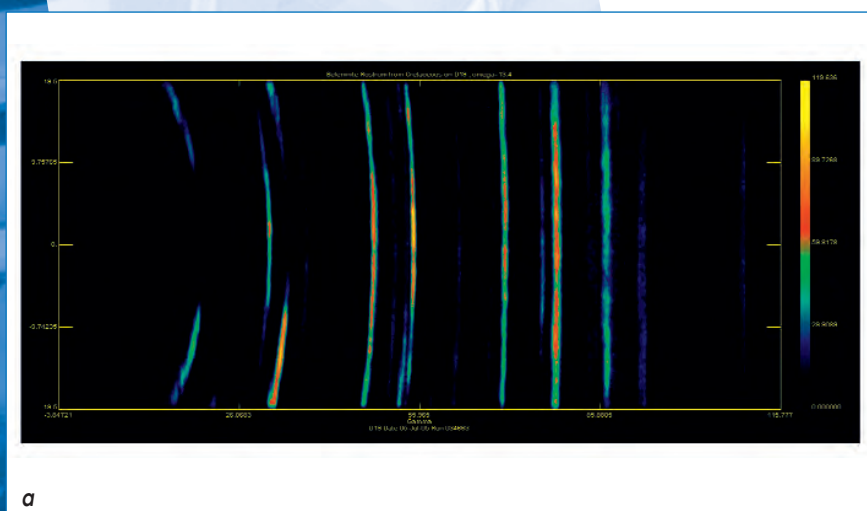


Figure 1a: Debye-Scherrer raw diagram for one orientation ( $\chi=0^\circ$ ,  $\varphi=0^\circ$ ) of the cretaceous Belemnite rostrum and b) corresponding required  $\chi$ -scan.

Such diagrams clearly reveal the presence of texture, with the strongly discontinuous rings of calcite (see for instance the two first rings from the left). One large advantage of such diagram is that its vertical axis simultaneously spans  $30^\circ$  in  $\theta$  roughly. This correspondingly diminishes the number of diagrams to be measured in  $\theta$  from 19 to 4 (figure 1b), i.e. a theoretical gain in acquisition time of nearly 5. Furthermore, less motor positioning (less dead time) is required. Data reduction is operated in the following sequence. First, a flat field correction is applied on each Debye-Scherrer diagram, in order to take account of cells efficiency, absorption and apparent surface irradiation. Then the Debye rings are developed to straight lines, in order to calculate equivalent  $2\theta$  diagrams. This latter step has been operated on a  $5^\circ$  binning scheme, in order to generate 19 diagrams (equivalent to 19  $\theta$  positions) out of the 4 detector positions, for each  $\varphi$  value. Data binning could have been operated to any desired resolution grid (e.g. with larger resolutions into  $1^\circ$  cells) using the same data set, for instance to analyse narrower crystallite dispersions. It is another advantage of this detecting approach which is only limited to the intrinsic cell size of the detector, and is less conditioned by the texture strength.

Data analysis is then carried out through Rietveld refinement of the whole dataset. In this step the previously extracted  $2\theta$  diagrams are directly interpreted using the combined analysis [2] implemented in the MAUD software. The angular transformations from the diffractometer space to the pole figure space are obtained using classical relations for CPS detectors [2]. The refinement of the Orientation Distribution Function allows subsequently recalculating any pole figures of interest. Figure 2 compares the pole figures for the main axes of the belemnite rostrum as measured using the previously validated D20 (figure 2a) [3], and the D19 (figure 2b) diffractometers. In this figure the rostrum axis is the perpendicular to the pole figures. Using both datasets the same texture is obtained, with calcite c-axes ( $\{006\}$  pole figure) strongly aligned around the rostrum axis, and at random around it forming the predicted planar texture. Correspondingly, the calcite

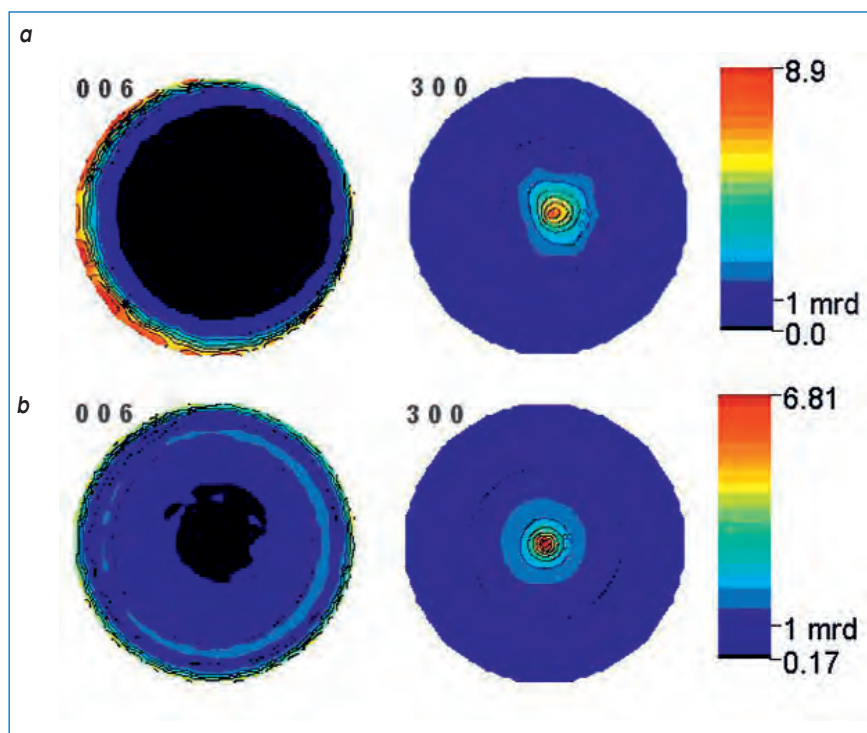


Figure 2:  $\{006\}$  and  $\{300\}$  pole figures for the Belemnite rostrum recalculated from the ODF refined on a) D20 and b) D19 data.

$\alpha$ -axes are distributed throughout the  $\{300\}$  pole figure with a gradual and slight reinforcement towards the centre due to the progressive lack of c-axes in this region. The weak tilt of the  $\{006\}$  planes observed on D20 data is only due to a slight misalignment on the diffractometer. The maximum orientation density is around 9 and 7 times the random orientation (9 and 7 m.r.d.) for the D20 and D19 instruments respectively. The observed difference of 2 m.r.d. is related in a worse reliability factor in the latter case (Rwp = 27 % and 44 %, respectively) and is attributed to small artefacts introduced during data reduction, which still need improvements. For instance, the blind zone at the left extremity of the detector together with the large curvature of the rings in this region makes a small bias in the actual correction, though the refined cell parameters are identical.

This study aimed at checking the quality of the approach developed for quantitative texture analysis using two-dimensional position-sensitive detectors. Although the level

of the data processing is still to be optimised, already good results are obtained, with the shortest acquisition times world-wide for this grid resolution using neutrons.

## References

- (1) H.-J. Bunge and C. Esling, *Quantitative Texture Analysis*, DGM, Germany (1982) 450p
- (2) D. Chateigner, *Combined analysis: structure-texture-microstructure-phase-stresses-reflectivity analysis by X-ray and neutron scattering (2004) 147p.* <http://www.ecole.ensicaen.fr/~chateign/texture/combined.pdf>
- (3) D. Chateigner, L. Lutterotti and T. Hansen: *ILL Annual Report 97 (1998)*, 28-29



# Experimental and user programme



- User programme
- Instrument list
- Beamtime allocation
- Instrument performance

And now, welcome to Belgium and Poland!

As Europe grows, so too does the European Research Area (ERA). Europe's future competitiveness, as far as research is concerned, depends most probably on its ability to develop its scientific expertise through the processes of innovation and exchange.

At its own level, the ILL too is extending its horizons. Over the last twelve months, for example, we have been joined by four new Scientific Members, Poland being the latest country to acquire ILL membership, after the recent accession of Sweden, Hungary, and Belgium.

#### **The ILL member countries**

- 1 - France
- 2 - Germany
- 3 - United Kingdom
  
- 4 - Czech Republic
- 5 - Italy
- 6 - Russia
- 7 - Spain
- 8 - Switzerland
  
- 9 - Belgium
- 10 - Hungary
- 11 - Poland
- 12 - Sweden

## User operation

The ILL User Support is there to assist all our users. If you are coming to the ILL to carry out experiments, the User Office is here to give you the organisational and administrative support you need for the successful operation of your experiments. Neutron beams and instrument facilities are free of charge for proposers of accepted experiments. Scientists affiliated to ILL member countries will also, in general, be assisted with necessary travel and daily subsistence for a limited period. The User Support Team makes all arrangements for accommodation and transport and will process claims for expenses after you have completed your experiment.



The ILL user support team (from left): Katja Jenkins, Giovanna Cicognani and Anne Dale.

### The ILL Visitors Club

All administrative tools for our scientific visitors are grouped together and directly accessible on the web, thanks to the Visitors Club. All information is presented in a user-friendly environment. After having logged in with your own personal identification, you can directly access all the available information which concerns you. Users with particular responsibilities have privileged access to other tools, according to their role. The ILL Visitors Club includes the electronic proposal and experimental

reports submission procedures and makes available additional services on the web, such as acknowledgement letters, subcommittee results, invitation letters, user satisfaction forms and so on.

Moreover, we have developed an Electronic Peer Review of the proposals submitted to the ILL, with a new application within the Visitors Club, which uses a web-based interface to the SCO Oracle database. This speeds up considerably the process of evaluation of the proposals.

You can join the Club by registering at: <http://club.ill.fr/cv/>



Peter Schurtenberger (Fribourg, Switzerland) is the Chairman of the Scientific Council sub-group working on the Partnership for Soft Condensed Matter (PSCM).

### Proposal submission

There are three different ways of submitting a proposal to the ILL:

- Standard submission of a research proposal - twice a year (in the first and third quarters)
- Director's discretion time (DDT) - no time restriction
- Special access for proprietary research and industrial users

#### Submission of a standard research proposal

Applications for beamtime should be submitted electronically, via our Electronic Proposal Submission system (EPS), available on the Visitors Club web-site. Proposals can be sub-

mitted to the ILL twice a year, usually in February and in September. The web system is activated two months before each deadline.

Submitted proposals are divided amongst the different colleges, (see indent) according to their main subject area.

Proposals are judged by a Peer Review Committee of the Subcommittees of the ILL Scientific Council. Subcommittee members are specialists in relevant areas of each College and they evaluate the proposals for scientific merit, assigning priorities and beamtime to accepted proposals.

### The ILL scientific life is organised into 10 colleges

- College 1** - Applied Physics, Instrumentation and Techniques
- College 2** - Theory
- College 3** - Nuclear and Fundamental Physics
- College 4** - Magnetic Excitations
- College 5A** - Crystallography
- College 5B** - Magnetic Structures
- College 6** - Structure and Dynamics of Liquids and Glasses
- College 7** - Spectroscopy in solid-state Physics & Chemistry
- College 8** - Structure and Dynamics of Biological Systems
- College 9** - Structure and Dynamics of Soft-condensed Matter

Before the meeting, the subcommittee receives a report on the technical feasibility and safety of a proposed experiment from the appropriate College at the ILL. Two proposal review rounds are held each year, approximately six weeks after the deadline for submission of applications.

There are normally 4.5 reactor cycles a year, with a full cycle lasting 50 days. Accepted proposals submitted by February will receive beamtime in the second half of the year and those submitted by September, in the first half of the following year. More detailed information on application for beamtime and deadlines are given on our web-site at:

[www.ill.fr/pages/science/User/UProposals.htm](http://www.ill.fr/pages/science/User/UProposals.htm)

### **Submission of a proposal to the Director's Discretion Time (DDT)**

This option allows a researcher to obtain beamtime quickly, without going through the peer-review procedure. DDT is normally used for hot topics, new ideas, feasibility tests and to encourage new users. Applications for Director's Discretion Time can be submitted to the Head of the Science Division, Dr. Christian Vettier, at any time. During the major refit programme of the ILL's reactor spanning the 2003-2006 period (see p.106) - DDT was suppressed in order to offer a larger fraction of the available beamtime to users.

### **Access for proprietary research and industrial users**

The ILL's mission is to provide neutrons for both public and industrial research. Our Industrial Liaison and Consultancy Group (ILC) ensures rapid access and total confidentiality to industrial companies, and provides a specialised staff. The ILC Group is in fact composed of scientists with considerable experience and expertise in neutron techniques applied to industrial R&D, and it facilitates and co-ordinates all aspects of industrial R&D at the ILL: initial enquiries, contractual questions, planning, experimental operations. All industrial research programmes are confidential and can be organised at short notice. To apply for proprietary beamtime, please contact the ILC at [industry@ill.fr](mailto:industry@ill.fr) or consult the web site under <http://www.ill.fr>, **Industrial Use**.

During the three reactor cycles of 2006 commercial contracts were signed with three companies (selling beamtime on D11, D22 and OrientExpress). New contracts have been established with

three potential future customers for the use of SALSA and D22 in 2007. A long term commercial user of D11 has already announced his intention of buying beamtime in the second half of 2007.

### **Experimental reports**

Users are asked to complete an experimental report on the outcome of their experiments. Following a recommendation of the ILL Scientific Council, the submission of an experimental report is now compulsory for every user who obtains access to ILL beamtime. Failure in doing so may in fact lead to rejection in case of application for beamtime for a continuation proposal. All ILL Experimental Reports are now software-archived and accessible via the web server as PDF files (under <http://www.ill.fr>, Publications). You can search for a report by experimental number, instrument, college, date of experiment, title, experimental team, local contact or institute.

Experimental reports for experiments performed in 2006 are included in the attached CD-ROM.

### **Out of hours support**

We have actively strengthened the level of technical support outside working hours. To date Out of Hours Support (OHS) has been implemented within the Instrument Control Service, the Detector Service and the Sample Environment Service.

### **Deuteration Laboratory**

A common ILL/EMBL deuteration laboratory is available to external users. The aim of the laboratory is to provide a focus for European scientists wishing to make their own deuterated materials for neutron scattering or NMR experiments. Information about the availability of this facility for external users is given on the ILL website (<http://www.ill.fr>, Users & Science, user Information, Proposal Submission). Please contact the Head of the Deuteration Facility, Michael Härtlein ([haertlein@ill.fr](mailto:haertlein@ill.fr)) for further details.

### **Facility for Materials Engineering**

The joint ILL-ESRF Facility for Materials Engineering (FaME38) provides a range of support to our users, from advice with experiment proposals to advanced sample metrology. In particular, FaME38 works with users to optimise the experimental methodology before the start of an experiment. This takes the form of standardised specimen mounting, digitisation of samples,

definition of measurement macros and liaising with the instrument responsible. It is recommended that users arrive at the ILL a day or two prior to the start of an experiment to enable these off-line preparations to be performed. The extra subsistence costs may be available from the SCO if requested beforehand. More information about this support may be found on the FaME38 website ([www.ill.fr/FaME38](http://www.ill.fr/FaME38)).

### **Partnership for Structural Biology**

The Partnership for Structural Biology (PSB) is a collaboration between the ILL, ESRF, EMBL and the neighbouring 'Institut de Biologie Structurale' (IBS). As a centre of excellence in the field of structural genomics, the PSB concentrates its research programmes on proteins and other biomolecules selected for their medical interest. It shares its office and laboratory space (located in the Carl-Ivar Brändén Building, CIBB) with the 'Institut de Virologie Moléculaire et Structurale' (IVMS) of the Joseph Fourier University.



*The Carl-Ivar Brändén Building (CIBB).*

# Instrument list - January 2007

## ILL's instruments

<b>D1A</b> (50%)	powder diffractometer	operational
<b>D2B</b>	powder diffractometer	operational
<b>D3</b>	single-crystal diffractometer	operational
<b>D4</b> (50% with IN1)	liquids diffractometer	operational
<b>D7</b>	diffuse-scattering spectrometer	operational
<b>D9</b>	single-crystal diffractometer	operational
<b>D10</b>	single-crystal diffractometer	operational
<b>D11</b>	small-angle scattering diffractometer	operational
<b>D16</b>	small momentum-transfer diffractometer	operational
<b>D17</b>	reflectometer	operational
<b>D19</b>	single-crystal diffractometer	operational
<b>D20</b>	powder diffractometer	operational
<b>D22</b>	small-angle scattering diffractometer	operational
<b>IN1</b> (50% with D4)	three-axis spectrometer	operational
<b>IN3</b>	three-axis spectrometer	operational
<b>IN4</b>	time-of-flight spectrometer	operational
<b>IN5</b>	time-of-flight spectrometer	operational
<b>IN6</b>	time-of-flight spectrometer	operational
<b>IN8</b>	three-axis spectrometer	operational
<b>IN10</b>	backscattering spectrometer	operational
<b>IN11</b>	spin-echo spectrometer	operational
<b>IN14</b>	three-axis spectrometer	operational
<b>IN16</b>	backscattering spectrometer	operational
<b>IN20</b>	three-axis spectrometer	operational
<b>PF1</b>	neutron beam for fundamental physics	operational
<b>PF2</b>	ultracold neutron source for fundamental physics	operational
<b>PN1</b>	fission product mass-spectrometer	operational
<b>PN3</b>	gamma-ray spectrometer	operational
<b>SALSA</b>	strain analyser for engineering application	operational
<b>VIVALDI</b>	thermal neutron Laue diffractometer	operational

## CRG instruments

<b>ADAM</b>	reflectometer	CRG-B operational
<b>BRISP</b>	Brillouin spectrometer	CRG-B commissioning
<b>D1B</b>	powder diffractometer	CRG-A operational
<b>D15</b>	single-crystal diffractometer	CRG-B operational
<b>D23</b>	single-crystal diffractometer	CRG-B operational
<b>IN12</b>	three-axis spectrometer	CRG-B operational
<b>IN13</b>	backscattering spectrometer	CRG-A operational
<b>IN22</b>	three-axis spectrometer	CRG-B operational
<b>S18</b>	interferometer	CRG-C operational

## Jointly funded instruments

<b>DB21</b> (50%)	single-crystal diffractometer	operational with EMBL
<b>LADI</b> (50%)	Laue diffractometer	operational with EMBL
<b>IN15</b>	spin-echo spectrometer	operational with FZ Jülich and HMI Berlin

## Test and characterisation beams

<b>CT1, CT2</b>	detector test facilities
<b>OrientExpress</b>	Laue diffractometer
<b>T3</b>	neutron optics test facility
<b>T13A, C</b>	monochromator test facility
<b>T17</b>	cold neutron test facility



# Beamtime allocation

## The ILL User Community

The ILL welcomed 1489 users in 2006. Approximately 87% came from the member countries including 361 from France, 272 from Germany and 329 from the UK (**Figure 1**). Many of our visitors were received more than once (for a total of about 1500 visits).

We value feedback from our users as an indicator of how well our facility is fulfilling their needs and to initiate actions when this is not the case. The user feedback forms, the *User Satisfaction Form*, are one measure of gathering the opinion of our users in order to raise a mirror up to ourselves. Users who have just finished an experiment at the ILL are asked to complete the questionnaire and to give us their views on different topics. User comments are made available to managers for their information and actions when appropriate.

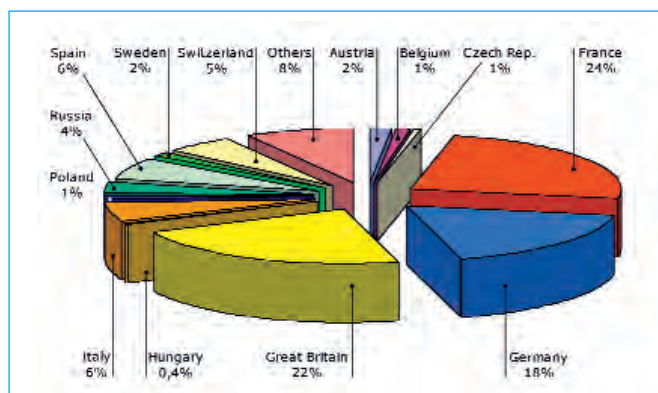


Figure 1: National affiliation of ILL users during 2006.

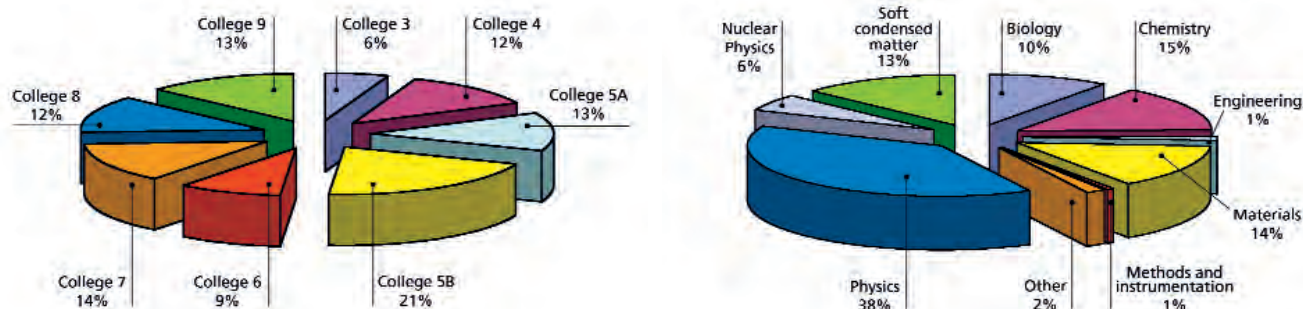


Figure 2: Beamtime allocation in 2006: distribution amongst the different research areas and colleges.

## Instruments

The instrumental facilities at the ILL are shown in the schematic diagram on page 99.

Besides the 25 ILL instruments, there are 9 CRG-instruments, which are operated by external Collaborating Research Groups. There are currently three different categories of CRG instruments.

- **CRG-A** in which the external group leases an instrument owned by ILL. They have 50% of the beamtime at their disposal and for the remaining 50% they support ILL's scientific user programme.

- **CRG-B** own their instrument and retain 70% of the available beamtime, supporting the ILL programme with the other 30%.

- Finally, **CRG-C** instruments are used full time for specific research programmes by the external group, which has exclusive use of the beam.

DB21, LADI and IN15 have a special status, since they are joint ventures of the ILL with other laboratories: in the case of DB21 and LADI with EMBL, and for IN15 with FZ Jülich and HMI Berlin.

The list of instruments as of December 2006 is summarised below (CRG instruments are marked with an asterisk \*):

- powder diffractometers: D1A, D1B\*, D2B, D20, SALSA
- liquids diffractometer: D4
- polarised neutron diffractometers: D3, D23\*
- single-crystal diffractometers: D9, D10, D15\*
- large-scale structures diffractometers: D19, DB21, LADI, VIVALDI

- small-angle scattering: D11, D22
- low momentum-transfer diffractometer: D16
- reflectometers: ADAM\*, D17
- diffuse scattering and polarisation analysis spectrometer: D7
- three-axis spectrometers: IN1, IN3, IN8, IN12\*, IN14, IN20, IN22\*
- time-of-flight spectrometers: BRISP\*, IN4, IN5, IN6
- backscattering and spin-echo spectrometers: IN10, IN11, IN13\*, IN15, IN16
- nuclear physics instruments: PN1, PN3
- fundamental physics instruments: PF1, PF2

The interferometer S18 is a CRG-C instrument and it is normally not available as a 'user' instrument, although some beamtime is made available for prototype tests of USANS.

Details of the instruments can be found on the web under <http://www.ill.fr> (Users & Science / Instrument groups & Theory).

## Beamtime allocation and utilisation for 2006

Overall, the Subcommittees of the Scientific Council scrutinised 710 proposals requesting 5071 days for 2006, out of which 572 proposals received beamtime, allocating 3319 days of beamtime on the different instruments. The distribution of beamtime for these experiments amongst the different research areas and colleges is shown in **Figure 2**.

The distribution of beamtime requested and allocated amongst the different countries is shown in **Table 1a**. In 2006, the member countries of the ILL were: France, Germany, UK, Spain, Switzerland, Austria, Italy, the Czech Republic, Russia, Sweden, Hungary and Belgium.

Poland joined in the second half of the year. The beamtime for the three reactor cycles in 2006 was allocated during the subcommittee meetings in April 2006. This is the reason why Poland does not appear as a member country of the ILL in **table 1**.

In calculating the statistics of beamtime per country, shown in **Table 1a**, the attribution is based on the location of the laboratory of the proposers, not their individual nationality. For a proposal involving laboratories from more than one member country, the total number of days is divided amongst the collaborating countries, and weighted by the number of people for each country. Local contacts are not counted as proposers except when they are members of the research team.

In **Table 1b**, the beamtime requested by and allocated to ILL, ESRF and EMBL is distributed amongst the member countries according to their financial contributions to the institutes. In this same table, when a proposal involves collaboration with a non-member country, the allocated time is attributed entirely to the collaborating member country (or countries), and weighted by the number of people for each member country. Proposals for which all proposers are from non-member countries therefore do not appear in this table.

**Table 1a:** Distribution amongst the different countries of beamtime requested and allocated in 2006 during the Subcommittees of the Scientific Council.

**Table 1b:** Distribution amongst the Associate and scientific-member countries of beamtime requested and allocated in 2006 during the Subcommittees of the Scientific Council.

Beamtime request and allocation, all countries (Table 1a)

All countries				
Country	Requested days	Requested in %	Allocated days	Allocated in %
AR	9,00	0,18	7,60	0,23
AT	<b>43,74</b>	<b>0,86</b>	<b>38,34</b>	<b>1,16</b>
AU	11,17	0,22	8,17	0,25
BE	55,08	1,09	30,47	0,92
BG	7,50	0,15	7,50	0,23
BR	10,17	0,20	5,67	0,17
BY	0,67	0,01	0,67	0,02
CA	2,67	0,05	0,67	0,02
CH	<b>121,13</b>	<b>2,39</b>	<b>73,28</b>	<b>2,21</b>
CN	3,00	0,06	4,00	0,12
CZ	<b>56,04</b>	<b>1,11</b>	<b>27,58</b>	<b>0,83</b>
DE	<b>811,59</b>	<b>16,00</b>	<b>574,23</b>	<b>17,30</b>
DK	10,66	0,21	11,10	0,33
EMBL	<b>61,83</b>	<b>1,22</b>	<b>18,84</b>	<b>0,57</b>
ES	<b>265,06</b>	<b>5,23</b>	<b>187,63</b>	<b>5,65</b>
ESRF	<b>24,23</b>	<b>0,48</b>	<b>10,06</b>	<b>0,30</b>
FI	16,06	0,32	1,00	0,03
FR	<b>992,75</b>	<b>19,58</b>	<b>684,01</b>	<b>20,61</b>
GB	<b>879,81</b>	<b>17,35</b>	<b>604,14</b>	<b>18,21</b>
GR	14,17	0,28	14,29	0,43
HU	<b>7,93</b>	<b>0,16</b>	<b>5,33</b>	<b>0,16</b>
IE	7,50	0,15	5,50	0,17
IL	3,00	0,06	3,00	0,09
ILL	<b>624,38</b>	<b>12,31</b>	<b>398,81</b>	<b>12,02</b>
IN	12,93	0,26	8,00	0,24
IT	<b>264,93</b>	<b>5,22</b>	<b>193,78</b>	<b>5,84</b>
JP	34,90	0,69	19,88	0,60
KR	1,38	0,03	1,25	0,04
LV	18,67	0,37	-	0,00
NL	14,92	0,29	12,00	0,36
NO	4,20	0,08	3,00	0,09
NZ	4,30	0,08	2,32	0,07
PL	33,20	0,65	21,43	0,65
PT	3,80	0,07	-	0,00
RU	<b>299,15</b>	<b>5,90</b>	<b>160,27</b>	<b>4,83</b>
SE	<b>66,03</b>	<b>1,30</b>	<b>33,61</b>	<b>1,01</b>
SG	3,00	0,06	2,00	0,06
SI	4,00	0,08	4,00	0,12
SK	1,67	0,03	1,33	0,04
TH	8,00	0,16	7,00	0,21
UA	5,60	0,11	3,00	0,09
US	248,89	4,91	121,41	3,66
ZA	2,33	0,05	2,33	0,07
<b>Total</b>	<b>5071,00</b>	<b>100,00</b>	<b>3318,50</b>	<b>100,00</b>

Beamtime request and allocation, only member countries (Table 1b)

Only member countries				
Country	Requested days	Requested in %	Allocated days	Allocated in %
AT	59,33	1,19	47,84	1,47
BE	60,47	1,21	35,52	1,09
CH	168,34	3,37	102,92	3,15
CZ	62,94	1,26	30,52	0,93
DE	<b>1094,40</b>	<b>21,88</b>	<b>735,57</b>	<b>22,53</b>
ES	328,36	6,57	217,10	6,65
FR	<b>1305,17</b>	<b>26,10</b>	<b>873,66</b>	<b>26,75</b>
GB	<b>1182,21</b>	<b>23,64</b>	<b>772,35</b>	<b>23,65</b>
HU	11,40	0,23	7,61	0,23
IT	332,12	6,64	230,84	7,07
RU	321,60	6,43	172,52	5,28
SE	74,65	1,49	39,04	1,20
<b>Total</b>	<b>5001,00</b>	<b>100,00</b>	<b>3265,50</b>	<b>100,00</b>

# Instrument performance

**Table 2** also gives a summary of instrument performance for 2006. For each cycle, a record is kept of any time lost from the total available beamtime and the reasons for the lost time are analysed for all instruments. The table gives a global summary for the year.

During 2006 the reactor operated for only 3 cycles, because of the work scheduled for the REFIT programme (see § Reactor Operation, p.106). This represented 143 days of neutrons (first cycle, 46 days at maximum power; second cycle, 3 days lost because of impurities in the deuterium of the vertical cold source; third cycle, 50 days).

Overall 3848 days were made available to our users in 2006 on ILL and CRG instruments, which represents about 70% of the total days of operation. 326 days were used by ILL scientists to carry out their own scientific research. About 14% of the total beamtime available

on the ILL instruments was allowed for tests, calibrations, scheduling flexibility and recovery of minor breakdowns (**figure 3**). Therefore, beam days delivered for science during the three reactor cycles (143 days) amount to 4174 in 2006. A total of 623 experiments were scheduled.

In 2006, about 583 days were lost due to various malfunctions, which represent 10% of the total available beamtime. This might seem pretty high (the average beamtime loss in normal operation is about 5%), but we are rather proud of this achievement, given the particularly challenging situation which we faced in 2006. The reactor restarted after a 10-month shutdown, during which many instruments were totally dismantled and rebuilt again with a very tight schedule, and the three reactor cycles were all concentrated in the second half of the year. The breakdown of beamtime losses is shown in **figure 4**.

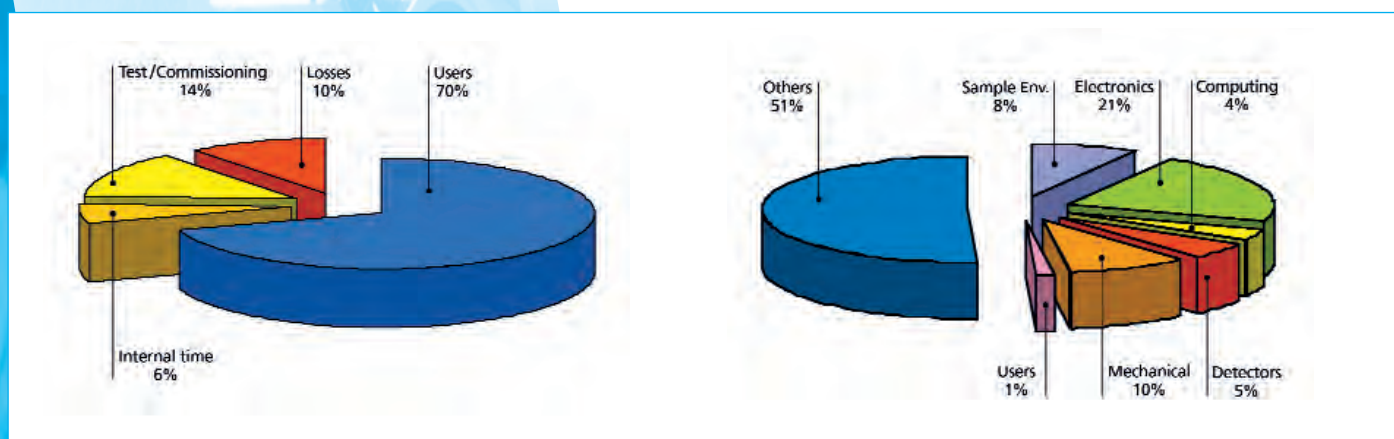


**Figure 3:** Use of ILL beamtime in 2006 (left) and reasons for beamtime losses (right).

Detailed comments on the larger beamtime losses (20 days or more) are as follows:

- D19, D20 and D2B suffered from problems related to the H11 guide;
- D3 had several minor problems (failure of electronic modules, computer crashes, motor failures...);
- D9 lost one week because of the delayed reactor restart (and consequent shift of experiments); in addition, several minor problems occurred (mainly in electronics and mechanics);
- IN15 lost an entire cycle because of beam shutter failure;
- IN4 was down for an entire cycle due to both electronic and mechanical failures;
- PN1 lost four weeks overall because of gas effluents interruption during the first and third cycles;
- PN3 was non operational for four weeks due to PZT-controller failure.

# Instrument performance

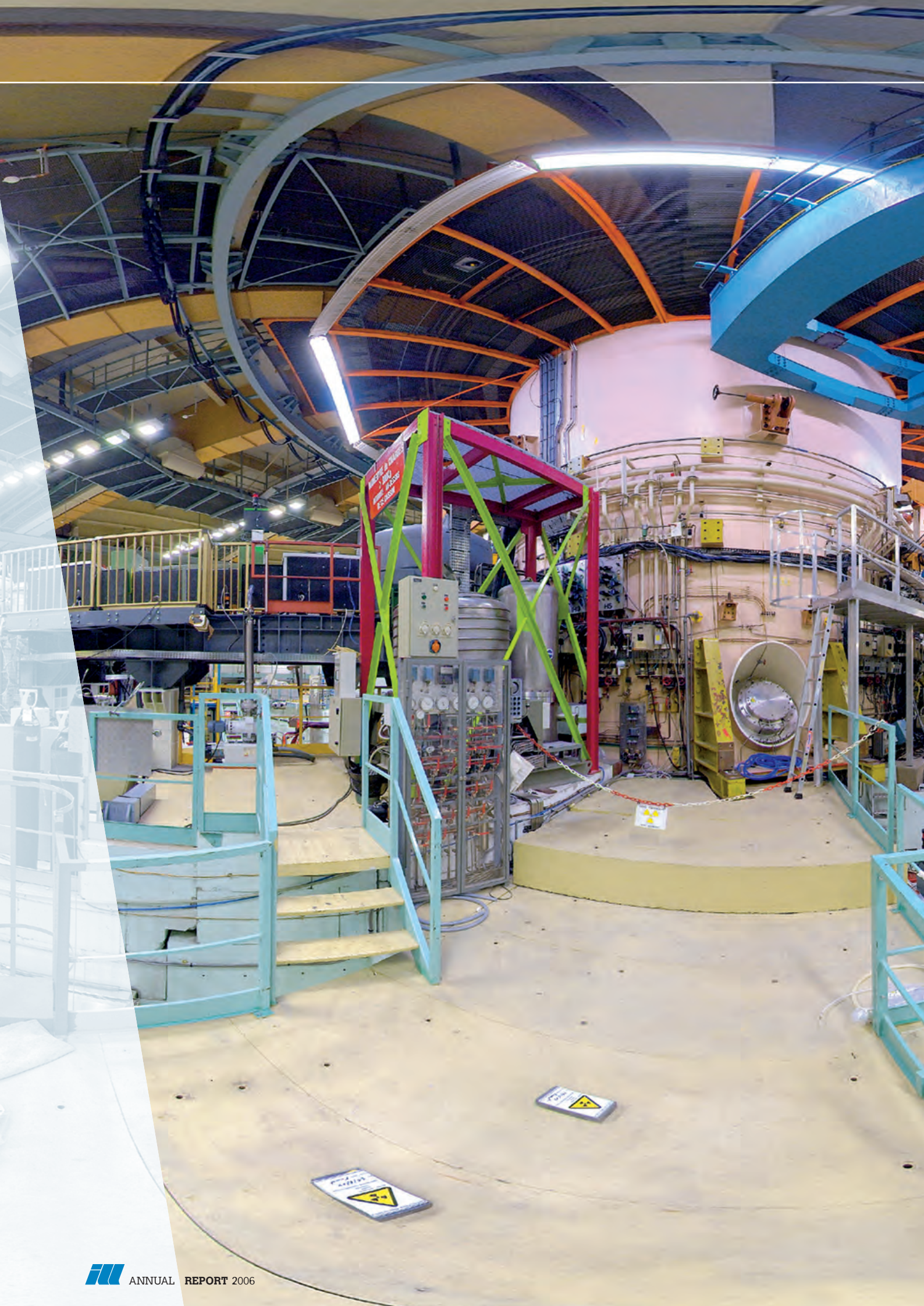
Instrument	Days requested	Days allocated *	Number of scheduled experiments	Days used for users **	Days lost	Days for commissioning /test/training	Days for internal research
ADAM	78	60	10	141	4	2	0
D10	122	106	13	116	11	12	4
D11	154	114	49	114	5	24	0
D15	8	20	3	55	78	8	0
D16	87	89	12	85	15	44	0
D17	182	113	29	121	8	11	3
D19	139	101	10	57	53	31	2
D1A	64	70	25	91	0	12	40
D1B	68	65	25	129	7	4	6
D20	269	105	49	87	39	14	3
D22	261	109	41	109	4	23	7
D23	13	15	2	128	9	6	0
D2B	135	83	37	97	26	14	6
D3	108	83	11	79	25	26	13
D4	108	60	15	60	6	7	6
D7	68	60	11	68	5	40	30
D9	84	84	9	92	24	27	0
DB21	49	49	2	46	3	1	0
IN1	93	56	8	45	2	5	12
IN10	40	95	10	104	1	38	0
IN11	93	95	10	119	2	17	5
IN12	31	30	4	128	5	6	4
IN13	67	62	8	127	8	15	0
IN14	233	93	14	102	7	17	17
IN15	107	66	9	74	52	17	0
IN16	224	98	18	101	13	24	5
IN20	149	77	12	83	5	45	10
IN22	39	41	6	99	5	4	42
IN3	45	55	3	58	16	22	47
IN4	68	65	13	65	50	17	11
IN5	157	126	27	125	11	5	3
IN6	134	91	18	116	1	23	3
IN8	151	104	15	101	3	31	8
LADI	262	72	18	70	1	42	30
PF1B	295	143	4	136	3	4	0
PF2/5 ***	149	112	12	143	0	0	0
PN1	265	108	11	87	29	27	0
PN3	230	141	7	78	28	37	0
SALSA	107	97	21	108	4	22	9
VIVALDI	135	106	22	104	15	24	0
<b>Total</b>	<b>5071</b>	<b>3319</b>	<b>623</b>	<b>3848</b>	<b>583</b>	<b>748</b>	<b>326</b>
<b>Percentage of the total available beamtime</b>				<b>70%</b>	<b>10%</b>	<b>14%</b>	<b>6%</b>

**Table 2:** Beamtime request/allocation (via standard subcommittees and DDT together) by instrument and instrument performance. CRG instruments are in blue. The reactor operated for 143 days in 2006.

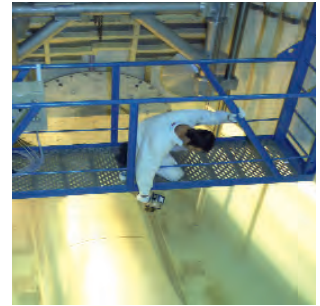
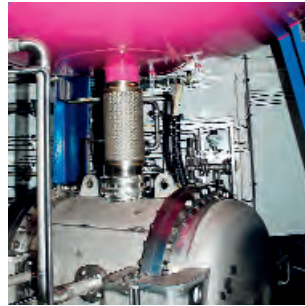
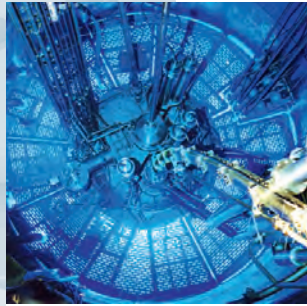
\* 'days allocated' refers to only those days reviewed by the subcommittees (i.e. excluding CRG days and DDT)

\*\* 'days used' refers to the total number of days delivered to users (i.e. including CRG and DDT days)

\*\*\* PF2 consists of 5 different set-ups where several experiments are running simultaneously



# Reactor operation



## ILL's neutrons are produced by its High-Flux Reactor

Refurbished between 1993 and 1995, it produces the most intense neutron flux in the world:  $1.5 \times 10^{15}$  neutrons per second per  $\text{cm}^2$ , with a thermal power of 58.3 MW.

The reactor operates continuously for 50-day cycles, each followed by a shut-down for changing the fuel element and carrying out a number of controls. In addition, there is a longer shut-down to enable necessary maintenance of equipment.

Normally there are 4.5 cycles a year, providing 225 days for science. However, the number of reactor cycles was reduced to 3 cycles per year during the 2003-2005 periods because of reinforcement work of the reactor (REFIT programme).

# Reactor operation

The three reactor cycles scheduled in 2006 provided for 146 days of scientific activity. There was very little disruption to operations despite the need to replace the deuterium in the cold source in the break between the first two cycles. The reactor operated to perfection, with maximum use of the fuel.

Since 2002 the ILL has been engaged in a major refit programme to ensure compliance with new seismic safety standards. This involved the reinforcement of its buildings to ensure their stability under seismic conditions. By 2006 the essentials had been completed and 2007 will therefore see a return to 4 reactor cycles of 50 days each. Throughout the refit ILL managed to maintain 3 annual cycles for user experiments.

Cycle no.	Start of cycle	End of cycle	Number of days of operation/days scheduled	Number of EFPD <sup>1</sup> scheduled	Number of unscheduled shutdowns
143	26.06.06	11.08.06	46/46	45.6/45.6	One 90-minute stoppage due to loss of offsite power
144	05.09.06	22.10.06	47/50	45.6/45.6	0
145	31.10.06	20.12.06	50/50	46/45.6	0
<b>Total</b>			<b>143/146 (98%)</b>	<b>137.2/136.8</b>	<b>1</b>

<sup>1</sup>EFPD: Equivalent Full Power Days



**Figure 1:** The installation of a new zircalloy beam tube thimble, with a life-time well beyond that of the reactor itself - the old aluminium tubes needed to be replaced every 5 - 8 years.

The main operations accomplished in 2006 were the following:

## 1. Buildings

- Phase 1 of the seismic reinforcement of the rear part of ILL 4 (main office building adjoining the reactor), following the reinforcement of the front part of the building in 2005
- Reactor building
- dismantling of structures on level D (ventilation, relaying fuel handling columns, rear area of the hot cell). 1500 tons of waste were generated by this work, conventional waste and two bins of low-level radioactive waste
- reinforcement of the floor using carbon fibre tissue
- anchoring of level D floor slab to the containment (the 'comb' technique) adjustment of the shims

## 2. Securing the reactor block, reactor pool, and transfer canal penetrations

3. Commissioning of the emergency water makeup system and its testing as part of the internal safety exercise
4. End of the H1/H2 beam tube liner replacement
5. End of the operation to install the H11 zircalloy beam tube liner
6. Reassembly of the H1/H2 guides: the upgrade of the guides and their realignment has doubled the flux available in the guide halls
7. Testing of the new digital control system for the vertical cold source
8. Important work prior to reactor start-up on 26 June:
  - drying of the reactor block prior to refilling with D<sub>2</sub>O
  - purification of the cold source D<sub>2</sub>O circuits
  - changing of the control rod, column, and new control system
  - testing of the handling columns and new control system
  - testing of the ventilation system
  - extensive pre-start-up testing
  - testing of the new start-up chambers (having submitted a request for authorisation, with a view to increasing the count rate by a factor of ten)
9. The first 58.3 thermal MW cycle with the new control rod was taken as a reference for the studies underway to optimise the reactor fuel element.

Work on the reactor itself was also scheduled in the ten-month shutdown required by the seismic refit programme. In fact, the work planned under the new Key Reactor Components programme (H1/H2 guides, fuel column controls, vertical cold source) would in any case have required a ten-month shutdown at a later date.

The recent reactor stoppage was therefore particularly complex and demanded a significant input of external resources (project planning, engineering, automation). The reactor was nevertheless able to start up as planned. The three cycles proceeded to technical perfection with optimum fuel burn-up.

The ILL's activities in 2006 generated waste and effluents respecting the regulatory limits applicable to our installation, as shown in the tables below:



Gaseous effluents	Released in 2006
Rare gas (TBq)	8.2E-01
Tritium (TBq)	4.4E+00
Gaseous halogen and aerosols (GBq)	1.7E-01

Liquid effluents	Released in 2006
Activation products, except tritium (GBq)	2.8E-01
Tritium (TBq)	1.2E-01

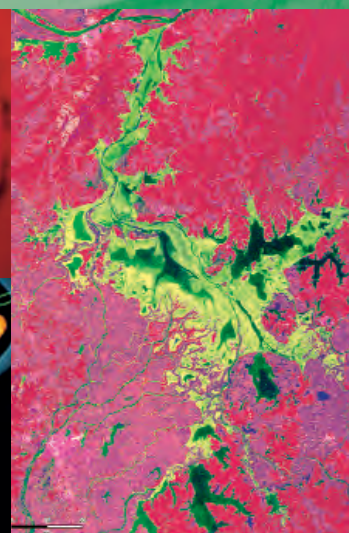
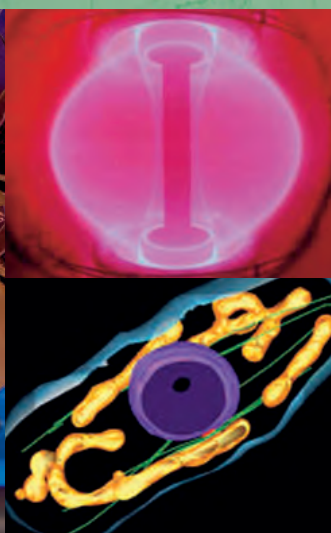
Evacuation of radioactive waste	Quantity
Decay bin (60 l)*	1
5 m <sup>3</sup> pre-concreted crate (low and intermediate level waste)	2
5 m <sup>3</sup> crate (low and intermediate level waste)	6
200 l drums of 'incineratable' (low-level waste)	41
HDPE drums 120 l (low-level waste)	35

\*Waste stocked in these decay bins is still quite active and requires several years of interim storage before meeting ANDRA's specifications for processing as intermediate-level waste.



**Figure 2:** When changing the vertical cold source's digital control system, other strategic equipment was also changed or modified, following the lessons learnt over the last 40 years. This is the vertical cold source tank under 18 m<sup>3</sup> of deuterium ballast. It houses the isolation valves and the analysis and conditioning circuits. It is designed to resist a deuterium explosion.

**Figure 3:** Slicing the irradiated H1/H2 thimble in its swimming pool. H1/H2 channels ILL's neutrons to the ILL7 guide hall. The procedures developed and tested by our teams ensured that this operation was performed in record time with minimum risk to the operators. For the first time at the ILL we were able to section the tube and ensure its transformation into properly packaged waste in one and the same operation.



## EIROforum: serving European science

Science is a team effort and for progress to be made, it often needs large specific facilities, some of which require resources beyond the means of any single country. Europe has a great history of scientific endeavour, and since the early 1950s, a number of intergovernmental research organisations have been established to fulfill the needs of Europe's scientists.

EIROforum (<http://www.eiroforum.org/>) is a partnership of Europe's seven largest intergovernmental research organisations, and the ILL is one of them.

After one year of chairmanship, on 30 June 2006 the ILL handed over EIROforum's presidency to the ESRF. It was certainly a year of great involvement for ILL representatives. This year good contact was established with the European Commission. A meeting was held in Brussels with the European Parliament's Committee on Industry, Research and Energy (ITRE), and EIROforum was prominent in several of the activities run by the Commission.

### The seven EIROforum members are:

- CERN** - European Organisation for Nuclear Research
- EFDA** - European Fusion Development Agreement
- EMBL** - European Molecular Biology Laboratory
- ESA** - European Space Agency
- ESO** - European Southern Observatory
- ESRF** - European Synchrotron Radiation Facility
- ILL** - Institut Laue-Langevin

In EIROforum, these organisations pursue joint initiatives, combine resources, and share best practices. Collaboration between the seven members is contributing positively to the development of the European Research Area. Joint initiatives have already resulted in an important impact in the areas of Outreach and Education.

High-profile activities such as Science on Stage (<http://www.scienceonstage.net/>) involve thousands of European science teachers in a joint effort to raise interest in science and technology studies. The next Science on Stage festival will be held in Grenoble (2-6 April 2007) and is jointly organised by the ILL and the ESRF.

Another important achievement is the publishing (4 times a year) of the European journal *Science in School* (<http://www.scienceinschool.org/>), which promotes inspiring science teaching.



## Workshops in which ILL was a major player in 2006

- **ThALES's meeting** (10-11 March, Rencurel)  
- M. Böhm, S. Roux and A. Hiess (ILL)
- **3<sup>rd</sup> International Workshop on Dynamics in Confinement, CONFIT 2006** (23-26 March)  
- M. Koza, B. Frick (ILL) and  
R. Zorn (Forschungszentrum Jülich)
- **Applications of Gamma-Ray Diffraction, APGRADE** (26-28 October)  
- M. Jentschel, B. Lauss, P. Mutti and J. Krempel (ILL)
- **The second ILL Millennium Symposium** (27-29 April)  
- ILL Management
- **ILL Soft Matter User Meeting** (22-24 November)  
- T. Forsyth, G. Fragneto, B. Frick, I. Grillo,  
P. Lindner, P. Timmins and C. Vettier (ILL).



### ThALES's Meeting

Thales (Three-Axis Low Energy Spectroscopy) is a project studying the development of the ILL's next generation of cold three-axis spectrometers, in terms of higher count-rates, easy-to-use polarisation options, larger kinematic range and experimental zones adapted to high-field magnets.

To discuss in detail the scientific case and to obtain feed-back from potential users on instrument layout, a 2-day meeting was organised in Rencurel, in the Grenoble region, where many of our users joined the ILL team and enjoyed excellent scientific talks and many fruitful discussions.



### 3<sup>rd</sup> International Workshop on Dynamics in Confinement (CONFIT 2006)

Hosted by the ILL, CONFIT 2006 was a continuation of two very successful meetings held in 2000 and 2003. The workshop aimed at an update of the scientific progress, new developments and latest achievements made over the last three years in the field of confined matter research.

The research in confined media spans a wide range of fields from glass and polymer physics, through fundamental aspects of quantum systems and biology to industrial application.

110 scientists contributed to lively debates at the CONFIT 2006 meeting. There were 19 invited and 25 contributed oral presentations given. 58 posters were on display.

website: <http://www.ill.fr/YellowBook/IN6/confit2006/confit-2006.html>



### Applications of Gamma-Ray Diffraction

The APGRADE-06 workshop, organised and hosted by the ILL's Nuclear and Particle Physics Group from 25 to 27 October, attracted a number of top researchers to our Institut. The goal of the meeting was to lay out the scientific future of the GAMS Gamma-Ray Spectrometers. The presentations were focused on future research topics for GAMS: more precise neutron binding energy measurements for metrology, a tunable gamma-ray source and the use of GAMS for Positron Annihilation Spectroscopy.





## The second ILL Millennium Symposium

The second ILL Millennium Symposium was held at the end of April to demonstrate the achievements of the Millennium Programme to date, and to boost the ILL's ambitious plans for the coming decade. It was also an opportunity to renew old acquaintances. Prof. Dirk Dubbers, the father of the Millennium Programme, was the honorary chairman, and we were also honoured by the sprightly presence of two other former ILL Directors, Bernard Jacrot and Peter Schofield.

The scientific programme included presentations of scientific results and frontier achievements in methods and neutron techniques, mostly by our users. ILL scientists and engineers also presented their ambitious plans for instrument developments and analysis techniques in the coming decade. Seven parallel sessions allowed intense discussion and feedback from the users in smaller groups. No holds were barred, yet all criticism will be considered in depth. The hectic schedule of 21 plenary talks, 49 talks in parallel sessions, 3 summary talks, and 73 posters, many on instrument developments at other neutron facilities, ensured lively discussions at the coffee breaks.

A document 'Future Perspectives and Opportunities for the ILL', which includes projects for instruments, infrastructure and user interface facilities as well as renewal plans of key components of the reactor, moderators and neutron guides, has been published.

Feedback from the users, expressed during the Symposium, or on the Symposium web site, will guide these objectives.

<http://vitraill.ill.fr/symposium/welcome.jsp>

## ILL Soft Matter User Meeting

The ILL organised the first ILL Soft Matter User Meeting from 22 to 24 November (kindly hosted by ESRF). The meeting gathered more than 110 scientists whose interest was to apply neutron methods to their own soft matter research and it offered opportunities to present and discuss recent neutron scattering research in this field and to identify the needs of the soft matter community at the ILL. In particular, questions such as on-site characterisation and preparation of samples, complementary methods or optimisation of the use of beamtime, were discussed.

In view of the future Partnership for Soft Condensed Matter (PSCM) on the ILL-ESRF site, this workshop provided an excellent opportunity to raise users' interest in the scope, structure and scientific orientation of the PSCM at its very early stages.

The meeting was very successful with lively and productive discussions. There was a general agreement for a paradigm change from a neutrons-only user facility to the creation of a stimulating and vibrant scientific environment from which users could profit enormously. The PSCM is strongly endorsed by the user community. It is seen as a great opportunity for experienced as well as new users and the way forward to allow « soft matter » users to make better use of neutrons.

website: <http://www.ill.fr/softill2006/>



## Workshops and events



**1** - Carl-Ivar Brändén Building (CIBB) inauguration (13 January)

**2** - Visit of the German General Consul, M. Heiner Model (22 February)

**3** - Visit of the British Ambassador, Sir John Holmes (8 March)

**4** - EIROforum Directors General meeting with Janez Potočnik - European Research Commissioner (22-23 May)

**5** - UK honours ILL scientists: Giovanna Fragneto (in the photo) and Katy Wood have been awarded the BTM Willis 2006 prize (end of March)



# A year in photos



Workshops and events

## Comings and goings

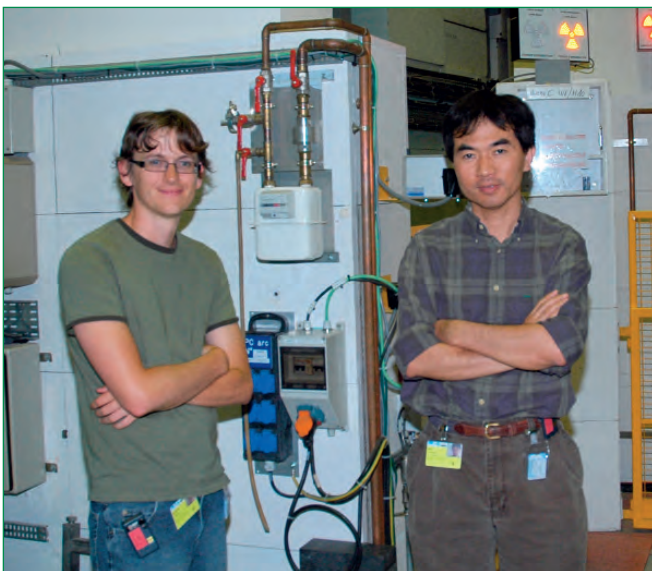
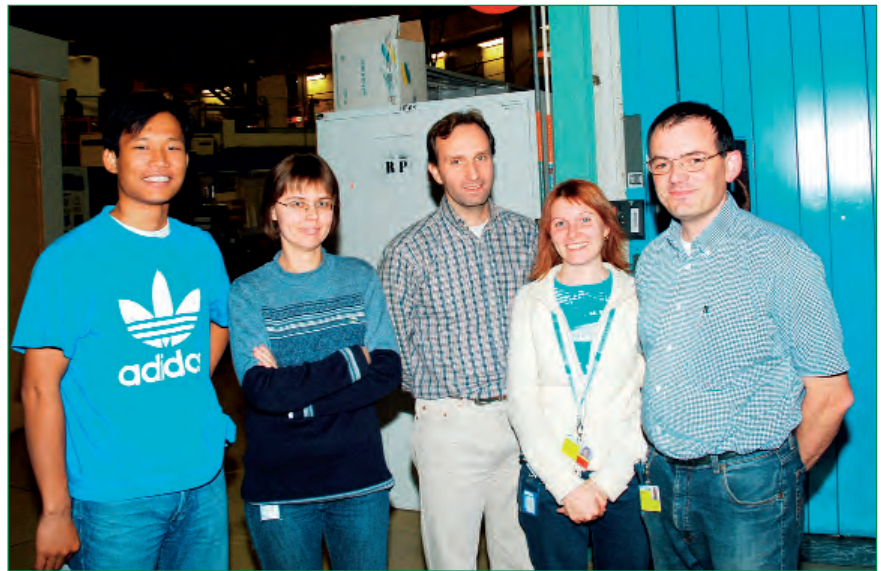
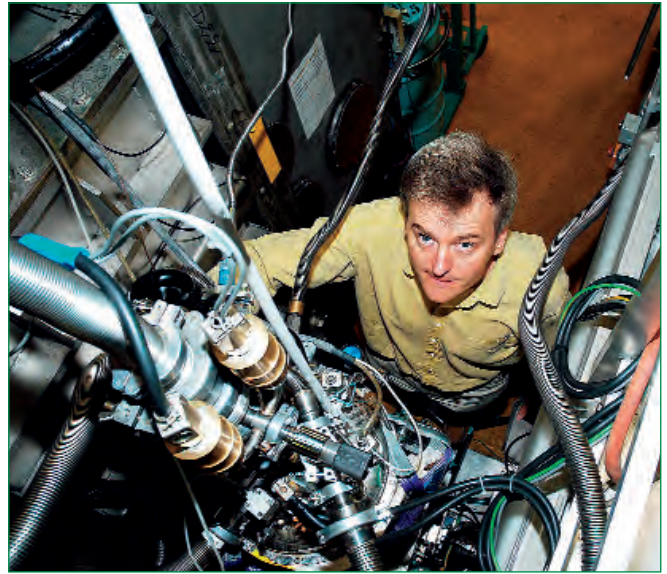
**6** - Colin Carlile leaves the ILL (27 September) and Richard Wagner takes over the Institut's leadership

**7** - Hands-on for the handover!

# French science festival



# Happy users at the ILL



Workshops and events

The ILL's Administration Division is responsible for the following areas of activity: human resources, finance and accounting, purchasing, building and site maintenance, and translations. The interactivity of its services and their close collaboration with the ILL's other divisions ensure that the administrative and organisational support they provide is efficient and reliable. Staff in the Administration Division is also involved in a continuous process of streamlining procedures, regulations and workflows to meet the changing needs of an international research centre. In 2006 all the Division's services were also heavily involved in the management of the Refit Programme.

### Human Resources

2006 was marked by major changes in personnel, due in particular to a high number of staff taking retirement. Recruitment has therefore been a top priority. Furthermore, a "competence approach" in order to be able to retain individual knowledge and know-how has been stated. In addition to this a new on-line recruitment system has been implemented with a positive impact on the speed of recruitment. Staff leave is now for the most part managed on-line via the Human

Resources Toolkit, thus allowing staff to track their personal leave entitlement from their desktops. The Training Unit has begun work on a detailed repertoire of all the professions represented at the ILL and has recently started to implement new legislation on vocational training entitlements.

Every effort is made to achieve a broad representation of the ILL's member countries amongst the ILL staff, and of course to promote gender equality. A package of relocation and support services ("Staff integration

support fund") is available to newcomers at the Institut, and to non-French nationals in particular, providing a smoother adjustment to life at the ILL and in the Grenoble region.

### Finance

The work of the Economic and Financial Service (SEF) includes preparations to meet the major annual milestones: the budget and final accounts, and the annual inspections by the Audit Commission and Fiscal Experts. In addition to the SEF's regular activities of



*Norbert Koenig left the ILL on 15 September, after a period of 5 years as the head of the Administrative Division.*



*Amin Saidoun is the new leader of the Administration Division.*

cash management (payments, invoicing, investments) and the negotiation and management of contracts, the Service focused its efforts in 2006 on the renewal of agreements with the ILL's banking partners. It also launched a project to bring the Institut's fixed assets management system into line with the new French accounting standard CRC 2002-10. The consultancy firm Mazars from Lyon has been brought in to assist with this process. More generally, the SEF has upgraded its QUALIAC accounting software and enhanced the security of the IT tools used to produce the financial statements and budgetary reports. Finally, in 2006 the SEF assumed responsibility for the financial management of the CIBB building house the PSB/IVMS structural biology partnership.

## Purchasing

Almost half of the ILL's budget is spent on procurement. Every year some 6000 purchase requests are processed by the ILL's buyers for issue as purchase orders to our many suppliers.

In 2006 the creation of a joint ESRF-ILL goods reception bay made a significant contribution to optimising logistics on the site. The success of this project has encouraged the institutes to establish a joint stores facility, responsible for managing the 1000 items of stock available to the scientists, engineers and technicians of both institutes. Progress of this sort can also be noted in the closer collaboration between the ILL and ESRF buyers. In practical terms, this includes the issuing of joint calls for tender, thus offering the institutes access to more competitive purchase conditions with external suppliers.

The ILL's Purchasing Service issues international calls for tender whenever possible, with the aim of ensuring a reasonable distribution of purchases in the member countries.

## Building and Site Maintenance

The Building and Site Maintenance Service is responsible for ensuring that the ILL's complex of buildings remains in a good state of repair. In 2006 the Service's resour-

ces were committed to the seismic reinforcement of the ILL's main office building ILL4 and the final stages of reconstruction of the experimental halls ILL7 and ILL22. The Service was also closely involved in studies to set up the instruments FIGARO and D11B. Other activities included the deviation of the fluid circuits in ILL4 and the transfer of staff from ILL4 to ILL17, a temporary measure required by the seismic reinforcement operations. Finally, a study has been launched for the redevelopment of the site's open spaces, including the planting of trees, and work has begun on upgrading the locking systems for access to site buildings.

## Translation

The ILL's in-house translation service is responsible for handling all the Institut's translation requirements into and out of the Institut's three official languages –

English, French and German. Its qualified staff translates a wide variety of administrative, scientific and technical documents, including the preparatory documents for meetings of the ILL's governing bodies, technical specifications for international calls for tender, and safety regulations. They also assist with the adaptation of scientific articles for non-specialist readers and are generally on hand to answer all questions of a linguistic nature. Interpreting services can also be provided if needed.

As part of its duties, the office takes charge of the translation of brochures and leaflets aimed at the general public. In 2006, its staff was involved in the preparation of a web site for "Science on Stage". The ILL and ESRF are the local organisers of the next edition of this European science teaching festival, which will be held in Grenoble in April 2007.



*The new ILL17 building.*

# The three European research institutes in Grenoble

European Molecular Biology Laboratory (**EMBL**)

European Synchrotron Radiation Facility (**ESRF**)

Institut Laue Langevin (**ILL**)



welcome

# SCIENCE *on Stage* 2

Grenoble, France  
2-6 April 2007

**Science teaching festival:  
The very best of today's science education**

- 500 teachers
- 30 European countries

organised by *EIROforum* (CERN, ESA, ESO, EMBL, EFDA, ESRF, ILL, EPS, EAAE)  
and supported by the European Commission as part of *Nucleus*.



[www.scienceonstage.net](http://www.scienceonstage.net)



# Facts and figures

• **Name** Institut Max von Laue - Paul Langevin (ILL)

• **Founded** 17 January 1967. International Convention (renewal) signed until 31 December 2013.

• **Associates**

- France

Commissariat à l'Energie Atomique (CEA)

Centre National de la Recherche Scientifique (CNRS)

- Germany

Forschungszentrum Jülich (FZJ)

- United Kingdom

Council for the Central Laboratory of the Research Councils (CCLRC)

• **Countries with Scientific membership**

- Spain

Ministerio de Educación y Ciencia (MEC)

- Switzerland

Bundesamt für Bildung und Wissenschaft

- Italy

Istituto Nazionale per la Fisica della Materia (INFN)

Consiglio Nazionale delle Ricerche (CNR)

- Russia

Federal Agency for Atomic Energy (FAAE)

- CENI (Central European Neutron Initiative)

Consortium, composed of

- Austria: Österreichische Akademie der Wissenschaften

- Czech Republic: Charles University of Prague

- Hungary: Research Institute for Solid State Physics and Optics affiliated to the Budapest Neutron Centre (BNC-RISP)

- Sweden

Swedish Research Council (SRC)

- Belgium

Belgian Federal Science Policy Office (BELSPO)

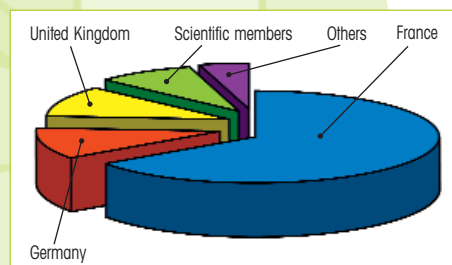
- Poland

The Henryk Niewodniczański Institute of Nuclear Physics (Polish Academy of Sciences)

• **Staff**

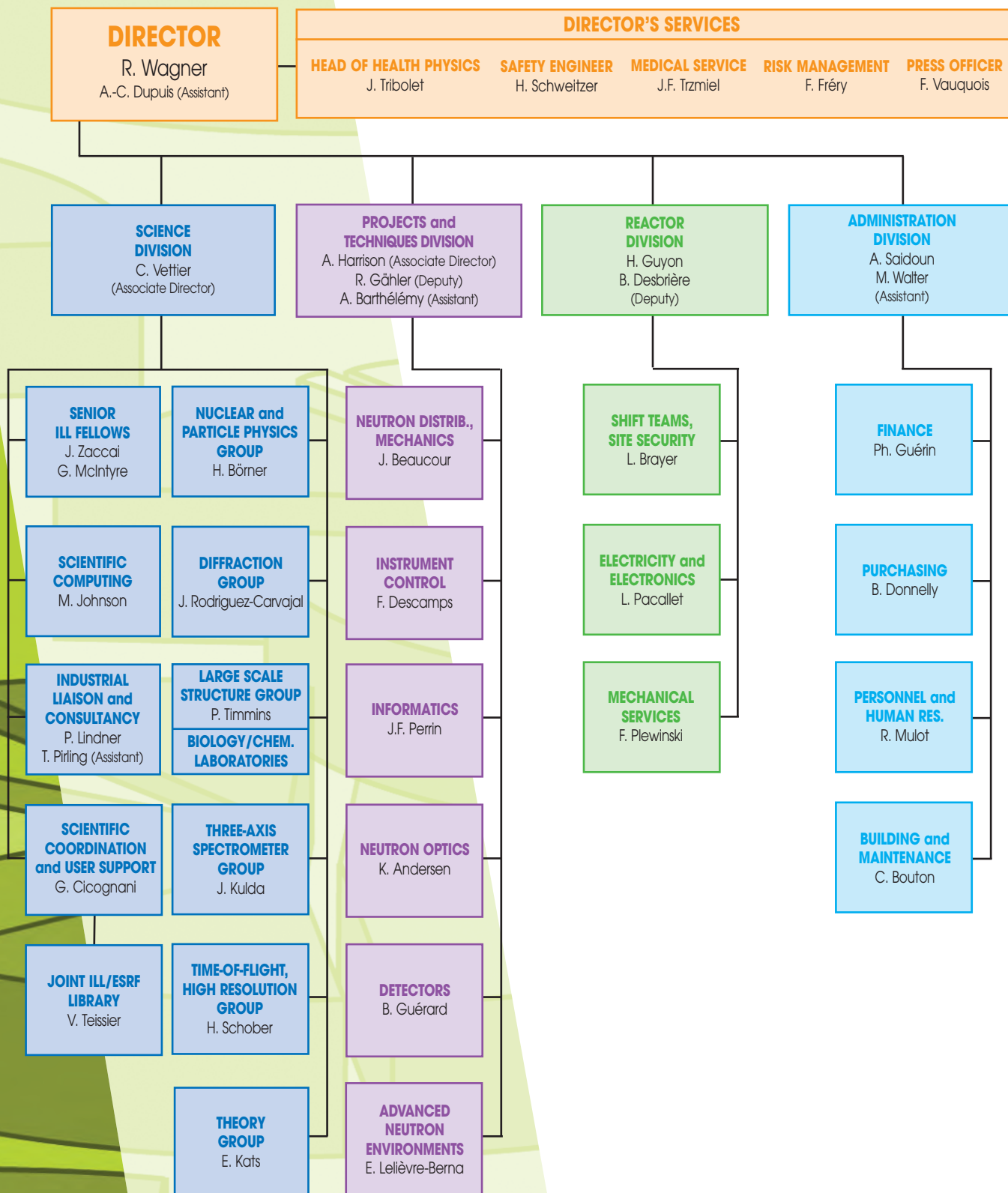
449 people including 60 experimentalists in the scientific sector and 20 thesis students.

292 French, 50 German, 49 British, 39 Scientific member countries and 19 others

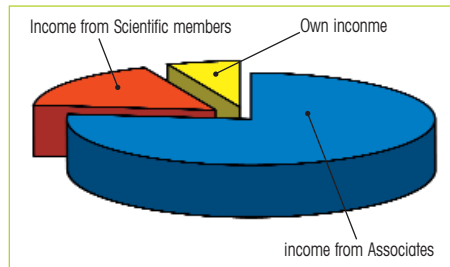


Staff on 31/12/2006		%
France	292.5	65.14
Germany	49.5	11.02
United Kingdom	48.5	10.80
Scientific members	39	8.69
Others	19.5	4.34
<b>Total</b>	<b>449</b>	<b>100</b>

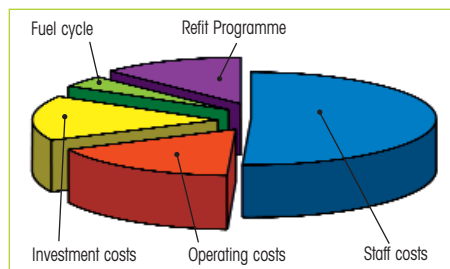
# Organisation chart - January 2007



• **Budget 2006 73.9 M€ (excluding taxes)**

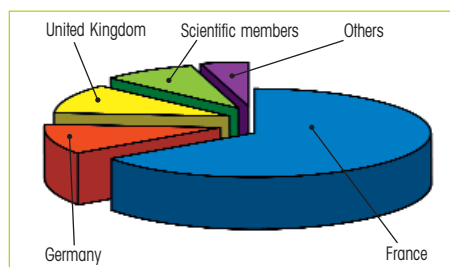


Income	(M€)	%
Income from Associates	56.7	76.73
Income from Scientific members	12.5	16.91
Own income	4.7	6.36
<b>Total</b>	<b>73.9</b>	<b>100</b>



Expenditure	(M€)	%
Staff costs	37.5	50.74
Operating costs	12.6	17.05
Investment costs	11.6	15.70
Fuel cycle	3.0	4.06
Refit Programme	9.2	12.45
<b>Total</b>	<b>73.9</b>	<b>100</b>

• **Distribution of ILL purchases (M€, excluding taxes)**



Purchases	(M€)	%
France	20.94	76.82
Germany	2.57	9.43
United Kingdom	1.06	3.90
Scientific members	1.36	4.99
Others	1.33	4.88
<b>Total</b>	<b>27.26</b>	<b>100</b>

• **Supervisory and Advisory Bodies**

- Steering Committee, meeting twice a year
- Subcommittee on Administrative Questions, meeting twice a year
- Audit Commission, meeting once a year
- Scientific Council with 9 Subcommittees, meeting twice a year

• **Reactor**

58 MW, running 3 cycles in 2006 (with cycles of 50 days)

• **Experimental Programme**

623 experiments (allocated by subcommittees) on 25 ILL-funded and 9 CRG instruments  
 1500 visitors coming from 36 countries  
 710 proposals submitted and 572 accepted

# Events calendar for 2007



- **17 January:** ILL 40<sup>th</sup> anniversary
- **23-27 January:** International Workshop on Laue Diffraction Methods
- **31 January - 2 February:** International Workshop on dynamics of molecules and materials
- **6 March:** Proposal submission deadline
- **2-6 April:** Science on Stage Festival
- **17-19 April:** Scientific Council and Subcommittee Meetings
- **26-27 April:** SAQ
- **14-15 June:** Steering Committee meeting
- **18 September:** Proposal submission deadline
- **25-26 October:** SAQ
- **6-9 November:** Scientific Council and Subcommittee Meetings
- **29-30 November:** Steering Committee meeting

## Reactor cycles for 2007:

Cycle n° 146 (071)	From To	20/02/2007 11/04/2007
Cycle n° 147 (072)	From To	24/04/2007 13/06/2007
Cycle n° 148 (073)	From To	28/08/2007 17/10/2007
Cycle n° 149 (074)	From To	30/10/2007 19/12/2007

*Start-ups and shut-downs are planned at 8:30 am.*



In 2006,  
the ILL received  
notice of  
639 publications by  
ILL staff and users

**The distribution by subject is as follows:**

Applied physics, instrumentation and techniques	67
Theory	34
Nuclear and particle physics	62
Magnetic excitations	48
Crystallography	94
Magnetic structures	133
Liquids and glasses	37
Chemistry	52
Biology	45
Soft matter	67





# 2006

Annual Report

2006

Annual Report

Institut Laue - Langevin

6, rue Jules Horowitz - BP 156  
38042 Grenoble Cedex 9 - France - <http://www.ill.fr>

